THE BELL SYSTEM TECHNICAL JOURNAL

JULY–AUGUST 1978
VOL. 57, NO. 6, PART 1 OF 2

ISSN0005–8580

ATLANTA FIBER SYSTEM EXPERIMENT

THE BELL SYSTEM TECHNICAL JOURNAL

THE BELL SYSTEM TECHNICAL JOURNAL is published monthly, except for the May-June and July-August combined issues, by the American Telephone and Telegraph Company, J. D. deButts, Chairman and Chief Executive Officer; C. L. Brown, President; W. G. Burns, Vice President and Treasurer; F. A. Hutson, Jr., Secretary. Editorial enquiries should be addressed to the Editor, The Bell System Technical Journal, Bell Laboratories, 600 Mountain Ave., Murray Hill, N.J. 07974. Checks for subscriptions should be made payable to The Bell System Technical Journal and should be addressed to Bell Laboratories, Circulation Group, Whippany Road, Whippany, N.J. 07981. Subscriptions $20.00 per year; single copies $2.00 each. Foreign postage $1.00 per year; 15 cents per copy. Printed in U.S.A. Second-class postage paid at New Providence, New Jersey 07974 and additional mailing offices.

THE BELL SYSTEM
TECHNICAL JOURNAL

DEVOTED TO THE SCIENTIFIC AND ENGINEERING
ASPECTS OF ELECTRICAL COMMUNICATION

Volume 57 July–August 1978 Number 6, Part 1

Atlanta Fiber System Experiment:

Overview

By IRA JACOBS

(Manuscript received December 29, 1977)

A complete 44.7-Mb/s lightwave digital transmission system was evaluated at the joint Western Electric and Bell Laboratories facility in Atlanta in 1976. An overview is provided to the papers describing the technology employed and some of the principal results of the experimental evaluation. Two interrelated themes are emphasized: (i) the importance of careful measurement and characterization, and (ii) the need for parameter control. Both the Atlanta Experiment and the follow-on Chicago installation have given confidence in the feasibility of lightwave technology to meet Bell System transmission needs.

On January 13, 1976 the Atlanta Fiber System Experiment was turned up, and 44.7 Mb/s signals were successfully transmitted over the entire system. The following papers in this issue describe the technology employed and some of the principal results of this experiment. Although there have been a number of conferences[1–6] and prior publications[7–10] in which some aspects of this experiment have been discussed, the present papers provide the first comprehensive report.

The purposes of the Atlanta Fiber System Experiment were:

(*i*) To evaluate lightwave technology in an environment approximating field conditions.

(*ii*) To provide a focus for the exploratory development efforts on fiber, cable, splicing and connectors, optical sources and detectors, and system electronics.

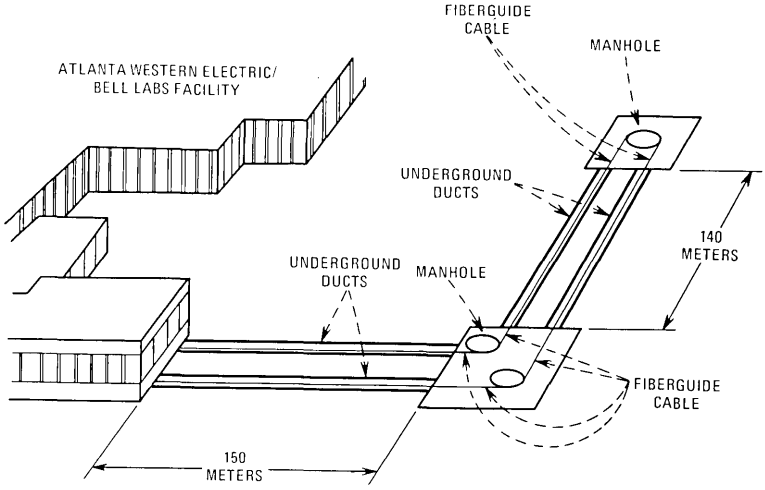

Fig. 1—Atlanta Fiber System Experiment ducts.

(*iii*) To address interface problems that arise when a complete system is being implemented (a system is more than the sum of its component parts).

In short, the purpose was to assess the technical feasibility of lightwave communications for Bell System application.

The locale of the experiment was the joint Western Electric and Bell Laboratories facility in Atlanta, Georgia where the fiber and cable were made, and where ducts, typical of those in metropolitan areas, were available. These ducts, including two in which temperature and humidity may be controlled, were installed when the Atlanta facility was constructed, and were intended as a test bed for new cables. The ducts terminate in a Bell Laboratories basement room and extend 150 meters to a manhole and then another 140 meters to a second manhole (Fig. 1). The fiberguide cables* are looped in the second manhole so that both ends terminate in the basement room. This room provides the office envi-

Table I—Atlanta System Experiment parameters and results

Transmission rate	44.7 Mb/s (672 voice channels)
Cable	144 graded-index fibers (12 × 12 ribbon array)
Average loss	6.0 dB/km (0.82 micron wavelength)
Average transmitter power	−3 dBm (0.5 mW)
Receiver sensitivity	−54 dBm (4 nW)
Calculated repeater spacing	7 km
Maximum repeater spacing	10.9 km

* Two cables, both made by Bell Laboratories, were installed. The first, containing fibers made solely by Western Electric, formed the principal cable for the experiments. The second cable was made with Western Electric, Bell Laboratories, and Corning Glass Works fibers.

ronment for the lightwave system; indeed, it simulates both end offices and intermediate offices in an interoffice trunk system.

The principal parameters and results of the experiment are summarized in Table I. The transmission was digital at a rate of 44.7 Mb/s corresponding to the third level (DS3) of the North American digital hierarchy. Lightwave systems tend to be power- rather than bandwidth-limited, and digital transmission is particularly desirable in such cases.[8] The transmission speed of 44.7 Mb/s was chosen as that hierarchical level at which lightwave systems might initially be most economic and practical.[11]

A ribbon-structured cable was chosen to facilitate splicing. The large number of fibers in the cable (144) was to gain experience in the making of large fiber-count cables. Also, since the total length of the installed cable was only 650 meters, many fibers were required so that long paths could be obtained by looping through the cable many times. The objective was to achieve at least 100 good fibers in the cable with an average loss of no more than 8 dB/km. The results achieved were 138 good fibers with an average loss of 6 dB/km.

The operating wavelength of 0.82 microns was chosen to be below the water absorption peak. Average transmitter power into the fiber from the GaAlAs laser was 0.5 mW, and the sensitivity of the APD receiver was 4 nW. A laser and an APD were used to maximize repeater spacing. With allowances for connector loss and system margin, a system repeater spacing of 7 km was calculated. Utilizing some of the lower loss fibers in the cable, error-free transmission was obtained with a repeater distance of 10.9 km.

The system in Atlanta contained all elements of an operational digital transmission system, including the three major subsystems (Fig. 2):

(*i*) Cable.
(*ii*) Distribution system.
(*iii*) Terminal electronics.

The first four papers in this issue relate to the cable, starting with the characteristics and reproducibility of the graded-index germania borosilicate fibers (DiMarcello and Williams), then treating the preform fabrication and fiber drawing (Myers and Partus), and the cable manufacture and performance characterization (Santana, Buckler, and Saunders), and concluding with optical crosstalk evaluations (Buckler and Miller).

The key element in the interconnection system is the molded plug single-fiber connector used both on the distributing frame and on the optical regenerators. The structure and performance of these connectors is described in the paper by Runge and Cheng.

The next sequence of four papers covers the system electronics. There are two papers on the detector, one (Hartman, Melchior, Schinke and

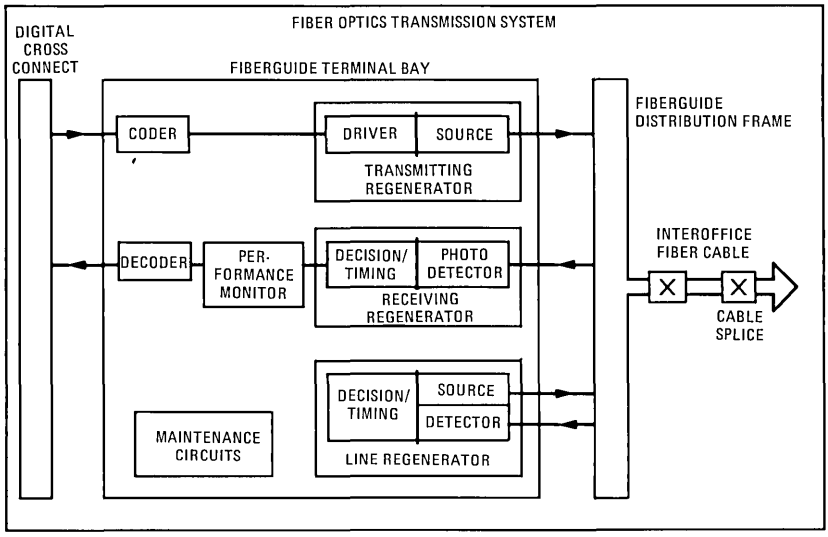

Fig. 2—Atlanta Fiber System Experiment transmission system.

Seidel) on the avalanche photodiode and one (Smith, Brackett, and Reinbold) on the detector package including the transimpedance preamplifier. The transmitter package, including the GaAlAs laser, is covered in the paper by Shumate, Chen, and Dorman. The design and performance of the optical regenerator, including timing recovery and decision functions in addition to the transmitter and receiver, is covered in the fourth paper (Maione, Sell, and Wolaver) of this sequence.

Following the papers on the technology and subsystems, Kerdock and Wolaver describe the experiments performed and the results obtained. In all cases, the system met or exceeded expectations.

Two themes run through all these papers. First is the importance of careful measurement and characterization. The loss of a multimode fiber or of a single fiber connector is critically dependent on how they are measured, and particular attention is paid in these papers not only to the results obtained, but to how they are obtained. Most of these results are of a statistical nature, and the second recurrent theme is the "tail of the distribution." From a research standpoint, one is often interested in the best result achieved. But from an exploratory development standpoint, the other end of the distribution is of importance, and technical feasibility means achieving the knowledge and understanding to control the low-performance tail of the distribution. The Atlanta Experiment has provided important inputs of this nature, but it is only one of many steps in the exploratory development phase prior to specific design and development.

The system in Atlanta accepted standard DS3 (44.736 Mb/s) signals,

and the system was interfaced with an M13 multiplex and a D3 channel bank, and voice, data, and television were transmitted over the system. But it is one thing to set up an experimental link on premises, and it is another to incorporate a system into the telephone network carrying actual customers' signals. The results achieved in Atlanta gave us confidence that we were ready for this next step. A trial system was installed in Chicago early in 1977, and has been carrying a wide range of services on a trial basis since May 11, 1977. Although the evaluation of this trial system is still in progress,[12,13] a brief article (Schwartz, Reenstra, Mullins, and Cook) is included in this issue describing the Chicago installation and the results to date. Both the Atlanta experiment and the Chicago installation have given confidence in the feasibility of lightwave technology to meet Bell System transmission needs.

REFERENCES

1. J. S. Cook, J. H. Mullins, and M. I. Schwartz, "An Experimental Fiber Optics Communications System," 1976 IEEE/OSA Conference on Laser and Electro-Optical Systems, San Diego, May 1976.
2. R. G. Smith, C. A. Brackett, H. Melchior, H. W. Reinbold, D. P. Shenke, T. C. Rich, and M. DiDomenico, Jr., "Optical Detector Package for the FT3 Fiberguide Experiment," *ibid.*
3. M. I. Schwartz, R. A. Kempf, and W. B. Gardner, "Design and Characterization of an Exploratory Fiber-Optic Cable," Second European Conference on Optical Fiber Communication, Paris, Sept. 1976.
4. J. S. Cook and P. K. Runge, "An Exploratory Fiberguide Interconnection System," *ibid.*
5. I. Jacobs and J. R. McCrory, "Atlanta System Experiments Overview," Topical Meeting on Optical Fiber Transmission II, Williamsburg, Feb. 1977.
6. R. S. Kerdock and D. H. Wolaver, "Performance of an Experimental Fiber-Optic Transmission System," National Telecommunications Conference, Dallas, Dec. 1976.
7. I. Jacobs, "Lightwave Communications Passes Its First Test," Bell Laboratories Record, *54*, Dec. 1976, pp 291–297.
8. I. Jacobs and S. E. Miller, "Optical Transmission of Voice and Data," IEEE Spectrum, *14* (Feb. 1977), pp. 32–41.
9. C. M. Miller, "A Fiber-Optic Cable Connector," B.S.T.J. *54*, No. 9 (November 1975), pp. 1547–1555.
10. T. L. Maione and D. D. Sell, "Experimental Fiber Optic Transmission System for Interoffice Trunks," IEEE Trans. Commun., *COM-25* (May 1977), pp. 515–523. pp. 515–523.
11. I. Jacobs, "Telecommunication Applications of Fiber Optics," National Telecommunication Conference, Los Angeles, Dec. 1977.
12. M. I. Schwartz, W. A. Reenstra, and J. H. Mullins, "The Chicago Lightwave Communications Project," 1977 International Conference on Integrated Optics and Optical Fiber Communication (Post-Deadline Paper), Tokyo, July 1977.
13. J. H. Mullins, "A Bell System Optical Fiber System—Chicago Installation," National Telecommunications Conference, Los Angeles, Dec. 1977.

THE BELL SYSTEM TECHNICAL JOURNAL
Vol. 57, No. 6, July–August 1978
Printed in U.S.A.

Atlanta Fiber System Experiment:

Reproducibility of Optical Fibers Prepared by a Modified Chemical Vapor Deposition Process*

By F. V. DiMARCELLO and J. C. WILLIAMS

(Manuscript received January 21, 1977)

The reproducibility of low-loss glass-fiber optical waveguides prepared from preforms produced by a "modified" chemical vapor deposition process was determined. The fibers have a multimode, graded-index core of germania borosilicate glasses and a cladding of fused silica. The quality of the fibers is expressed in terms of core/cladding dimensions, circularity, and concentricity, as well as loss spectrum, normalized index-of-refraction difference Δ, and graded-index profile characteristic α.

I. INTRODUCTION

A variety of multimode, low-loss glass fibers consisting of a core of germania borosilicate glasses and a cladding of fused quartz have been prepared over the past several years using the modified chemical vapor deposition (MCVD) process. The primary purpose has been to provide experimental glass fibers in response to in-house requests. Most of the early fibers used for prototype fiber optic cable studies leading to the Atlanta Fiber System Experiment[1] were prepared in this laboratory. The requests for fibers were seldom alike in terms of core/cladding dimensions, index profiles, index differences, and other properties. Although the conditions of preparation and properties of these fibers were monitored, it became desirable to establish the reproducibility of the process. Equally important, this would enable us to determine where and possibly how we should make improvements if needed.

* Part of this work was presented as a paper at the First European Conference on Optical Fiber Communication at London, The Institute of Electrical Engineers, September 16–18, 1975.

A series of fibers was to be fabricated on the basis of an arbitrarily chosen set of objectives listed in Table I. All process parameters selected for meeting these requirements were attempted to be held constant. The reproducibility achieved in these fibers is to be expressed in terms of properties such as core/cladding dimensions, loss spectrum, normalized index difference Δ, graded index profile characteristic α, circularity, and core/cladding concentricity as well as their comparison to the objectives.

II. PROCEDURE

The MCVD process,[2] as practiced for this study, is summarized here in conjunction with the schematic shown in Fig. 1.

A chemically cleaned tube (12 mm × 14 mm × 92 cm) of fused quartz is rotated in a glass working lathe. An oxy-hydrogen torch, while moving to the right at slow speed (0.35 cm/s), heats the tubing to ~1650°C. The torch returns to the left, at a faster speed (1.5 cm/s) and lower flame temperature, to complete one cycle. Throughout the torch cycle, controlled proportions of semiconducting grades of B, Ge, and Si chlorides in an oxygen carrier gas flow through the fused quartz tube. The deposition and simultaneous fusion of a thin layer of core glass occurs along the internal surface of the tube in the region of the torch as it moves from left to right only.

The flow conditions of the reactants at an ambient temperature of 23° to 25°C are listed in Table II. An initial layer of borosilicate glass is deposited during the first two torch cycles. The numbers in parentheses are the flow rates of oxygen through the bubblers containing the Ge and

Table I — Fiber property objectives

Loss (0.82 μm)	$\leq$4 dB/km
Index profile, α	~2.0
Index difference, Δ	0.013
Core diameter	55 μm
Fiber diameter	110μm

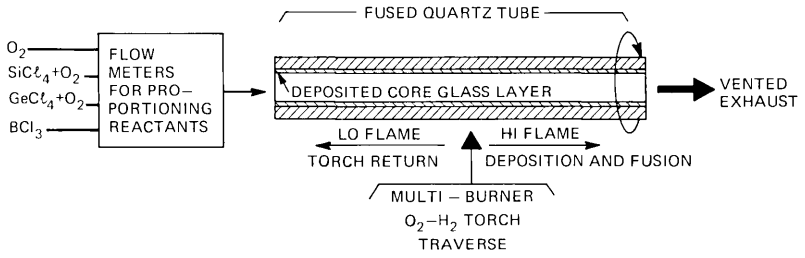

Fig. 1 — Schematic diagram of the modified chemical vapor deposition (MCVD) process.

Table II — Flow conditions of reactants (cc/min)

Torch Cycles	BCl_3	$SiCl_4$	$GeCl_4$	Additional O_2
2	24	81 (255)	—	500
47	8	81 (255)	4.5–47.4 (70–500)	500

( ) = oxygen to bubblers.

Si tetrachlorides. To obtain the 2:1 diameter ratio of the cladding to core in the final fiber, an additional 47 torch cycles were required for depositing the germania borosilicate core glass. The flow rate of the $GeCl_4$ was increased automatically in 47 increments, or one per torch cycle, over the range from 4.5 to 47.4 cc/min. This provides the compositional gradient in the core glass required for the graded-index profile.

The fused quartz tubing is then collapsed into a solid rod within three additional torch cycles, at which time the speed of the torch is reduced (0.2, 0.1, and 0.03 cm/s) to raise the transient temperature of the tubing to the level of 1850° to 1950°C. During collapse, the flow of reactants was stopped except for oxygen until the last cycle of the torch. This produces a preform as seen in Fig. 2, measuring ~8 mm in diameter and 60 cm in length, that yields 3 km of 110-μm diameter fiber.

The preforms were drawn into fibers using the apparatus shown in Fig. 3. The basic components consist of a preform support and feed mechanism at the top, a high temperature heat source, a fiber diameter monitoring unit, and a winding mechanism at the bottom. An experimental coating system, shown just above the winding drum, was not used in this study. The overall assembly is mounted on a heavy aluminum frame measuring ~1.2 × 1.8 × 2.4 m.

The feed mechanism consists of a variable speed motor and control system* capable of providing less than 1 percent variation and full torque at low speeds of 0.5 to 1.5 cm/min. The heat source is a graphite resistance furnace† provided with a zirconium oxide‡ muffle tube and oper-

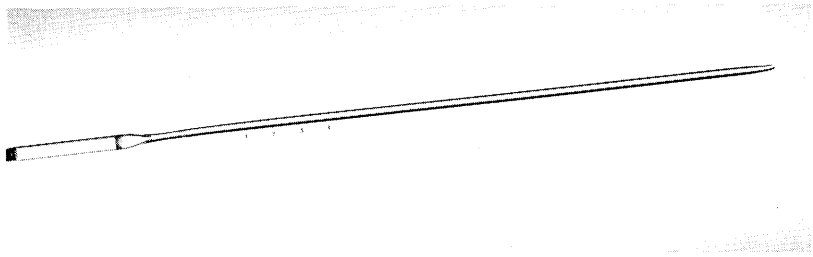

Fig. 2 — Collapsed glass preform obtained from the MCVD process (8 mm dia. × 60 cm).

* Motomatic E550M, B & B Motor and Control, N.Y., N.Y.
† Model 6000-2020, Astro Industries, Santa Barbara, California.
‡ No. 1706 Zircoa Div., Cohart Refractories, Solon, Ohio.

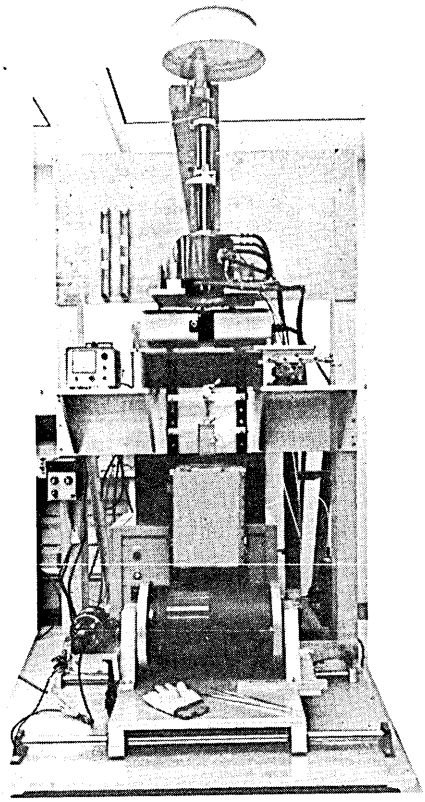

Fig. 3 — Overview of the laboratory fiber drawing facility.

ated with a 50/50 mixture by volume of He and Ar (8–10 L/min.) gases to prevent oxidation of the graphite heating element.

The winding mechanism consists of a black anodized aluminum drum (28 cm diam. × 45 cm) driven by a variable speed motor.* A gear belt connects the drum drive to a lead screw that traverses the drum to give a 0.30-mm (0.012-in.) pitch to the fiber winding. Typically, a 1100-m length of fiber is wound on a drum in a single layer. A drawing speed of 1 m/s was used in this work.

The diameter of the fiber was monitored during drawing by means of the device† mounted just below the furnace. It employs an optical comparison technique with the window located about 12 cm below the furnace. The shadow of the fiber is compared to a pre-set illuminated slit opening that has been calibrated previously. The size of the fiber

* Bodine NSH34RH, B and B Motor and Control, New York, N.Y.

† Model SSE-SR Milmaster, Electron-Machine Corp., Umatilla, Fla.

relative to the slit opening is indicated on a nullmeter having a precision of ±0.13 μm (±0.000005 inch). Normally, the preform feed speed and furnace temperature are held constant while the speed of the winding drum is adjusted manually to maintain a constant fiber diameter.

Initially, 18 lengths of fused quartz tubing* were selected at random. Prior to cleaning, each tube was numbered for identification by means of a diamond scribe at the designated left-hand end. An axial mark at the same end served to indicate the "north" orientation of the tubing when viewed from either end. The minimum and maximum outside diameter (O.D.) and wall thickness corresponding to the four main compass directions at either end were determined by means of a vernier caliper. Variations ranging in outside diameter from 0.02 to 0.13 mm and in wall thickness from 0 to 0.16 mm were found in the 18 lengths of tubing. In addition, the location and amount of the maximum warp along the length of the tubing was determined using a feeler gauge to measure the maximum clearance between the tubing and a ground stone reference plane as the tube was rotated about its axis. The warp was typically in the form of a bow that ranged from a minimum of 0.13 to a maximum of 0.61 mm. A further characterization of the quality of the fused quartz tubing was attempted by a cursory inspection for visual blemishes as revealed by illuminating the tubing from either end by means of a high-intensity fiber-optic lamp. The predominate type of blemish manifested itself as a bright speck of scattered light that resulted, in most cases, from small bubbles within the glass tubing. Several tubes contained <10 specks/in., while others ranged up to ~50 specks/in. In addition, a number of scratches, smears, and hazy areas were recorded for many of the tubes. No correlation has been established between the visual quality of the tubing and the quality of the resulting fiber.

Fibers were prepared from 12 of the 18 lengths of tubing selected. Tubes numbered 2, 6, 13, 14, 15, and 17 were excluded from this study because of accidental breakage before preform preparation (nos. 2 and 6), excessive variation in wall thickness causing oval cores in the collapsed preforms (nos. 13, 14, and 15), and being classified as a spare preform (no. 17).

III. RESULTS AND DISCUSSION

In this study, two 1-km lengths of fiber were drawn from each preform using the above drawing facility. The following data were obtained from an examination of these fibers and provide an indication of their quality and reproducibility.

Figure 4 is a composite semilog plot of the loss spectrum of a kilometer length of fiber from each of 11 preforms and two 1-km lengths from one other preform. The Arabic number identifies the preform, while the

* Commercial Grade T08, Amersil Corp., Sayreville, New Jersey.

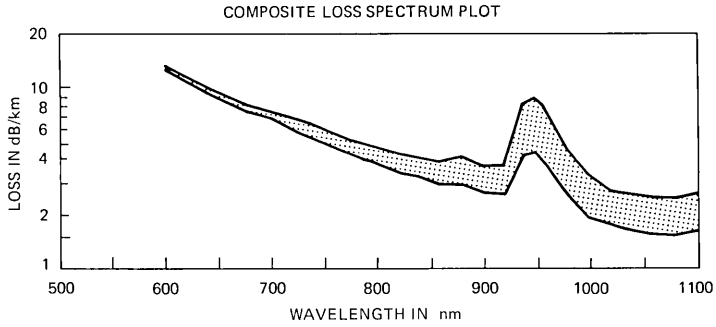

OPTICAL LOSS IN dB/km

PREFORM —FIBER	WAVELENGTH IN nm		
	820	900	1060
1-I	3.9	3.0	1.9
3-I	3.8	3.1	1.8
4-II	3.5	2.6	1.5
5-II	4.4	3.7	2.5
7-I	4.1	3.5	2.0
8-I	3.6	2.7	1.6
9-I	3.9	3.0	1.8
10-I	3.5	2.9	1.7
11-I	3.7	2.9	1.6
11-II	3.9	3.1	1.8
12-I	3.8	2.9	1.6
16-II	3.5	2.6	1.6
18-I	3.7 (RMS = 3.8)	3.0	1.8

Fig. 4 — Composite loss spectrum plot and tabulated loss values (13 1-km fibers among 12 preforms, GeO_2-B_2O_3-SiO_2 core and fused silica cladding).

Roman numeral refers to the first or second kilometer drawn from that preform. The curves fall within narrow limits. The corresponding tabulated values at wavelengths of 820, 900, and 1060 nm include minimum values of 3.5, 2.6, and 1.5 dB/km, respectively, with most of the fibers being within ½ dB or less of these minima. The RMS value at 820 nm is 3.8 dB/km.

The graded-index profile characteristic α and the normalized maximum index of refraction difference Δ were obtained by a technique developed by Wonsiewicz et al.[3] The method provides a computer-generated plot of the index profile in Δn versus fiber radius as illustrated in Fig. 5. The data are obtained from the pattern of a thin, polished cross-section of a fiber as viewed in an interference microscope. A computer program also determines the value of α corresponding to the curve that fits the data best in accord with the basic equation shown in the diagram. The maximum normalized Δ is determined from the maximum Δn of the plot. The dip at the center among the data points results from a depletion of Ge along the center of the fiber by volatilization during the collapsing of the preform. The existence of this condition has not been shown to be detrimental to the transmission characteristics of the fiber.

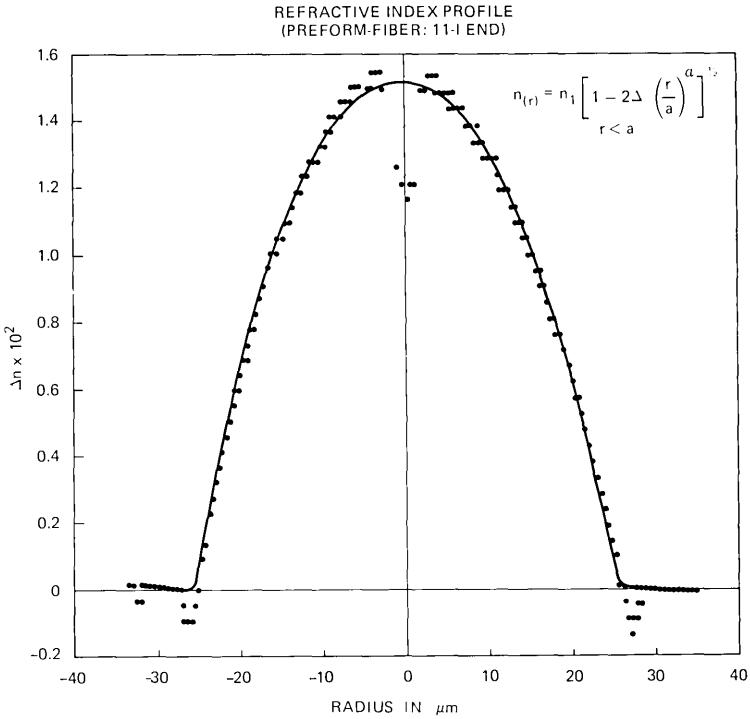

Fig. 5 — Index of refraction profile for preform—fiber: 11-I.

The dip at either edge of the profile corresponds to the borosilicate layer at the core cladding surface.

Figure 6 compares the range of values for α and Δ determined from "four" fiber samples within each preform, as indicated by the height of the bar, and among preforms. The RMS values for α were calculated to be 2.14 and for Δ to be 0.012. The precision of measurement for α is ± 0.05 and for Δ is ± 0.001. Although the observed α values are higher than intended, they could be corrected by adjusting the flow rates of the reactants and other parameters. The values for Δ in this study tend toward the low side for two reasons: (*i*) a decrease in the germania concentration at the center of the core and (*ii*) the thickness of the central region of the core of the thin section sample being less than the apparent value because of preferential abrasion during polishing.[4]

While the diameter of the fiber was monitored and controlled manually during drawing, it was measured subsequently at a precision of $\pm 1/4$ μm by an off-line forward light scattering technique described by Watkins.[5] The diameters along 556 m from each of several randomly selected fibers were determined at the rate of one measurement per meter. Figure 7 illustrates a typical linear plot of the diameter variation for such a length. The minimum, maximum, and average diameters and

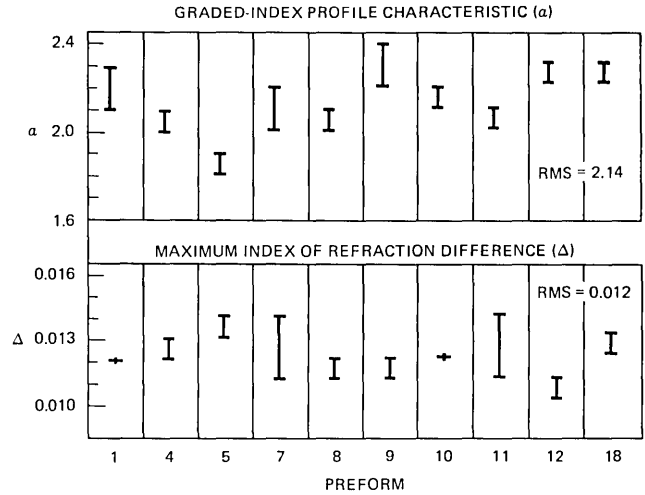

Fig. 6 — Graded-index profile characteristic (α) and maximum index of refraction difference (Δ) vs preform (interference microscopy; sample thickness ~50 μm).

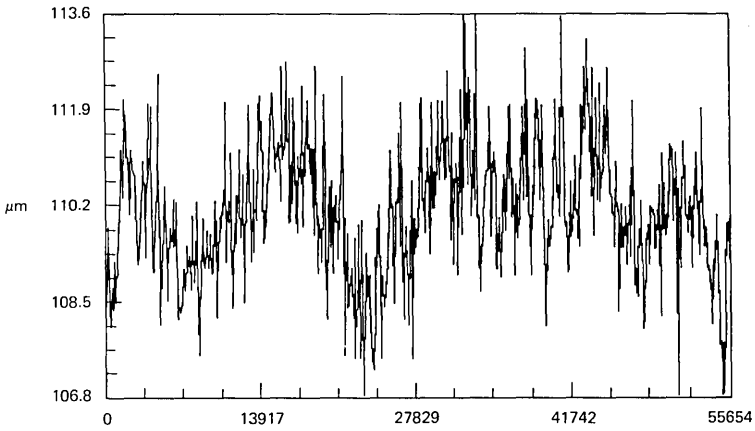

PREFORM –FIBER	MIN	MAX	AVG	% STND DEV
5-1	107.0	113.1	110.2	1.02
8-1	105.7	113.2	109.7	1.30
11-1	104.8	114.5	109.6	1.72
12-1	105.7	112.5	109.0	1.09
12-2	104.9	113.5	109.7	1.45
16-1	106.7	115.0	109.7	1.13

Fig. 7 — Fiber diameter variation vs. 556-m length of preform—fiber: 5-I; and minimum, maximum, average, and percent standard deviation of fiber diameter within and among preforms.

the percent standard deviation within and among preforms are tabulated. Considering that diameter control was by manual feedback during drawing, the average values are relatively close to the objective of 110 μm.

The circularity and concentricity of the core and cladding are important properties related to fiber alignment when splicing. They were determined by microscopic examination of four fiber samples per preform corresponding to the positions shown in the diagram at the top of Fig. 8. The minimum and maximum diameters were determined by means of dividers and a calibrated micrometer scale from a photograph of a cross-section of the fiber, such as that shown on the left.

Circularity for either the core or cladding is expressed as the ratio of the minimum and maximum diameter of each. The concentricity of the core-cladding is defined as the separation (Δcp) expressed in micrometers between the center points formed by the intersection of the minimum and maximum diameters for each of the core and cladding.

In Fig. 9, the minimum-maximum diameter ratios of the core and cladding are shown for fiber samples among each of 12 preforms. Each dot represents a diameter ratio measurement. The numerical range of values observed for the diameters among the four samples within each preform is also shown. In general, the circularity of the cladding is better than that of the core both within a preform and among preforms. The circularity of the core becomes fixed, essentially during the collapsing stage of the preform, while that of the cladding may be upgraded during the drawing step. The circularity of the core and cladding vary independently of each other as seen in the case of preforms 4, 9, and 18. It was also observed that the variation in core circularity increases with the variation in wall thickness of the deposition tubing.

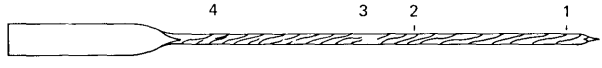

MCVD PREFORM

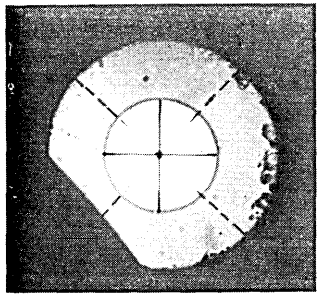

CIRCULARITY = $\frac{\text{MIN (d)}}{\text{MAX (d)}}$

FOR CORE AND CLADDING

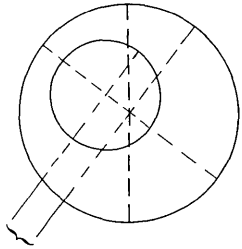

Δcp = CONCENTRICITY

Fig. 8 — Core-cladding circularity and concentricity as defined and positions tested along preform.

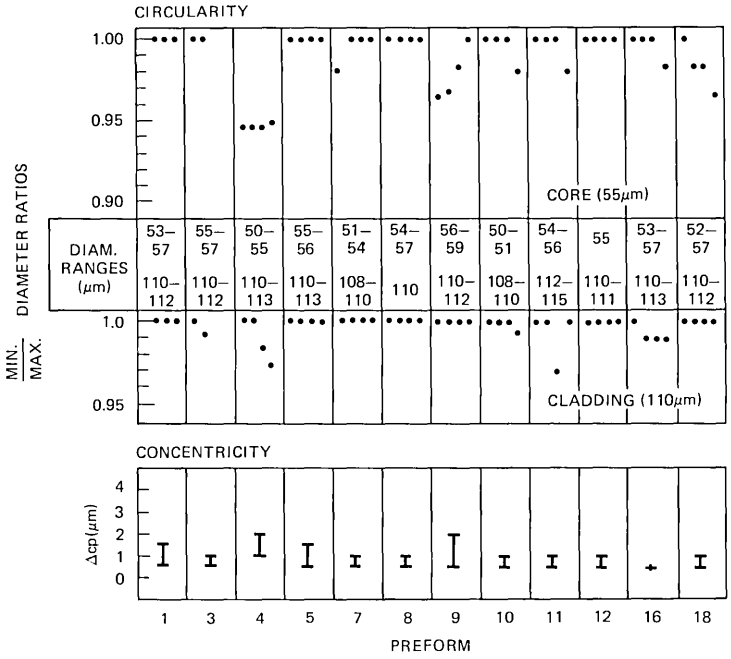

Fig. 9 — Circularity and concentricity of fiber core and cladding within and among preforms.

The concentricity values of the core-cladding (Fig. 9), represented by four determinations within each preform, are typically low in magnitude and range. The separation between center points is usually less than a micrometer, while the maxima of 2 micrometers occur with preforms exhibiting poorer circularity.

The objective and observed RMS values for the properties of interest in this study are compared in Table III. The table also summarizes the reproducibility of fibers prepared by a "modified" CVD process with our equipment. The percent standard deviations within a preform for loss, α, and core diameter are about one-half that observed among preforms,

Table III — Reproducibility summary (MCVD:GeO_2-B_2O_3-SiO_2 core; fused quartz cladding)

Property	Objective	Observed rms value	Percent standard deviation	
			Within preform	Among preforms
Optical loss (0.82 μm)	≤4 dB/km	3.8	2.5	6.5
Index profile (α)	~2.0	2.14	3.0	6.0
Index difference (Δ)	0.013	0.012	5.0	5.0
Core diameter	55 μm	54.8	1.5	3.2
Fiber diameter	110 μm	109.9	1.27	1.28

while the standard deviations for Δ and fiber diameter are about the same within and among preforms. The data indicate that the "modified" CVD process and equipment as discussed are capable of providing low-loss optical fibers of adequate quality and reproducibility for many applications. The following process and equipment modifications are suggested for enhancing the uniformity of dimensional and optical properties.

(*i*) There is a need for better dimensional uniformity and precision in the fused-quartz tubing. In particular, there is a marked dependency of core circularity upon the uniformity of the wall thickness of the preform tubing. A 3-percent variation appears to be the upper limit that can be tolerated for the change in wall thickness of the tubing used in this study and a 0.4-percent variation as the upper limit on the outside diameter of the tubing. The presence of blemishes of the type discussed earlier did not affect the optical properties of the fibers. However, they are recognized as possible factors affecting the strength of the fibers and are being included in other studies initiated recently.

(*ii*) Improved control of the MCVD reactant flows and a more uniform deposition temperature are expected to aid in achieving improvements to Δ and α. These experiments have shown that maintaining a uniform deposition temperature is important for optimizing the reproducibility of the MCVD process. This applies not only to the temperature along the length of the silica tubing during each torch cycle as it traverses from left to right, but also throughout the deposition process of a preform and from preform to preform. Temperature variations of as much as 40° to 50°C were observed to have occurred at all of these stages in the course of conducting the above study.

In a subsequent series of experiments, a more uniform deposition temperature was attained by more careful monitoring and by frequent manual adjustments of the torch gases. This resulted in lowering the range of α values (for 14 samples from among three preforms) to within the precision of error of the measurement technique. These preliminary experiments indicate that electronically controlled flow valves for both the reactants and the torch gases as well as a feedback system to control the tube temperature would significantly improve the reproducibility of the process.

(*iii*) The incorporation of a capstan-drive, fiber-diameter monitoring by means of a laser and electronic feedback controls to the fiber drawing apparatus should improve control of the fiber diameter.

IV. ACKNOWLEDGMENTS

The authors wish to express their appreciation for the assistance received in the following phases of the investigation from C. L. Collins and R. A. Becker for discussions about the statistical design of the experi-

ments, M. Drohn for preform preparation, L. S. Watkins and P. H. Krawarik of Western Electric Engineering Research Center for diameter analysis, E. A. Sigety for polishing fiber cross sections, J. R. Simpson for spectrum loss, index, and profile data, and W. G. French for data processing.

REFERENCES

1. "Experimental System Brings Lightwave Communication Closer," Bell Laboratories Record, *53,* No. 11 (December 1975), pp. 444–445.
2. J. B. MacChesney, P. B. O'Connor, F. V. DiMarcello, J. R. Simpson, and P. D. Lazay, Proc. Xth International Glass Congress, *6* (1974), pp. 40–45.
3. B. C. Wonsiewicz, W. G. French, P. D. Lazay, and J. R. Simpson, "Automatic Analysis of Interferograms: Optical Waveguide Refractive Index Profiles," Appl. Opt., *15,* No. 4 (April 1976), pp. 1048–1052.
4. J. Stone and R. M. Derosier, "Elimination of Errors Due to Sample Polishing in Refractive Index Profile Measurements by Interferometry," Review of Scientific Instruments, *47* (July 1976), pp. 885–887.
5. L. S. Watkins, "Instrument for Continuously Monitoring Fiber Core and Outer Diameters," Technical Digest of Topical Meeting on Optical Fiber Transmission, *tua 4-1,* Williamsburg, Va., Jan. 7–9, 1975.

THE BELL SYSTEM TECHNICAL JOURNAL
Vol. 57, No. 6, July–August 1978
Printed in U.S.A.

Atlanta Fiber System Experiment:

Preform Fabrication and Fiber Drawing by Western Electric Product Engineering Control Center

By D. L. MYERS and F. P. PARTUS

(Manuscript received November 16, 1977)

Optical fibers for the Atlanta Fiber System Experiment were produced in the Western Electric Product Engineering Control Center development laboratory. The processing methods and facilities used in preform fabrication and fiber drawing are described. The results obtained in terms of yield and process control factors are also presented.

I. INTRODUCTION

In 1974, the acquisition of a fiber-optics development laboratory was started by the Western Electric Product Engineering Control Center in Atlanta. This facility was intended to provide the experience needed by Western Electric to establish manufacturing methods and machinery in the new field of fabricating low-loss optical fibers. The first preform fabrication facility and its companion tube-cleaning installation became operational in April 1975. Operation of the fiber-drawing machine started in August 1975, and fiber delivery to Bell Laboratories commenced in September. All fibers were characterized by Bell Laboratories in Atlanta and subsequently used in their ribbons and cables. The delivery of fibers for the Atlanta Fiber System Experiment was completed in November 1975.

II. TUBE PREPARATION

The facility for acid-etching, fused-quartz starting tubes (Fig. 1) consisted of a bench-mounted cleaning chamber containing a rack for seven tubes. Adjacent to the chamber was a work position for mixing and

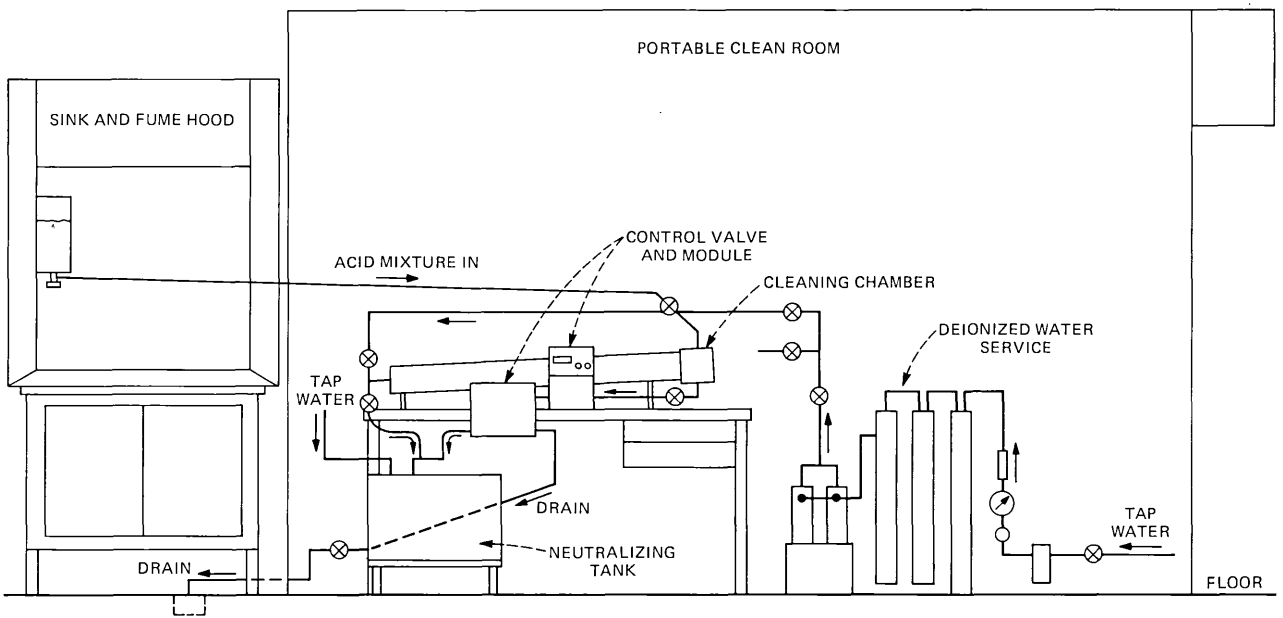

Fig. 1—Tube cleaning facility.

supplying the acid mixture to the cleaning chamber. A commercial deionized water system provided clean rinsing water, and a marble chip vat permitted neutralization and dilution of the acid mixture after each etching cycle.

The 12 × 14-mm diameter, 0.91-m long tubes (Amersil* T08 grade) were etched in a 50-percent solution of nitric acid, hydrofluoric acid, and deionized water. After etching and a thorough deionized water rinsing, the tubes were dried with nitrogen and then capped to maintain a clean inside tube surface.

III. PREFORM FABRICATION

Although two preform fabrication installations were provided in anticipation of future development and fiber needs, only one was initially used. Both installations were identical (Fig. 2) and were modeled after facilities used at Bell Laboratories in Murray Hill, N.J. for modified chemical-vapor deposition.[1,2]

The glass working lathe was equipped with an oxygen-hydrogen torch mounted on a motorized burner carriage. Tube temperature was monitored with an infrared pyrometer, while oxygen and hydrogen flow rates were controlled by flowmeters.

The chemical system consisted of stainless steel bubblers containing liquid silica tetrachloride ($SiCl_4$) and germanium tetrachloride ($GeCl_4$). The third chemical, boron trichloride (BCl_3), was supplied in a commercial cylinder. Oxygen to the bubblers and the extra oxygen added in the chemical vapor stream were supplied from the liquid oxygen tank also used to supply the burner. The chemical system O_2 supply line was equipped with a purifier and filter. All chemical vapors and the extra

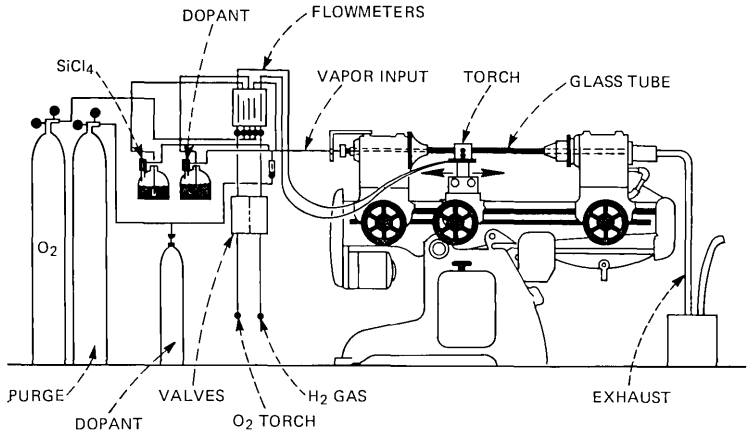

Fig. 2—Modified chemical-vapor deposition process.

* Amersil, Inc., Sayerville, New Jersey.

O_2 flow rates were controlled by means of flowmeters, which were calibrated for O_2 flow rates.

A typical run was very similar to that reported by DiMarcello and Williams.[3] Table I gives the details of such a run. Note that in Steps 4 and 5, BCl_3 and O_2 are passed into the tube without $SiCl_4$. Instead of building a barrier layer as previously done, BCl_3 was used to try to eliminate surface water. The graded-index profiling is accomplished in Steps 6 through 50 by increasing the $GeCl_4$ flow rate for each step.

IV. FIBER DRAWING

The fiber-drawing machine design was also based on exploratory equipment used at Bell Laboratories. The main frame consisted of two vertical I beams on a base frame which was shock-mounted and stabilized. The subassemblies for drawing and tandem coating were attached to the main frame (Fig. 3). At the top was the feed mechanism utilizing a traverse unit for lowering the preform into the drawing furnace.

The drawing furnace was a graphite resistance furnace modified to operate without a muffle tube. Operating such a graphite furnace in the 2000°C region requires careful control of an inert gas atmosphere such as argon. A high argon flow rate reduces element deterioration but creates a turbulence detrimental to drawing stability. Thus, a restriction of the furnace entrance and exit was provided to reduce the argon flow.[4]

The furnace entrance restriction was a disk slightly larger than the preform. The furnace exit restriction was a pair of interlocking, adjustable sliding plates, separated at start-up to provide a large opening for grasping the tip of the preform. After start-up, the plates were moved together so that the fiber passed through a small hole. An electronic micrometer was positioned near the furnace exit to monitor fiber diameter.

Table I — Deposition sequence

Operation	Step No.	$SiCl_4$ gms/min	O_2 to $SiCl_4$ cc/min	$GeCl_4$ gms/min	O_2 to $GeCl_4$	BCl_3 cc/min—cmj.k-min—°C	Torch Vel. cc/min	Temp	Extra O_2
Polish	1	—	—	—	—	—	—	1500	750
Polish	2	—	—	—	—	—	25.4	↓	750
Polish	3	—	—	—	—	—	↓	↓	750
BCl_3 to tube	4	—	—	—	—	10	↓	↓	515
BCl_3 to tube	5	—	—	—	—	↓	↓	↓	↓
$SiCl_4$ and	6	0.6	260	0.02	75	↓	↓	1580	↓
$GeCl_4$ to tube for deposit	↓	↓	↓	↓	↓	↓	↓	↓	↓
End deposit	50	0.6	260	0.43	515	10	25.4	1590	515
Collapse	51	—	—	—	—	—	15.8	1740	
Collapse	52	—	—	—	—	—	8.8	1750	515
Collapse	53	—	—	—	—	—	3.2	1770	—

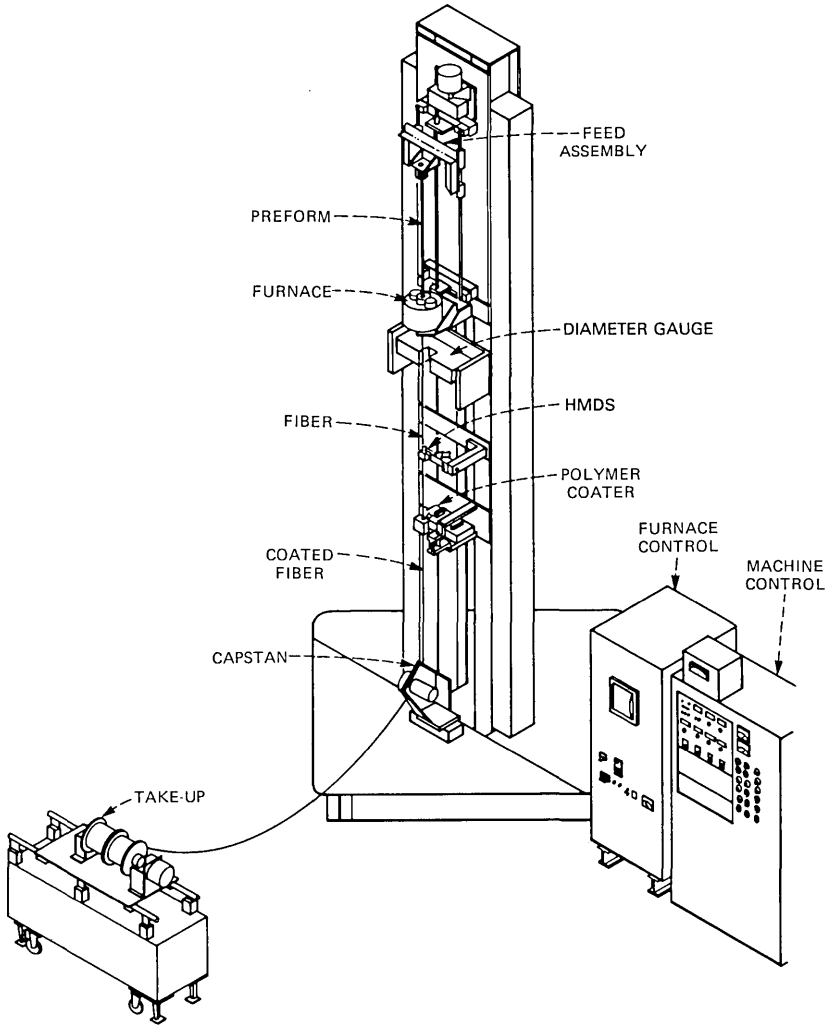

Fig. 3—Fiber-drawing machine.

Two coating applicators were provided. The first was a compressed polyurethane foam wiper to apply hexamethyldisilizane (HMDS). The HMDS was dripped onto the pads to maintain a wet condition and minimize frictional contact with the fiber. Directly below this applicator was a radiant-heat-tube furnace, which vaporized the excess silane.

The second coating mechanism was a polymer applicator which applied a solution of ethylene-vinyl acetate (EVA).[5] This applicator consisted of a heated reservoir attached to a coating die cavity such that a nearly constant solution level was maintained above the die. The die and die cavity were a split design to permit alignment of the fiber in the die

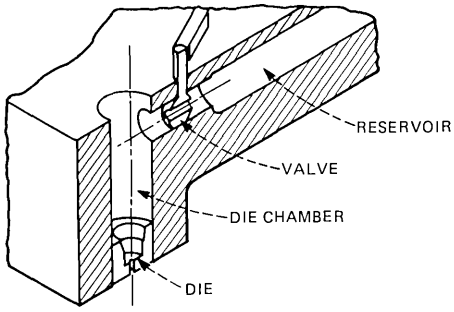

Fig. 4—Fiber coater.

hole (Fig. 4). The entire coating assembly was mounted in an X-Y positioning arrangement. The EVA used was mostly Dupont Alathon* 3172 although a small quantity of fiber was coated with Alathon 3170 (Elvax* 460). The solution mixture was 28.3 gms EVA to 100 ml 1,1,1 trichloroethane.

The distance between the coating applicator and drawing capstan permitted a 2-s gelation time at 0.8 m/s draw speed. This was sufficient to prevent distortion of the coating in the belt-type drawing capstan where a minimum belt pressure was used.

The reel take-up was positioned a few feet from the capstan so that a fiber catenary could be maintained for minimum winding tension. The take-up was capable of supporting two 15-cm-diameter expanded

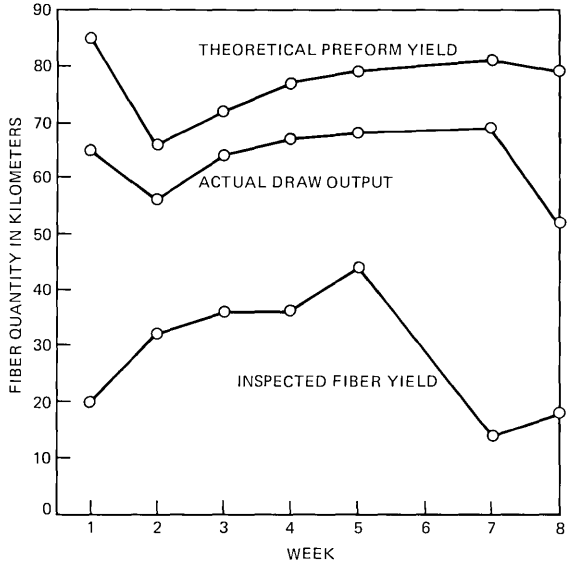

Fig. 5—Fiber drawing results.

* Trademarks of E. I. DuPont de Nemours and Company.

Table II — Fiber rejection, Atlanta Experiment

		Percent Rejection
1.	Cladding diameter ($110\ \mu \pm 2.5\%$)	10
2.	$\frac{\text{Cladding diameter}}{\text{Core diameter}}$ ratio ($2.0 \pm 6\%$)	9
3.	Core ellipticity $\left(\frac{\max - \min}{\min} \text{ dia.} \leq 6\%\right)$	2
4.	Bandwidth (200 MHz – km)	0
5.	Loss @ $0.82\ \mu$m (≤ 7.0 dB/km)	18
6.	Proof testing (30K psi)	16
Total		55

polystyrene reels, one for start-up and one for accumulating the fiber length in a loosely wrapped package.

The drive motors were dc permanent magnet servo type with integral optical tachometers. These were used in a frequency and phase-locked loop digital circuit for superior speed control.[6] In the operational mode used, the draw speed control capstan was set at a speed of 0.8 m/s. The take-up tracked the capstan while partially compensating for the diameter change as the reel filled. Preform feed speed was manually selected as a ratio based on preform-to-fiber diameter.

V. RESULTS

Figure 5 shows fiber drawing output results for the eight-week period during which most of the fibers were drawn. The theoretical output is the number of preforms drawn multiplied by the expected 2.2-km length for each preform. The length of fiber drawn is that quantity delivered to Bell Laboratories for quality measurement. The difference between the two curves represents machine failures, general processing difficulties, and preforms that would not yield the full 2.2 km.

The yield curve is simply the fiber passing the quality measurement criteria. The early low yield was due to problems associated with the diameter monitor. After procedures were established for calibrating and adjusting the gauge, a gradual improvement was realized. The dip near the end occurred when loss problems were experienced. Conditions contributing to the high loss, primarily oxygen impurity, were subsequently cleared and higher yields returned. Table II shows the six criteria limits for fiber quality and the percent rejection for each parameter.

As previously described, fiber diameter was controlled manually by adjusting preform feed velocity. With this technique, the time required for the diameter to respond to a step change in feed speed was too long,

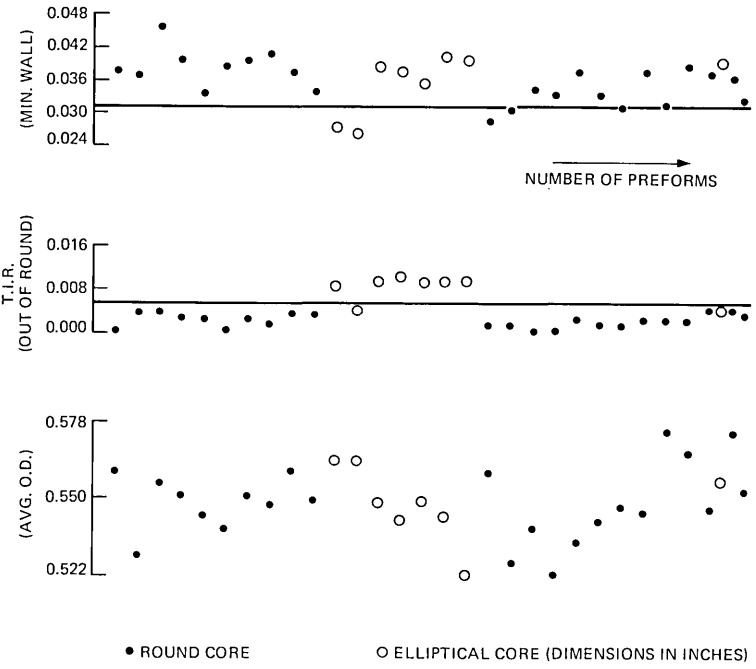

Fig. 6—Glass-tube dimension vs preform core.

and most diameter charts showed a sinusoidal variation. Preform nonuniformity also affected the fiber diameter. Starting tube diameter and wall thickness variations coupled with short-term variations in deposition rates result in diameter changes along a preform. A random sample of 37 preforms showed this variation to be as much as 5 percent. These factors, along with the diameter monitor inaccuracies, furnace turbulence, and preform particle contamination caused by the furnace seal, were major concerns in fiber diameter control.

Core-to-cladding ratio variations are a function of starting tube diameter, wall thickness differences, and long-term deposition rate drift. These variations are strongly related to tube dimensions and are larger than the short-term variations previously mentioned. Therefore, the ratio limits are larger than the fiber diameter limits.

Core ellipticity was originally a difficult problem. Nineteen of the first 67 preforms (28 percent) failed to meet limits. A study of 31 starting tubes was made, and the results of fiber drawn from these are shown in Fig. 6. The study illustrated that tube out-of-roundness and wall thickness variation at a cross-section were the important factors determining core ellipticity. Therefore, 0.006-inch (0.152-mm) limits were placed on each, which lowered the rejections to 2 percent.

Losses greater than 7.0 db/km at 0.82 μm were generally the result of impure materials and material-handling procedures. It was found that

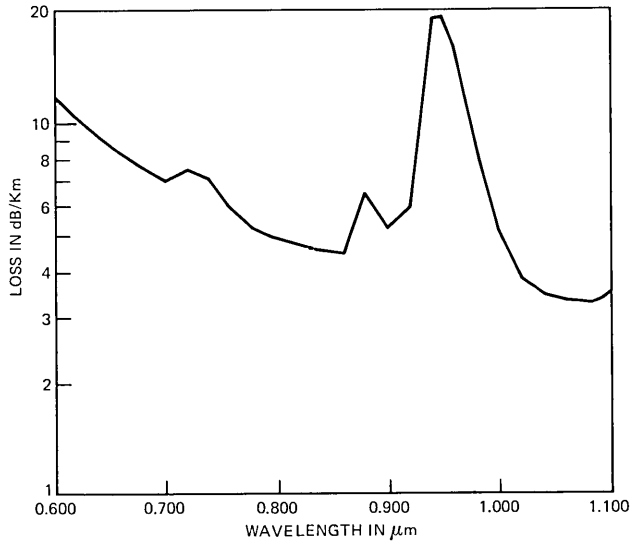

Fig. 7—Typical fiber loss.

purging all lines prior to installing a refilled bubbler was very important. If not done properly, it was common to have a high-loss preform on the first run. Leaks in the system also resulted in high loss fibers. They were difficult to eliminate when Teflon* fittings were used. Leaks also developed in the oxygen supply line from the liquid oxygen tank. This problem was eliminated by using high-purity oxygen obtained in bottles. High loss could also be induced by inadequately fusing the doped silica layers during deposition. Since the tube temperature was manually controlled, the H_2-O_2 flow increases for each deposit pass depended on the accuracy of the flow meter settings. If the tube wall thickness varied significantly, a large temperature change was noted. Figure 7 shows a typical fiber loss curve, and Fig. 8 shows the loss distribution for the fibers.

Proof test failures stemmed from a number of processing conditions. Obviously, methods of handling tubes and preforms could cause damage. Preforms were in contact with the top furnace seal, and the drawn fiber would at times contact the die in the coating apparatus.

The bandwidth requirement was low and could be met without difficulties. The average bandwidth was approximately 450 MHz—km. A high value of nearly 1200 MHz—km was measured.

In all, the above specifications led to a 45-percent yield. This yield was considered a reasonable accomplishment, but certainly pointed to the need for improvement in all aspects of fiber preparation.

* Registered trademark of E. I. DuPont de Nemours and Company.

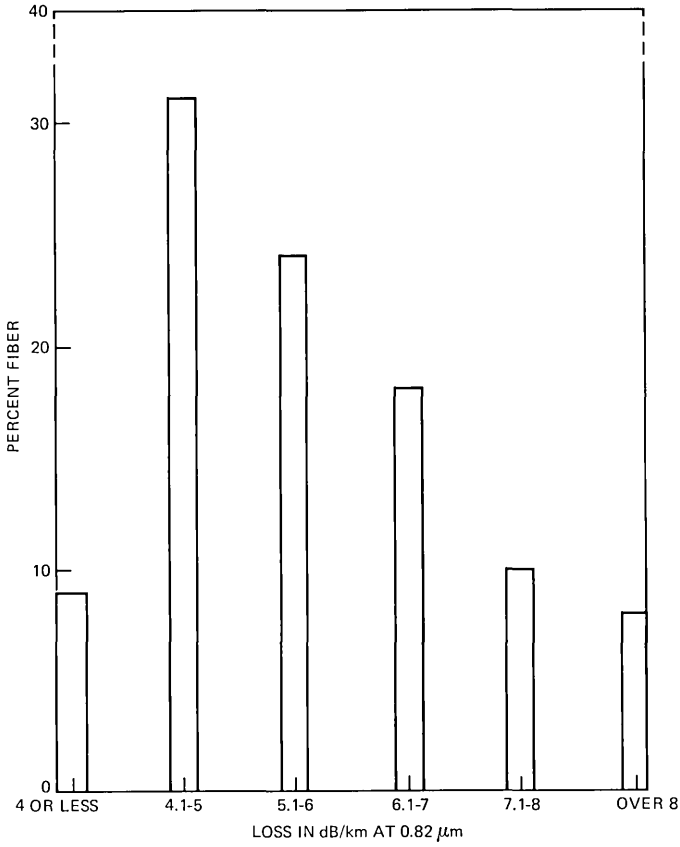

Fig. 8—Fiber loss distribution.

VI. ACKNOWLEDGMENTS

Making fibers for the Atlanta Experiment could not have been accomplished without the immense support of a host of Bell Laboratories personnel. Special mention is made of the efforts of W. B. Gardner, B. R. Eichenbaum, M. J. Buckler, and L. D. Tate. The highest accolade belongs to the authors' co-workers in the PECC laboratory, whose untiring and enthusiastic performance made success a realization. They were M. J. Hyle, E. A. Haney, R. L. Center, M. L. Vance, and T. A. Karloff.

REFERENCES

1. J. B. MacChesney, P. B. O'Connor, F. V. DiMarcello, J. R. Simpson, and P. D. Lazay, Proc. Tenth Int. Congr. Glass, Kyoto, Japan, July 1974.
2. J. B. MacChesney, P. B. O'Connor, and H. M. Presby, "A New Technique for the Preparation of Low-Loss and Graded Index Optical Fibers," Proc. IEEE, *62*, No. 9 (Sept. 1974), pp. 1278–1279.
3. F. V. DiMarcello and J. C. Williams, Conf. Pub. No. 132, IEEE, First European Conf. on Opt. Fiber Comm., *37* (1975).
4. P. Kaiser, "Method for Drawing Fibers," U.S. Patent 4-030-901. See also Appl. Opt., *16* (1977), p. 701.
5. B. R. Eichenbaum, unpublished work.
6. L. D. Tate, unpublished work.

THE BELL SYSTEM TECHNICAL JOURNAL
Vol. 57, No. 6, July–August 1978
Printed in U.S.A.

Atlanta Fiber System Experiment:

Lightguide Cable Manufacture and Performance

By M. J. BUCKLER, M. R. SANTANA, and M. J. SAUNDERS

(Manuscript received December 5, 1977)

The manufacture of the optical fiber ribbons and the optical cable used in the Atlanta Fiber System Experiment is described. Yields and added loss in each step of cable manufacture and installation are covered, along with the bandwidth changes resulting from packaging the optical fibers in the lightguide cable. Mechanical performance in tension and in bending are also considered, as well as the thermal stability of cable performance.

I. INTRODUCTION

As part of the Bell Laboratories Atlanta Fiber System Experiment, a small, ruggedized, high-capacity, optical fiber cable was designed, manufactured, and characterized both optically and mechanically. After manufacture and evaluation of the fiber optic cable, it was installed in underground ducts, typical of those used by telephone companies, and characterized once again. In the present paper, we describe the optical fiber ribbon and cable designs used for the Atlanta Experiment and their performance results. In addition, the cable environmental performance is also discussed. These results provide initial indications of the manufacturability of the cable design, including yield information.

II. FABRICATION OF OPTICAL FIBER RIBBONS

In 1970, a proposal was made to put optical fibers together into easily handled units for optical communication purposes.[1] This proposal suggested "the use of fiber ribbons consisting of linear arrays of fibers embedded in a thin, flexible supporting medium as components of a cable for fiber transmission systems." Such a medium is attractive from the splicing standpoint, since groups of fibers can be handled at once with relaxed alignment requirements needed to accomplish mass field

splicing.[2] Moreover, this linear array provides increased size and mechanical support, thereby improving the human handling qualities of the fibers.

Optical fibers can be assembled into a linear array structure in many different ways. The method chosen here was to sandwich 12 optical fibers between two layers of polyester-backed adhesive (adhesive sandwich ribbon, ASR).[3] The machine for making the ASR is described in Ref. 3. Figure 1 shows a sketch of the completed ribbon cross section. Each of the ASRs contained twelve Western Electric optical fibers which were coated in-line with ethylene-vinyl-acetate and proof-tested at 207 MN/m^2 (30 ksi). The fibers[4] supplied by Western Electric for the Atlanta Experiment were germania-doped borosilicate, multimode, graded-index, and were made using a modified chemical vapor deposition process (MCVD).[5] The ASRs manufactured using these fibers were then incorporated into the optical fiber cable for the Atlanta Fiber System Experiment.[6,7]

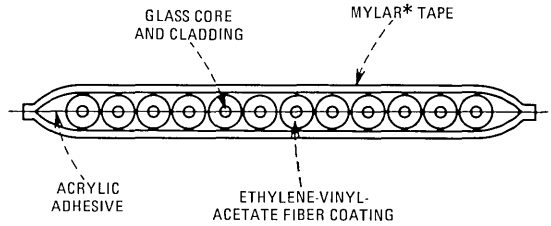

Fig. 1—Ribbon cross section.

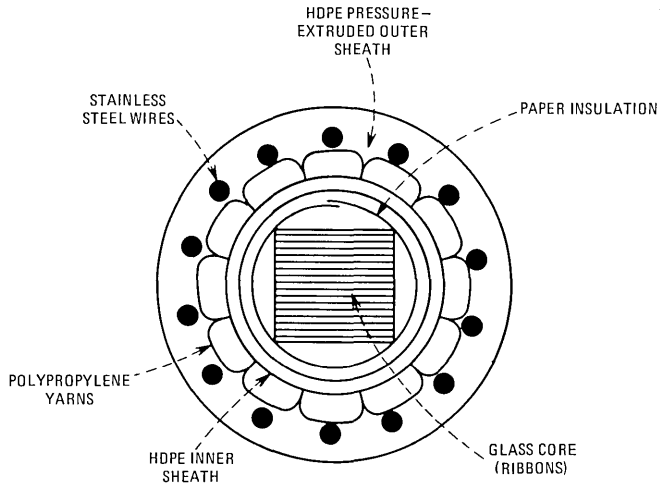

Fig. 2—Optical cable cross section.

* Registered trademark of E. I. DuPont de Nemours and Company.

Since the coated fibers are contiguous within the ribbon, any roughness in the coating results in microbending,[8] which increases the fiber loss. Indeed, it was found that this added loss due to microbending was essentially eliminated when the coated fibers were not contiguous within the ribbon. With contiguous fibers, increased pressure from the compliant rollers in the ribbon machine pushes the fibers together. It was found that, by adjusting this pressure, the added loss in the ribbon could be varied in certain coated fibers from about 1 to 19 dB/km.

A total of 16 ASRs, all approximately 1050 m in length, were made by Bell Laboratories. Four of the ribbons were discarded because of multiple fiber breaks. The 12 ASRs selected for the optical cable had a total of seven fiber breaks. Since that time, better fiber-winding techniques and improved ribbon machine design have substantially reduced the number of fiber breaks occurring during ribbon fabrication.

III. FABRICATION OF OPTICAL FIBER CABLE

The major consideration in the Bell Laboratories optical fiber cable design was the simplification of the difficult task of splicing the optical fibers. This provided the motivation for selecting a cable design based on linear array fiber ribbons.

Figure 2 shows a developed view of the fiber optic cable design used for the Atlanta Experiment. The cable core consisted of 12 ASRs (each containing 12 fibers) stacked in a rectangular array to facilitate the application of factory-applied cable connectors. This stacked ribbon core was twisted into a helix with about a 15-cm lay, to improve the cable bending characteristics. A paper thermal insulation layer was longitudinally applied over the core, and a high density polyethylene (HDPE) inner jacket was extruded over the paper layer. This loosely fitting jacket provides enough space for the glass core to move, and thus allows relaxation of manufacturing and installation-induced stresses that otherwise could result in optical fiber breakage or excessive microbending loss.[8]

The reinforced outer sheath consists of helically applied strands of fibrillated polypropylene twine which provide thermal and mechanical isolation. The cable load-bearing strength members are helically applied stainless steel wires over which an HDPE outer sheath is pressure ex-

Table I — Mechanical data for the cable components

Cable Component	Tensile Stiffness (N/percent)
Glass (144 fibers)	934
Mylar (12 ribbons)	40
HDPE (inner jacket)	56
Polypropylene twine	209
Steel wire	2732
HDPE (outer sheath)	109

truded. This outer sheath provides chemical as well as mechanical protection for the entire structure. Table I contains a listing of the cable components and their respective material and cable assembly properties. Optical and mechanical performance results for this cable design are discussed in the following sections.

IV. OPTICAL PERFORMANCE

Optical fibers are incorporated in protective coatings, ribbons, and cables for protection during handling and installation. However, during this packaging process, microscopic perturbations of the fiber axis from straightness[9] can cause mode coupling, and thus add loss (microbending loss),[8] and reduce pulse delay distortion.[10] For our particular fiber design, coupling between guided modes and lossy radiation modes occurs when the fiber's longitudinal axis is deformed with periods of the order of 1 mm and amplitudes as small as a micrometer. Field-worthy cables must inhibit fiber axis deflections of this microscopic nature and yet allow for normal installation and handling procedures.

In this section, we discuss the optical transmission performance and the yield after each cable manufacturing step.

4.1 Transmission loss

The transmission loss versus wavelength characteristic of each unpackaged fiber was measured using an incoherent source and seven filters between 0.63 and 1.05 μm.[11] In addition, since in this wavelength region the added loss due to microbends is essentially independent of wavelength,[8] the added losses induced by packaging the fibers in ribbons and

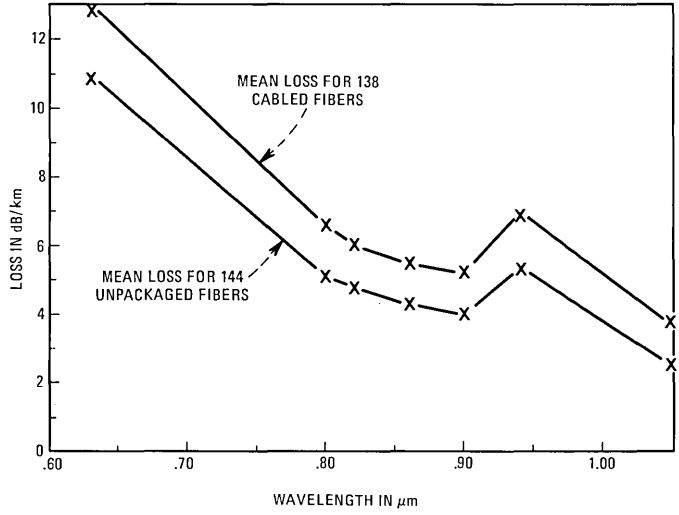

Fig. 3—Spectral loss before and after cable manufacture.

cables were measured using a He-Ne laser source. The use of 0.63-μm coherent radiation to measure packaging-induced loss provided the capability of visually locating and diagnosing high scattering loss regions in the packaged fibers. These two loss measuring sets had their launch optics adjusted to match the average 0.23 numerical aperture of the Western Electric fibers. For both measurement sets, the two-point technique was used, where first the optical power received at the end of a long fiber is measured and second, the fiber is broken at about 0.5 m from the launch end and the output power from the short length is measured. The ratio of the received power from the long fiber to that of the 0.5-m pigtail was used to calculate the transmission loss. The agreement between the two sets at 0.63 μm and the measurement repeatability are both about $\pm$0.2 dB for a 1-km fiber length.

4.1.1 Unpackaged fiber losses

Western Electric at Atlanta fabricated the 144 in-line coated optical fibers used for the Atlanta Experiment cable (12 ribbons each with 12 fibers). One hundred thirty-two fibers were coated with Alathon* 3172, and 12 were coated with Elvax* 460. The spectral loss of each unpackaged fiber was measured at seven different wavelengths between 0.63 and 1.05 μm. The lower curve in Fig. 3 is a plot of the mean spectral loss curve for the 144 unpackaged fibers measured, where the standard deviation at each wavelength is approximately 1 dB/km. At the Atlanta Experiment transmission wavelength of 0.82 μm (transmitter source was a GaAlAs laser operating at 0.82 μm), the mean unpackaged fiber loss was 4.7 dB/km.

4.1.2 ASR loss results

Twelve 1-km adhesive sandwich ribbons, each containing 12 fibers, were used in the Atlanta Experiment cable. The added loss due to packaging the fibers in the ribbon structure was measured using the He-Ne laser loss set. Due to the mechanical relaxation of the fibers within the ASR structure, the added packaging-induced microbending loss decreases with time after completion of ribbon manufacture. It has been found that the added loss due to ribboning relaxes to a quasi-steady-state minimum value within about 50 hours after the completion of ribboning. Table II shows the results for each of the 12 ASRs. For each ribbon listed in Table II, the manufactured ribbon length, fiber yield, and the mean added loss just after the completion of ribboning (t = 0 hours) and just before cable manufacture (t > 200 hours after ribboning) is shown. For the 137 transmitting fibers in these 12 ASRs, the mean added loss just before cable manufacture was 0.8 dB/km.

* Alathon and Elvax are ethylene-vinyl-acetate resins that are registered trademarks of E. I. DuPont de Nemours and Company.

Table II — ASR loss and yield results

Ribbon Designation	Manufactured Length (m)	Number of Transmitting Fibers	Mean Ribboning Added Loss (dB/km)	
			$t = 0$	$t > 200$ Hours
ASR 281	1043	12	3.4	0.8
ASR 282	1054	12	6.0	1.1
ASR 284	1092	10	2.9	0.9
ASR 286	1067	12	2.8	0.6
ASR 287	1050	11	3.1	1.5
ASR 288	1092	10	3.1	0.4
ASR 290	1050	12	3.3	1.1
ASR 291	1146	12	3.3	0.7
ASR 292	1101	10	2.3	0.1
ASR 294	1047	12	3.9	0.8
ASR 295	1036	12	4.7	0.8
ASR 296	1081	12	4.1	1.3

4.1.3 Cable loss results

Using the 12 ribbons described, a 1023-m length of cable was manufactured for the Atlanta Experiment. The added loss due to cable manufacture was measured with the 1023-m length of cable wound loosely on a cable reel. The mean added loss due to cable manufacture was 0.5 dB/km for the 134 transmitting fibers in the cable (there were three fiber breaks during cabling). Figure 4 is a histogram of the total added losses due to ribbon and cable manufacture. The mean total packaging induced loss was +1.3 dB/km with a standard deviation of 1.3 dB/km for the 134 transmitting fibers in the 1023-m cable length. A 658-m section of this cable (with 138 transmitting fibers) was installed in a standard plastic underground duct network (see Fig. 5) at the Bell Laboratories/Western Electric Atlanta facility. The ducts terminate in a basement room and extend 150 m to a manhole, and then another 140 m to a second manhole. The lightguide cable was looped in the second manhole so that both ends could be terminated in the basement room. The remaining 365 m of cable not installed underground was cut off and used for mechanical and environmental tests described later in this paper. After completion of installation of the 658-m cable segment, the spectral loss was measured for each of the 138 transmitting fibers. The upper curve of Fig. 3 shows the mean spectral loss curve for the 138 fibers. Comparing the loss measurements between 0.63 and 1.05 μm for the unpackaged fibers and the installed-cable fibers (Fig. 3, lower and upper curve, respectively) indicates that the microbending loss is essentially independent of wavelength for this spectral region, as predicted.[8] These results also indicate that there was no measurable change in cabled fiber transmission loss due to installation. The mean installed-cable fiber loss at the source wavelength of 0.82 μm was 6.0 dB/km with a standard deviation of 1.9 dB/km.

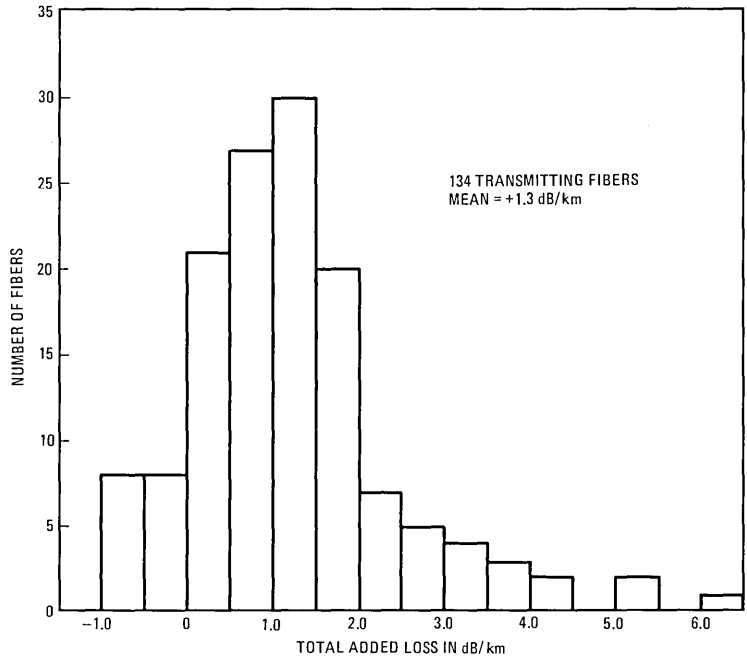

Fig. 4—Histogram of cabled fiber added losses.

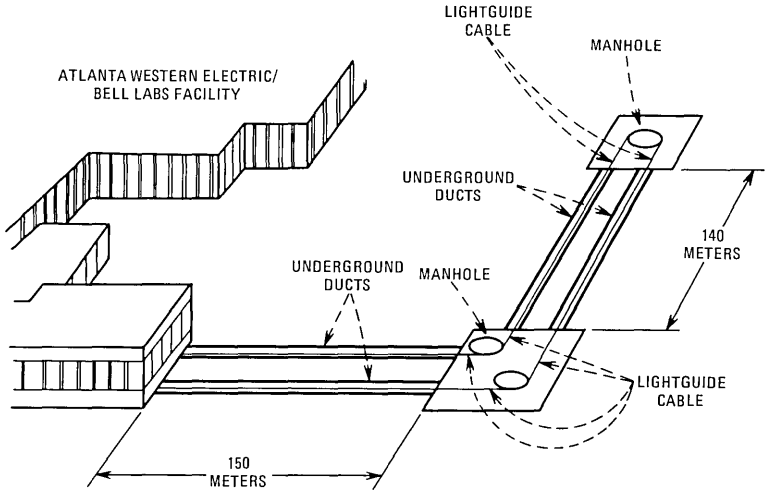

Fig. 5—Atlanta installation route.

4.2 Pulse delay distortion

Pulse spreading in a multimode optical fiber is reduced when the geometry (microbends) of the waveguide induces power mixing among the propagating modes (mode coupling).[12] In a waveguide with strong ran-

dom coupling among its guided modes, it has been predicted that for long enough lengths the width of the impulse response will increase with the square root of the fiber length. Thus, the length dependence of pulse spreading for a particular fiber of a given length can vary between linear and square root, depending on the strength of the intermodal coupling.

The pulse delay distortion or pulse spreading characteristics of 72 of the 144 fibers in the experiment cable were obtained from impulse response measurements. The impulse response was measured at 0.82 μm using techniques and equipment described elsewhere.[13] The 3-dB bandwidth, i.e., the baseband frequency at which the Fourier transform of the fiber impulse response has decreased to $\frac{1}{2}$ of its dc loss value, will be used here as a figure of merit.

4.2.1 Unpackaged fiber bandwidths

The 72 unpackaged fibers characterized for the Atlanta Experiment cable varied in length between 1.1 and 2.3 km. Thus, in order to determine the effects of packaging on fiber pulse delay distortion, it is necessary to normalize the fiber pulse spreading results to a common length. Independent studies using fibers like those used for the Atlanta Experiment indicate that the unpackaged fiber pulse spreading is approximately linear with length (i.e., the coupling length was usually larger than 2.3 km). Using this approximation for the unpackaged fiber bandwidths, the mean, measured, unpackaged fiber-optical-3-dB-point bandwidth was 438 MHz for a 1-km length (with a standard deviation of 224 MHz).

4.2.2 ASR bandwidth results

The 72 unpackaged fibers measured for impulse response were all contained within six of the 12 ASRs used in the optical cable. The pulse spreading characteristics of the 68 of these 72 fibers that survived ribboning were remeasured after the completion of ribbon manufacture. Due to the fiber mode coupling induced by the ribbon package (as seen in Section 4.1.2), the ribboned fiber bandwidth is assumed to be inversely proportional to the square root of length (complete mode mixing). Since the six ribbons measured varied in length between 1043 and 1092 m, there is a minimum of ribboned fiber bandwidth data shifting required to normalize the data to a 1 km length. Using this length dependence assumption, the mean measured ribboned fiber bandwidth was 633 MHz for a 1-km length. However, it should be noted that the ribboned fiber bandwidths were usually measured right after the completion of ribbon manufacture. As mentioned in Section 4.1.2, the time decaying component of the ribboning added loss was not relaxed until about 50 hours after the completion of ribboning. Thus, the ribboned fiber bandwidths

measured are probably slightly high, since initially the fibers have additional mode mixing due to the unrelaxed ribboned fiber microbends.

4.2.3 Cable bandwidth results

For the 1023-m length of cable manufactured, 65 of the 72 fibers which had been measured in the unpackaged state survived ribbon and cable manufacture. The mean 3-dB point bandwidth measured for the 1023-m length of cabled fibers was 553 MHz (with a standard deviation of 309 MHz). For the 658-m length of installed cable, 68 of the 72 fibers were transmitting and had a mean 3-dB bandwidth of 690 MHz (with a standard deviation of 286 MHz). Using the measured bandwidth data for the 1023-m length of cabled fibers and the 658-m length of installed-cabled fibers, the 3-dB bandwidth was calculated to be proportional to $(\text{length})^{-0.50\pm0.17}$. This result provides excellent agreement with previous predictions of square-root-of-length dependence for complete mode mixing.[14] Using this measured square-root-of-length dependence, the mean cabled fiber bandwidth normalized to a 1-km length was calculated to be 559 MHz. Thus, the mean 3-dB bandwidth increase in going from unpackaged to cabled fibers was 121 MHz (with a standard deviation of 249 MHz) for a 1-km length. However, this increase in bandwidth was accompanied by a mean increase in loss of 1.3 dB/km.

V. ENVIRONMENTAL PERFORMANCE

Unless special precautions are taken during storage, shipment, and installation of cables, they may encounter a large range of temperature exposures. Dimensional changes within the optical fiber cable structure, due both to linear thermal expansion of materials and polymeric shrinkback, can result in variations in the optical transmission properties of the fiber, thus possibly impairing system performance.

To evaluate how temperature variations affect the optical performance of the Atlanta Experiment fiber optic cable, a 156.4-m section was installed in a thermally insulated, underground, temperature-controlled, copper duct. The temperature of this duct can be controlled to about ±1°F over the range of +30°F to +150°F. Ribbons at one end of the cable were spliced together in pairs with six ribbon splices,[15] thus providing 72 fiber links, each 312.8 m in length. Four of these 312.8-m fiber links were spliced together at the other cable end using three low-loss, loose-tube, individual fiber splices,[16] thus forming a single 1251.2-m cabled fiber link. This 1251.2-m link was used to determine environmental effects on loss and pulse delay distortion at 0.82 μm. Forty of the 312.8-m cabled fiber links were each measured for the environmental effects on the loss at 0.63 μm.

During the environmental tests at exposure temperatures above

+70°F, the cable was allowed to stabilize for 72 hours before measurements were made. Twenty-four-hour exposure was assumed sufficient at low temperatures. To better ascertain the nature (reversible or not) and magnitude of the effect of the temperature exposure, the cable was always returned to +70°F before any subsequent temperature exposure.

Figure 6 shows a plot of the sensitivity of cable loss to thermal history measured at 0.63 μm for the forty 312.8-m fiber links. Figure 7 shows a plot of the sensitivity of cable bandwidth to thermal history, measured at 0.82 μm, for the single 1251.2-m fiber link. Correlation of the data measured for the 0.82-μm loss and bandwidth changes induced by the +30°F to +150°F exposure temperatures shows that the 3-dB bandwidth increased by 9.9 ± 0.5 MHz (3.0 percent) for a loss increase of 1.0 dB (6.2 percent), with a coefficient of correlation of 0.86. Moreover, there was essentially unity correlation between the 0.63-μm and 0.82-μm loss changes, suggesting that these temperature-induced microbending loss variations are essentially linear with length and independent of wavelength over this wavelength range, as expected.[8] The environmental results presented here clearly show that the cabled fiber loss and

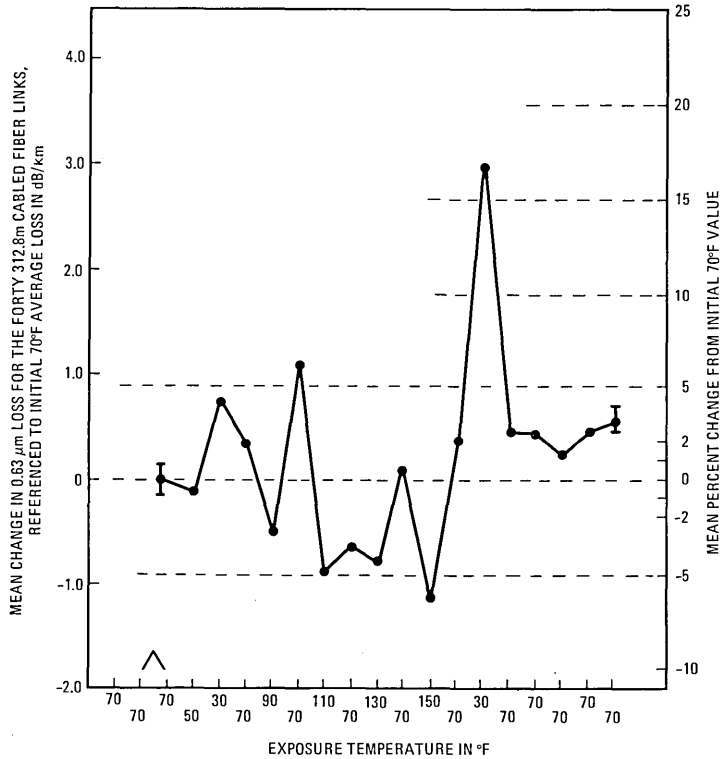

Fig. 6—Change in 0.63-μm loss vs. exposure temperature.

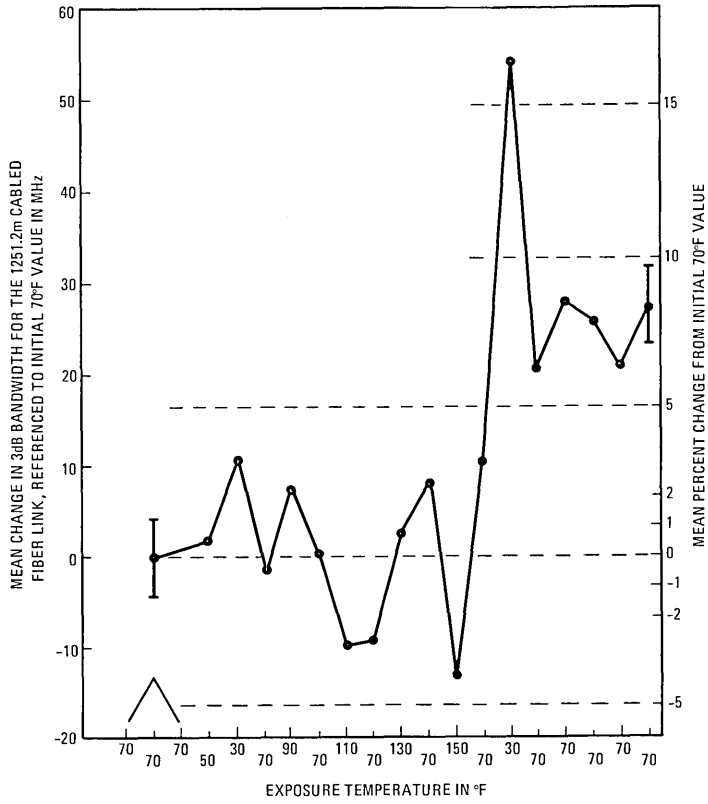

Fig. 7—Change in 0.82-μm bandwidth vs. exposure temperature.

bandwidth changes for this cable depend not only on cable exposure temperature but on thermal history as well.

Design modifications of the "Atlanta type" optical cable are in progress, with the goal of reducing temperature-induced loss variations to less than 0.5 dB/km over a temperature range from at least −20°F to +150°F.

VI. MECHANICAL PERFORMANCE

Mechanical tests were conducted on a number of segments of the Atlanta Experiment cable. The cable segments were subjected to both tensile and bending tests. Figure 8 shows a typical curve obtained for cabled fiber survival versus cable load and strain. No fiber breaks occurred until the cable load exceeded 1779 Newtons, with more than 85 percent of the fibers still surviving at a load of 4448 N. Also, cable reverse bends, which consisted of a 90-degree bend with a 12.5-cm radius followed by a second 90-degree bend of 12.5-cm radius in the opposite di-

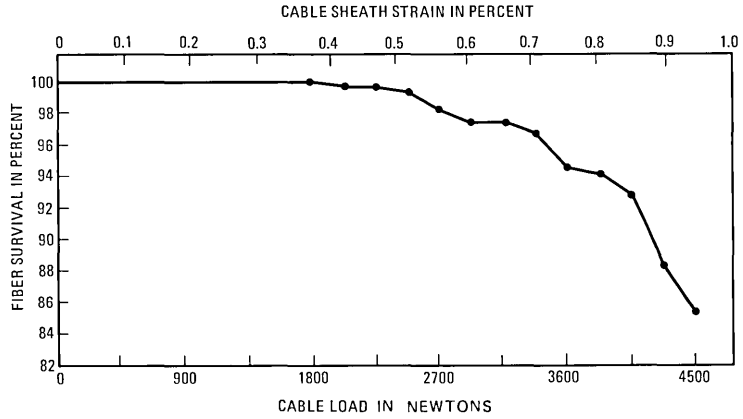

Fig. 8—Percent fiber survival versus cable load.

rection, caused no fiber breaks or cable degradation. These results provide further proof that small, ruggedized, lightweight (the Atlanta cable weighs only 934 N/km) fiber optic cables can be designed to package hundreds of high-capacity lightguides.

VII. CONCLUSIONS

The design and characterization of the optical fiber ribbons and cable used in the Atlanta Experiment have been described. The cable performed well, and results of the optical cable tests indicate that high performance, large-capacity, optical-fiber cables are feasible. The successful integration of this optical cable with the other necessary fiber-optic transmission system components is described in companion papers in this B.S.T.J. issue. This optical cable design was the stepping-stone to the installation of optical fiber cables for the Bell System's Chicago Lightwave Communications Project.[17] In the Chicago Project, the optical cables are of the same design, but contain only a two-ribbon core (24 fibers), and are being evaluated under actual live customer traffic.

As a result of the design and evaluation of the Atlanta Experiment optical cable, new designs and material changes are being investigated. The goal of these efforts is to improve performance and increase the compatibility of the cable with real-world handling and environmental conditions.

VIII. ACKNOWLEDGMENTS

The successful completion of the Atlanta Experiment optical cable is due to the efforts of many individuals at Bell Laboratories and Western Electric. In particular, we would like to acknowledge the efforts of W. P. Maxey in cable manufacture, W. L. Parham in ribbon manufacture, and L. Wilson in optical characterization.

REFERENCES

1. R. D. Standley, "Fiber Ribbon Optical Transmission Lines," B.S.T.J., *53,* No. 6 (July–August 1974), pp. 1183–1185.
2. M. I. Schwartz, "Optical Fiber Cabling and Splicing," Technical Digest of Papers of the Topical Meeting on Optical Fiber Transmission I, Williamsburg, Virginia, January 1975, p. WA2.
3. M. J. Saunders and W. L. Parham, "Adhesive Sandwich Optical Fiber Ribbons," B.S.T.J., *56,* No. 6 (July–August 1977), pp. 1013–1014.
4. D. L. Myers and F. P. Partus, "Fiber Optics for Communications," Wire Journal, *9,* No. 10 (October 1976), pp. 72–77.
5. J. B. MacChesney, P. B. O'Connor, and H. M. Presby, "A New Technique for the Preparation of Low-Loss and Graded-Index Optical Fibers," Proceedings of the IEEE, *62,* No. 9 (September 1974), pp. 1280, 1281.
6. S. J. Buchsbaum, "Lightwave Communications—An Overview," Physics Today, *29,* No. 5 (May 1976), pp. 23–27.
7. J. S. Cook, J. H. Mullins, and M. I. Schwartz, "An Experimental Fiber Optics Communications System," 1976 IEEE/OSA Conference on Laser and Electro-Optical Systems, San Diego, May 1976.
8. W. B. Gardner, "Microbending Loss in Optical Fibers," B.S.T.J., *54,* No. 2 (February 1975), pp. 457–465.
9. D. Gloge, "Optical-Fiber Packaging and Its Influence on Fiber Straightness and Loss," B.S.T.J., *54,* No. 2 (February 1975), pp. 245–262.
10. D. Marcuse, "Losses and Impulse Response of a Parabolic Index Fiber with Random Bends," B.S.T.J., *52,* No. 8 (October 1973), pp. 1423–1437.
11. M. J. Buckler, L. Wilson, and F. P. Partus, "Optical Fiber Transmission Properties Before and After Cable Manufacture," Technical Digest of Papers of the Topical Meeting on Optical Fiber Transmission II, Williamsburg, Virginia, February 1977, p. WA1.
12. S. D. Personick, "Time Dispersion in Dielectric Waveguides," B.S.T.J., *50,* No. 3 (March 1971), pp. 843–859.
13. J. W. Dannwolf, S. Gottfried, G. A. Sargent and R. C. Strum, "Optical-Fiber Impulse-Response Measurement System," IEEE Transactions on Instrumentation and Measurement, *IM-25,* No. 4 (December 1976), pp. 401–406.
14. L. G. Cohen and S. D. Personick, "Length Dependence of Pulse Dispersion in a Long Multimode Optical Fiber," Applied Optics, *14,* No. 6 (June 1975), pp. 1357–1360.
15. A. H. Cherin and P. J. Rich, "A Splice Connector for Joining Linear Arrays of Optical Fibers," Technical Digest of Papers of the Topical Meeting on Optical Fiber Transmission I, Williamsburg, Virginia, January 1975, p. WB3.
16. C. M. Miller, "Loose Tube Splices for Optical Fibers," B.S.T.J., *54,* No. 7 (September 1975), pp. 1215–1225.
17. A. R. Meier, " 'Real-World' Aspects of Bell Fiber Optics System Begin Test," Telephony, *192,* No. 15 (April 11, 1977), pp. 35–39.

THE BELL SYSTEM TECHNICAL JOURNAL
Vol. 57, No. 6, July–August 1978
Printed in U.S.A.

Atlanta Fiber System Experiment:

Optical Crosstalk Evaluation for Two End-to-End Lightguide System Installations

By M. J. BUCKLER and C. M. MILLER

(Manuscript received October 14, 1977)

A visual photometric method of measuring lightguide cross-coupling is described. Cross-coupling losses up to 100 dB can be measured with a resolution of ±1 dB. The end-to-end cross-coupling losses were measured for the Bell System's 1976 Atlanta Fiber System Experiment and 1977 Chicago Lightwave Communications Project installations. In the Atlanta experiment, the crosstalk was also measured for the unconnectorized lightguide cable and fanout ribbons, separately. Worst-case cross-coupling losses were measured to be 55 dB for far-end output-to-output and 70 dB for near-end. Results presented here confirm that properly designed parallel lightguides have negligibly small levels of optical crosstalk. However, it is shown that future optical interconnection devices that involve high-fiber packing densities will have to take crosstalk considerations into account.

I. INTRODUCTION

The Bell System uses many types of transmission media to carry telephone calls, computer data, and television signals. One of the newest telecommunications medium under development is the glass fiber lightguide medium.[1] The first telephone plant application of lightwave systems will probably be between central offices in metropolitan areas—where duct and manhole space are at a premium, the volume of traffic is high, and central offices are close enough so that manhole repeaters are not needed.

In 1976 Bell Laboratories successfully demonstrated an experimental lightwave communications system at its facility shared with Western Electric in Atlanta.[2] This system, designated FT3, which uses solid-state

lasers as light sources, could carry the equivalent of nearly 50,000 telephone calls through a one-half-in. diameter cable containing 144 fiber lightguides. Following this successful experiment, the Bell System's first lightwave system to be evaluated under actual service traffic conditions was installed in Chicago (Illinois Bell Telephone Company) in early 1977.[3]

Advantages of optical fibers over conventional copper links include small size, freedom from interference, immunity to ground-loop problems, large information capacity, and potential economy. Data available thus far on early lightwave systems have, for the most part, been limited to optical loss and signal distortion (pulse spreading),[4] which can be related directly to economic viability. However, for telecommunication applications in congested metropolitan areas, the trend is toward higher fiber packing density. Therefore, as the lightguides are packed closer together and as the connectorization schemes become more miniaturized, the effects of lightguide cross-coupling will be enhanced. As a result, lightguide crosstalk could directly influence system applications and engineering rules, as well as system immunity to outside intrusion.

Although the theory of optical crosstalk for parallel lightguides has been studied by others,[5–9] a search of the literature turned up no actual measurements for a complete optical fiber transmission system. This paper presents the in-depth optical crosstalk data measured for the Bell System's lightwave systems in Atlanta and Chicago. These results show, as others have predicted,[5–9] that crosstalk levels in parallel lightguides arranged in our cable geometry are extremely low. Moreover, it is seen that there are measurable levels of system end-to-end optical crosstalk; however, the source of this crosstalk is believed to be the interconnection hardware. The laser measurement technique and equipment used for these optical crosstalk evaluations are described in the next section.

II. CROSS-COUPLING MEASUREMENT TECHNIQUE

It is well known that the human eye is incapable of making an absolute measurement of the amount of light entering it; we can look at two sources and estimate that one appears "brighter" than the other if there is sufficient difference between them, but we cannot form a reliable judgment as to how much they differ.[10] However, the eye can decide with very good accuracy whether two adjacent surfaces appear equally bright; this was the basic premise used for our visual photometric measurement of lightguide cross-coupling.

According to the law of Weber,[10] the smallest perceptible difference of apparent brightness or luminosity is a constant fraction of the luminosity ($\Delta L/L$ = constant). This fraction, known as Fechner's fraction,

is, over a large range of luminosities, about 1 percent. The eye can therefore distinguish between two adjacent surfaces that differ in luminance by this amount.[10]

The measurement setup for photometrically measuring the cross-coupling between optical fibers is shown in Fig. 1. The optical excitation source used for these measurements was a 2.5-mW helium-neon laser having an approximately Gaussian distribution of light in the TEM_{00} mode. This laser output beam is expanded, collimated, and focused to a numerical aperture of 0.23 to match the average numerical aperture of the optical fibers to be tested. The procedural steps of optically measuring the cross-coupling between optical fibers are as follows:

(*i*) Only one of the fibers is illuminated in the packaged fiber structure to be tested.

(*ii*) The end of the fiber being energized is covered at the far end of the structure being tested.

(*iii*) The far-end observer uses a loupe to observe the He-Ne luminance in a cross-coupled-to fiber.

(*iv*) The near-end observer (and source operator) now places a neutral density filter in the laser beam path.

(*v*) The far-end observer uncovers the far end of the energized fiber and observes the He-Ne luminance with the loupe.

(*vi*) The far-end observer covers the energized fiber and the near-end observer removes the neutral density filter.

(*vii*) Steps (*iii*), (*iv*), and (*v*) are repeated in rapid succession with different amounts of neutral density filtering until the far-end observer notes that the energized fiber with filter has the same luminance as the cross-coupled-to fiber.

The amount of neutral density filtering required to equalize these luminances is the same as the equal-level far-end output-to-output cross-coupling for that fiber pair. This is essentially a null-comparison type measurement process in that it attempts to maintain a balance by suitably applying an effect balancing that which is generated by the cross-coupling.[11] All the cross-coupling experiments were performed

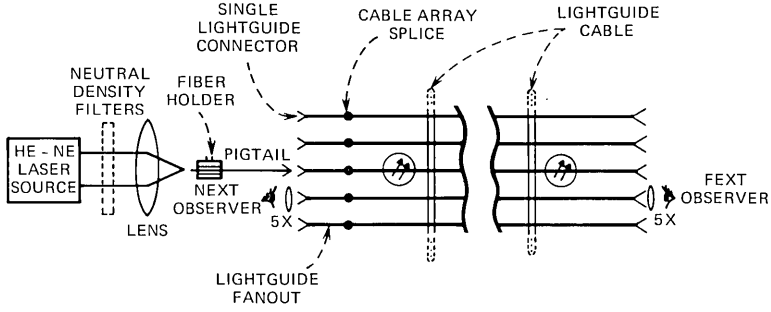

Fig. 1—Cross-coupling measurement setup.

under darkened ambient conditions. For these conditions, it was found that input-to-input or output-to-output cross-coupling losses of up to 100 dB could be detected.

With parallel lightguides, not only is there far-end crosstalk (FEXT) due to parallel interference, but there can also be near-end crosstalk (NEXT) caused by antiparallel interference. The procedures for measuring the near-end optical cross-coupling are essentially the same as those stated above for FEXT. For near-end cross-coupling, neutral density filters are inserted into the laser beam path until the energized fiber pigtail output luminance equals the luminance of the near end of the cross-coupled-to fiber. Using this visual photometric method of measuring lightguide cross-coupling, the optical crosstalk was measured for the Bell System's end-to-end lightguide installations in Atlanta and Chicago.

III. CROSSTALK MEASUREMENTS FOR THE ATLANTA FIBER SYSTEM EXPERIMENT

In the past several years, many fundamental advances have been made at Bell Laboratories in lightwave communications technology. Low-loss optical fibers have been fabricated, cabling and splicing techniques devised, long-lived laser transmitter packages constructed, and optical repeater technology advanced. The 1976 Atlanta Fiber System Experiment brought all these components together into a working system to evaluate system performance in an environment approximating field conditions. The experimental system contained all the elements of an operational 44.7-Mb/s digital transmission system. Plastic underground ducts, typical of those used in metropolitan areas, provided the outside plant environment for the lightguide cable (see Fig. 2).

The 658-m cable is 12 mm in outer diameter and has 144 optical fibers arranged in 12 fiber ribbons—each encapsulating 12 graded-index optical fibers manufactured by the Western Electric Company at Atlanta.[12] The 12 ribbons are stacked and twisted together as shown in Fig. 3. The stacked ribbon structure permits simple interconnection of cables via array splice "butt" joints.[13] An important part of the central office environment is the transition (fanout) from the cable end to the individual fiber connectors on a fiberguide distributing frame. This fanout is composed of 12 laminated fiber ribbons,[14] each containing 12 fibers, where one end has a single 12 × 12 array connector[13] for splicing to the cable end and the other end has 144 individual fiber connectors[15] for interconnection at the fiberguide distributing frame. This complete Atlanta end-to-end installation of 658-m 144-fiber cable, two array splices, and 24 fanout ribbons was measured for optical crosstalk.

Because of the large number of fibers in this installation and the tedious nature of these measurements, the 144-fiber cross section was first

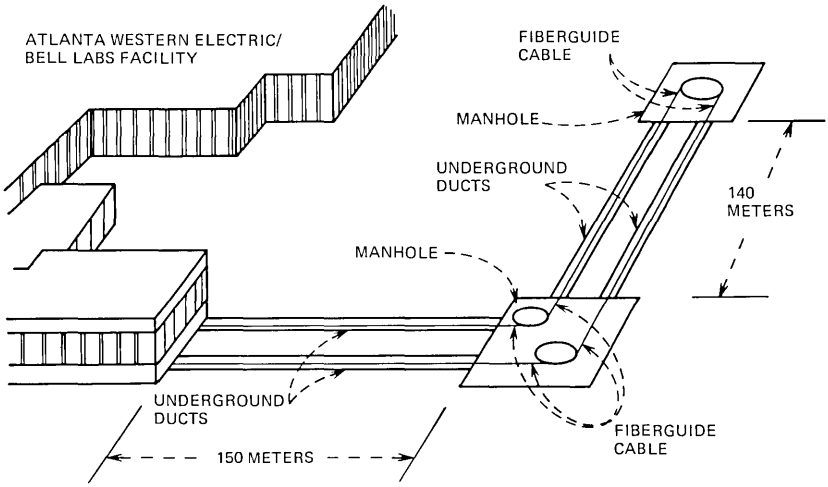

Fig. 2—Atlanta installation route.

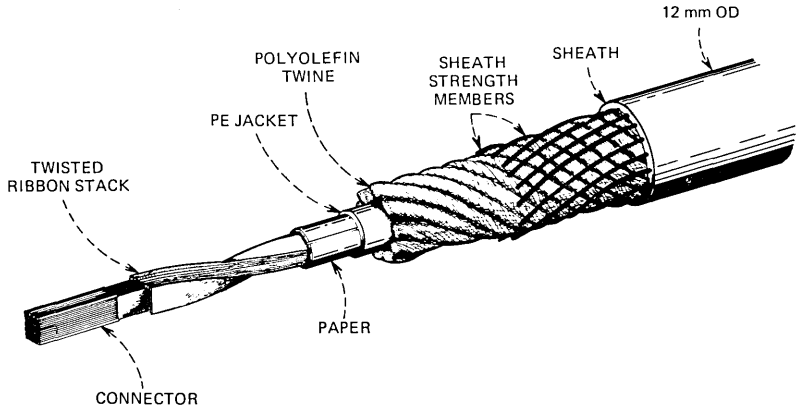

Fig. 3—Lightguide cable design.

quickly searched for fibers exhibiting abnormal amounts of cross-coupling. Only one energized fiber caused significant crosstalk at the far end. In this case, the output-to-output cross-coupling loss to the two adjacent fibers in that ribbon was 55 dB. Using an interfering digital signal and error rate analyses with computer simulations, Wolaver[16] has obtained exactly the same result for these two fiber pairs. It should be noted that, with present technologies, the digital receiver sensitivities are such that cross-coupling losses of greater than $\simeq$65 dB cannot be detected using these error rate analysis techniques, but at least this single comparison has given additional credence to the photometric method of measuring cross-coupling losses.

Once all the fibers were scanned, six energized fibers showing the largest far-end cross-coupling were selected and their measurable cross-coupled-to near neighbors (14 in this case) were measured for cross-coupling loss (to the nearest decibel). Output-to-output far-end crosstalk was converted to input-to-output far-end crosstalk by increasing the numerical value in decibels by the cable, array splice, and fanout ribbon attenuation. The far-end cross-coupling losses in decibels are presented in the format:

mean output-to-output, mean input-to-output
worst case output-to-output

Figure 4 shows the results for the far-end cross-coupling losses measured for the end-to-end Atlanta lightguide installation. Since ribbons are horizontal in Fig. 4, the primary far-end cross-coupling mechanism appears to be intra-ribbon induced, while secondary effects seem to be associated with inter-ribbon mechanisms. For the complete Atlanta end-to-end installation, there was no measurable near-end cross-coupling. To try to isolate the system components causing the cross-coupling mechanisms, further tests were performed for the various segments of the end-to-end transmission medium.

Crosstalk measurements on a second 144-fiber cable fabricated for the Atlanta Experiment, which were without connectors or a ribbon fanout and which contained both Western Electric and Corning fibers, showed that there was not a single case of measurable cross-coupling in the cable. In fact, a different He-Ne laser source of 17-mW output was used in the measurement setup of Fig. 1 and still no measurable crosstalk was observed. Crosstalk was also measured for a 3-m long unconnectorized laminated fiber ribbon like those used for the fanouts from the connectorized cable. For this laminated fiber ribbon, the mean far-end output-to-output cross-coupling loss was 83 dB for adjacent fibers and

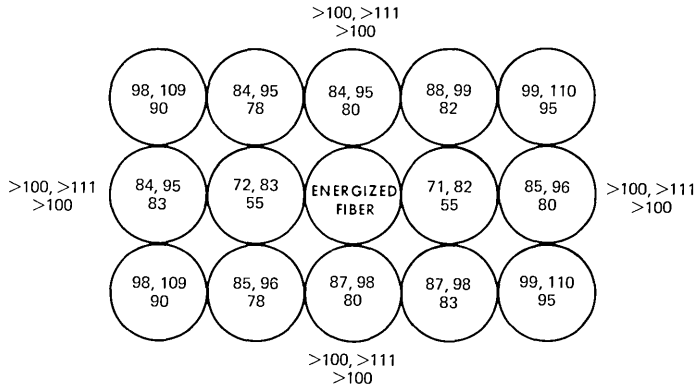

Fig. 4—Far-end cross-coupling losses in decibels for the Atlanta Experiment installation.

98 dB for fibers two positions apart. These data, along with the data of Fig. 4, indicate that for the Atlanta end-to-end installation, the primary far-end crosstalk inducing mechanism was the 12 × 12 array splices with the secondary contributor being the laminated fiber fanout ribbons. It should be pointed out that the measured crosstalk levels were sufficiently small that their effect on system performance was negligible. No near-end cross-coupling was found for the unconnectorized cable or the fanout ribbons separately. This is not surprising, since the end-to-end installation had no measurable NEXT even for the connectorized case.

IV. CROSSTALK MEASUREMENTS FOR THE CHICAGO LIGHTWAVE COMMUNICATIONS PROJECT

Upon the completion of the 1976 Atlanta Experiment, the Bell System's first lightwave system to be evaluated under actual field conditions was installed in Chicago in early 1977. A total of 10 lightguide cable segments, each having the same make-up (except for the core) as those in Fig. 3, were successfully installed in conventional ducts and manholes along a 2.65-km route in downtown Chicago (see Fig. 5). There are 12 cable array splices on this route—five in manholes and seven in the three buildings involved. In the Chicago project, the cable core consists of two 12-fiber ribbons stacked and twisted as in Fig. 3 (all other cable parameters are the same as those of the Atlanta Experiment cables). Thus, the cable segments are joined together with 2 × 12 cable array splices. The central office fanout from the cable end to the fiberguide distributing frame is accomplished this time with unribboned fibers, where one end has a single 2 × 12 array connector and the other end has 24 individual fiber connectors.

Crosstalk for the Chicago Lightwave Communications Project was measured from distributing frame to distributing frame for the Franklin-to-Wabash 1.62-km route and for the Franklin-to-Brunswick 0.94-km route. The characteristics of each route are listed below:

Route	Length	Number of Cable Segments	Number of Array Splices
Franklin-Wabash	1.62 km	6	7
Franklin-Brunswick	0.94 km	4	5

Each route also has two fanouts—one at each end location. To reduce the measurement time per fiber so that all of the fibers could be measured, the crosstalk was measured to the nearest 5 dB instead of to the nearest decibel.

Figure 6 shows the cross-coupling losses measured, both far-end and near-end, for the Franklin-to-Wabash route. The format for the far-end cross-coupling losses (shown in Fig. 6a) is the same as in Fig. 4. The near-end cross-coupling losses shown in Fig. 6b are in the format:

mean input-to-input, worst case input-to-input

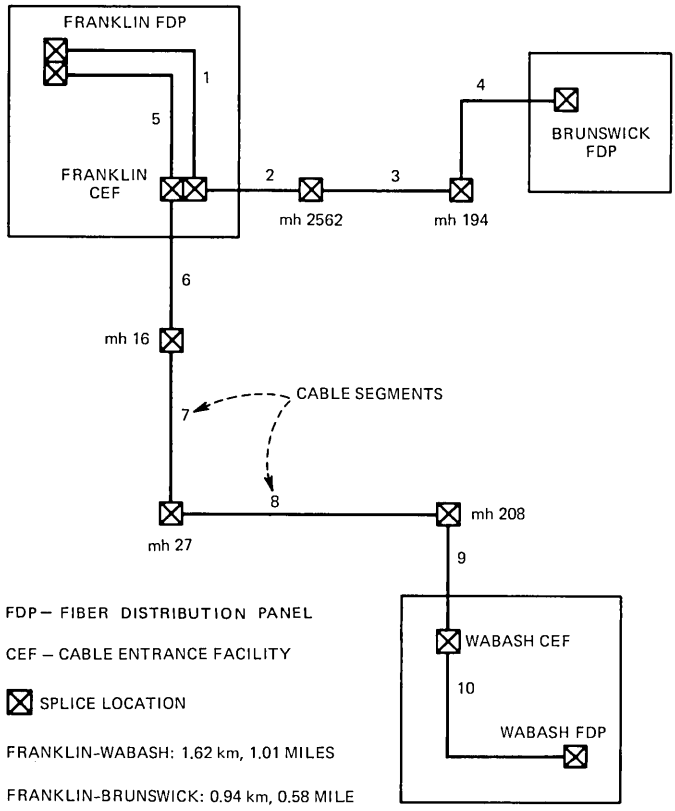

Fig. 5—Chicago route plan.

Figure 7 shows the cross-coupling losses for the Franklin-to-Brunswick route. As can be seen from Figs. 6 and 7, far-end cross-coupling is almost totally intra-ribbon effects most probably induced by the numerous array splices. Unlike the Atlanta Experiment, the Chicago Project installation had near-end cross-coupling. The data of Figs. 6 and 7 show that the primary mechanism for near-end cross-coupling is also intra-ribbon effects, with a secondary mechanism of inter-ribbon effects (both are probably array splice effects). In fact, in the Atlanta array connectors, the intra-ribbon fiber spacing was 9 mils with inter-ribbon fiber spacing of 11 mils, whereas for the Chicago array connectors the intra-ribbon fiber spacing was 9 mils, with inter-ribbon fiber spacing of 21 mils. The major differences between the Atlanta and Chicago end-to-end installations are the number and size of the array splices, the presence of fanout ribbons for Atlanta, and the installed length of the lightguide medium. The numerous cable array splices with their inherent mirror-like end-face cavity construction is most probably the cause of the Chicago near-end cross-coupling. The Atlanta installation had only a single

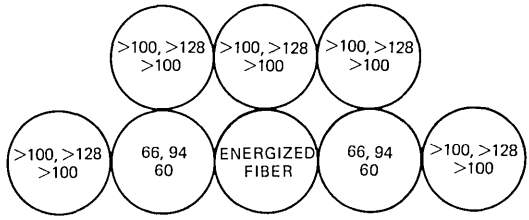

a) FAR-END CROSS-COUPLING LOSSES (dB)

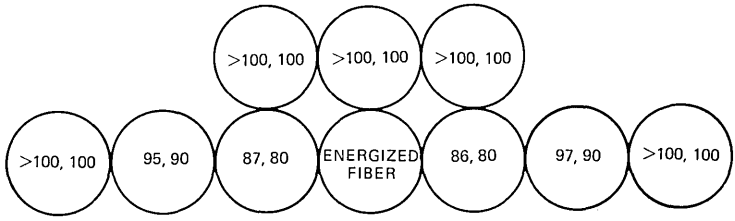

b) NEAR-END CROSS-COUPLING LOSSES (dB)

Fig. 6—Cross-coupling losses in decibels for the Franklin-to-Wabash Chicago route.

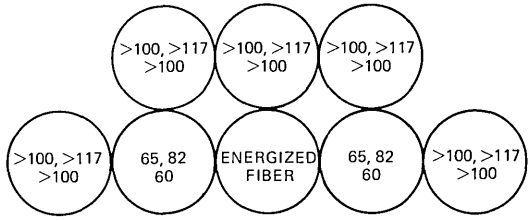

a) FAR-END CROSS-COUPLING LOSSES (dB)

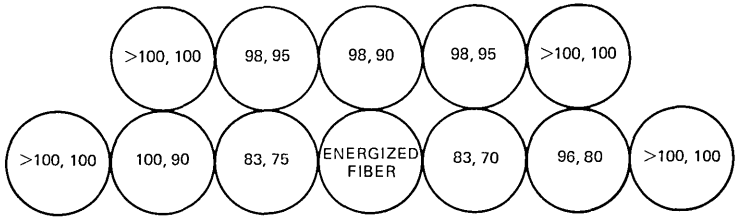

b) NEAR-END CROSS-COUPLING LOSSES (dB)

Fig. 7—Cross-coupling losses in decibels for the Franklin-to-Brunswick Chicago route.

array splice at each end, thus possibly explaining why no near-end cross-coupling was observed there.

V. SUMMARY AND CONCLUSIONS

A visual photometric method of measuring lightguide cross-coupling has been described. Cross-coupling losses up to 100 dB can be measured

with a resolution of ±1 dB. These concepts could be used to build cross-coupling measurement instrumentation using sensitive optical detection devices, such as a photomultiplier tube.

The end-to-end cross-coupling losses were measured for the Bell System's 1976 Atlanta Fiber System Experiment and 1977 Chicago Lightwave Communications Project installations. In the Atlanta Experiment, the crosstalk was also measured for the unconnectorized lightguide cable and fanout ribbons separately. For the Atlanta Experiment, it was found that the primary far-end crosstalk-inducing mechanism was the cable array splices, with the fanout ribbons having a secondary effect. There was no measurable near-end cross-coupling. For the Chicago project, both far-end and near-end cross-coupling were measured and the primary mechanism was intra-ribbon effects that are probably associated with the array connectors.

The worst case cross-coupling losses measured were 55 dB (far-end output-to-output) for the Atlanta installation, and 70 dB (near-end) for the Chicago installation. These results confirm one of the important advantages of optical fiber transmission; namely, that crosstalk is not a serious fundamental problem. However, it has been shown that, even though parallel lightguides can be designed to produce little crosstalk, optical components that are desirable for system operation introduce measurable amounts of crosstalk. Future optical cable and interconnection devices that involve high fiber packing densities will have to take crosstalk considerations into account.

VI. ACKNOWLEDGMENT

W. B. Gardner shared the burden of the many crosstalk measurements made for the Chicago project, and his efforts are very gratefully acknowledged.

REFERENCES

1. T. L. Maione and D. D. Sell, "Experimental Fiber-Optic Transmission System for Interoffice Trunks," IEEE Trans. Commun., *COM-25,* No. 5 (May 1977), pp. 517–523.
2. J. S. Cook, J. H. Mullins, and M. I. Schwartz, "An Experimental Fiber Optics Communications System," 1976 IEEE/OSA Conference on Laser and Electro-Optical Systems, San Diego, May 1976.
3. A. R. Meier, " 'Real-World' Aspects of Bell Fiber Optics System Begin Test," Telephony, *192,* No. 15 (April 11, 1977), pp. 35–39.
4. M. J. Buckler, L. Wilson and F. P. Partus, "Optical Fiber Transmission Properties Before and After Cable Manufacture," Technical Digest of Papers of the Topical Meeting on Optical Fiber Transmission II, Williamsburg, Virginia, February 1977, p. WA1.
5. A. H. Cherin and E. J. Murphy, "Quasi-Ray Analysis of Crosstalk Between Multimode Optical Fibers," B.S.T.J., *54,* No. 1 (January 1974), pp. 17–45.
6. A. W. Snyder, "Coupled-Mode Theory for Optical Fibers," J. Opt. Soc. Am., *62,* No. 11 (November 1972), pp. 1267–1277.
7. A. W. Snyder and P. McIntyre, "Crosstalk Between Light Pipes," J. Opt. Soc. Am., *66,* No. 9 (September 1976), pp. 877–882.
8. A. L. Jones, "Coupling of Optical Fibers and Scattering in Fibers," J. Opt. Soc. Am., *55,* No. 3 (March 1965), pp. 261–271.
9. D. Marcuse, *Light Transmission Optics,* New York: Van Nostrand Reinhold, 1972, pp. 407–437.

10. H. A. E. Keitz, *Light Calculations and Measurements,* New York: St. Martin's Press, 1971, pp. 233–263.
11. E. O. Doebelin, *Measurement Systems: Application and Design,* New York: McGraw-Hill, 1966, pp. 9–71.
12. M. I. Schwartz, R. A. Kempf, and W. B. Gardner, "Design and Characterization of an Exploratory Fiber Optic Cable," Paper X.2, Second European Conference on Optical Fiber Communications, Paris, September 1976.
13. C. M. Miller, "Fiber-Optic Array Splicing with Etched Silicon Chips," B.S.T.J., *57,* No. 1 (January 1978), pp. 75–90.
14. C. M. Miller, "Laminated Fiber Ribbon for Optical Communication Cables," B.S.T.J., *55,* No. 7 (September 1976), pp. 929–935.
15. J. S. Cook and P. K. Runge, "An Exploratory Fiberguide Interconnection System," Second European Conference on Optical Fiber Communications, Paris, September 1976.
16. R. S. Kerdock and D. H. Wolaver, "Performance of an Experimental Fiber-Optic Transmission System," 1976 National Telecommunications Conference, Dallas, November/December 1976.

THE BELL SYSTEM TECHNICAL JOURNAL
Vol. 57, No. 6, July–August 1978
Printed in U.S.A.

Atlanta Fiber System Experiment:

Demountable Single-Fiber Optic Connectors and Their Measurement on Location

By P. K. RUNGE and S. S. CHENG*

(Manuscript received December 20, 1977)

The transfer-molded, single-optical-fiber connector and the fiberguide distribution system implemented for the Atlanta Fiber System Experiment are described. A new technique for measuring the connector and connectorized fiber cable loss in the field was implemented and the results are reported. More recent results of the evolutionary versions of the connector are also reported.

I. INTRODUCTION

The Atlanta Fiber System Experiment was a first test of fiberguide equipment to explore the feasibility of using optical fibers for digital metropolitan trunk transmission systems. It was realized at the onset that high-density systems using cables containing up to 144 fibers[1] would require a fiber interconnection system within the central offices to allow convenient access to all fibers and to permit connecting any number of fibers end to end and to the electronics. A fiberguide interconnection system was therefore implemented for the Atlanta Experiment. This paper describes the interconnection system and the single-fiber connector on which it is based.

II. THE FIBERGUIDE INTERCONNECTION SYSTEM

Figure 1 shows the schematic of the fiberguide interconnection system. The equipment bay containing the fiber optic transmitter and receiver plug-ins and the bay containing the fiberguide distributing frame stand side-by-side and are optically connected by "bay jumpers." The transmitter and receiver circuit boards have fiberguide plugs mounted at the

* P. K. Runge is responsible for the design of the single-optical-fiber connector and S. S. Cheng for their measurement on location.

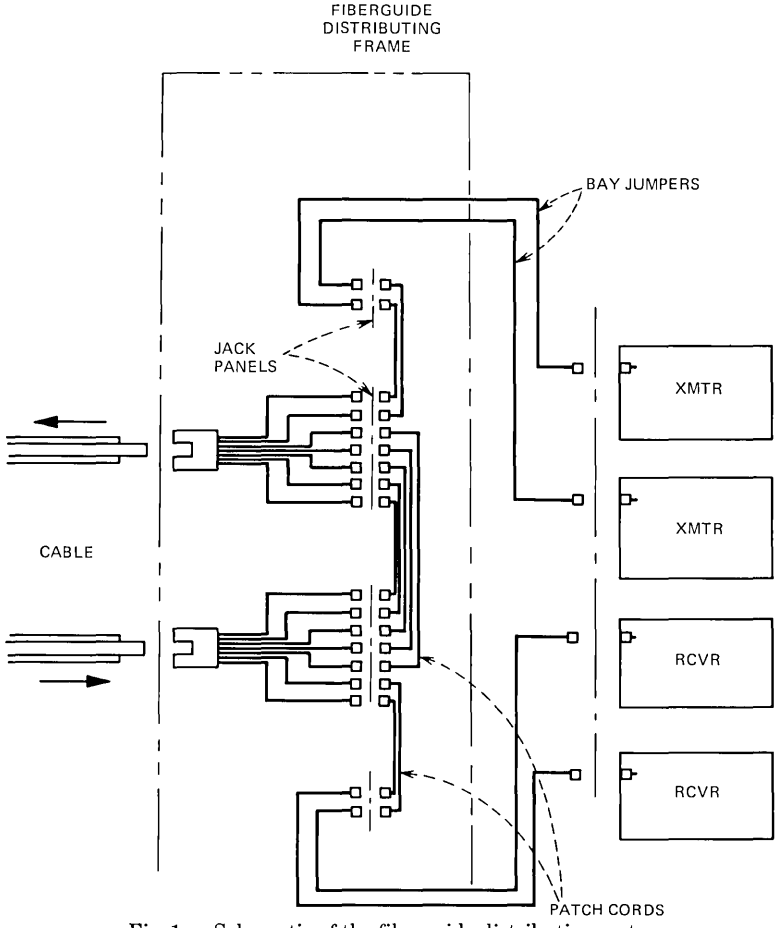

Fig. 1 — Schematic of the fiberguide distribution system.

back so that optical connections to the bay jumpers are made simultaneously with electricrical connections upon insertion. The bay jumpers terminate on a jack panel in the distributing frame. Adjacent to that panel are two jack fields that provide access to both ends of all 144 fibers in the fiberguide cable.

Fiberguide patch cords, typically ½ to 1 meter long, are plugged into the jack fields to provide cable end-to-end connections as shown in Fig. 2. Patch cords also provide the optical link from the equipment jack panel to the cable panels. Optical reconfigurations are all done by moving patch cords at the distributing frame.

The jacks of the distributing frame are connected to cable splice connectors[2] through the individual fibers of the "fan-out" unit. Figure 3 shows a photograph of one fan-out unit taken from the back of the distributing frame at the time the cable splice connection was made. (The

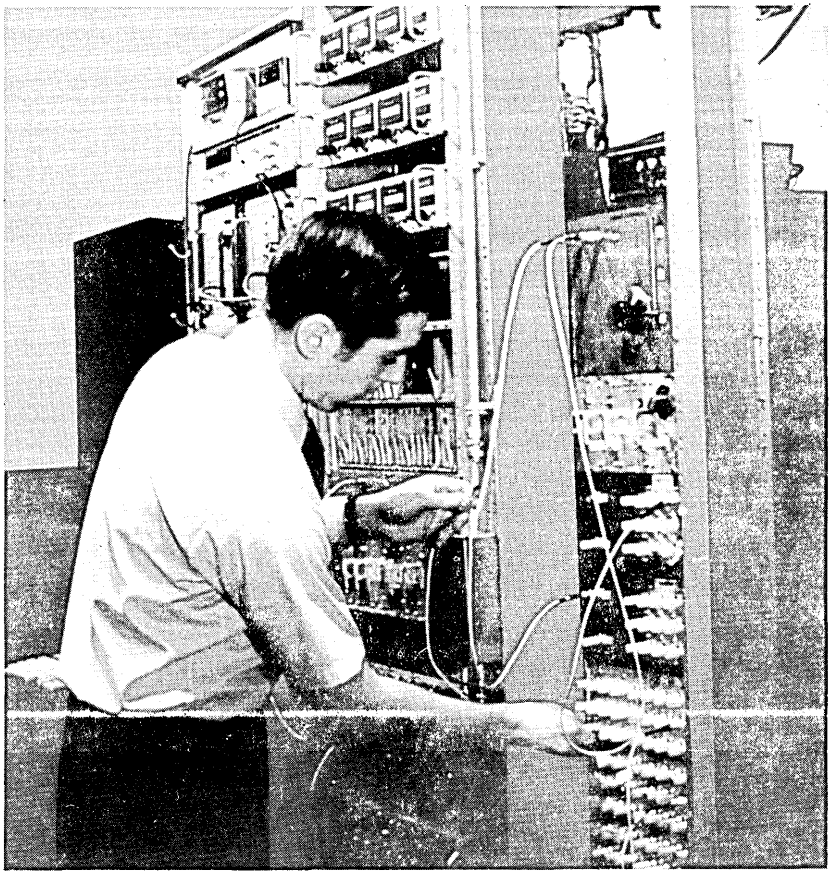

Fig. 2 — The fiberguide distribution frame.

fiberguide cable rises at the left edges of the fan-out units.) The stack of 12 fiberguide ribbons fans out into individual ribbons containing 12 fibers each, each ribbon leading into one organizer tube. Inside the tube, each ribbon fans out into its 12 individual fibers addressing the group of jacks at the opposite end of the tubes. Two of these fan-out units in Fig. 3 were stacked in the back of the distributing frame.

III. SINGLE FIBER CONNECTOR

The heart of the distribution system is the single fiber connector. The connector butt joins two single optical fibers having nominally 110-μm outside diameter and a 55-μm-diameter graded-index core. The mechanical tolerances that have to be maintained in each connection become apparent in Fig. 4. The measured transmission loss is plotted versus axial and lateral misalignment error between two fiber ends with the same core parameters. The loss data were taken with light-emitting diode

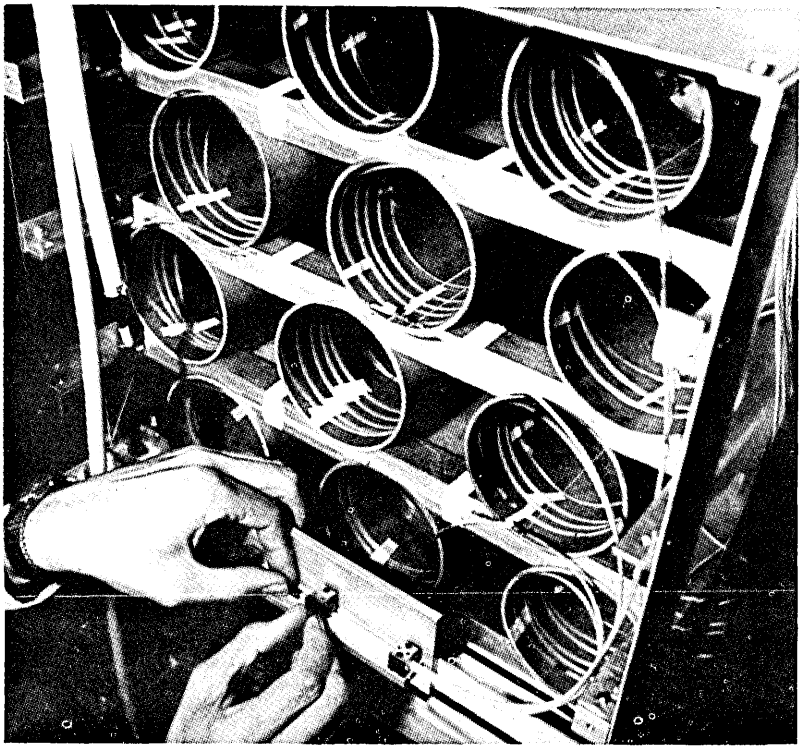

Fig. 3 — One fiberguide fan-out box for 144 fibers.

excitation and glycerin as index-matching media in the gap of the joint. The lateral misalignment error contributes mostly to this extrinsic loss of a fiber connection, and for this fiber the sensitivity ratio of small lateral and axial errors is about 20:1.

When fibers are connected at random, variations in their parameters, as diameter, numerical aperture, and profile of the distribution of index of refraction, lead to an additional, intrinsic loss in the connection. Assuming that a connector with 1-dB average transmission loss has 0.5-dB intrinsic loss leaves only 0.5 dB extrinsic loss for the connector design itself. According to Fig. 4, the total lateral offset error then has to be held below about 5 μm. For the development of a demountable connection, that constitutes a formidable task.

Besides the unprecedented tolerance requirements, the total cost of the single-fiber connector will also be a decisive parameter, since a large number of connectors will be needed, and ultimately optical fiber systems have to compete economically against copper facilities. In addition, since, for the Atlanta Experiment itself plus the assorted test equipments, over 1000 plugs (a plug is the male part of the connector containing the optical fiber) were needed, a mass producible connector was desired.

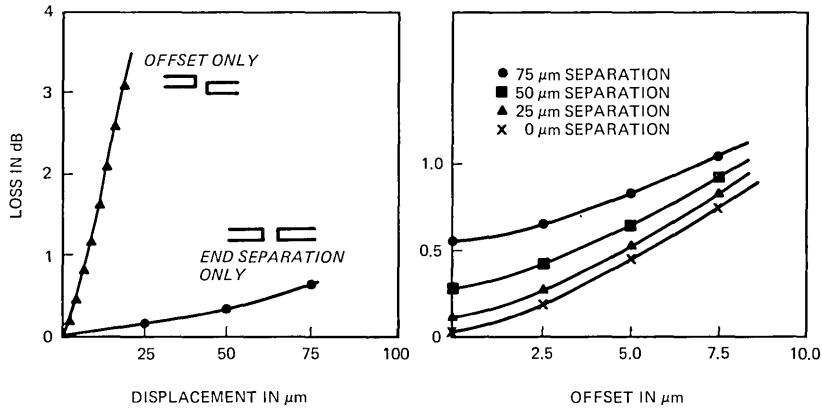

FIBER CLADDING DIAMETER = 110 μm
FIBER CORE DIAMETER = 55 μm
GRADED INDEX CORE; LED EXCITATION

Fig. 4 —Transmission of a single fiber butt joint.

A precision transfer-molding process was developed to produce the plugs shown in Fig. 5. The connector alignment is provided by concentric conical surfaces at the tips of the plugs and by a biconic socket. The molded plug bodies have grooves for additional outside hardware to provide an axial force to seat the connector. The cutout in Fig. 5 is an exploded view of the two optical fiber ends embedded in flexible index-matching cushions.

We have selected the transfer molding process as a mass production process for thermosetting materials that is most gentle on the optical

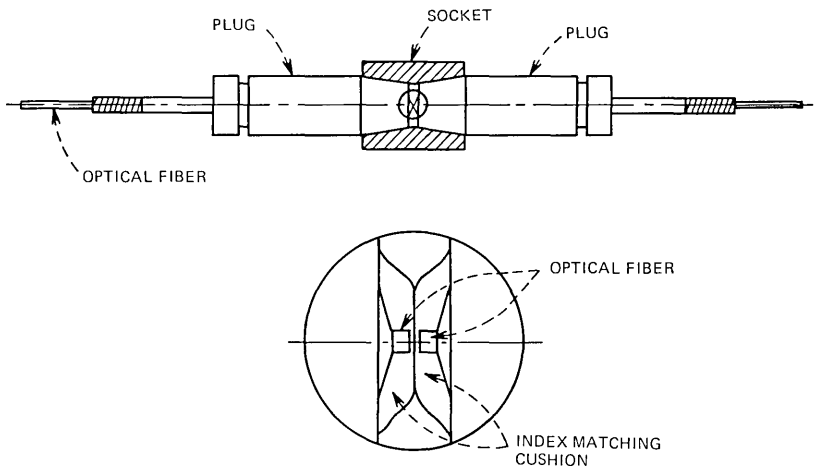

Fig. 5 — Cross section of the single fiber connector detail shows elastomeric index matching cushions.

fiber and guarantees that the mechanical impact of the molding material rarely causes fiber breakage and minimizes deflection. The key part of the mold is a precision die that is cylindrically symmetric without parting lines. It possesses a centering guide hole of nominally 115 μm in diameter, concentric to better than a fraction of a micron with respect to the axis of the tapered surface that constitutes the aligning surface of the molded plug. The diameter of the guide hole equals the nominal fiber outside diameter plus three standard deviations.

A taper was chosen as the aligning surface for a number of reasons.

(*i*) It accommodates molding materials with a varying rate of shrinkage, as long as the material shrinkage is isotropic. Variations from molding to molding do not manifest themselves in lateral misalignments, but rather in the less critical axial error.
(*ii*) It allows easy insertion for low abrasion and good performance reproducibility.
(*iii*) The geometry allows fibers of different diameters to be interfaced.

The molding material is a heavily silica-filled epoxy, which yields plugs of excellent mechanical integrity, extreme toughness, and good surface qualities, including excellent abrasion resistance. After molding, about 2 cm of unprotected fiber protrudes beyond the epoxy body. The angular misalignment between the optical fiber and the taper axis was measured for a large number of plugs by inserting the plug into a brass socket with complementary taper, rotating it, and measuring the walkout of the exposed fiber. The results for the first 397 plugs are indicated in Fig. 6. Ninety percent of all plugs have an angular misalignment of less than 0.8 degree, which is well within the design limit of 1 degree. If desired, a reduction of this angle is possible by improving the guidance of the bare optical fiber in the mold.

We cut the fiber end by inserting the plug into a reference socket and by scoring the fiber at a fixed position with respect to the socket such that two plugs mating in a double conical socket would consistently have a 30-μm gap between fiber ends. The cutting technique of Gloge et al.[3] was employed, where the fiber is simultaneously bent and stressed and then scored.

The most critical tolerance of the fiber optic connector is the eccentricity of the fiber with respect to the axis of the tapered aligning surface. To measure the eccentricity, we used a Ge-doped graded-index fiber that possessed a small depression of the index of refraction at the center of the core. This depression shows up as a dark spot at the center of the illuminated core, about 1 μm in diameter, and allowed us to measure the plug eccentricity to within 0.5 μm.

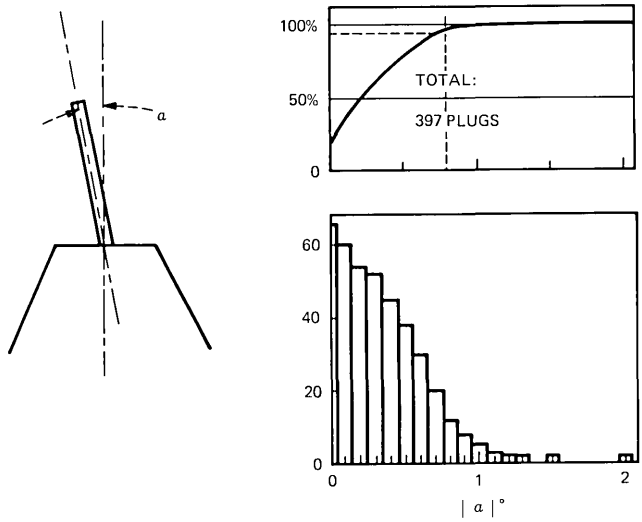

Fig. 6 — Angular error of the first 397 molded plugs.

For this measurement, the plug is inserted into a single steel socket mounted rigidly under a microscope with 400× magnification. By rotating the plugs in this socket, the eccentricities of the optical fibers with respect to the taper axis can be determined. As an example, Fig. 7 shows the location of the centers of 24 plugs molded in die 5 as obtained by this method. Within the accuracy of the measurements, the samples are scattered at random and do not reveal a systematic error. Figure 8 is a plot of the results of 144 measurements of the absolute value of the eccentricity (the angular information is lost). The average error is about 1.2 μm, and 90 percent of the measured plugs had an error of less than 2 μm. A few plugs had eccentricities in excess of 4 μm, but these could be traced to moldings imperfections as, for example, entrapped air bubbles on the critical taper surfaces or a deformation of the taper itself on demolding.

The measured eccentricity, of course, includes the eccentricity of the fiber itself. Although it would have been desirable to obtain statistical information about the eccentricity of the fiber, these data are very difficult to measure to an accuracy of a fraction of a micron. A few sample measurements indicate an average fiber eccentricity of 0.75 and a maximum value of 1.2 μm. Eccentricities in the centering mechanism account for an additional error of the order of 0.5 to 1 μm. The average eccentricity of about 1.2 μm in Fig. 8 thus can easily be explained in terms of those two factors. In view of these facts, we have to conclude that the eccentricity of the plug resulting from nonlinear shrinkage of the epoxy is not dominant and must, on an average, be smaller than about 1 μm.

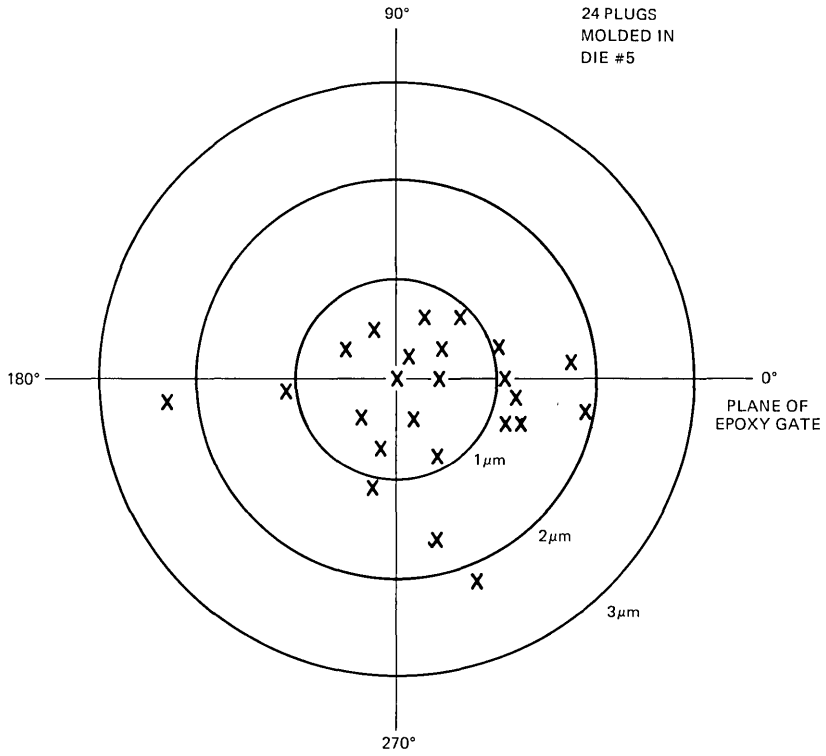

Fig. 7 — Distribution of core center location for first 24 plugs molded in one die.

The process for molding the precision biconic socket was not developed in parallel with the process for plug molding, so that at the time of the Atlanta Experiment only metallic sockets were available. Figure 9 is a photograph of plugs molded on nylon coated fibers mated in a machined brass biconic socket.

The socket in Fig. 9 has an observation hole through which the shadowgraphs of Figs. 10 and 11 were taken. Figure 9 shows the two fiber ends opposing each other with an air gap of about 41 μm. To reduce the transmission loss from Fresnel reflection and refraction and also to protect the fiber ends from contamination, transparent cushions of silicone rubber were applied to each plug. Figures 11a through 11c are three steps in a sequence showing two plugs being pulled apart. As Fig. 11c demonstrates, an index-matching medium without interface is formed between the fiber ends. This medium reduces the transmission loss by about 0.4 dB when compared to the loss in the air gap of Fig. 10. (Figures 10 and 11 have the same magnification.)

Two types of metallic biconic sockets were available for the experiment: sockets made by hydroforming copper sleeves onto precision steel mandrels and sockets machined from solid brass. The hydroformed

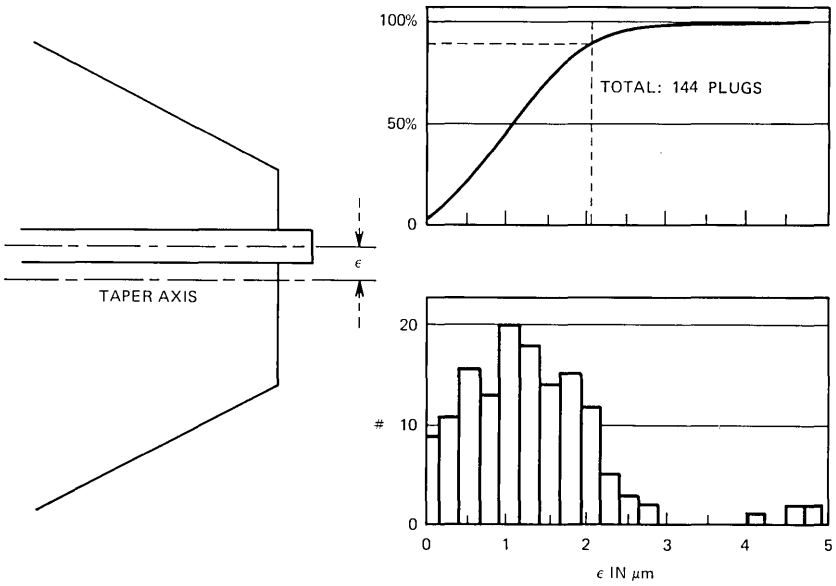

Fig. 8 — Distributions of eccentricity errors of the first 144 molded plugs.

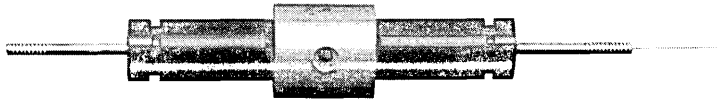

Fig. 9 —Two plugs mated in a brass biconic socket. Note the observation hole.

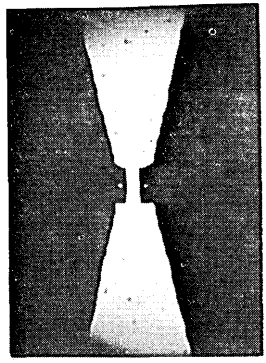

Fig. 10—Shadowgraph of opposing fiber ends of two plugs mated in the socket of Fig. 9.

sockets showed eccentricities between 5 to 10 μm and had too much resiliance on insertion of the plugs, so that the gap between fiber ends had to be increased to 100 μm. The machined brass sockets had eccentricities in the range from 0 to 5 μm and were in addition stiffer, which allowed the gap to be reduced to 65 μm.

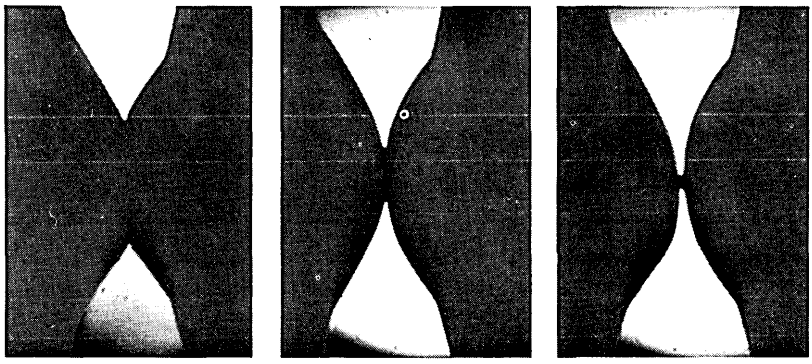

(a) (b) (c)

Fig. 11—(a) Shadowgraph of two plugs with flexible transparent "buttons" for index match mated in the biconic socket (same magnification as Figure 10). (b) and (c) One connector is gradually unseated; button surfaces cling together.

IV. INTERCONNECTION HARDWARE

The quick connection at the rear of the transmitter and receiver cards is provided by mounting the molded plug in the spring-loaded jig as shown in Fig. 12. Two pins guide the plug into the floating biconic socket mounted on the frame. The plug is connected to the receiver or transmitter package on the circuit board by a "pigtail," which is a nylon-

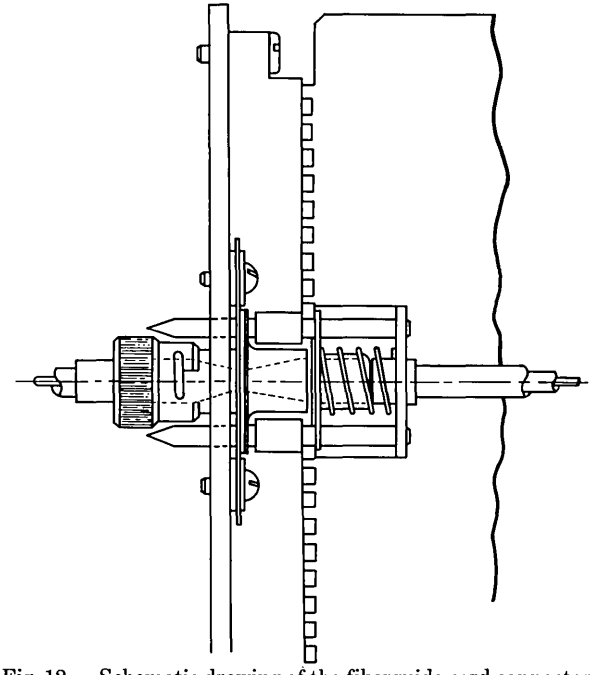

Fig. 12 — Schematic drawing of the fiberguide card connector.

coated fiber in a loose protective sheath that is looped to permit easy motion when the plug engages. Figure 13 shows the three plug-ins that comprise a full repeater photographed from the connector side.

The armor for an optical fiber patch cord must protect the fiber against excessive bending, compression, and elongation forces, yet it should be flexible and light in weight to ease the forces on the optical connectors. The experimental patch cords utilized the standard protection of a miniature coax cable with the optical fiber replacing the center conductor. Its Teflon® inner jacket protects the optical fiber from contact with the metallic braid and offers protection against sharp bends of the cable. The metallic braid protects, within limits of about 20 kg, against elongating forces. The optical connectors were molded directly onto the ends of the patch cord. The cords have not been tested systematically to failure, but they are surprisingly rugged, and to our knowledge there have been no failures in normal usage from a fiber breaking in the sheath.

The fiber connector of Fig. 3 required some outside hardware to exert the seating force and also to protect the connector ends. For convenience, the outer shell of a standard BNC coax connector was modified and served that purpose well. Thus, the patch cords being handled in Fig. 2 only look like coax cables; in reality they are fiberguides.

The fan-out was constructed by molding plugs onto 2-m-long, nylon-coated fibers. These were assembled into ribbons, 12 at a time, leaving about one-half meter of coated fiber between the ribbon and plug. The 12 plugs were mounted on a 12-jack panel, the panel was mounted on the distributing frame, and the ribbon was coiled loosely in the organizer tube behind each panel. The ribbons were then brought together at the back of the distributing frame and mounted into a stack of grooved wafers for connection to the cable.

V. A STATISTICAL LOSS MEASUREMENT METHOD

The loss measurement set (Fig. 14) consists of an optical transmitter with a stable laser as the source, and an avalanche photodiode detector (APD) operating in the linear range as the optical power detector. The optical link may consist of up to three jumpers and two fibers. These fibers are part of the 144 fibers in the 640-m long fiber cable in the Atlanta Experiment.

Figure 14 shows a simplified measurement sequence that statistically determines the loss of three jumpers and two fibers. The first setup is for the baseline calibration; the transmitter is connected to the receiver via a variable optical attenuator and/or reference jumpers and fibers for setting a proper input level. The baseline level is chosen such that the received power level for all subsequent setups will be within the linear operating range of the APD. In each setup, the received power is measured

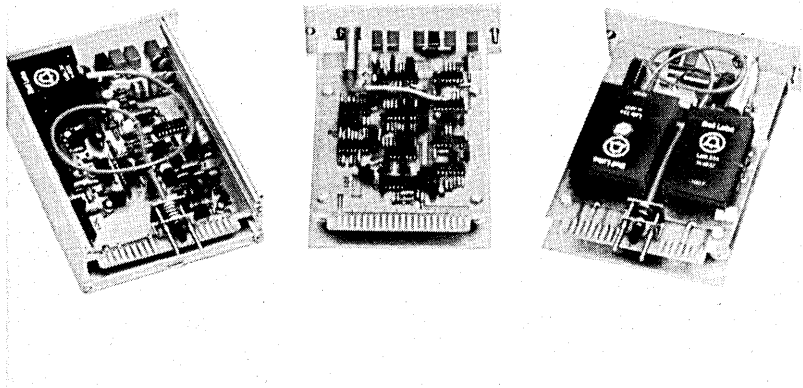

Fig. 13—A complete fiberguide regenerator with: Left: receiver module with fiberguide card connector. Center: decision and retiming module. Right: laser transmitter module with fiberguide card connector.

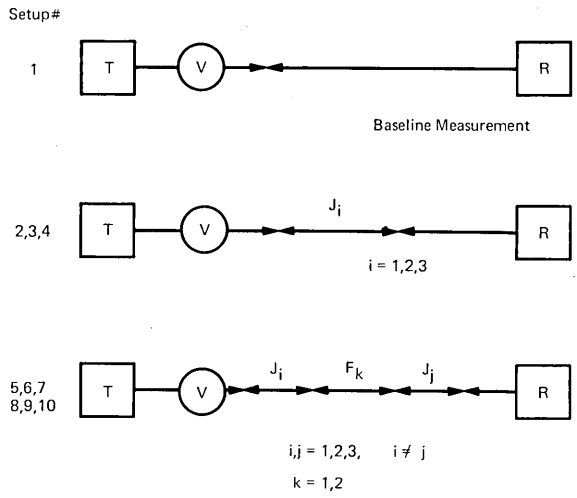

NOTES:

(1) IN EACH SETUP, AT LEAST 10 POWER MEASUREMENTS ARE MADE TO ENABLE A MEANINGFUL AVERAGING OF MEAN AND RMS.

(2) V REPRESENTS A VARIABLE ATTENUATOR AND/OR SEVERAL REFERENCE JUMPERS AND FIBERS FOR SETTING A PROPER BASELINE LEVEL.

Fig. 14 —A simplified sequence of statistical loss measurement.

many times so that a mean and an rms level can be determined. In each measurement, the connection between the transmitter and the receiver jumpers is disconnected and then reconnected with a slightly different

orientation. The purpose is to enable a meaningful averaging of loss over all possible connector orientations.

In setups 2 through 4, one of the three jumpers is added to the optical link. Again, in each power measurement, the jumper is disconnected on both ends and reconnected at a different angle. Setups 5 through 10 consist of the set and one possible combination of two jumpers and one fiber. Here, in each measurement, both jumpers are disconnected and reconnected each time.

At the conclusion of all measurements, a least-square technique is applied to these data to determine the best fits for the six unknowns (five loss elements and the baseline level of the set). The simultaneous determination of many loss elements reduces the inconsistency that may occur in the measurement. The loss is represented by a mean value and an rms value. The rms value is contributed partially by the measurement inaccuracy and partially by the offset and the angular dependence of the connector loss. The mathematical basis for such an approach is presented in the appendix.

The success of this method depends on the following assumptions and precautions:

(*i*) The APD should be operated in a linear range to serve as an optical power detector. For the optical receiver, −10 to −45 dBm is a suitable range. The stability of the laser is also important. Overnight monitoring of the laser power indicates a variation of less than 0.1 dB.

(*ii*) The loss of various components in the optical link must add up linearly. To insure this, additional mode mixing is introduced through one variable optical attenuator and/or additional reference jumpers and fibers in front of the loss elements to be measured. Once the attenuator position is set and the reference jumpers and fibers are in place, they remain intact throughout the rest of the measurement sequence. The reference jumper and fiber are chosen on the basis that the connection yields a minimum uncertainty in the repeated baseline measurements. With carefully chosen reference jumper and fiber, the uncertainty is typically 0.06 dB.

(*iii*) To take full advantage of the redundant measurements, a jumper-to-fiber mix of 3 to 2 is preferred over 3 to 1 or 4 to 1. The ratios of number of measurements to number of unknowns are 10 to 6, 7 to 5, and 9 to 6 respectively. The increased redundancy reduces the contribution from poor or inconsistent measurements.

An HP 9830A calculator was programmed to perform the power measurement and the data reduction. To double-check the results, we made other measurements that include some previously measured jumpers and fibers. Two such measurements were made at more than a 1-month

interval using different transmitters and receivers. The agreement has been quite good and was sufficient to indicate that these measurements are reliable and repeatable.

VI. MEASURED LOSS OF CONNECTORS AND FIBERS IN THE ATLANTA EXPERIMENT

Tables I and II summarize the measured jumper and fiber loss. The consistency among these measurements is generally good. That is, the difference between the mean loss of two measurements is usually less than the combined uncertainty of the measurements. Out of the 27 elements measured, there are three exceptions to this rule, J72, F1-4, and F3-1. The reason for some of them may be purely statistical, but more likely it may be because of a permanent deterioration of the surface condition at the fiber tip of the connector. This is concluded on the basis that the increase in loss invariably occurs after hundreds of times of handling and that, once the loss is increased, it is irreversible.

The average insertion loss of jumpers using hydroformed sockets ranges from 1.0 to 3.1 dB with an uncertainty between 0.1 to 0.4 dB. The average loss of all such jumpers measured is 1.75 ± 0.26 dB.

Jumpers using machined sockets have a mean loss ranging from 0.5 to 1.9 dB and an uncertainty from 0.1 to 0.4 dB. The average loss of this

Table I — Jumper loss in dB

Jumper No.*	1st	2nd	3rd	Avg.
72	2.4 ± 0.3	3.6 ± 0.4		2.4 ± 0.3†
76	1.6 ± 0.3			1.6 ± 0.3
77	3.1 ± 0.4	2.5 ± 0.2	2.5 ± 0.2	2.7 ± 0.3
80	1.7 ± 0.3			1.7 ± 0.3
82	2.0 ± 0.3			2.0 ± 0.3
84	1.5 ± 0.2			1.5 ± 0.2
87	1.0 ± 0.1			1.0 ± 0.1
91	1.0 ± 0.3	1.1 ± 0.1		1.0 ± 0.2
149	1.6 ± 0.3			1.6 ± 0.3
150	0.9 ± 0.2	0.6 ± 0.2		0.7 ± 0.2
154	1.6 ± 0.1	1.7 ± 0.1		1.6 ± 0.1
157	1.1 ± 0.3			1.1 ± 0.3
160	1.5 ± 0.2	1.7 ± 0.3		1.6 ± 0.2
161	1.2 ± 0.2			1.2 ± 0.2
168	0.7 ± 0.3			0.7 ± 0.3
169	1.8 ± 0.4			1.8 ± 0.4
172	1.4 ± 0.2	1.9 ± 0.4		1.6 ± 0.3
174	1.2 ± 0.2	1.2 ± 0.2	1.3 ± 0.1	1.3 ± 0.2
176	0.5 ± 0.2	0.8 ± 0.1	0.8 ± 0.2	0.7 ± 0.2
180	0.5 ± 0.1	0.7 ± 0.2		0.6 ± 0.1

* Jumpers No. 72 through 91 are with hydroformed socket, No. 149 and up are with machined socket.
† The second measurement is excluded because the jumper by then might have suffered permanent degradation due to repeated use.

Table II — Fiber loss in dB

Fiber No.	1st	2nd	3rd	4th	Avg.
1-4	6.5 ± 0.2	8.0 ± 0.4*			6.5 ± 0.2†
1-11	8.1 ± 0.4*	8.3 ± 0.6	8.1 ± 0.3	8.3 ± 0.3*	8.2 ± 0.4
2-1	4.7 ± 0.3	4.7 ± 0.3			4.7 ± 0.3
2-8	4.9 ± 0.4*	5.6 ± 0.5			5.2 ± 0.5
3-1	5.0 ± 0.3	5.9 ± 0.2			5.0 ± 0.3†
5-2	5.5 ± 0.4	5.2 ± 0.6*			5.4 ± 0.5
7-2	6.6 ± 0.5*	6.8 ± 0.4			6.7 ± 0.4

* Jumpers with hydroformed socket.
† The tips on the fiber connectors might have suffered permanent degradation after repeated use. The last measurement is excluded in obtaining the average loss.

type of jumper is 1.22 ± 0.21 dB, indicating convincingly that this type of socket is superior to the former type. As indicated before, machined sockets have tighter tolerances, thus providing better alignment and less loss. The small improvement in the loss uncertainty (from 0.26 to 0.21 dB) suggests that the measurement uncertainty may dominate the angular loss variations of the connectors.

Fiber loss (Table II) consists of the loss incurred in the 640 M glass fiber, two array splices, and the two half-connectors on the distribution frame. The average loss of the seven fibers measured is 5.96 ± 0.40 dB. Subtracting from it a mean loss of 0.55 dB for each array splice and 3.5 dB for the average fiber loss, the average full jumper loss would be 1.36 dB. Considering the small size of fiber sample measured, this crudely defined connector loss with mixed sockets lies within the bounds of the previously established loss of 1.75 dB with hydroformed socket and 1.22 dB with machined socket. This was also the first time the end-to-end absolute loss of a fiber in the field environment was accurately determined.

The loss measurement method described and tested can be applied to several areas of interest:

(*i*) To evaluate the comparative merits of optical jumpers with various types of connectors or sockets.
(*ii*) To perform precision loss measurement of optical fibers in a field environment.
(*iii*) To provide a means to estimate the aging and environmental effects on the optical fibers, jumpers, splices, and connectors.
(*iv*) When the absolute loss of a large number of jumpers or fibers needs to be determined, we may use this method to determine the absolute loss of a few elements. Then one can quickly switch over to simpler means such as using a variable attenuator, a transmission loss set, or an optical power meter to determine the relative loss between these elements and the rest.

The method, though tedious, is capable of making a simultaneous loss determination of six elements. Twenty-seven jumpers and fibers have been successfully measured. Some of them were measured many times to check consistency. The agreement among various measurements is generally good. Three elements show a definite increase of loss after hundreds of times of handling, indicating a possible permanent dirt penetration or surface damage on the connectors. A clear understanding and a substantial reduction, if not complete elimination, of such phenomena is needed before the real system usage.

It is also shown convincingly that connectors with machined sockets perform better than those with hydroformed sockets. However, even with machined sockets, the jumper loss variation of 0.5 to 1.9 dB is larger than desirable, particularly from the viewpoint of setting engineering rules for fiberguide systems.

VII. EVOLUTION OF THE SINGLE-FIBER CONNECTOR AFTER THE ATLANTA EXPERIMENT

The single-fiber connector obviously was in the initial development phase at the beginning of the Atlanta Experiment. Nevertheless, valuable information could be gained by the experiment itself, which led to a number of significant improvements. A molded biconic sleeve was developed by W. C. Young,[4] and the performance of the connector improved significantly. The mechanical tolerances of molded sleeves can be held more tightly than those of machined sleeves. The eccentricity error is less than 2 μm and, because of tighter control of the length parameter, the nominal end separation between fibers could be reduced to 25 μm.

A second significant change lies in the preparation of the fiber ends. The protruding fiber stub, as in Fig. 5, was found to be much too vulnerable to impact, and a fiber end flush with the plug was desirable. The breaking method of Gloge et al.[2] does not lend itself to produce flush ends. It was found that breaking a fiber closer to the plug body would result in break faces that were no longer perpendicular to the fiber axis, but showed progressively larger break angles (up to 60 degrees, when the fibers were scored somewhat inside the epoxy). We have therefore adopted a quick lapping and polishing process, which produces good, square fiber ends flush with the plug body.

More recently reported results[4] of 0.4-dB transmission loss for LED excitation and index match were a consequence of these implemented changes plus the improved characteristics of the optical fiber itself. The results were obtained by measuring the average transmission loss of 50

jumper cables against a standard connector as the final step in their inspection. Perhaps more indicative of the present state of the fiber and connector technology is the result obtained in January 1978. Twenty randomly selected jumper cables of the newest variety were connected in series at random connector orientations and excited with an LED. The measured connector losses had a mean of 0.54 dB and a standard deviation of 0.3 dB without index match between the fiber ends.

VIII. CONCLUSION

The Atlanta Fiber System Experiment was the testing ground for the first generation of fiber-optic interconnection hardware and has yielded valuable information for subsequent system experiments. An attempt was made to meet the challenge with a mass-produced single-fiber connector. While the technology was not completely developed at the time of the experiment, satisfactory results were nevertheless obtained.

IX. ACKNOWLEDGMENTS

We would like to thank our colleagues T. C. Chu, L. Curtis, A. R. McCormick, L. Maggi, C. R. Sandahl, and W. C. Young for their invaluable contributions to this success. The assistance by L. Wilson in loss data collection is also appreciated.

APPENDIX

Matrix Formulation of Maximum Likelihood Loss Measurement

Let x_i, $i = 1,5$ represent the loss of three jumpers and two fibers respectively and x_6 the baseline level of the set. The measured power level and its uncertainty are represented by y_i and σ_i, $i = 1,10$. The measurement sequence follows the order outlined in Fig. 14. Elements of x_i and y_i can be related in a matrix equation

$$Ax = y, \tag{1}$$

where x and y are column matrices. A is a 6-by-10 configuration matrix whose element is either 1 or 0, depending on whether the particular loss

element in question is present in the link. In the measurement

$$A = \begin{array}{c} \text{Loss element} \\ \\ \\ \\ \\ \\ \\ \\ \\ \\ \\ \end{array} \begin{array}{c} \begin{array}{cccccc} \text{J1} & \text{J2} & \text{J3} & \text{F1} & \text{F2} & \text{Set} \end{array} \\ \left|\begin{array}{cccccc} 0 & 0 & 0 & 0 & 0 & 1 \\ 1 & 0 & 0 & 0 & 0 & 1 \\ 0 & 1 & 0 & 0 & 0 & 1 \\ 0 & 0 & 1 & 0 & 0 & 1 \\ 0 & 1 & 1 & 1 & 0 & 1 \\ 1 & 0 & 1 & 1 & 0 & 1 \\ 1 & 1 & 0 & 1 & 0 & 1 \\ 1 & 1 & 0 & 0 & 1 & 1 \\ 1 & 0 & 1 & 0 & 1 & 1 \\ 0 & 1 & 1 & 0 & 1 & 1 \end{array}\right| \end{array} \tag{2}$$

The sequence of measurements is chosen to minimize the number of changes of loss elements from one setup to another.

Since there are more equations than unknowns in the matrix equation (1), an exact or unique solution for x does not exist. However, a best-fit can be found by using a multiparameter least-square-fit technique[5] that is widely used by experimental physicists.

If we consider the measured results y_i to be Gaussian, then the likelihood function is proportional to

$$L(x_1,x_2,\cdots,x_n) = \prod_{i=1}^{N} \frac{1}{\sqrt{2\pi}\sigma_i} \exp\left[-\frac{(y_i - \xi_i)^2}{2\sigma_i^2}\right], \tag{3}$$

where $N = 10$ is the number of measurements and $n = 6$ is the number of unknowns. $\xi_i = \xi_i\,(x_1,x_2,\cdots x_n)$ is the "theoretical" value or the best fit value of y_i.

To maximize the likelihood L is equivalent to minimizing the exponent

$$\sum_{i=1}^{N} \frac{(y_i - \xi_i)^2}{2\sigma_i^2},$$

which leads to the condition of least-square fit, namely,

$$\sum_{i=1}^{N} \left(\frac{y_i - \xi_i}{\sigma_i^2}\right) \frac{\partial \xi_i}{\partial x_m} = 0, \quad m = 1,2,\cdots,n. \tag{4}$$

Since

$$\xi_i = \sum_{m=1}^{n} A_{im} x_m, \; i = 1,2,\cdots,N$$

from eq. (1), the maximum likelihood condition of eq. (4) becomes

$$\sum_{i=1}^{N} \frac{A_{im} y_i}{\sigma_i^2} = \sum_{i,l=1}^{N} \frac{A_{im} A_{il}}{\sigma_i^2} x_l. \tag{5}$$

In matrix form, eq. (5) becomes

$$Y = Mx, \tag{6}$$

where

$$Y_m = \sum_{i=1}^{N} \frac{A_{im} y_i}{\sigma_i^2}, \quad m = 1,2,\cdots,n \tag{7}$$

is a modified data vector and

$$M_{ml} = \sum_{i=1}^{N} \frac{A_{im} A_{il}}{\sigma_i^2} = M_{lm}, \quad m,l = 1,2,\cdots,n \tag{8}$$

is a symmetric square matrix called the measurement matrix. The solution of eq. (6) is

$$x = M^{-1} Y. \tag{9}$$

The standard error in x_m is

$$\Delta x_m = (M_{mm}^{-1})^{1/2}, \quad m = 1,2,\cdots,n. \tag{10}$$

Because of the above property, M^{-1} is referred to as the error matrix. From eqs. (9) and (10), it is clear that a symmetric matrix inversion routine of rank 6-by-6 constitutes the bulk of the data reduction. The expected measured power is defined as

$$\xi_i = \sum_{m=1}^{n} A_{im} x_m \quad i = 1,2,\cdots,N \tag{11}$$

and the expected measured uncertainty

$$\eta_i = \left[\sum_{m=1}^{n} A_{im} \Delta x_m^2 \right]^{1/2}, \quad i = 1,2,\cdots,N \tag{12}$$

Comparison of ξ_i, η_i with y_i, σ_i can give a qualitative feeling of the quality of the loss measurement and the least-square fit.

REFERENCES

1. M. I. Schwartz, W. A. Reenstra, J. M. Mullins, and J. S. Cook, "The Chicago Lighwave Communications Project," B.S.T.J., this issue, pp. 1881–1888.
2. C. M. Miller, "Fiber-Optic Array Splicing with Etched Silicon Chips," B.S.T.J., *57*, No. 1 (January 1978), pp. 75–90.
3. D. Gloge et al., "Optical Fiber End Preparation for Low-Loss Splices," B.S.T.J., *52*, No. 9 (November 1973), pp. 1579–1588.
4. P. K. Runge, L. Curtis, W. C. Young, "Precision Transfer Molded Single Fiber Optic Connector and Encapsulated Devices," Topical Meeting on Fiber Optics, Williamsburg, February 1977.
5. J. Mathews, R. L. Walker, *Mathematical Methods of Physics,* New York: W. A. Benjamin, 1965, pp. 365–367.

THE BELL SYSTEM TECHNICAL JOURNAL
Vol. 57, No. 6, July–August 1978
Printed in U.S.A.

Atlanta Fiber System Experiment:

Planar Epitaxial Silicon Avalanche Photodiode

By H. MELCHIOR, A. R. HARTMAN, D. P. SCHINKE, and T. E. SEIDEL

(Manuscript received March 1, 1978)

A silicon avalanche photodiode (APD) has been developed for optical fiber communications systems. It has been optimized for optical wavelengths of 800 to 850 nm and exhibits a quantum efficiency greater than 90 percent. The APD operates between typical voltages of 100 and 400 V, exhibiting photocurrent gains of approximately 8 and 100, respectively, at those biases. The device has a short response time of ~1 ns and low excess noise characterized by an excess noise factor approximately 5 times the shot noise limit for operation at a photocurrent gain of 100. The APD has a four-layer n^+-p-π-p^+ structure and is fabricated on large-diameter epitaxial wafers using planar technology. Uniform avalanche gain, low dark currents, and good reliability are achieved through the use of (i) a diffused guard ring, (ii) a diffused channel stop, (iii) metal field plates, (iv) the removal of impurities in the surface oxides and the bulk of the APD, (v) passivation with silicon nitride and (vi) a processing sequence that maintains low dislocation density material.

I. INTRODUCTION

Solid-state photodetectors are particularly well suited to optical communications. The detectors, fabricated from semiconducting materials, are small, fast, highly sensitive and relatively inexpensive.[1] Two widely employed detectors are the PIN photodiode, which in reverse bias collects the photogenerated minority carriers, and the avalanche photodiode, which has a high field region that multiplies the photocurrent through the avalanche generation of additional electron-hole pairs.

The avalanche photodiode (APD) designed specifically for the FT3 optical communications system[2] will be described in this paper. At a bit

rate of 44.7 Mb/s, the APD allows an increase in system sensitivity by approximately 15 dB over the same receiver with a PIN detector.[3] This improvement is possible because the shot noise in the photocurrent of the PIN diode is much smaller than the equivalent input noise of a receiver amplifier having sufficient bandwidth to carry the 45 Mb/s signal.[4] The gain in the APD increases the signal intensity and system sensitivity until the noise in the multiplied current is comparable to the noise of the amplifier. The avalanche photodiode is not, however, an ideal multiplier. It adds a substantial amount of noise because of fluctuations in the avalanche gain. The excess noise depends on the device structure and the electron and hole ionization rates of the material chosen for the detector.[5] The avalanche photodiode for the FT3 application was designed to minimize excess noise and maximize the quantum efficiency without compromising manufacturability or reliability.

In Section II, the design and operation of the APD are described. The fabrication is outlined in Section III, and the optical and electrical characteristics are given in Section IV.

II. DESIGN AND OPERATION

Since the wavelengths of the GaAlAs double heterostructure laser employed in the FT3 system are 800 to 850 nm, the choice of silicon as the detector material is the obvious one. These wavelengths require photocarrier collection lengths of 20 to 50 μm, which lie well within the range of achievable space charge layer widths in lightly doped material.

For lowest noise, McIntyre[5] has shown that in silicon the avalanche should be initiated by pure electron injection into a relatively wide gain region. This results from the high ratio of the electron-to-hole ionization rates favoring electron multiplication by a factor of 10 to 50 for the electric fields of importance.[6] The avalanche photodiodes combining the highest efficiency and speed (in the 800- to 900-nm wavelength range) with high uniform current gains and low excess noise are then constructed from silicon as n^+-p-π-p^+ structures and operated at high reverse bias voltages with fully depleted p-π regions. In these devices, incident light in the 800- to 900-nm range is mainly absorbed in the π region. From the π region, the photogenerated electrons drift into the n^+-p high field region where they undergo avalanche carrier multiplication. This device structure is referred to as a reach-through structure.[7–9] To achieve the lowest noise operation associated with pure electron injection, the light should be incident through the p^+ contact and fully absorbed in the π region. These APDs must be bulk devices thinned to 50 to 100 μm before metallization[8] or epitaxial devices having n^+ substrates and two sequential epitaxial p and π layers.[10]

A device construction more amenable to fabrication on large-diameter

silicon wafers with good control of the doping profile utilizes π-type epitaxial silicon on p^+ substrates and forms the n^+-p-π-p^+ structure through ion implantation and diffusion. This construction, as shown in cross section in Fig. 1, dictates that the light be incident through the n^+ contact on the epitaxial surface of the device. The noise penalty brought about by the resultant generation and injection of electrons and holes into the high-gain region is minimized by tailoring the field profile. With a shallow n^+ and a deeply diffused p-type region, the electric field profile in the p-region is essentially triangular with the maximum field at the n^+-p junction. Employing the noise analysis of Webb et al.,[5] the triangular field profile results in lower noise operation for front-illuminated APDs, when compared to a rectangular field profile. The electrons injected from the π into the p-region encounter a low field and the holes generated within and in front of the gain region encounter a large field, both of which are shown by this analysis to be beneficial for low-noise carrier multiplication.[11]

While the noise of the gain process for front-illuminated epitaxial devices is somewhat larger than for back-illuminated bulk devices, the difference has only a small influence of approximately 1 dB on the overall receiver sensitivity. Device construction from epitaxial silicon makes fabrication with large-diameter wafers possible and avoids thinning and handling bulk wafers.

Referring to the cross section of the device, the epitaxial π region is typically 40 μm thick, has a resistivity in excess of 300 Ω-cm, and is grown

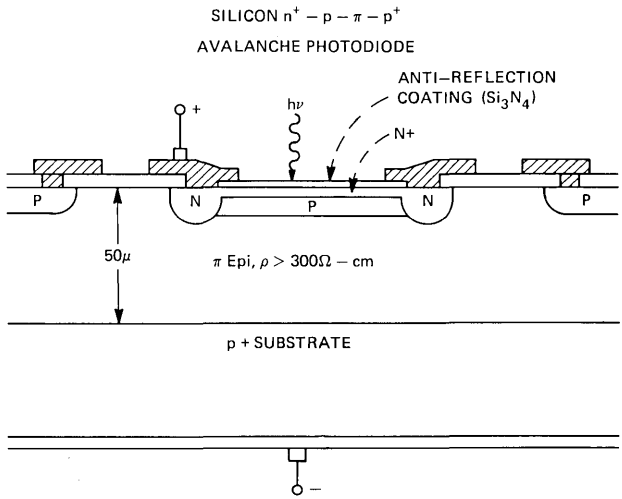

Fig. 1 — Cross-sectional view of epitaxial silicon n^+-p-π-p^+ avalanche photodiode made for illumination through the n^+ contact layer. Diameter of the light-sensitive high-gain region is 100 μm.

on dislocation-free boron-doped substrates. The light doping of the π region is required to minimize the voltage required to deplete the entire region between the n^+ contact and the p^+ substrate. The p^+ channel stop diffusion surrounding the device cuts off surface inversion channels, limits the lateral spreading of the depletion region, and ensures that the depletion region will not extend to surface areas beyond the immediate perimeter of the device. The doping in the p-control charge region is determined by a boron ion implantation and subsequent drive-in. Deeper drive-in produces lower excess noise but increases the operating voltage. The n^+ contact under the optical window is made very shallow to minimize both the carrier recombination and the hole injection from the n^+ region to the p-region, which would increase the noise of the device. To avoid the low breakdown voltage associated with the small radius of curvature of the shallow n^+-π junction, an n guard ring is diffused around the perimeter of the junction. This guard ring also reduces constraints on the metal contact by providing a deep junction under the contact windows. The device is passivated over the exposed π region with SiO_2 and Si_3N_4 layers. Over the optical window, Si_3N_4 is deposited to a controlled thickness as an antireflection coating for normally incident radiation.

The metal contacts are arranged to overlap the metallurgical n-π and π-p junctions. These field plates prevent the buildup of charge within and at the surface of the SiO_2 and Si_3N_4 layers near the edges of the junctions. If charges on the surface of the dielectric were permitted to build up there, they could induce sufficiently large electric fields to cause bursts of avalanche and zener breakdown currents.[12] High levels of surface charge concentrations would ultimately lead to increased leakage currents and reduced breakdown voltages. The field plates also increase the breakdown voltage at the perimeter of the n-π junction by effectively increasing the radius of curvature of the guard ring diffusion.[13–15] The avalanche breakdown of the APD is then a bulk rather than surface effect because of the additional charge in the p-region. Similarly, the region of high multiplication lies within the optical window and has a diameter of $\sim$100 μm.

The planar epitaxial n^+-p-π-p^+ avalanche photodiode described above provides both high reliability and processing capability in large diameter silicon wafers. Similar epitaxial structures are achieving attention, as indicated in several recent publications.[3,10,16–19]

III. FABRICATION

The actual device fabrication begins with the growth on p^+ substrates of (>300 Ω-cm p-type) 50-μm thick epitaxial material. The structure of Fig. 1 is formed by first diffusing the n-type guard ring and p-type channel stop. A carefully controlled boron dose is then implanted and

diffused into the center region of the APD. A heavily doped phosphorus layer is diffused into the back of the wafer to getter deep level impurities in the silicon. This gettering substantially reduces the dark currents. A shallow n^+ (phosphorus) contact is deposited and the time of its drive-in diffusion is adjusted to control the current gain-voltage characteristics of the device. The wafers are annealed in an HCl ambient to reduce the mobile ion content of the surface oxide, and Si_3N_4 is deposited to passivate the structure. The Si_3N_4 is impervious to ionic contamination such as Na^+.

The n^+ diffused layers are removed from the back of the wafer, and an ohmic contact is formed by ion implantation of boron. At this point, the wafer is approximately 450 μm thick and has good mechanical strength. The front surface metallization is Ti-Pt-Au formed over sintered PtSi, and the back metal is Ti-Au.

PIN photodetectors are obtained with this fabrication sequence by omitting the boron ion implantation. Like the APDs, the PIN detectors have low leakage and capacitance and excellent reliability.

IV. CHARACTERISTICS

A relatively large number of optical and electrical characteristics contribute significantly to the performance of the avalanche photodiode. The characteristics of the n^+-p-π-p^+ APD that are of interest in the FT3 application are:

(*i*) Quantum efficiency.
(*ii*) Current gain-voltage characteristics.
(*iii*) Dynamic range.
(*iv*) Temperature and wavelength dependence of the gain-voltage characteristics.
(*v*) Uniformity of the gain under the optical window.
(*vi*) Excess noise as a function of wavelength and nominal gain.
(*vii*) Speed of response.
(*viii*) Capacitance.
(*ix*) Temperature dependence of the dark current.
(*x*) Reliability for 300-V operation.

The subject of system performance is treated in other papers in this volume.

4.1 Quantum efficiency

Consider first the quantum efficiency of the front-illuminated structure for normally incident radiation. The spectral response characteristics of Fig. 2 show the quantum efficiency of these avalanche photodiodes to be greater than 90 percent over the wavelength range from 680 to 860 nm. The accuracy of the measurements is $\sim\pm5$ percent.

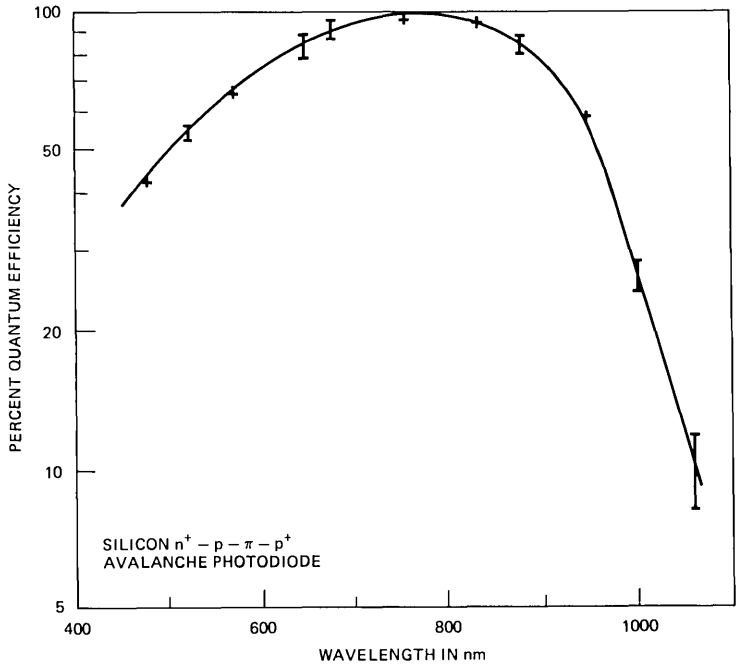

Fig. 2 — Spectral response curve of silicon n^+-p-π-p^+ avalanche photodiode with 40-μm wide π-type carrier collection region and SiO_2-Si_3N_4 antireflection coating.

The antireflection coating keeps the surface reflection to less than ~3 percent at 800 nm. Recombination in the thin n^+ contact and at the surface becomes substantial for wavelengths less than 600 nm. The response drops rapidly beyond 900 nm as the radiation penetrates deeply into the p^+ substrate.

4.2 Gain-voltage characteristics and dynamic range

Typical gain-voltage characteristics for different temperatures and with excitation at 825 nm are shown in Fig. 3. The operating bias range of these avalanche photodiodes extends from the onset of current gain at 60 V and complete sweepout around 100 V to avalanche breakdown at 250 to 400 V. At sweepout, the current gains (M) are between 5 and 10, and before breakdown they increase to values of several hundred.

In the FT3 system, the bias on the APD is decreased to reduce the gain for high levels of radiation. This current gain control adds to the dynamic range of the receiver. For the APD of Fig. 3, the dynamic range is given by the ratio of the maximum gain (M = 80 in the FT3 system) to the minimum gain ($M \simeq 6.5$ at 150 V bias), which is 11 dB of optical power. The minimum bias is determined by the speed of response requirements discussed in Section 4.5.

To preserve the dynamic range in the APD, the control charge doping was precisely adjusted to obtain the above characteristics. It is well

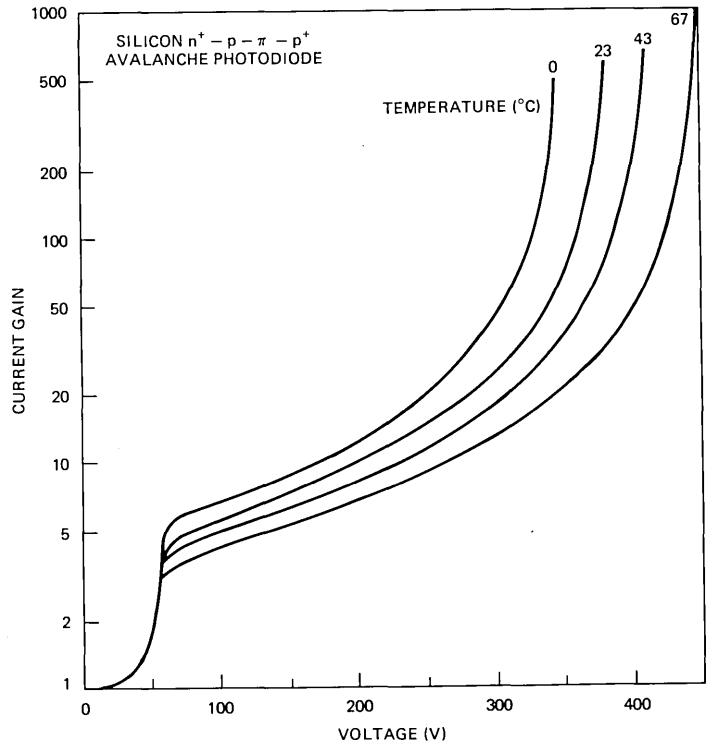

Fig. 3 — Current gain-voltage characteristic of silicon n^+-p-π-p^+ avalanche photodiode at different temperatures measured with excitation at 825 nm.

known that the breakdown voltage of n^+-p-π-p^+ structures are very sensitive to the charge of the p region.[20] A small increase of approximately 10 percent in the p region doping reduces the breakdown voltage by more than 100 V, but simultaneously increases the gain at the minimum bias. Lower voltage APDs are then characterized by lower dynamic range. For the front-illuminated APD with high resistivity epitaxy, the operating voltage range could be reduced from 150 V minimum–400 V maximum to 120 V minimum–200 V maximum (23°C), where the only engineering trade-off would be a reduction in the dynamic range from 12:1 (11 dB) to 4:1 (6 dB of optical power).

The gain-voltage characteristics show a pronounced dependence on temperature. As can be seen from Fig. 3, a bias voltage change of 1.4 V/°C is needed to keep the gain constant as a function of temperature. In addition, the gain-voltage characteristics show some dependence on wavelength of excitation, especially at short wavelengths, as shown in Fig. 4. The decrease in gain throughout the operating bias range at short wavelengths is due to mixed initiation of the avalanche by electrons and holes when most of the light is absorbed in the n^+-p region close to the silicon surface. The ionization coefficient for holes is smaller than that for electrons causing a reduction in the total current gain.

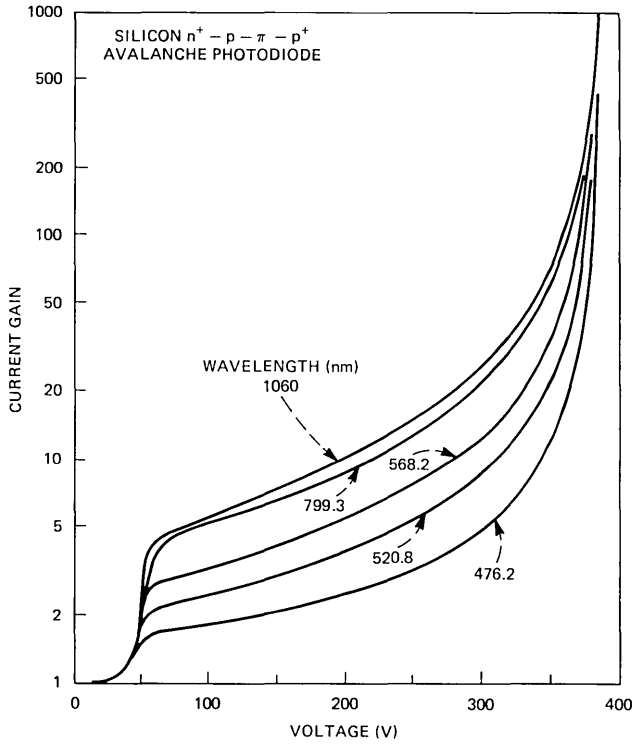

Fig. 4 — Current gain-voltage characteristics of silicon n^+-p-π-p^+ avalanche photodiode at room temperature for different wavelengths of optical excitation.

4.3 Current gain uniformity

The current gain uniformity is extremely important for the noise performance of the APD. Nonuniformities arise from two primary sources—crystalline defects and doping density fluctuations in the p-region.

Certain defects lead to premature breakdown spots or microplasmas. At their onset, the microplasmas generate irregularly fluctuating spikes of current that render the detectors useless for weak light signals. Through proper measures such as the choice of low dislocation materials and processing that does not introduce additional defects, the number of devices with disturbing microplasmas can be kept small.

All avalanche photodiodes exhibit high noise at the onset of bulk breakdown.[21,22] The breakdown noise is first observed as current pulses or spikes. In good devices, the breakdown noise threshold is substantially above the voltage for an average optical gain of 100, typically by 20 V. As the device is operated at higher gains, the regions of locally higher electric field develop a rapidly increasing tendency to support very large multiplication. Equivalently, the tail of the probability distribution extends rapidly to higher multiplications. A finite probability develops

that a single incident electron will produce a very large number of secondaries (i.e., 1000 to 10,000 carriers). The voltage onset of the avalanche noise is then believed to depend on the region of highest electric field in the APD.

A second source of electric field enhancement, after crystalline defects, is local fluctuations in the doping of the p region. When operating at an optical gain of 100, the APD will experience approximately 10 percent increase in gain for a doping fluctuation of 0.1 percent. The importance of the uniformity of the ion implantation for the p region cannot be overstated.

In the APD fabricated in this work, the avalanche carrier multiplication is quite uniform over the center part of the light-sensitive area of the diodes. This can be seen from Fig. 5, where the current gain as a function of position of the photoexcitation is shown for different bias voltages. At a maximum gain of 100, the gain is uniform within ±5 percent over a diameter of 75 μm and ±10 percent over a diameter of 90 μm.

4.4 Excess multiplication noise

The multiplication process in the avalanche photodiode increases the noise in the output current beyond the multiplied shot noise of the photocurrent. The source of the excess noise lies in the fluctuations in the avalanche process. The incident electrons are accelerated by the high

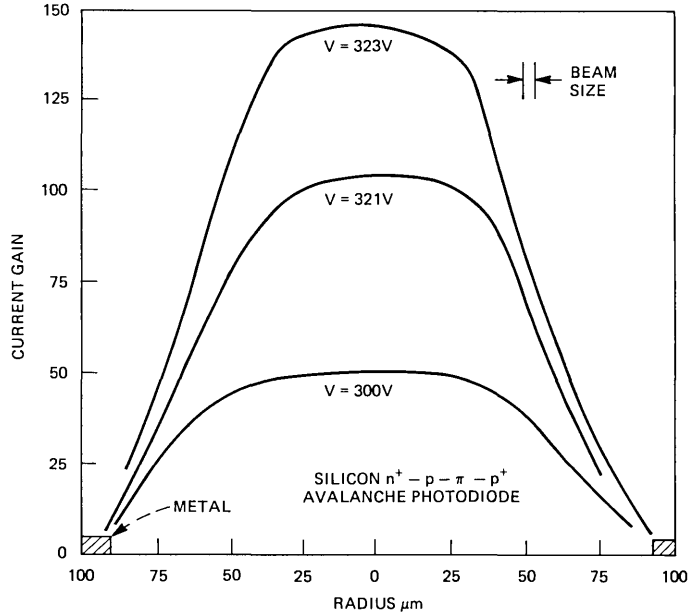

Fig. 5 — Spatial variation of the current gain across the light-sensitive area of an avalanche photodiode at different bias voltages. Measurements were done by scanning with a 3-μm light spot at 799.3 nm.

electric field and at the same time experience various inelastic scattering processes. When they achieve sufficient energy above the band gap, they can generate secondary electron-hole pairs. These charge carriers in turn gain sufficient energy to create additional electron-hole pairs. An ideal multiplier would provide exactly the same number of secondary electrons for each incident electron. In practice, the random nature of the scattering processes produces a broad distribution of multiplication factors. The current gain M of the APD is the average of the distribution of the multiplication factors. This statistical variation in the multiplication process increases the noise fluctuations of the output current.

A measure of the excess noise is given in the equation below, where the excess noise factor,

$$F(M) = \frac{\langle i_m^2 \rangle}{\langle i_{ph}^2 \rangle \times M^2}, \tag{1}$$

is defined as the measured mean-square noise current $\langle i_m^2 \rangle$ at the output of the avalanche photodiode divided by the product of the mean square noise $\langle i_{ph}^2 \rangle$ of the primary photocurrent and the square of the average gain M. Equivalently, the noise spectral density of the APD current is written as

$$\frac{d}{df} \langle i^2 \rangle = 2q \langle i_{ph} \rangle M^2 F(M). \tag{2}$$

The noise factor increases with gain reflecting a broadened distribution of multiplication factors. The development of a long tail in the distribution toward high multiplication factors at high electric fields was discussed in the previous section in connection with breakdown noise. The detailed dependence of $F(M)$ on M determines the optimum avalanche gain to be used with a given receiver front end and ultimately the optimum sensitivity of the receiver. The quantity $F(M)$ is often approximated by the relation $F(M) = M^X$, but a more exact expression, and one which is equally tractable mathematically, is[5]

$$F(M) = M\left[1 - (1 - k)\left(\frac{M - 1}{M}\right)^2\right] \tag{3}$$

or

$$F(M) = 2(1 - k) + kM, M \gg 1. \tag{4}$$

where k is the effective ratio of the ionization coefficients of holes and electrons, suitably averaged over the high field region where avalanche occurs. The value of k depends upon the detailed electric field profile within the avalanche region and also upon the extent to which the avalanche is initiated by holes.

Shown in Fig. 6 is the excess noise factor of an APD as a function of

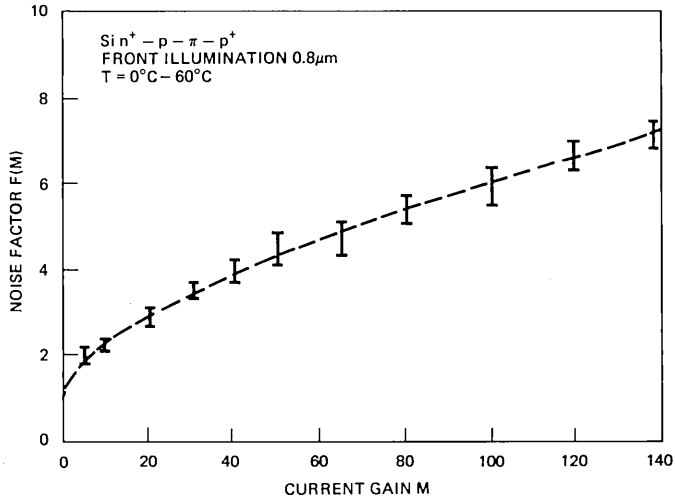

Fig. 6 — Noise factor $F(M)$ as a function of average current gain M for silicon n^+-p-π-p^+ avalanche photodiode at 800 nm. The measurement bars give an indication of the noise spread measured on devices made from different wafers.

gain. The measurement was done at room temperature; however, the excess noise factor is quite independent of temperature, at least over the 0° to 60°C range investigated. The excess noise at an average gain of 100 for excitation at 800 nm is only a factor of 5 to 6 higher than the shot noise limit of an ideal multiplier. This noise factor compares favorably with the noise factor of $F(M = 100)$ of 3 to 5 measured for the best bulk n^+-p-π-p^+ devices with illumination through the p^+ contact and pure electron initiation of the avalanche.[10] The value of k extracted from Fig. 6 at 800 nm is ~0.04.

Lower excess noise and k values are obtained for small increases in the width of the high field region. An extension of the multiplication region allows lower electric fields where the ratio of hole-to-electron ionization coefficients becomes even smaller.[8] However, the knee of the current gain-voltage characteristic (at 60 V in Fig. 3) corresponding to the depletion voltage of the p region moves to higher voltages increasing the voltage requirements for the APD. Additionally, for front-illuminated devices, wider p regions cause a larger fraction of the multiplication to be initiated by holes. For wide p regions, this effect determines the noise of the APD. Consequently, an optimum doping profile exists for the desired wavelength range. As discussed in Section II, the front-illuminated devices show lower noise for a triangular rather than a square electric field profile, where the initiating electrons first encounter a low electric field. To the first order, the electric field of the p region is essentially triangular because of the doping profile after drive-in.

Noise factor measurements on another APD with excitation at different wavelengths are shown in Fig. 7. While the lowest noise, $F(M = 100) =$

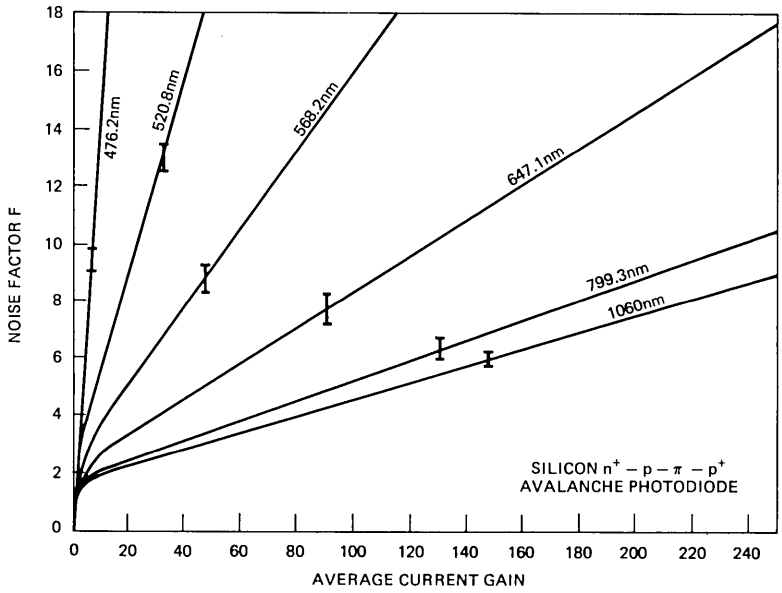

Fig. 7 — Noise factor $F(M)$ as a function of average current gain for optical excitation at different wavelengths.

4, is observed for excitation at long wavelengths at 1060 nm, the noise at 799 nm is not significantly higher, $F(100) \sim 5$. Actually, the diodes are quite low in excess noise even for mixed injection at 647 nm.

The overall penalty in optical sensitivity at $\lambda = 825$ nm incurred by the mixed injection of holes and electrons was $\lesssim 1$ dB of optical power. The ability to fabricate this device structure with a planar, high-voltage process is judged to outweigh the loss of 1 dB in sensitivity.

4.5 Response time and capacitance

To gain a measure of the speed of response, the duration of the multiplied output current pulses was investigated as a function of bias voltage for excitation with short laser spikes of 220 ps duration from a GaAlAs laser at 838 nm. The output pulses are quite symmetric in their rise and fall times without any tails at the end of the pulses. As depicted in Fig. 8, the duration of the output pulses at full depletion above 100 V is at most a few nanoseconds. At high bias voltages, where the holes drift with almost saturation-limited velocity through the π region, the pulse duration at 50 percent amplitude is less than 1 ns. At bias voltages less than 100 V, the pulse response becomes slower due to lower drift velocities and carrier diffusion within the undepleted π region.

The FT3 application requires a pulse width of 20 ns. To minimize jitter, the rise and fall times of the APD should be on the order of 1.0 to 2.0 ns. This requirement sets the minimum bias voltage at 150 V.

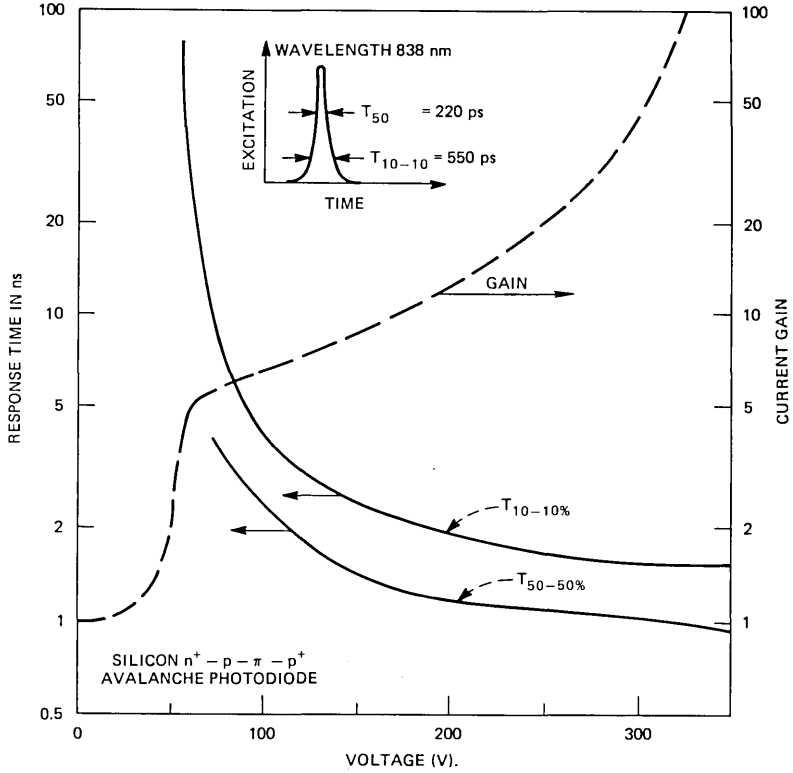

Fig. 8 — Response time and gain of multiplied photocurrent as a function of bias voltage for a silicon n^+-p-π-p^+ avalanche photodiode excited with pulses from a GaAlAs laser at 838 nm. The insert shows the shape and duration of the laser spikes as measured with a fast germanium photodiode.

Over the range of operating voltages, the capacitance of the avalanche photodiode is nearly independent of voltage. For a 40-μm π region, the capacitance is ~0.3 pF. The capacitance-voltage characteristic at lower voltages is given in Fig. 9. The gradual drop in capacitance between 0 and 50 V reflects the movement of the depletion layer through the p region. The rapid drop around 55 V corresponds to the movement of the depletion layer into the π region. The APD reaches full sweepout at ~85 V bias.

4.6 Leakage currents

Leakage or dark currents in the avalanche photodiode can be generated in the bulk of the depleted region due to thermal generation of carriers, or they can originate at the surface and bulk terminations of the space charge regions. The major part of the leakage of a typical APD is collected at the perimeter in a low field portion of the junction. These currents simply create a small offset that is not of importance to the

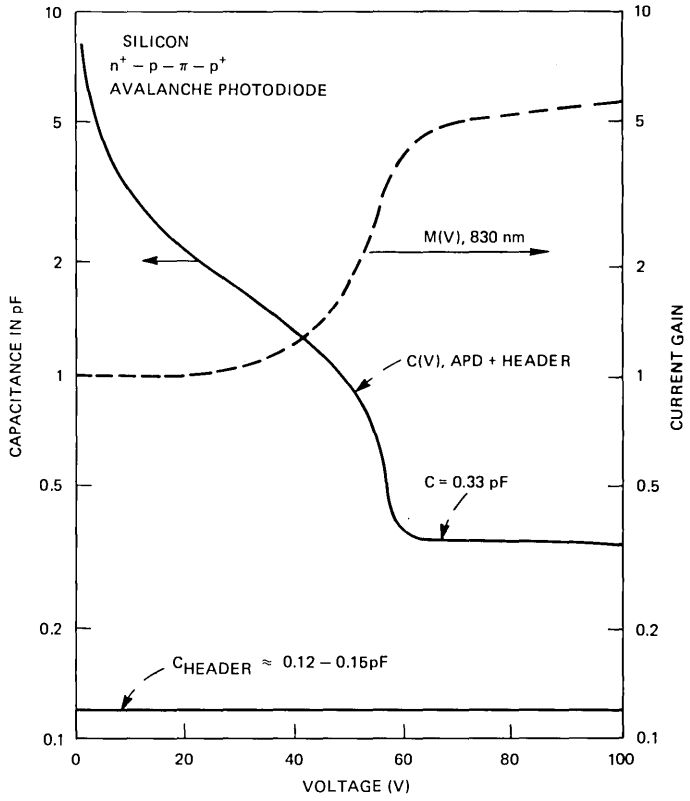

Fig. 9 — Capacitance and gain of an avalanche photodiode on a header as a function of bias voltage. From the difference between the total capacitance of the device and header and the capacitance of the header, it can be inferred that the capacitance of the device chip is between 0.2 and 0.3 pF at full depletion.

optical repeater. The leakage current collected in the high field portion of the junction is a potential source of noise since it experiences 80-fold multiplication in the APD. If the leakage current that is to be multiplied approaches the photocurrent induced by the laser in its off state, the noise of the APD would be increased. The smallest laser off-state photocurrents before multiplication fall between 10^{-10} and 10^{-9} A. By comparison, the leakage current to be multiplied is less than 10^{-12} A (at 23°C), and is negligible over the full temperature range of 0 to 60°C. Low leakage is achieved in these devices through the use of low dislocation materials, processes that avoid defect formation, and a back surface phosphorus diffusion gettering to eliminate fast-diffusing, deep-level impurities.

In Fig. 10, the dark current of a well-gettered APD with a 100-μm diameter active region is plotted as a function of reciprocal temperature. The dark current around room temperature is due to carrier generation

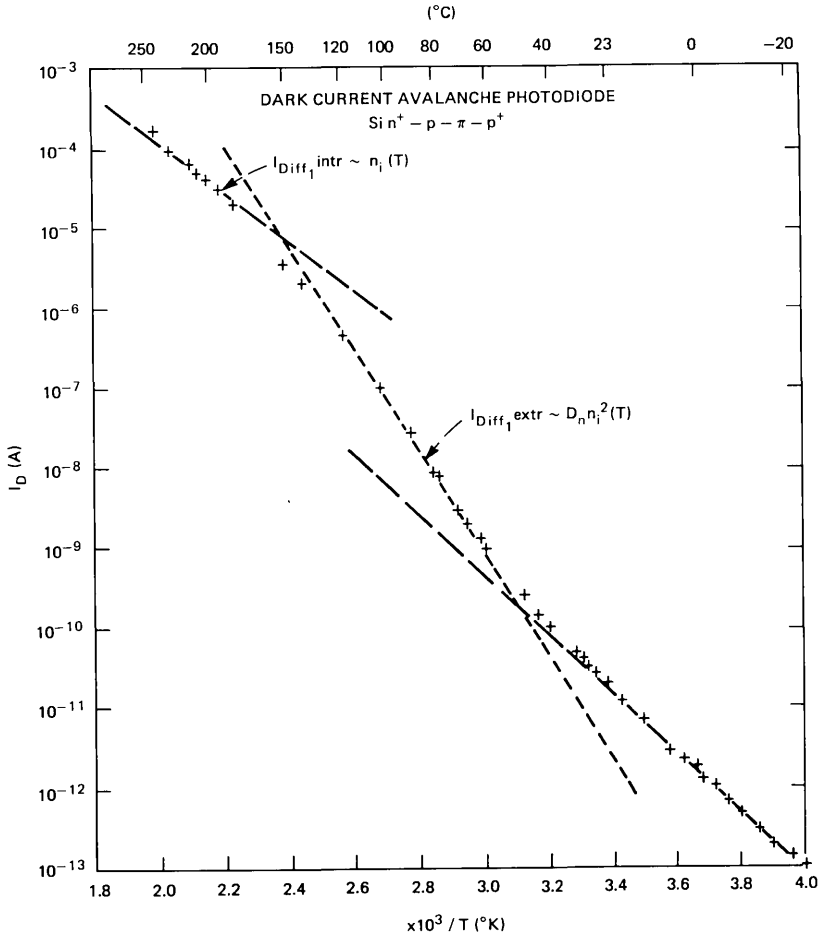

Fig. 10 — A plot of dark current as a function of reciprocal temperature for an avalanche photodiode with a 100 μm diameter high gain region and an overall diameter of 360 μm of fully depleted π region (40 μm thick).

from impurity centers with energy levels close to the middle of the bandgap. From the temperature dependence of the current between −20° and +40°C, the thermal activation energy for the carrier generation in these well-gettered devices is estimated to be 0.66 to 0.69 eV.

At higher temperatures between 40 and 150°C, the dark current increases with temperature in proportion to the square of the intrinsic carrier density as

$$n_i^2(T)D_n(T), \tag{5}$$

where $D_n(T)$ is the temperature-dependent diffusion constant of the electrons. Based on numerical estimates and measurements on devices of different diameters, it is suggested that this dark current component

is due to the diffusion of electrons out of the undepleted high resistivity π-type sidewalls of the device.

For temperatures in excess of 150°C, the intrinsic carrier concentration exceeds the doping in the π region. The leakage resulting from electron diffusion out of the APD's perimeter then increases in proportion to the intrinsic carrier concentration.[23]

4.7 Reliability

The avalanche photodiodes are reliable, having mean times to failure in excess of 10^3 hours at 200°C and 300-V bias in hermetic packages. Assuming an activation energy of 0.7 eV, which is estimated from the accelerated aging of several groups at different temperatures, the mean time to failure is in excess of 10^7 hrs at room temperature. This reliability results from the silicon nitride passivation, the gettering of mobile ions, and the use of field plates as discussed in Section II. Failures occur in devices without field plates because of surface charge accumulation over doped regions of the device. The surface charge induces high electric fields which reduce the breakdown voltage or produce breakdown noise.

V. SUMMARY

Front-illuminated, epitaxial silicon avalanche photodiodes having an n^+-p-π-p^+ structure are well suited to the detection of 800- to 900-nm radiation in fiber waveguide systems. The APD-developed for the FT3 system is a state-of-the-art device providing high quantum efficiency, ~1-ns response times, and low excess noise and dark currents. The APD allows ~15-dB improvement in receiver sensitivity, when compared to a nonavalanching photodiode. Its fabrication as a planar device on large-diameter, high-resistivity epitaxial wafers provides substantial improvements in manufacturability and reliability.

VI. ACKNOWLEDGMENTS

We are greatly indebted to R. P. Deysher and R. G. McMahon of Western Electric for the development and fabrication of the high-resistivity epitaxial material and to R. E. Carey and R. S. D'Angelo who contributed to the process development. Many helpful discussions with G. A. Rozgonyi, R. A. Moline, R. Edwards, R. G. Smith, A. U. MacRae, and M. DiDomenico are also acknowledged.

REFERENCES

1. H. Melchior, Physics Today, *30* (1977), p. 32.
2. J. S. Cook, J. H. Mullins, and M. I. Schwartz, paper presented at Conference on Lasers and Electro-optical Systems, San Diego, Calif. (1976), p.25.
3. H. Melchior and A. R. Hartman, Technical Digest of the International Meeting on Electron Devices (Wash., D.C.), IEEE, New York (1976), p. 412.

4. S. D. Personick, *Fundamentals of Optical Fiber Communications,* New York: Academic Press, 1976, p. 155.
5. R. J. McIntyre, IEEE Trans Electron Dev., *ED-13* (1966), p. 164.
6. C. A. Lee, R. A. Logan, J. J. Kleimack, and W. Wiegman, Phys. Rev., *A134* (1964), p. 716.
7. H. Ruegg, IEEE Trans. Electron Dev., *14* (1967), p. 239.
8. P. P. Webb, R. J. McIntyre, and J. Conradi, RCA Rev., *35* (1974), p. 234.
9. J. Conradi and P. P. Webb, IEEE Trans. Electron Dev. *22* (1975), p. 1062.
10. T. Kaneda, H. Matsumoto, T. Sakurai, and T. Yamaoka, J. Appl. Phys., *47* (1976), p. 1605.
11. H. Melchior, D. P. Schinke, and A. R. Hartman, unpublished work.
12. S. R. Hofstein and G. Warfield, IEEE Trans. Electron Dev., *ED-12* (1965), p. 66.
13. S. M. Sze and G. Gibbons, Solid State Electron., *9* (1966), p. 831.
14. D. S. Zoroglu and L. E. Clark, IEEE Trans. Electron Dev., *ED-19* (1972), p. 4.
15. L. E. Clark and D. S. Zoroglu, Solid State Electron., *15* (1972), p. 653.
16. H. Kanbe, T. Kimura, Y. Mizushima, and K. Kajiyama, IEEE Trans. Electron Dev., *ED-25* (1976), p. 1337.
17. T. Kaneda, H. Matsumuoto, T. Sakurai, and T. Yamaoka, J. Appl. Phys. *99* (1976), p. 1151.
18. S. Takamiy, A. Kondo, and K. Shirahata, Meeting of the Group on Semiconductors and Semiconductor Devices, Inst. of Elect. and Comm. Engr. of Japan, Tokyo, Japan, 1975.
19. H. Kanbe, T. Kimura, and Y. Mizushima, IEEE Trans. Electron Dev., *ED-24* (1977), p. 713.
20. T. E. Seidel, D. E. Iglesias, and W. C. Niehaus, IEEE Trans. Electron Dev., *ED-21* (1974), p. 523.
21. R. J. McIntyre, IEEE Trans. Electron Dev., *ED-19* (1972), p. 703.
22. R. J. McIntyre, IEEE Trans. Electron Dev., *ED-20* (1973), p. 637.
23. A. S. Grove, *Physics and Technology of Semiconductor Devices,* New York: John Wiley, 1967, p. 176.

THE BELL SYSTEM TECHNICAL JOURNAL
Vol. 57, No. 6, July–August 1978
Printed in U.S.A.

Atlanta Fiber System Experiment:

Optical Detector Package

By R. G. SMITH, C. A. BRACKETT, and H. W. REINBOLD

(Manuscript received February 10, 1978)

The optical detector package used in the Atlanta Fiber System Experiment is described. The detector subsystem consists of an avalanche photodetector and a transimpedance amplifier packaged in a dual in-line configuration, with a connectorized optical-fiber pigtail for optical interfacing. We describe here the design, operation, and construction of the amplifier circuit, the gain and noise characteristics of the avalanche photodetector, and the experimental performance of 53 completed packages. The design is found to meet or exceed all system performance goals. The measured performance of the 53 subsystem packages gives an average optical sensitivity of −54.1 dBm (BER = 10^{-9}) with a standard deviation of 0.28 dB, a transimpedance of 13.7 kΩ, a dynamic range of 76 dB (38 dB of optical power), an effective quantum efficiency of 69 percent, and a frequency response corresponding to complex poles located at −70 ± j56 MHz. The optical sensitivity was found to be unchanged within experimental error when measured at 50°C. Preliminary life testing of 32 units, 10 of which are operating at 60°C, has produced no failures in over 7×10^5 equivalent device hours. These are very encouraging results and imply a device reliability approaching that required for system applications.

I. INTRODUCTION

This paper describes the design, packaging, and performance characteristics of the optical detector packages used in the receiver portion of the regenerator employed in the Atlanta Fiber System Experiment recently completed in Atlanta, Georgia.

The goal of this development effort was to design a self-contained optical detector package containing the photodetector along with the associated preamplifier which would operate at the DS3 transmission

rate (44.7 Mb/s), achieve good sensitivity, possess a wide dynamic range, and be easily interfaced both optically and electrically to the printed circuit board and backplane. The design was also to produce a level of performance representative of a manufacturable unit. This latter constraint affected several of the engineering choices made during this development.

The optical detector package, to be described in detail below, employs an avalanche photodiode as the optical detector and a transimpedance amplifier as the interface between the detector and the remainder of the linear channel. The combination is enclosed in an EMI shield and potted in plastic to provide mechanical rigidity. Optical interfacing is accomplished by use of a short piece of optical fiber connected on one end to the APD and on the other end to an optical connector. Electrical interfacing is achieved via pins designed to fit either into a socket or on to a printed circuit board.

The performance of 53 detector packages fabricated and evaluated for this project includes a measured optical sensitivity of −54.1 dBm with a standard deviation of 0.3 dB for a bit error rate of 10^{-9} and a dynamic range of 38 dB of optical power compared to design goals of −53 dBm and 30 dB, respectively. Measured performance at 50°C showed no degradation from room temperature results.

II. CIRCUIT DESCRIPTION

The front end of an optical receiver consists of a photodetector, generally a PIN or avalanche photodiode, along with some form of amplifying stage or stages. The overall combination of the detector, amplifier, and subsequent filtering is designed to respond to the input light signal in such a way as to provide an output pulse shape—usually with a raised cosine spectrum—appropriate for presentation to the digital decision circuit. The combination, referred to as the linear channel, must therefore have sufficient bandwidth to respond properly to the input pulse. It should also contribute as little noise as possible in order to give a good optical sensitivity.

A number of approaches to the design of the input amplifier or front end have been investigated. The most straightforward method is to terminate the detector in a load resistor, R, chosen such that in combination with the input capacitance of the amplifier, C, the RC time constant is sufficiently small to reproduce the input pulse shape. This approach, though straightforward, has been shown to be excessively noisy.[1-3]

An alternative to this approach, usually referred to as the high impedance or integrating front end, used extensively in nuclear engineering, has been analyzed in detail by Personick.[1] He shows that it has less noise and results in considerable improvement in optical sensitivity compared

to the technique discussed above. Receivers have been designed and built using integrating front ends, verifying the predicted noise reduction and sensitivity improvement.[2,3]

The essential feature of the design of a low-noise front end is minimizing the contributions of the various sources of noise, including those resulting from leakage currents in the photodiode, thermal noise associated with biasing resistors, and noise associated with the amplifying transistors. If the input signal source is a photodiode, which looks like a current source shunted by a capacitor,[4] minimizing the noise is accomplished by increasing the values of biasing resistors, reducing all associated capacitances, and minimizing leakage currents.[1] For a bipolar transistor, choice of an optimum collector current is also required.[5] Such an optimization results in an amplifier which has a bandwidth considerably smaller than that required to reproduce the desired pulse shape. This situation is remedied by subsequent equalization which can be performed with little or no noise penalty.

Although this approach has been shown to give optimum performance, there are several drawbacks. First of all, the degree of equalization will depend upon the parasitics of the circuit. This introduces the possibility that circuits would require equalization on an individual basis—an undesirable step from a manufacturing point of view. The most serious drawback, however, is the loss of dynamic range resulting from the equalization.[6]

A third approach, and the one employed here, is to use a shunt feedback amplifier, commonly referred to as a transimpedance amplifier, which is essentially a current-to-voltage converter. A simplified diagram of the transimpedance amplifier is shown in Fig. 1. In the limit of large gain, the output voltage, V_o, is related to the input current, i, by the relation

$$V_o = -Z_F i, \tag{1}$$

where Z_F is the feedback impedance.

The feature of the transimpedance amplifier that makes it desirable for the present use is that, compared to an unequalized amplifier that does not employ feedback, it is less noisy for a given bandwidth or alternatively has more bandwidth for a given noise level. Compared to an

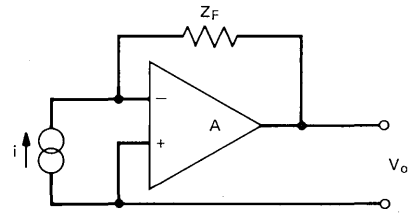

Fig. 1—Schematic representation of the transimpedance amplifier.

optimized, equalized amplifier of the high impedance design, a receiver employing the transimpedance amplifier along with an avalanche photodetector requires approximately 1 dB more optical power to achieve a given error rate. Circuit simplicity, eliminating the need to employ equalization, and obtaining increased dynamic range were judged worth the 1-dB loss in sensitivity.

A schematic diagram of the transimpedance amplifier used here is shown in Fig. 2. The first two transistors comprise the feedback pair or transimpedance portion of the circuit; the third stage provides additional gain and isolation. Q_1 was chosen to have as small an input capacitance as possible and was selected to have a high β. Q_2 and Q_3 were unselected devices of the same type, chosen for commonality in bonding technique. A tendency of early circuits to oscillate was eliminated by using a resistance in the base of Q_2. Other components shown in Fig. 2 are used for filtering and bypassing.

The basic transimpedance of the feedback pair is approximately given by the feedback resistor, in this case, 4 kΩ. To increase the output signal level to 4 mV peak to peak at the minimum optical signal level, the gain of the third stage was chosen to be 3.7, giving an effective transimpedance of 14.8 kΩ.

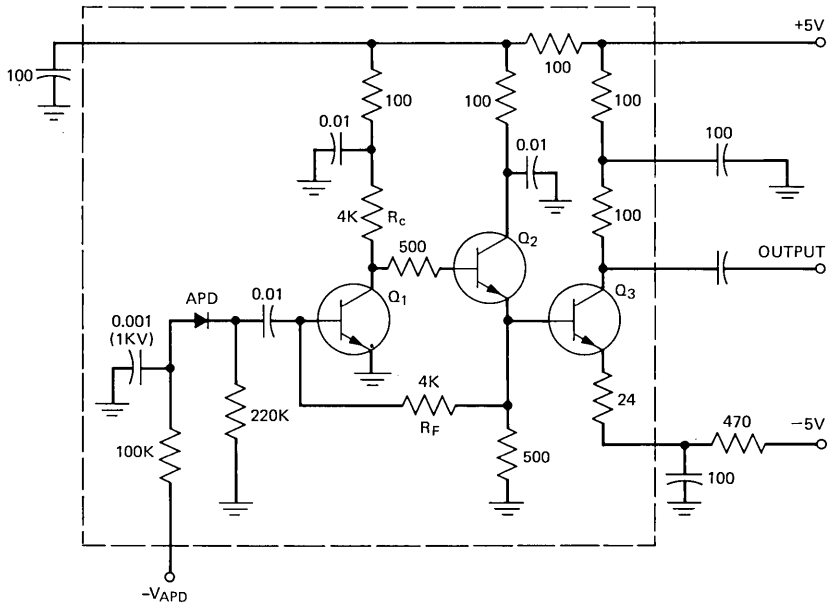

Fig. 2—Circuit diagram of the amplifier used. Components shown within the dotted line are included within the package.

III. AVALANCHE PHOTODIODE

The photodetector used in the optical detector package is an avalanche photodiode (APD). This detector, designed and developed for this application, is described in a companion paper.[7] The essential feature of the avalanche photodiode is that it provides internal multiplication of the photo-generated current that improves the sensitivity of the receiver.

A typical gain-versus-voltage curve for the avalanche photodetectors used is shown in Fig. 3. The important features of this curve are the rapid increase in the gain with voltage near 50 V reverse bias and again near 400 V. The first region is associated with the depletion of the device, the second with approach to self-sustained avalanche breakdown. The device must be operated at a voltage in excess of that required to deplete the π region in order to obtain adequate speed of response and below self-sustained breakdown where the device is excessively noisy. More specifically, the devices used here could operate with a minimum gain of approximately 6, at which point they were sufficiently fast, and were capable of producing gains in excess of 100. (As discussed later, the optimum gain was found to be 80.)

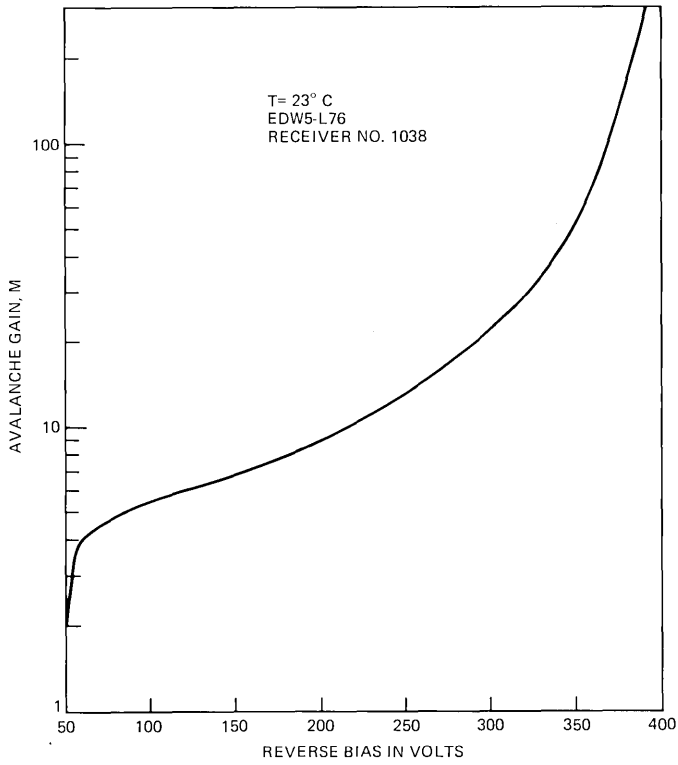

Fig. 3—Room temperature gain curve of an avalanche photodiode typical of those used in the detector packages.

The gain of the avalanche photodiode is temperature-dependent, requiring approximately 1.5 V per °C increase in bias voltage to achieve constant gain. To compensate for temperature variations and for varying input light levels, the bias to the diode, which is generated by an up-converting power supply located on the main board, is controlled by a feedback loop which maintains the signal level at the output of the linear channel at a constant value.[8] The range over which the APD gain is varied extends from a minimum value of approximately 6 (at high light levels) to 80 (corresponding to an error rate of 10^{-9} at the minimum detectable optical power level). Further discussion of the operation of the gain control of the linear channel may be found in Ref. 8.

IV. PACKAGE DESIGN

The physical design of the optical detector package was approached with the goal of designing a unit that would be physically sturdy and that could be easily interfaced with the circuit board and backplane both electrically and optically. Electrical interfacing was achieved using a standard electrical pin configuration to permit the package to be plugged into a socket on the printed circuit board. Optical interfacing was achieved through the use of an optical pigtail—a short piece of optical fiber protected by a plastic sheath—placed in proximity to the APD on one end with a molded optical connector on the other end. Fig. 4 is a photograph of the completed package.

In this design, the APD and the optical pigtail were packaged as a subassembly, and this subassembly was later attached to the ceramic circuit board. This approach was taken to simplify the package development and to permit separate testing of the APD and circuit. More recent packaging approaches coupled with improved circuit design have resulted in a detector package with the APD chip mounted directly to the circuit board, yielding a more compact package with improved performance.

The amplifier circuit was fabricated using thick-film technology. The transistors used were beam-lead, sealed-junction devices that were thermocompression-bonded to the thick-film circuit. The ceramic circuit board with the APD subassembly attached was placed within an EMI shield, and the entire assembly was potted in plastic to provide mechanical rigidity to the electrical pins and the optical pigtail.

V. PERFORMANCE CHARACTERISTICS

During the course of this development, approximately 100 detector packages were fabricated; of these, 53 were characterized in detail. The results and comparison with theory, where appropriate, are summarized below.

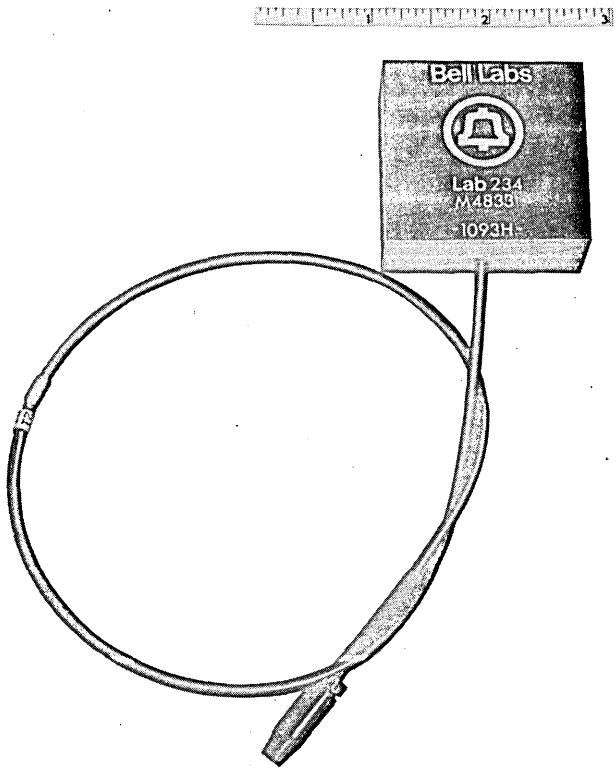

Fig. 4—Finished optical detector package.

5.1 Equivalent input noise current density

The optical sensitivity of an optical receiver is determined primarily by the equivalent input noise current density of the detector-amplifier combination and the avalanche characteristics of the APD. For a transimpedance amplifier of the type used here, there are several principal sources of noise including: (*i*) thermal noise of the feedback resistor, R_F, (*ii*) shot noise of the base current of Q_1, (*iii*) shot noise associated with the collector current of Q_1, and (*iv*) leakage currents in the photodetector. The APD used here was designed to minimize leakage currents and in all cases, even at elevated temperatures, noise associated with surface leakage and bulk dark currents was completely negligible. Further, for the collector current used in Q_1, the contribution from (*iii*) is expected to be small. The dominant noise sources for the present circuit

are thus the feedback resistor and the base current of Q_1. For these noise sources, the spectral density of the equivalent input noise current will be flat and is given by

$$\frac{d}{df}\langle i^2\rangle = \frac{4kT}{R_F} + 2qI_B, \tag{2}$$

where

k = Boltzmann's constant
T = absolute temperature
q = electronic charge
I_B = base current of Q_1
R_F = feedback resistor.

Using $R_F = R_C = 4\ \text{k}\Omega$ and $V_{cc} = 5$ V, eq. (2) reduces to

$$\frac{d}{df}\langle i^2\rangle = 4.14 \times 10^{-24}\left(1 + \frac{70}{\beta}\right), \tag{3}$$

where $\beta = I_C/I_B$ and T is taken to be 300 K. Taking $\beta = 150$, a typical value for the transistors used, eq. (3) has a value of 6.07×10^{-24} A^2/Hz.

The above noise current density is, by assumption, independent of frequency. The actual frequency dependence was determined by measuring the output noise spectral density with a spectrum analyzer, referring this to the input using the measured frequency response of the amplifier. The results are shown in Fig. 5, where the noise is found to be flat out to approximately 20 MHz with a 3-dB corner frequency of 87.5 MHz. When the frequency response of the filter used to limit the noise and shape the pulse is taken into account (the system response is down 10 dB at 40 MHz and 20 dB at 54 MHz), the contribution to the total output noise from the frequency dependent portion is found to be negligible. Thus, assuming a flat equivalent noise spectral density at the input introduces little error in receiver sensitivity calculations.

The absolute magnitude of the input noise spectral density was determined by measuring the total output noise power (after the filter, using a true rms power meter) and referring this to the input using known amplifier gains, the measured transimpedance, and the measured characteristics of the filter. The resultant mean input noise current density was found to be 6.92×10^{-24} A^2/Hz. The difference of 0.6 dB between the measured and calculated values may be due in part to noise sources that have been neglected, but a significant contribution is believed due to uncertainties in the determination of the transimpedance.

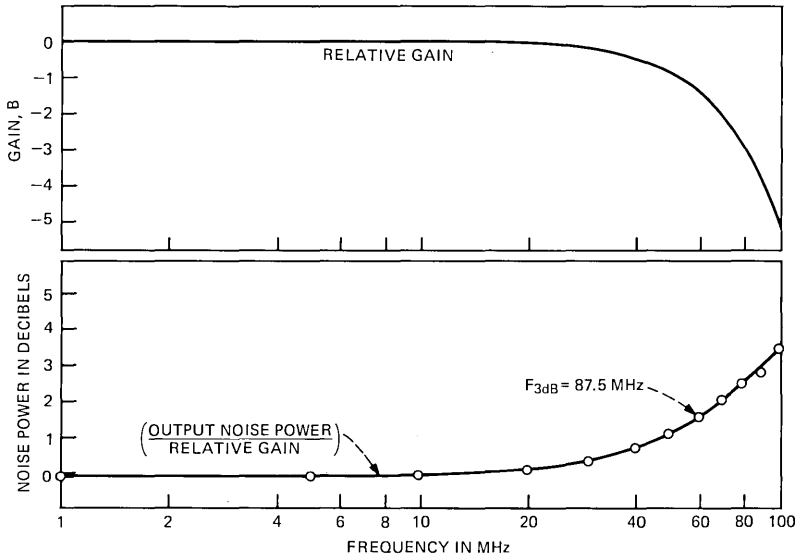

Fig. 5—Plots of relative gain and effective input noise current density as functions of frequency.

5.2 Receiver sensitivity

The sensitivity of an optical receiver is given by[2]

$$\eta\bar{p} = h\nu \frac{Q}{2}\left[\frac{Q\langle M^2\rangle B}{M^2} + \frac{2}{qM}(\langle i^2\rangle)^{1/2}\right], \tag{4}$$

where

η = the overall quantum efficiency of the diode and coupling structure

$\bar{p}$ = the average optical power required to achieve a given bit error rate (BER), assuming an equal population of ones and zeros

Q = a function of the bit error rate; $Q \cong 6$ for BER $= 10^{-9}$

$h\nu$ = energy of a photon $\approx 2.4 \times 10^{-19}$ J

q = electronic charge $= 1.6 \times 10^{-19}$ coulomb

B = bit rate (assuming the two-level coding)

$(\langle i^2\rangle)^{1/2}$ = root-mean-square noise current of the amplifier referred to the input

$M = \langle M\rangle$ = average avalanche gain

$\langle M^2\rangle = \langle M\rangle^2 F(M)$ = mean square avalanche gain

$F(M)$ = excess noise factor associated with the avalanche process.

Equation (4) has been derived assuming that the noise in the zero state

is independent of the signal level and that the noise has a Gaussian amplitude distribution.

For a given bit rate, B, and error rate determined by Q, the average optical power required to achieve the error rate is a function of the average avalanche gain, $\langle M \rangle$, and the excess noise factor, $F(M)$. The excess noise factor, $F(M)$, is given by[9]

$$F(M) = M\left[1 - (1 - k)\left(\frac{M - 1}{M}\right)^2\right], \tag{5}$$

where k is an effective ratio of the ionization coefficients of holes and electrons in the avalanche region. For the devices used here, $k \approx 0.035$ for a front-illuminated diode and a wavelength of 825 nm.[10] The value of $\eta\bar{p}$ required to achieve an error rate of 10^{-9} ($Q = 6$) as determined from eqs. (4) and (5) is plotted in Fig. 6 as a function of M, using the average measured input noise current, $(\langle i^2 \rangle)^{1/2} = 1.45 \times 10^{-8}$ A. The curve indicates that the sensitivity is maximum for an avalanche gain of approximately 140 with an optimum value $\eta\bar{p} = -56.6$ dBm. The sensitivity for $M = 1$, corresponding to a p-i-n diode is -38.9 dBm. Also shown by the cross in the figure is the average measured sensitivity of 53 devices taken at an avalanche gain of 80. This value of gain was found to yield the optimum sensitivity as constrasted to the predicted value of ≈ 140. The optimum value of threshold for the decision circuit was found to be approximately 45 percent of the peak eye height in contrast to a considerably smaller value predicted by the theory.

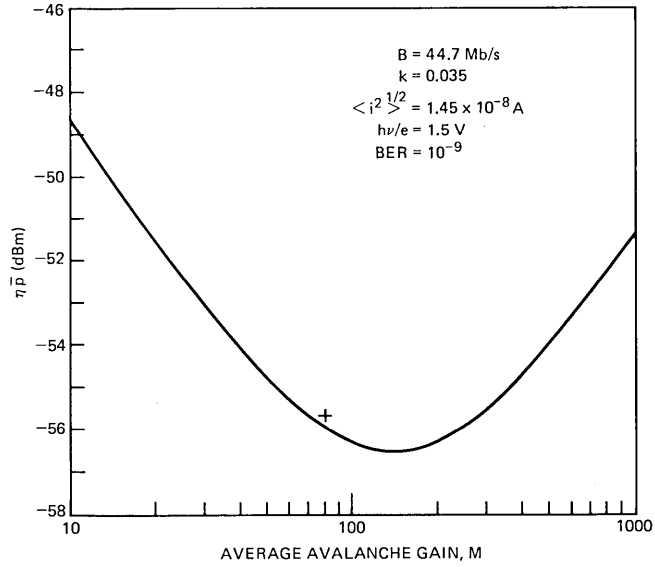

Fig. 6—Plot of the calculated optical sensitivity as a function of the average avalanche gain, M. The cross represents the average of the measured sensitivity of 53 receivers.

The primary reason for the above deviations is associated with the fact that the amplitude distribution of avalanche gain is not Gaussian, but is skewed toward higher gain values.[11–14] This has the effect of greatly enhancing the effective noise generated by current associated with the zero state of the incident light (determined by the extinction ratio of the source[15]). The rapid increase of this noise with avalanche gain effectively limits the extent to which the decision level can be lowered and hence reduces the optimum avalanche gain. Sensitivity calculations incorporating the non-Gaussian nature of the avalanche gain do, in fact, predict an optimum gain very close to the value of 80 determined here.[13] The measured sensitivity is seen to be in close agreement with that calculated from eq. (4) at a gain of 80.

A plot of the distribution of measured values of $\eta\overline{p}$ is shown in Fig. 7b. The mean value is −55.7 dBm with a standard deviation of 0.22 dBm.

5.3 Quantum efficiency

The sensitivity discussed above is expressed in terms of the product of the quantum efficiency, η, and the average optical power, $\overline{p}$. This is a convenient means of characterizing the sensitivity of receivers, as it requires only a measurement of the current drawn by the photodetector and a knowledge of the avalanche gain; it is not necessary to measure optical power, which can be difficult at such low power levels. By measuring the optical power, it is possible to determine $\overline{p}$ and thus to infer the quantum efficiency, η. A plot of the measured values of $\overline{p}$ is shown in Fig. 7a. The mean value is −54.1 dBm with a standard deviation of 0.28 dBm. Comparing the mean values for $\overline{p}$ and $\eta\overline{p}$, the mean quantum efficiency is calculated to be −1.6 dB, or 69 percent. Contributing to this value are coupling losses within the pigtail structure as well as the intrinsic quantum efficiency of the diode, which was typically 90 percent.

5.4 Temperature effects

The sensitivities of the optical detector packages were measured at

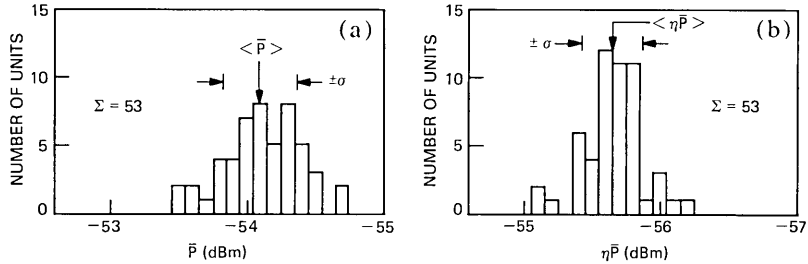

Fig. 7—Plots showing the distribution of optical sensitivities for a bit error rate of 10^{-9}.

50°C as well as at room temperature. Within ±0.1 dBm, and well within experimental error, the measured values were found to be the same at the two temperatures. There is thus no evidence of degradation in performance, at least to 50°C.

5.5 Pole locations

In the initial design of the amplifier, it was not known how accurately the pole locations could be controlled. It was thus decided to design the amplifier with sufficient bandwidth that any variations in its frequency response characteristics would not significantly affect the overall response of the linear channel including the final filter. The resulting amplifier design thus had a bandwidth in excess of that required for operation at 45 Mb/s, and its noise was correspondingly higher.

The frequency response of the detector package was measured by illuminating the APD with incoherent light and measuring the output noise spectrum with a spectrum analyzer. When the spectral density of the shot noise of the APD is much larger than that of the amplifier noise, the output noise is proportional to the amplifier response function. This response function was fitted, using a least-squares method, to a two-pole transfer function. The resulting pole locations were found to be complex with a mean value of $-70 \pm j56$ MHz. Although the poles are complex, they are sufficiently removed from the poles of the filter to have little effect on the overall system response. In amplifier designs performed subsequent to this development, careful attention to the reduction of parasitics has resulted in amplifiers with real poles and bandwidths in excess of those reported here.

5.6 Power supply requirements

The circuit was designed to operate from nominal +5 V, −5.2 V power supply voltages. No variation in performance of the detector package was observed for variations of ±1 V about these nominal values.

5.7 Dynamic range

One of the principal reasons for choosing the transimpedance design was to obtain a large dynamic range. The dynamic range of the amplifier is defined as the ratio of the maximum output voltage swing to the value when the receiver is operating at maximum sensitivity. For an error rate of 10^{-9}, $\eta\bar{p} = -55.7$ dBm and using $M = 80$, the peak input current to the amplifier is calculated to be 0.29 μA. With a measured transimpedance of 13.7 kΩ, the output voltage is 4 mV p-p. The maximum output voltage swing is found to be ±0.9 V, limited by the third-stage biasing and the use of ac coupling of the APD to the amplifier. The resultant dynamic range is then 53 dB electrical, or 26.5 dB of optical power.

The overall dynamic range of the optical detector package includes the range of available gain of the APD as well as the dynamic range of the amplifier. The ratio of the optimum gain ($M = 80$) to the minimum value where the device becomes slow ($M \cong 6$) gives an additional contribution to the dynamic range of 22.5-dB electrical or 11.3-dB optical. The overall dynamic range of the optical detector package is then approximately 76-dB electrical or 38-dB optical power, compared to a design goal of 30-dB optical power.

VI. SUMMARY

An optical detector package consisting of a silicon avalanche photodetector and a low-noise amplifier has been developed for experimental studies of a fiber-optic system operating at 45 Mb/s. The self-contained unit has been designed to plug into a printed wiring board and to interface optically via a connectorized optical pigtail.

The performance of the unit is characterized by an optical sensitivity of −54.1 dBm at a bit error rate of 10^{-9}, with a dynamic range in excess of 38 dB of optical power. Both values exceed the nominal specifications placed on the units. The range of measured sensitivities showed a rather tight standard deviation of 0.28 dBm, and performance was unchanged over the temperature range of 20°C to 50°C.

A number of units of this design have been successfully operated in the Atlanta Experiment and are currently being used in a field evaluation now under way in Chicago, Illinois.

VII. ACKNOWLEDGMENTS

The development of the detector package described here involved the contributions of many people within Bell Laboratories. In addition to those involved in the development of the avalanche photodiode, described in a companion paper, the authors wish to thank T. C. Rich for the package design; H. M. Cohen, W. B. Grupen, B. E. Nevis, E. L. Soronan, and A. E. Zinnes for supplying the thick-film circuits; M. M. Hower, F. M. Ogureck, and Tseng-Nan Tsai for providing transistors; A. W. Warner and W. W. Benson for supplying the fiber pigtails; M. F. Galvin, R. P. Morris, and J. R. Potopowicz for their excellent technical assistance; and D. P. Hansen and S. W. Kulba for fabricating the packages. The authors would like to express appreciation to G. L. Miller for many stimulating discussions and M. DiDomenico for his encouragement throughout the project.

REFERENCES

1. S. D. Personick, "Receiver Design for Digital Fiber Optic Communication Systems, Parts I and II," B.S.T.J., *52*, No. 6 (July–August 1973), pp. 843–886.
2. J. E. Goell, "An Optical Repeater With High-Impedance Input Amplifier," B.S.T.J., *53*, No. 4 (April 1974), pp. 629–643.

3. P. K. Runge, "An Experimental 50 Mb/s Fiber Optic PCM Repeater," IEEE Trans. Commun., *COM-24* (April 1976), pp. 413–418.
4. H. Melchior, *Laser Handbook,* Arecchi and Schulz-DuBois, eds., Amsterdam: North Holland, 1972, pp. 727–835.
5. J. E. Goell, "Input Amplifiers for Optical PCM Receivers," B.S.T.J., *53,* No. 9 (November 1974), pp. 1771–1793.
6. Y. Ueno, Y. Ohgushi, and A. Abe, "A 40 Mb/s and a 400 Mb/s Repeater for Fiber Optic Communication," Proceedings of the First European Conference on Optical Fiber Communication, 16–18 September 1975, IEEE Conference Publication, No. 132, pp. 147–149.
7. H. Melchior, A. R. Hartman, D. P. Schinke, and T. E. Seidel "Planar Epitaxial Silicon Avalanche Photodiode," B.S.T.J., this issue, pp. 1791–1807.
8. T. L. Maione and D. D. Sell, "Experimental Fiber-Optic Transmission System for Interoffice Trunks," IEEE Trans. Commun., *COM-25* (May 1977), pp. 517–522.
9. R. J. McIntyre, "Multiplication Noise in Uniform Avalanche Diodes," IEEE Trans. Electron Dev., *ED-13* (January 1966), pp. 164–168.
10. H. Melchior and A. R. Hartman, "Epitaxial Silicon n^+-p-π-p^+ Avalanche Photodiodes for Optical Fiber Communications at 800 to 900 Nanometers," Technical Digest IEDM Meeting, Washington, D.C., 1976, pp. 412–415.
11. R. J. McIntyre, "The Distribution of Gains in Uniformly Multiplying Avalanche Photodiodes: Theory," IEEE Trans. Electron Dev., *ED-19* (June 1972), pp. 703–713.
12. J. Conradi, "The Distribution of Gains in Uniformly Multiplying Avalanche Photodiodes: Experimental," IEEE Trans. Electron Dev., *ED-19* (June 1972), pp. 713–718.
13. S. D. Personick, P. Balaban, J. H. Bobsin, and P. Kumer, "A Detailed Comparison of Four Approaches to the Calculation of the Sensitivity of Optical Fiber System Receivers," IEEE Trans. Commun., *COM-25* (May 1977), pp. 541–548.
14. P. Balaban, "Statistical Evaluation of the Error Rate of the Fiberguide Repeater using Importance Sampling," B.S.T.J., *55,* No. 6 (July–August 1971), pp. 745–766.
15. P. W. Shumate, Jr., F. S. Chen, and P. W. Dorman, "GaAlAs Laser Transmitter for Lightwave Transmission Systems," B.S.T.J., this issue, pp. 1823–1836.

THE BELL SYSTEM TECHNICAL JOURNAL
Vol. 57, No. 6, July–August 1978
Printed in U.S.A.

Atlanta Fiber System Experiment:

GaAlAs Laser Transmitter for Lightwave Transmission Systems

By P. W. SHUMATE, JR., F. S. CHEN, and P. W. DORMAN

(Manuscript received February 16, 1977)

A feedback-stabilized GaAlAs injection laser optical-communication source for transmission of NRZ data at 44.736 Mb/s has been built and tested. The emitter-coupled driver circuit and the feedback scheme utilizing an operational amplifier are described. Two special hybrid packages contain the circuit components on thick-film substrates, and the package holding the laser provides laser heat-sinking as well as the interface between the laser and optical fiber. The laser source packages that were fabricated were capable of launching an average power of >0.5 mW into the 55-μm diameter core of a graded-index fiber (N.A. = 0.23). The sources draw a total of 0.9 W from the +5.0 V and −5.2 V (±5 percent) supplies and operate properly over a temperature range of 5° to 55°C.

I. INTRODUCTION

An experimental lightwave communication system has been designed and set up in an environment approaching field conditions at the Bell Laboratories facility in Norcross, Georgia to study the feasibility of optical fiber transmission systems in interoffice digital trunking.[1] The experimental system operates at the DS-3 signal rate (44.736 Mb/s, the third level of the Bell System digital hierarchy) using a binary (on-off) nonreturn-to-zero (NRZ) signal format. Terminal transmitters and line regenerators require an optical source to convert the ECL-level logic signals to optical signals of 0.5 mW average power into a transmission fiber. GaAlAs injection lasers are sources well suited for this application, as they can be on-off modulated at high speeds (with rise times of less than 1 ns) with low drive power. In addition, the laser light can be effi-

ciently coupled into low N.A. fibers, and the laser wavelength and linewidth are nearly optimum for digital transmission in low-loss glass fibers. However, some inherent disadvantages must be circumvented before GaAlAs lasers can be used in practical optical fiber systems, the most important of which is the temperature sensitivity of the laser.

A two-package GaAlAs laser source subsystem was designed and built to operate at 44.7 Mb/s over the temperature range 5° to 55°C. One package contains the GaAlAs double-heterostructure injection laser operating at 825 nm and the driver modulation circuitry. This package also interfaces the laser to the fiber. The second package contains circuitry to provide closed-loop feedback control of the laser output power, rendering this insensitive to changes in ambient temperature or changes in laser parameters due to aging. Sixty-two functioning subsystems were fabricated. This paper describes the circuits and packages and gives data on the overall source subsystem performance as a function of temperature including output power, power stability, pulse response, extinction ratio, and amplitude ripple.

II. DRIVER CIRCUIT

For the 44.736-Mb/s trunking application, the following requirements were specified. First, the peak light-pulse output must remain constant, regardless of changes in temperature or changes due to laser aging. Second, the extinction ratio (on-off ratio of the light pulses) should be $\geq$10 to avoid an excessive sensitivity penalty at the receiver.[2] Third, the delay time between the application of a current pulse and the onset of laser emission must be much shorter than the bit interval so that the light pulses accurately reproduce the digital input signal. Fourth, the relaxation oscillation of the light-output pulses excited by the application of fast current pulses should be damped. Depending on the design of the system, this oscillation may degrade the system's performance. The driver circuit described in this section, used with the laser bias circuit described in the next section, meets these four requirements for a 44.7-Mb/s source subsystem.

Figure 1 shows the response of a semiconductor laser diode to current through the device. A typical diode exhibits spontaneous or LED light for currents below about 100 mA, the lasing threshold. Above this threshold, the output is predominantly coherent laser light. The ratio between these two levels determines the on and off states in the digital signal. To operate at >10:1 on-to-off ratio in the laser transmitter, the diode is biased slightly below threshold at I_B (~90 mA) in the off or zero state. A high-speed driver then adds an additional current I_D (~20 mA) for a one state to bring the light level up to the on level. This scheme results in efficient, high-speed operation because the diode capacitance need not be charged repeatedly and the turn-on delay time of the laser

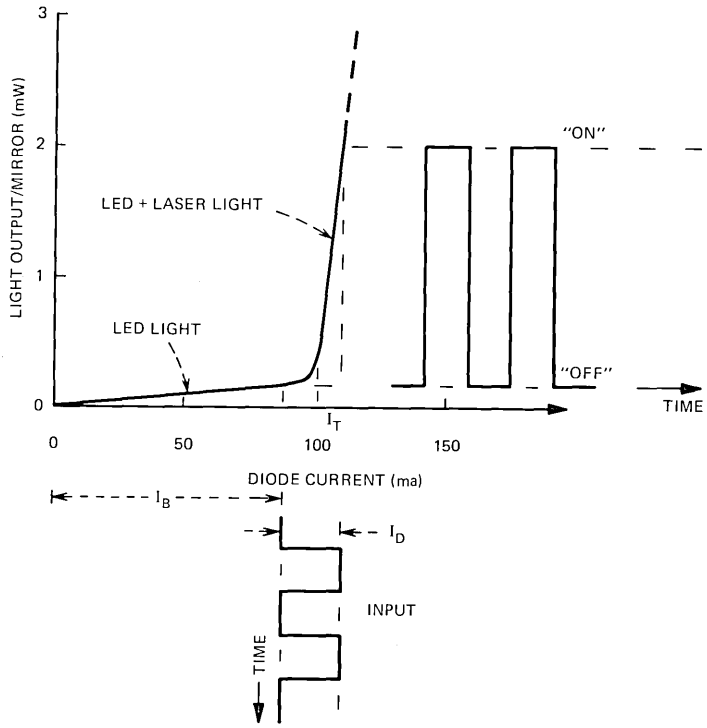

Fig. 1—Transfer characteristic of a semiconductor laser, shown with input (current) waveform and resulting light output.

emission is minimized. The demands placed on the high-speed switch are reduced since $I_D \ll (I_B + I_D)$. Undesirable effects due to pattern-dependent junction heating are minimized since the on and off power dissipations are nearly equal. Finally, the principal benefit of this biasing scheme is that the dc bias can be varied easily in a low-frequency, closed-loop manner to stabilize the light output of the laser. This can correct for slow changes in ambient temperature or gradual aging of the laser itself.

The drive current I_D is provided by an emitter-coupled current switch which supplies constant-amplitude pulses directly to the laser terminal. During assembly, these pulses, with switching speeds of approximately 2 ns, are adjusted in amplitude to match the particular laser being used and left unchanged as the laser ages. This driver circuit is shown in Fig. 2. Transistors Q_1 and Q_2, forming the current switch, are a conventional emitter-coupled pair. When the base of Q_1 is more positive than the base of Q_2, all the current ($= I_D$) from the current source is steered through the collector of Q_1 and no drive current passes through the laser. When the base of Q_1 is more negative than the base of Q_2, all

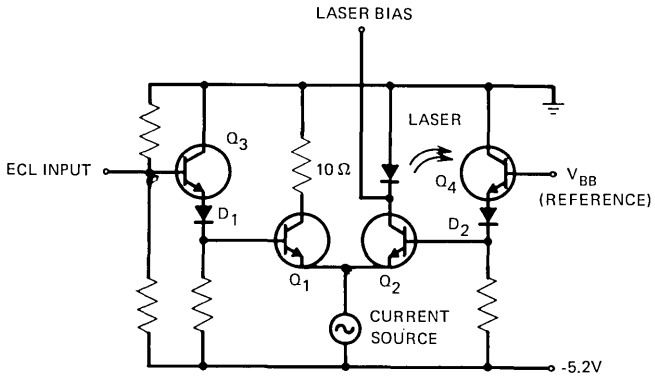

Fig. 2—Emitter-coupled driver circuit.

the drive current is steered through the laser. The selection of one of these conditions is made by an ECL input signal (one = −1.8 V, zero = −0.8 V) applied to the base of Q_1 after level shifting through Q_3 and diode D_1. The base of Q_2 is fixed at −2.6 V, a voltage midway between the shifted zero and one levels, by a temperature-compensated reference, V_{BB}.

With an emitter-coupled circuit and with proper choice of input voltage levels, none of the transistors can ever be driven into saturation. This results in fast switching since no stored charge need be removed from a saturated transistor. Another advantage of this driver configuration is its constant-current nature; minimum noise in the form of switching transients is placed on the power bus.

III. LASER BIAS CIRCUIT

Since the laser is a threshold device and the threshold changes with temperature and aging, the optical power level must be stabilized. This is accomplished using a feedback circuit (Fig. 3) to supply the dc bias I_B which is adjusted to maintain the peak light output constant relative to a reference. For these transmitters, light from the "back" mirror of the laser crystal is monitored using a p-i-n photodiode while light from the "front" mirror is coupled to the fiber. It was assumed for this development effort that the front and back intensities track each other as a function of temperature and aging, although they need not be equal in magnitude.

In a systems application, it is possible that the input signal may be removed from a channel for an extended period. A simple intensity regulator would tend to raise the bias during such an interval to maintain the average light level expected for ordinary random-data operation. This is not acceptable, since an idle channel would be transmitting half-intensity ones. With a reasonably fast bias circuit, this would occur even during long sequences of zeros in random data, thus generating errors.

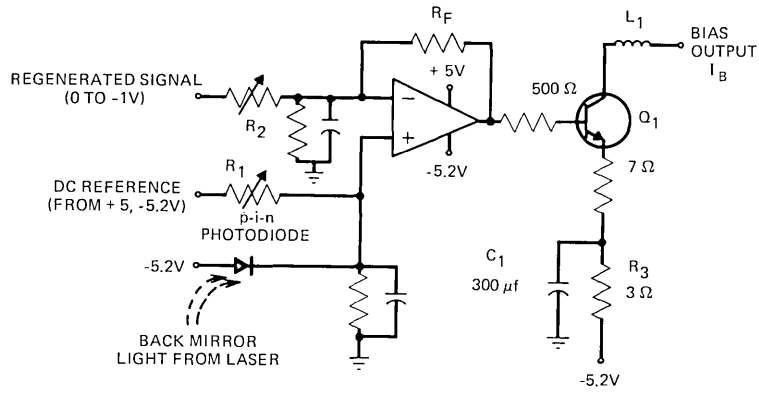

Fig. 3—Bias circuit that provides feedback stabilization of laser output.

To prevent this situation, the input signal pattern is fed to the feedback circuit so that the on, or lasing-light, level is compared with a one and the off, or LED-light, level is compared with a zero. In effect, the dc reference, through resistor R_1 in Fig. 3, sets the bias current at the proper operating point during long sequences of zeros. This bias current, when added to the drive current supplied by the circuit of Fig. 2, results in the desired peak output power. Resistor R_2 then balances the signal reference current against the p-i-n photocurrent for 50 percent duty ratio at 25°C. As the threshold of the laser changes, due either to aging or to changes in ambient temperature, the circuit automatically adjusts I_B so that the balance between the data reference and the p-i-n photocurrent is restored. The circuit will maintain the LED-light level during long sequences of zeros.

Since the input pattern serves as a precise reference, and also since ECL levels are temperature-dependent, the input signal is thus regenerated to temperature-independent 0-V and −1-V levels before reaching the feedback circuit. This regeneration uses an emitter-coupled driver very similar to Fig. 2 except the collector load resistances of Q_1 and Q_2 are large (500 Ω).

The operational amplifier of Fig. 3 sums the three inputs—p-i-n photocurrent, dc reference, and signal pattern reference—and provides an output voltage which results in the proper value of I_B through the action of transistor Q_1. This amplifier has unity gain at 800 kHz, permitting small bias corrections to be made in ~1 μs. This correction speed is desirable to prevent amplitude ripple effects resulting from pattern-dependent junction heating, but the circuit is slow enough to ensure stability with a loop gain of approximately 200.

Another function of the feedback circuit is to prevent a transient overshoot of light output from the laser when the power supplies common to both feedback and driver circuits are switched on and off. The scheme adopted here for the turn-on is to let the driver circuit and the

operational amplifier in the feedback circuit reach a steady-state operating condition first while the bias current is slowly increasing. The negative supply voltage to Q_1 in the feedback circuit (Fig. 3) is filtered by R_3 and C_1, providing an adequately long time constant of ~1 ms. Thus by the time the sum of the bias and the drive current reaches threshold, the feedback circuit is ready to limit the laser output to a predetermined magnitude with a minimum overshoot.

IV. OPTICAL INTERFACE

The transmission fibers used in the Bell Laboratories lightwave communications experiment had a 55-μm-diameter, GeO_2-doped, graded-index silica core and were clad with silica bringing the glass-fiber outside diameter to 110 μm. The fiber numerical aperture was approximately 0.23. Nylon jacketing was placed around the fiber for mechanical protection, bringing the diameter up to about 200 μm. The jacket has no optical function. Typical fibers with these parameters, when coated with DuPont ethylene-vinyl acetate (EVA) and assembled into transmission cables, display an average loss of 6 dB/km at 825 nm.[3]

A practical scheme for permanently affixing such a fiber near the stripe geometry laser is to use a single fiber optical jumper cable. This permits initial adjustment of the fiber for maximum coupling, yet still allows the package to be removed from system equipment along with the jumper and its optical connector without disturbing the laser-to-fiber interface. For this purpose a 40-cm jumper, or "pigtail," is assembled. The fiber, which is nylon-jacketed instead of EVA-coated for this application, is placed inside a 2.8-mm O.D. Teflon* sleeve, which provides additional mechanical protection. A special molded connector[4] is attached at one end, and several millimeters of fiber are left protruding from the Teflon at the other end. A spherical lens is melted on this end of the fiber, the lens raising the coupling from ≈35 percent without the lens to ≈55 percent, a gain of 2 dB.[5-7]

During packaging, the Teflon sleeve is attached to the package with a strain-relief bushing, and the free end of the fiber is positioned about 50 μm in front of the laser (see Fig. 4). A micropositioner is used to position the fiber for maximum coupling (the laser is operated as the light source), and the fiber is then cemented in place. This is a critical step. Coupling efficiencies of 50 to 55 percent are normally attained, but the sensitivity to transverse misalignment (i.e., parallel to plane of laser mirror) is high (see Fig. 5). For example, ±5 μm in either the x or the y direction results in 0.4-dB loss relative to maximum coupling.[8] As shown in Fig. 5, the longitudinal (z) direction is much less critical—the −1-dB point occurs after 40 μm of motion away from the laser mirror. Once

* Registered trademark of E. I. DuPont de Nemours and Company.

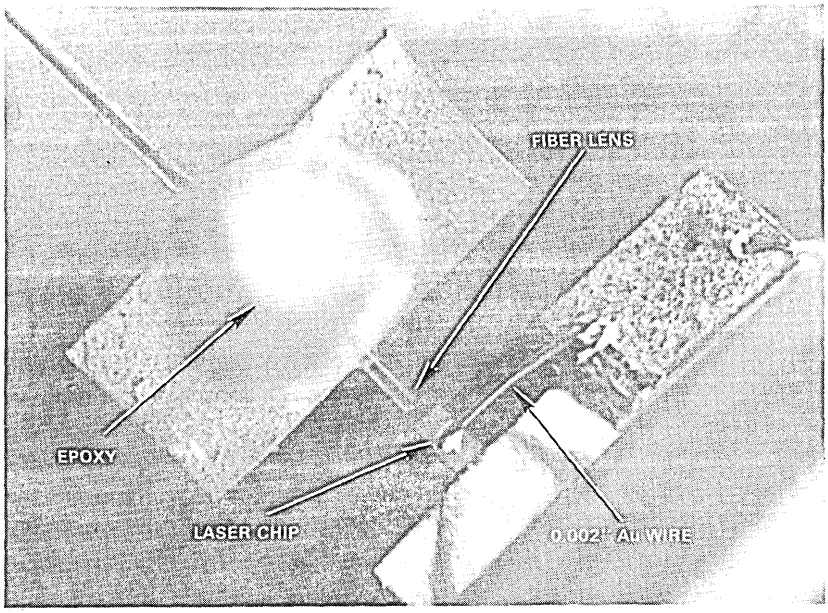

Fig. 4—Photomicrograph (40×) showing wire-bonded laser chip and lensed optical fiber cemented in position (cement is white material over fiber) after alignment.

cemented in place, however, the fibers in these packages have remained stably positioned.

V. PACKAGING

The two packages forming a complete transmitter subsystem are shown in Fig. 6. The laser and the driver circuit of Fig. 2 are placed in the larger of the two packages (5.1 × 7.0 cm) along with the fiber pigtail. The second emitter-coupled pair used to regenerate the signal for the feedback circuit is also placed in this package. The feedback circuit, including the series pass transistor for the bias current (Q_1 in Fig. 3), is in the smaller package (4.1 × 6.3 cm). This separation is done so that the power dissipated by the pass transistor will not interact thermally with the laser. The reasons for packaging the feedback components at all are so that high-reliability beam-lead silicon components can be used and so that all adjustments made during assembly will be sealed off from accidental changes, thus protecting the laser from damaging overdrives.

Components in both packages are bonded to thick-film, hybrid, integrated circuits. The metallization is Pd-Ag and the resistors are made using DuPont 1400 Birox-series paste. It was found that these resistors were stable in the presence of the amine potting epoxy (see the discussion below). Other materials used for resistors might be expected to show severe instability in the presence of amines.[9]

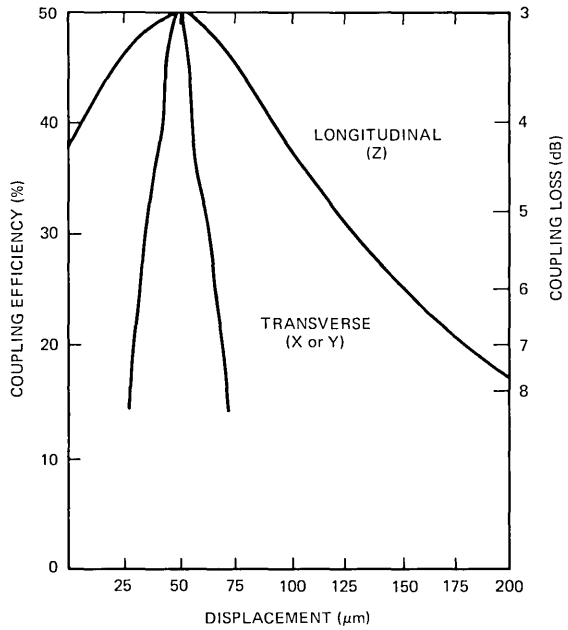

Fig. 5—Sensitivity of power coupled into a 55 μm-core fiber as functions of displacement perpendicular (longitudinal) and parallel (transverse) to plane of laser mirror.

The thick-film circuits, carrying pins for electrical connections, are attached to black-anodized, finned, aluminum heat sinks using silver-filled conductive epoxy. For the laser/driver package (Fig. 7 shows the internal details), a 2.5-cm dia. gold-plated copper header is placed under the thick-film circuit. This header was designed to facilitate heat flow between the laser and the aluminum heat sink. (The laser crystal is indium soldered to a gold-plated, rectangular copper pedestal. The pedestal, in turn, is indium soldered into a slot on the round head.)

As described above, the pigtail sleeve is secured to the driver heat sink. The fiber is positioned using the laser light as a monitor for maximizing the coupling, and the fiber end is cemented near the laser.

For both packages, the circuit is covered with an electromagnetic interference shield. Hysol 4179 potting epoxy is then added, filling out the package (the cavity in Fig. 7) to the outer dimensions of the aluminum heat sink. The p-i-n photodiode used to monitor the back laser mirror for feedback is mounted on a special standoff on the driver circuit (see Fig. 7). Potting materials are kept from obstructing the laser-photodiode optical path by using a plastic shield to create an internal cavity before potting.

One hundred package starts were attempted, resulting in 62 successful completions. Section VI summarizes the measurements made on these subsystems.

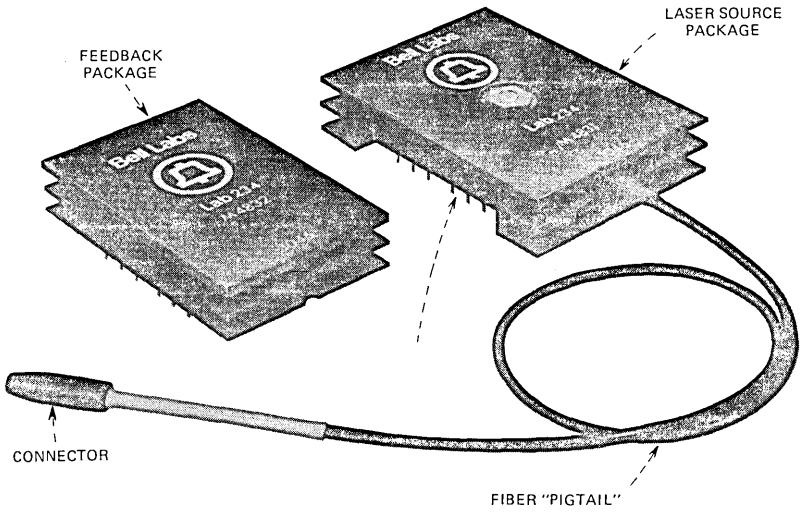

Fig. 6—Transmitter subsystem packages. The laser/driver package is shown on the right and the bias/feedback package on the left.

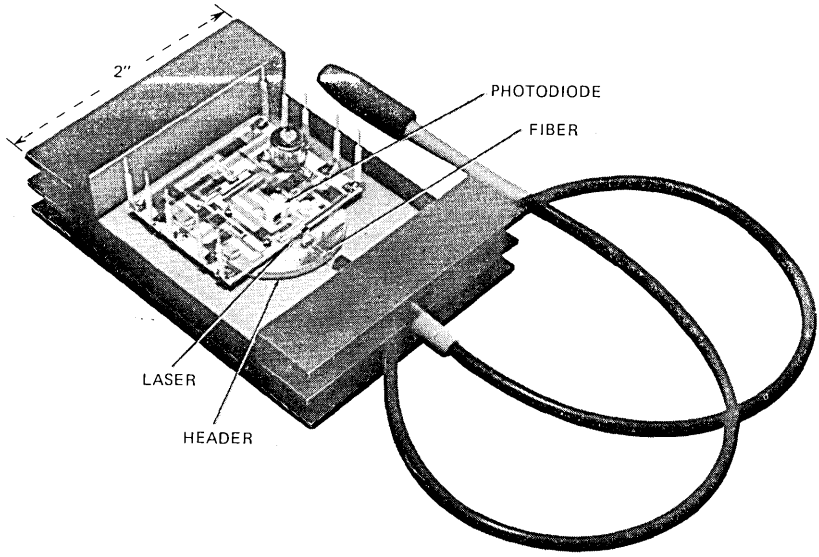

Fig. 7—Laser/driver package shown prior to final potting.

VI. PERFORMANCE CHARACTERISTICS

Table I lists the design goals for several parameters important to the systems application. These goals were selected for optimum performance of the experimental 44.736-Mb/s link. All goals were met for the completed units.

Table I — Summary of parameter design goals and measured values for 62 packages. Measurements were made at 25°C using a 1023-bit pseudo-random input word

Parameter	Goal	Measured
Average power output @ 25°C	≥0.5 mW	0.63 mW
Average power output @ 50°C	≥0.5 mW	0.63 mW
Amplitude variation (p-p)	≤10%	7%
Propagation delay*	<20 ns	5 ns
Extinction ratio	≥10:1	18:1
Operational temperature range	5–55°C	5–55°C
Power requirement	1.5 W	0.9 W

* Midpoint of ECL logic transition to midpoint of optical output.

6.1 Signal-pattern effects

Figures 8 and 9 show optical-output pulses under various conditions. In Fig. 8, a 500-MHz real-time oscilloscope was used in conjunction with an avalanche photodetector for a resultant rise-time of ≈1.5 ns. The output was measured at the connector end of the fiber pigtail. Figure 8a shows the optical output for a 0100110100 bit sequence (NRZ at 50 Mb/s). The spiking and relaxation oscillation of light-output pulses were reduced by choosing transistors and components to give a rise-time of ≈2 ns. (The spiking and oscillations disappear from Fig. 8a because of the slow response of the photodetector used.) Figure 8b shows an "eye" diagram—a superposition of pseudorandom zeros and ones. Such a trace includes the worst and best outputs and, since the pseudorandom sequence is relatively short (1023 bits), the worst-case bits are easily visible (from a duty-cycle point of view). Note that the eye is extremely clean with regard to amplitude ripple. Figure 8c shows the complete 1023-bit word twice using a slow sweep in the upper trace, while the lower trace shows that part of the sequence containing the worst-case pattern—9 zeros followed by 10 ones, at the 6.2-cm mark in the sweep. Notice that the pattern-dependent amplitude ripple is clearly less than 10 percent.

6.2 Temperature effects

Figure 9 shows the pulse-shape control supplied by the bias circuit as a function of temperature. For these data, a faster avalanche photodetector was used with a sampling oscilloscope for a resultant rise-time of ≈0.15 ns. Shorter data pulses lasting 10 ns were also used. The output was measured at the front mirror of the laser. No fiber was in the optical path. Figure 9a shows reasonably clean, constant-width pulses at 0°, 25°, and 45°C. Observe that the relaxation oscillation associated with the leading edge of each pulse is uniformly damped at each temperature. Figure 9b, however, shows the output degradation observed when the feedback loop, adjusted at 25°C, is opened and the temperature changed.

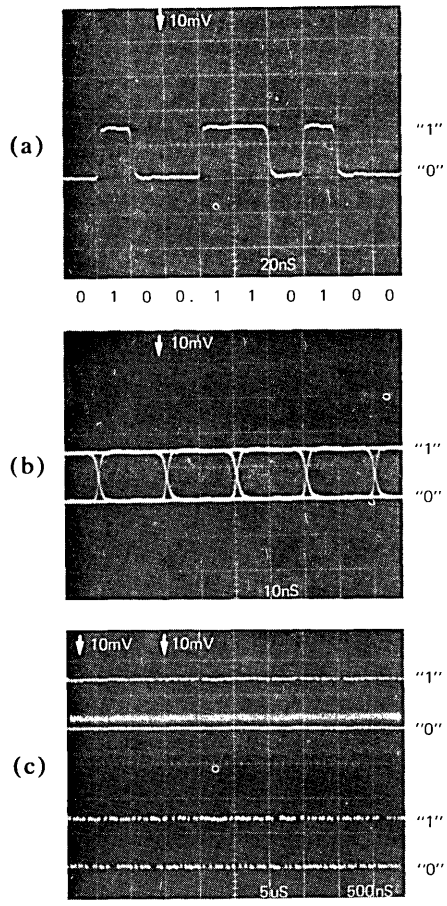

Fig. 8—Oscillographs of optical output as detected using an APD. Horizontal scales (t/div) are shown on each figure. (a) Individual NRZ bits. (b) Eye diagram using a 1023-bit pseudorandom sequence. (c) 1023-bit pseudorandom sequence showing the entire word (upper) and the worst-case sequence (lower), namely, ones after many sequential zeros near the 3, 6, and 9 cm ordinates.

At 35°C, the threshold rises. With the bias still at its 25°C value, the laser is biased too far below threshold, resulting in large relaxation oscillations and increased delay. In addition, the light output is down about 2 dB from its 25°C value. At 45°C, not shown in the figure, no lasing takes place because the sum of bias plus drive is now below threshold. Upon cooling to 0°C, which decreases the threshold, the pulses are excessively wide: biased very near threshold, the delay associated with reaching threshold is absent. The amplitude of the relaxation oscillations is decreased; this would be an advantage if it were not that this occurs only at a particular temperature. Finally, one notices that the light output increases although not as much as expected. This is because the partic-

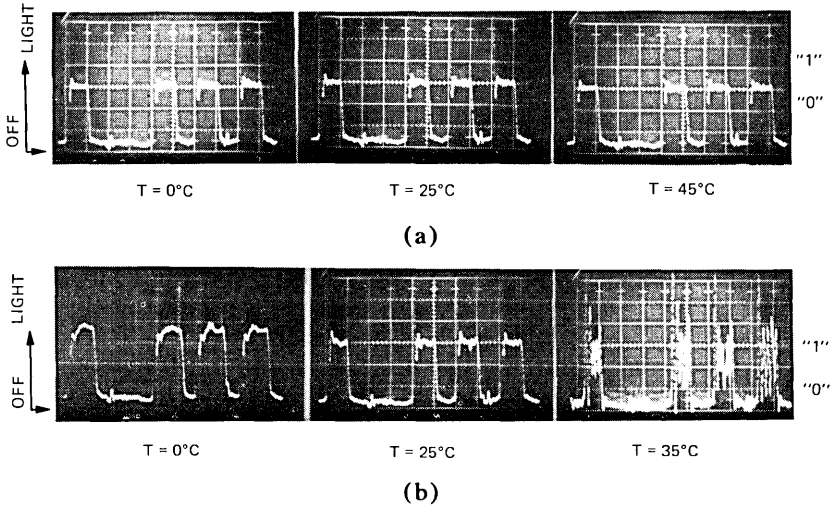

Fig. 9—Light-pulse patterns at various ambient temperatures detected using an APD. Horizontal scales are 10 ns/div. (a) With feedback circuit. (b) With feedback circuit disabled.

ular laser used for these photographs developed a nonlinearity in the operating region of its L-I characteristic at 0°C. Figure 9 clearly shows the stabilization provided by feedback control of the laser bias.

It is instructive to calculate the output-power regulation expected to be provided by the feedback circuit during changes in temperature. From an elementary closed-loop calculation, the light level subject to regulation can be related to temperature-induced threshold shifts as:

$$\frac{dP}{dT} = \frac{\partial P}{\partial I_T}\frac{dI_T}{dT} = -\frac{(1/4)\eta}{1 + A\beta}\frac{dI_T}{dT}, \tag{1}$$

where

P = average light power launched into fiber (mW)
T = temperature (°C)
I_T = laser threshold current (mA)
η = laser slope efficiency (mW/mA)
A = transfer gain of amplifier without feedback
β = reverse transmission factor.

The last factor β is a function of the p-i-n diode's quantum efficiency, the slope efficiency of the laser diode, and the coupling between the laser and the p-i-n diode. Typical values are:

P = 0.63 mW
I_T = 100 mA (T = 25°C)
η = 0.2 mW/mA (for each mirror)

$A = 23000$

$\beta = 0.01$

The factor of 1/4 in the numerator of (1) adjusts laser peak power for a 50-percent duty cycle (for random signals) and for the 50-percent coupling efficiency to the fiber. Since the threshold of these lasers shifts approximately +1 mA/°C, which is dI_T/dT, (1) gives

$$\frac{dP}{dT} = -0.2\,\mu W/°C. \tag{2}$$

Experimentally, a typical package showed a $\leqq 1$ percent power decrease as the package temperature was raised from 25°C to 50°C. For the data used above, this gives $dP/dT \approx -0.25\,\mu W/°C$, in very good agreement with the prediction in (2).

6.3 Aging effects

Approximately half the 62 completed units were used in the Bell Laboratories experiment, while the others were aged under normal operating conditions at 25° or 50°C. The principal aging characteristic of these lasers is a gradual increase of threshold current with time. Thus at either temperature, the closed-loop bias circuit should hold the output power quite constant with time until the circuit can no longer supply adequate current for a greatly shifted threshold. The circuit described here limits at about 225 mA. When the threshold, initially ~100 mA, reaches this value, the output power will begin to decrease as the laser continues to age. For both the 25° and 50°C packages, however, while some package outputs did remain constant with time, others showed increasing or decreasing power trends. Approximately as many packages showed increasing power as showed decreasing power.

A careful analysis of these packages showed that the feedback control circuitry was performing properly but that the front and back laser mirrors mistracked slightly.[10] Therefore, while the feedback circuit was maintaining constant power at the back mirror, the power launched into the fiber from the front mirror was not precisely regulated.

For power stability with aging, (1) can again be used if dI_T/dT is replaced by dI_T/dt, the value of, at most, +1 mA/1000 h.[11] Thus

$$\frac{dP}{dt} \leq -0.2\,\mu W/kh.$$

Due to the front-to-back mistracking, however, the output of our units varied from less than 10 to as much as 100 times more than this prediction, as well as changing in either direction, although the back-mirror power was maintained constant to within the resolution of our apparatus ($\pm 3\,\mu$W). For future transmitter designs, the power actually launched into the fiber should be monitored for feedback-control purposes unless lasers, at that time, demonstrate better front-to-back tracing.

VII. SUMMARY AND CONCLUSIONS

An optical communications source has been designed for use at 44.736 Mb/s. Sixty-two such transmitters were completed, meeting the design goals and clearly demonstrating the viability of using GaAlAs injection lasers for stable optical sources in lightwave communications. It is concluded that feedback control of laser bias is a practical solution for regulating output power. It was found, however, that unless the front and back mirrors of GaAlAs lasers can be made to track each other linearly, the light power actually launched into the transmission fiber should be monitored to assure maximum power stability.

VIII. ACKNOWLEDGMENTS

We thank B. C. DeLoach, R. W. Dixon, R. L. Hartman, and B. Schwartz for supplying the GaAlAs lasers used for this work, G. Moy for his careful measurements on all these devices, and D. R. Mackenzie for developing the soldering technique for mounting the laser pedestals. Thanks also go to D. D. Sell for his comments and suggestions concerning the feedback scheme, to P. K. Runge for supplying connectors for the pigtails, to the Thick-Film Technology Group at the Allentown laboratory of Bell Laboratories for supplying the thick-film circuits, and to W. W. Benson for the data used in Fig. 5. We thank M. DiDomenico for his guidance and technical suggestions that contributed substantially to the project. Finally, we especially thank E. E. Becker, D. P. Hansen, R. Pawelek and J. R. Potopowicz for their expert assistance in package assembly, and M. A. Karr for the package design and assistance with assembly.

REFERENCES

1. T. L. Maione and D. D. Sell, "Experimental Fiber-Optic Transmission System for Interoffice Trunks," IEEE Trans. Commun., to be published.
2. S. D. Personick, "Receiver Design for Digital Fiber Optic Communications Systems, II," B.S.T.J., *52*, No. 6 (July–August 1973), pp. 875–86.
3. M. I. Schwartz, R. A. Kempf, and W. B. Gardner, "Design and Characterization of an Exploratory Fiber-Optic Cable," Second European Conf. on Optical Fiber Communication, Paris 1976, paper X.2.
4. J. S. Cook and P. K. Runge, "An Exploratory Fiberguide Interconnection System," Second European Conf. on Optical Fiber Communication, Paris 1976, paper VIII.3.
5. D. Kato, "Light Coupling from a Stripe-Geometry GaAs Diode Laser into an Optical Fiber with Spherical End," J. Appl. Phys., *44* (1973), pp. 2756–2758.
6. L. G. Cohen and M. V. Schneider, "Microlenses for Coupling Junction Lasers to Optical Fibers," Appl. Opt., *13* (1974), pp. 89–94.
7. C. A. Brackett, "On the Efficiency of Coupling Light from Stripe-Geometry GaAs Lasers into Multimode Optical Fibers," J. Appl. Phys., 45 (1974), pp. 2636–2637.
8. W. W. Benson, private communication.
9. K. Asama, Y. Nishimura, and H. Sasaki, "Study on the Thick-Film Resistance Abrupt Change by Resin Packaging," Proc. 1969 Hybrid Microelectronics Symposium, pp. 51–62.
10. T. L. Paoli, "Nonlinearities in the Emission Characteristics of Stripe-Geometry (Al-Ga)As Double-Heterostructure Junction Lasers," IEEE J. Quantumn Electron., *QE-12*, No. 12 (Dec. 1976), pp. 770–776.
11. R. L. Hartman, private communication.

THE BELL SYSTEM TECHNICAL JOURNAL
Vol. 57, No. 6, July–August 1978
Printed in U.S.A.

Atlanta Fiber System Experiment:

Practical 45-Mb/s Regenerator for Lightwave Transmission

By T. L. MAIONE, D. D. SELL and D. H. WOLAVER

(Manuscript received June 15, 1977)

A 45-Mb/s optical regenerator using an avalanche photodiode and a GaAlAs injection laser has been designed for a field environment. Its design and performance are described here. Feedback control of the optical transducers permits operation over a temperature range of 0 to 60°C. The regenerator has simple power requirements, and optical connectors permit easy installation. Its input sensitivity and output power makes useful regenerator spacings possible with currently available optical fiber. The large AGC range permits a wide range of regenerator spacings. A novel phase-locked loop design achieves a wide pull-in range for the timing recovery circuitry.

I. INTRODUCTION

An optical regenerator* is essentially a digital regenerator with optoelectronic transducers at the input and output. The transducers used here are an avalanche photodiode and a GaAlAs injection laser. The regenerator includes the usual features of amplification, filtering, automatic gain control, retiming, and regeneration. Some features peculiar to a design for a lightwave transmission system are very high gain and wide dynamic range. Also, the characteristics of the transducers must be stabilized with feedback.

The optical regenerator described here is the prototype of a design for a field environment. The intended transmission medium is low-loss graded-index fiber.[1,16] The regenerator was initially used in the Atlanta Experiment, a study of a lightwave transmission system in an environment simulating field conditions.[2]

* A regenerator is a one-way repeater.

The feasibility of an optical regenerator operating at a data rate of 45 Mb/s has already been shown.[3] The objective here is a practical regenerator with simple power requirements, operation over a temperature range from 0° to 60°C, wide dynamic range, practical optical connectors, and a design that could be manufactured by present methods.

The selected data rate was 44.736 Mb/s, the DS3 level of the Bell System digital hierarchy. This rate makes use of the wide bandwidth of the fiber without incurring significant penalty from fiber dispersion. The signal format is binary nonreturn-to-zero* with scrambling to insure adequate balance and timing information.

The optical regenerator was constructed in three separate modules, as shown in Fig. 1. This design relaxed the requirements on size and isolation in order to focus effort on the requirements mentioned above. It also allowed the modules to be used for terminal regenerators. The functions performed in each module are shown in Fig. 2. The receiver module accepts an optical signal as low as −55 dBm at its optical connector and produces a 1-V p-p electrical output signal. The decider module extracts timing and regenerates the signal. The transmitter module converts the regenerated electrical signal to a regulated optical signal and couples a minimum of −3 dBm of average power into an optical connector.

Notice that the optical connectors[4] on the receiver and transmitter are designed to engage when electrical connection is made to the module. Electrical test points are brought to the face of each module.

The remainder of the paper describes the operation of the three modules. The regenerator performance reported is based on the measurement of 15 regenerators.

II. RECEIVER

The receiver module comprises the linear channel of the regenerator. It converts the received optical signal to an electrical signal and maintains a constant output by automatic gain control (AGC). The dispersion of the glass fiber medium is small enough that the receiver does not need to equalize for it. However, filtering is done to limit the noise. The circuit in Fig. 3 shows the functions performed in the receiver.

Special care was needed in the layout, shielding, and bypassing for this module. (Most of the bypassing is not shown in Fig. 3 to simplify the drawing.) Signal currents differing in level by 90 dB are present in the circuit.

* Light on corresponds to a logical "one"; light nominally off is a logical "zero."

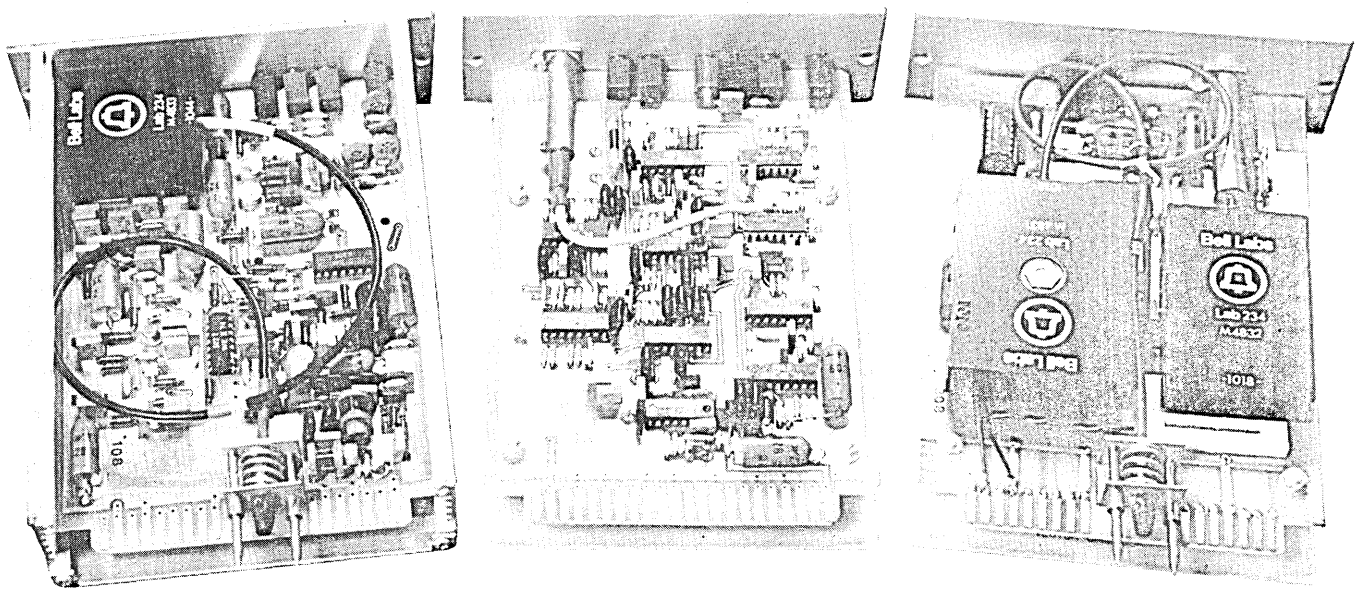

Fig. 1 — Optical regenerator. Each module is 6.5 × 4.5 × 1.5 in.

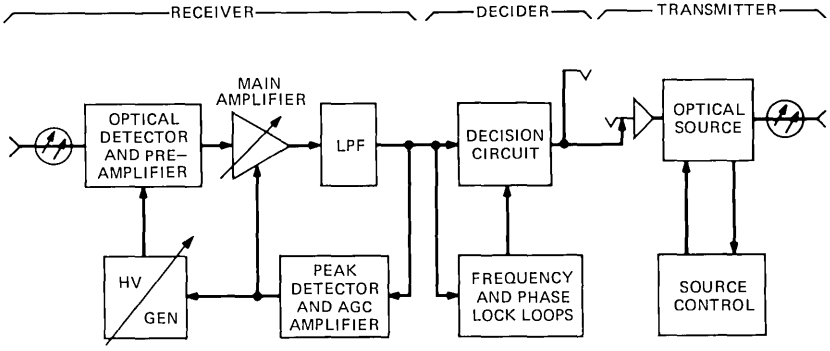

Fig. 2 — Optical regenerator.

2.1 Photodetection

The optical signal is detected by an avalanche photodiode (APD) capable of providing current gain in the range from 6 to 120. The dependence of the gain on the bias voltage is shown in Fig. 4. The bias, supplied by the dc-to-dc converter, can be varied from −150 to −420 volts by the p-n-p transistor loading down the converter's output. Zener diodes limit both the maximum and minimum voltages applied to the APD. The voltage limitation prevents excessive burst noise or damage that can occur at high voltages. It also avoids the slow APD response at low voltages.

The small current from the APD is amplified by a transimpedance preamplifier located in the same shielded package with the APD. The noise figure is not so low as that of a high-impedance preamplifier,[5,6] but the sacrifice in sensitivity is only 1 dB. The advantages of a transimpedance preamplifier are greater dynamic range and no equalization required.[7] Further details of the ADP and preamplifier performance are given by the designers and builders of the detector package in Ref. 8.

A useful measure of the received optical power level is the detected power $\eta\overline{P}$. This is the product of the average power $\overline{P}$ available at the optical connector and the combined efficiency η of the connector, pigtail, and APD.* The detected power $\eta\overline{P}$ is conveniently obtained by measuring the APD current for a known gain. For light of wavelength 825 nm, the perfect conversion to primary photocurrent would be 0.67 ampere per watt of optical power.

For a given error rate, an optimum APD gain will minimize the required optical power $\eta\overline{P}$. The optimum gain for 10^{-9} error rate was determined experimentally to be 80, and the receiver is aligned to realize this condition. The required $\eta\overline{P}$ is about −55 dBm.

The measured curve of error rate versus $\eta\overline{P}$ for a typical regenerator is shown in Fig. 5. For this range of low $\eta\overline{P}$, the APD gain was adjusted

* The efficiency η was measured to be about −1.5 dB.

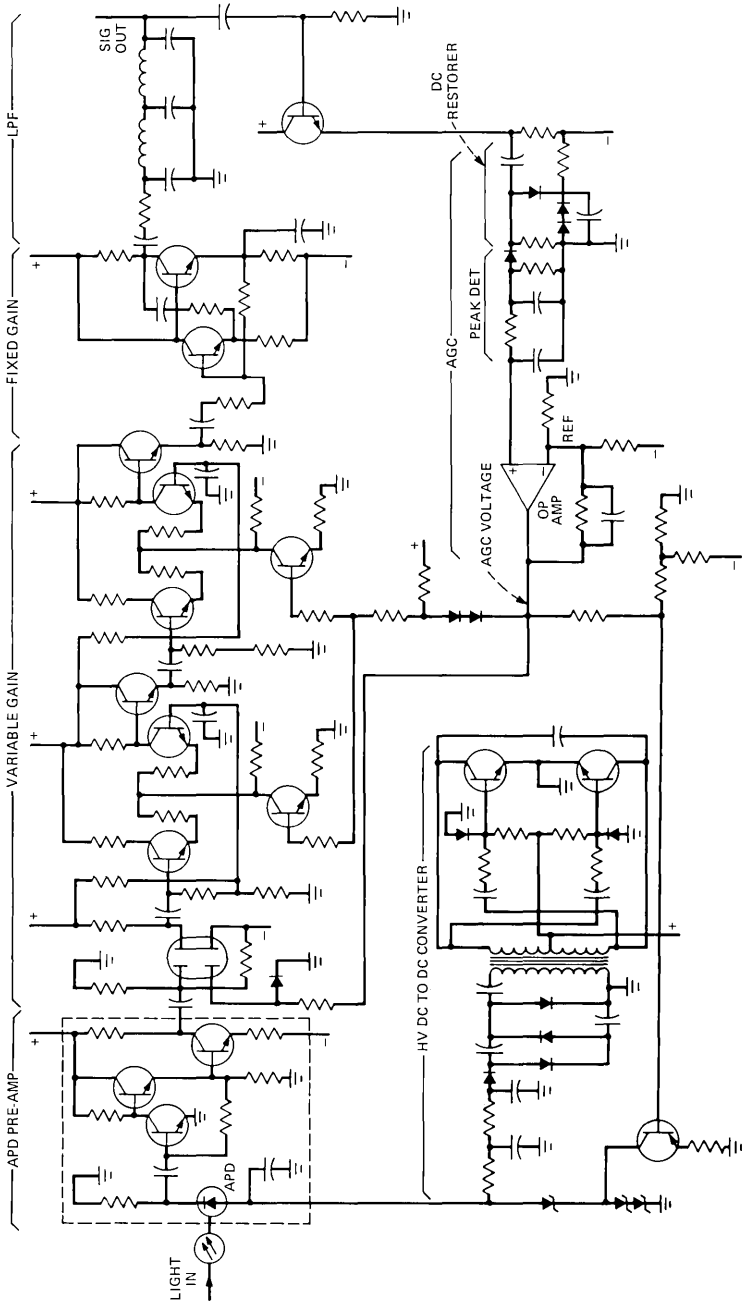

Fig. 3 — Receiver circuit.

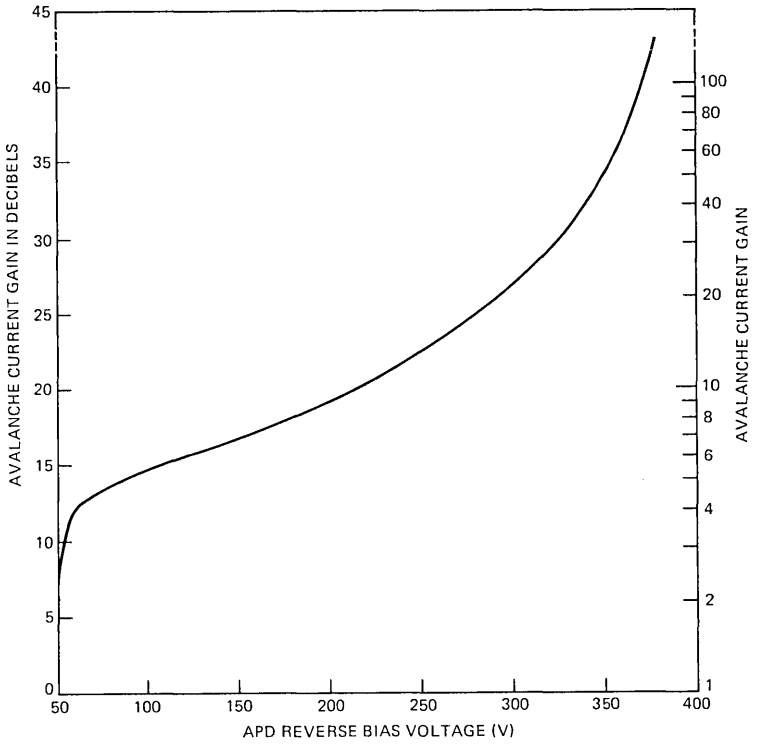

Fig. 4 — Avalanche photodiode gain characteristic.

by the AGC to maintain a constant output signal level. The performance of the regenerator is considered to be useful to an error rate of 10^{-6}, corresponding to a detected power $\eta\bar{P}$ of about −57 dBm and an APD gain of 120. (Burst noise can begin to occur at gains greater than 120.)

2.2 Main amplifier

The main amplifier consists of a variable-gain amplifier, a fixed-gain power amplifier, and a low-pass filter to limit noise.

The first stage of the variable-gain amplifier is a dual-gate FET. This device accepts a large signal input without distortion and achieves a gain variation of 20 dB. Each of the following two stages is an emitter-coupled pair with a gain variation of 14 dB. The fixed-gain amplifier provides a 2-V p-p signal to the low-pass filter. The signal at the output of the filter is maintained at 1-V p-p by the AGC.

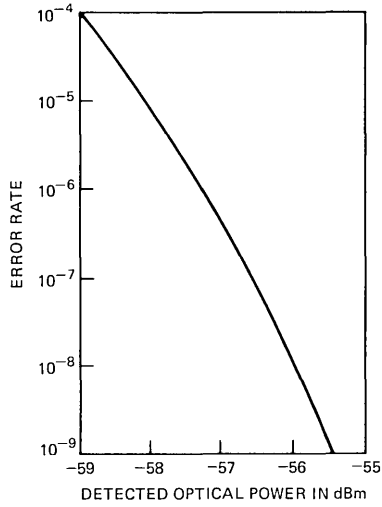

Fig. 5 — Error rate versus detected optical power.

2.3 Automatic gain control

The level of the output signal is monitored by a peak detector and compared against a reference by a comparator with a gain of 125. The peak detector includes a low-pass filter with a cutoff frequency of 0.12 Hz. The "AGC voltage" at the output of the comparator controls gain of both the APD (by varying the bias voltage) and the main amplifier.

Table I lists these gains and their ranges; 26 dB range for the APD and 48 dB for the main amplifier. Thus, the total AGC range is 74 dB. Note this is twice the 37-dB range indicated for the corresponding detected power $\eta\overline{P}$, since the APD is a square-law detector. The ranges indicated are the maximum for linear operation. $\eta\overline{P}$ can be extended 5 dB higher without incurring significant closing of the "eye."

If the APD and the main amplifier are in the active parts of their AGC ranges simultaneously, interaction and oscillation are possible. Therefore, the AGC is designed so their ranges do not overlap. For low detected power ($\eta\overline{P} < -44$ dBm) the APD gain is varied, and the main amplifier gain is at maximum (see Fig. 6). This maximum gain is accurately set, and the AGC acts to stabilize the APD gain over temperature as well as to accommodate changes in the detected power.

Table I — Receiver gains and levels

	Min.	Max.	Range
Detected power $\eta\overline{P}$	−57 dBm	−20 dBm	37 dB
APD current gain	6 (15.6 dB)	120 (41.6 dB)	26 dB
APD output (average)	0.16 μA	40 μA	
Preamp transimpedance	14 kΩ		
Preamp output	4.5 mV p-p	1120 mV p-p	
Main amplifier gain	−1 dB	47 dB	48 dB
Receiver output	1.0 V p-p		

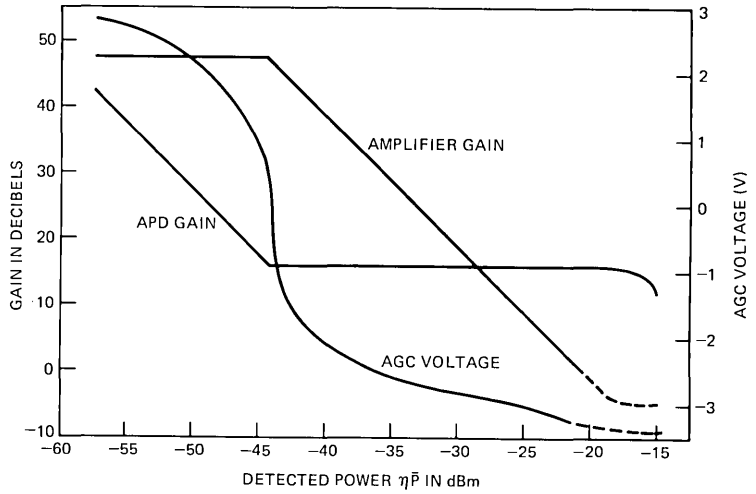

Fig. 6 — Receiver automatic gain control.

For $\eta\bar{P} > -44$ dBm, the main amplifier gain is varied, and the APD is at minimum gain. The value of the AGC voltage over the range is also shown in Fig. 6. The change in gain with AGC voltage is greatest at the extremes—about 30 dB/V, corresponding to an open-loop gain of 430 and a closed-loop bandwidth of 52 Hz.

2.4 Linear channel response

The low-pass filter at the output of the receiver shapes the frequency response of the linear channel to limit noise without introducing much intersymbol interference in the 44.7-Mb/s signal. An optimum design minimizes the detected power required for a given error rate. The filter used here introduces a complex pole pair at $24 \pm j38$ MHz and at $76 \pm j12$ MHz, and a real pole at 58 MHz. Roll-off due to parasitics in the linear channel can be modeled by two additional poles—one at 46 MHz and one at 54 MHz. This filter gives performance within 1 dB of the optimum design.[9]

The measured high-frequency roll-off of the linear channel is shown in Fig. 7. From this, the effective noise bandwidth is calculated to be 33.7 MHz. The low-frequency roll-off due to coupling capacitors is shown in Fig. 8. Cutoff is at about 650 Hz.

A single detected light pulse at the input can be modeled by a trapezoid with rise and fall times of 3 ns. The time response of the linear channel to this pulse was calculated by fast Fourier transform from the measured frequency response (see Fig. 9). Note that the time response is a little too narrow, reflecting the fact that the low-pass filter design is not the optimum. The measured eye pattern is shown in Fig. 10.

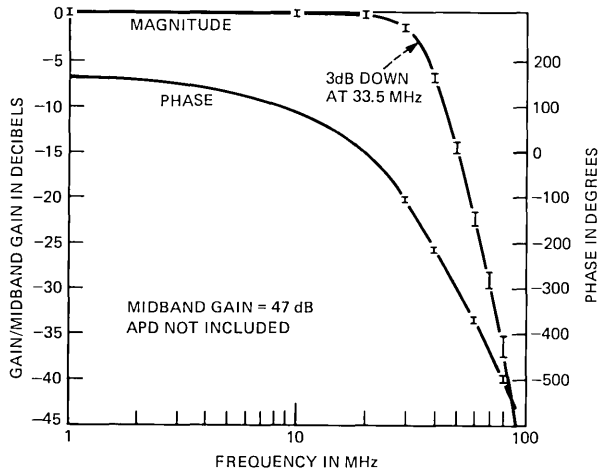

Fig. 7 — Receiver high-frequency electrical gain characteristic.

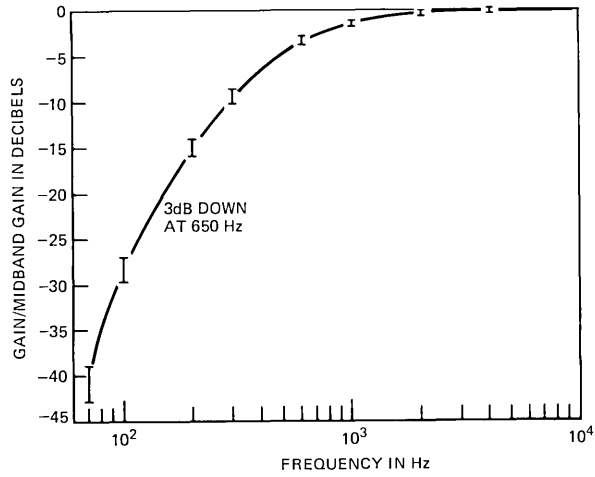

Fig. 8 — Receiver low-frequency electrical gain characteristic.

III. DECIDER

The decider module includes a decision circuit that samples the signal from the receiver and generates a logic-level output signal. The timing of sampling and of logic transitions is controlled by a clock recovered from the receiver output. A narrowband phase-locked loop is used to recover the timing. A circuit diagram of the decider is shown in Fig. 11.

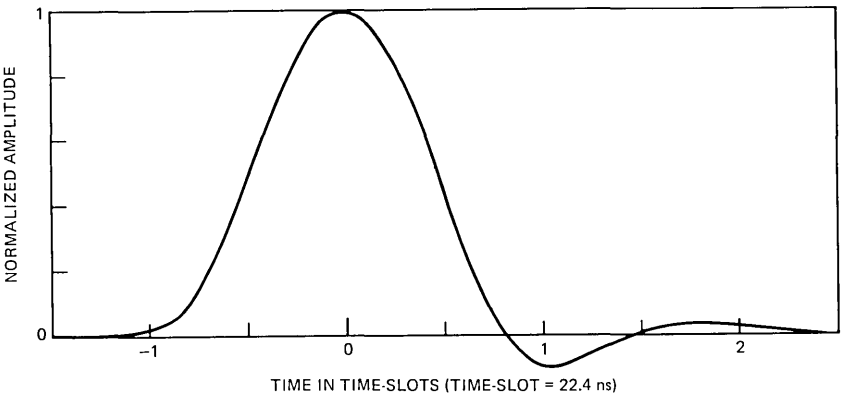

Fig. 9 — Nominal linear channel pulse response.

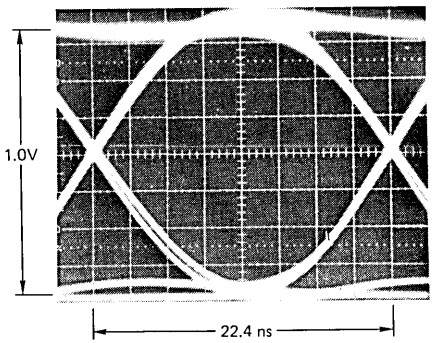

Fig. 10 — Typical eye pattern (receiver output).

3.1 Decision circuit

The decision circuit compares the SIGNAL IN with a threshold and decides, at sampling times determined by the recovered clock, whether the signal is "high" or "low." In a lightwave system, the signal is not symmetric; the high (light on) state has more noise associated with it than the low (light off) state.[6] For this reason, the optimum threshold is not at the center of the "eye" (0 V with ac coupling), but closer to the low state. A typical plot of error rate versus threshold is shown in Fig. 12. For the 1-V p-p eye, the optimum threshold averages about −70 mV.

Error rate is plotted as a function of the sampling time in Fig. 13. For timing within ±1.3 ns (±20.5 degrees), about the optimum, the error rate is not even doubled. The measured timing variation from circuit to circuit at room temperature is ±18 degrees. The stability of a timing recovery circuit over a range of 65°C is ±2.5 degrees with temperature compensation. This compensation (not shown in Fig. 10) consists of a thermistor in the load of the PLL phase comparator. (Without compensation, the variation would be ±10 degrees over a temperature range of 65°C.)

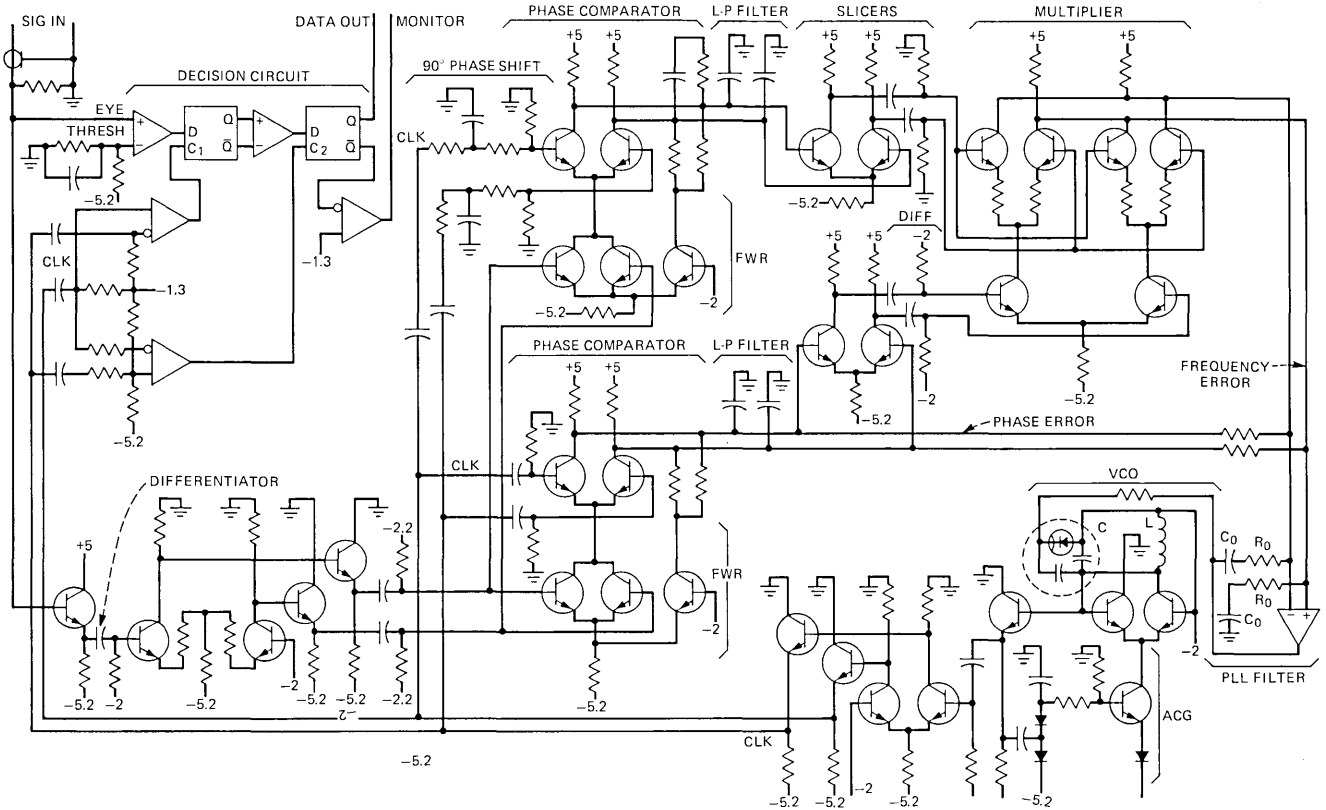

Fig. 11 — Decider circuit.

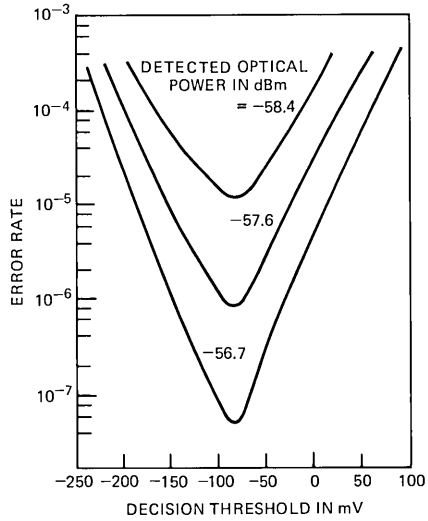

Fig. 12—Error rate versus decision threshold. Logic "1" = +500 mV; logic "0" = −500 mV.

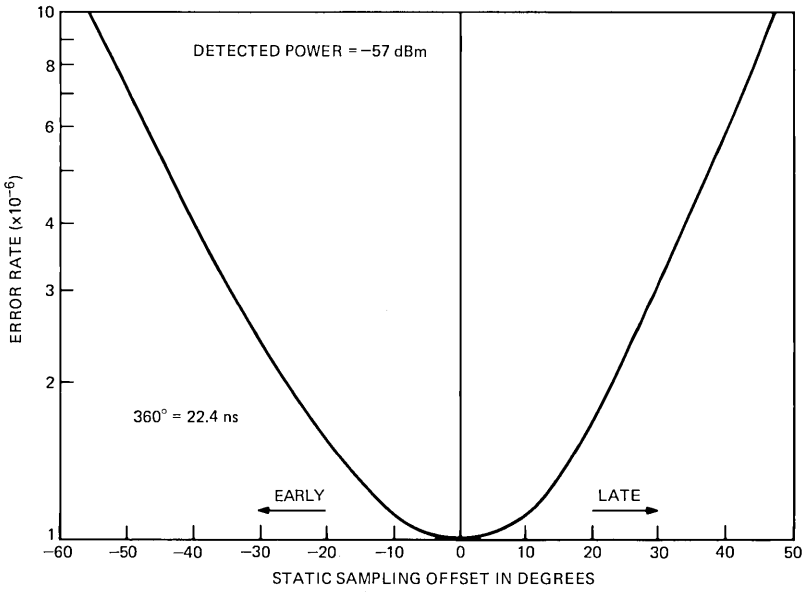

Fig. 13 — Error rate dependence on sampling time.

The decision circuit is a commercial integrated circuit MC1650 connected as a master-slave D-type flip-flop. As shown in Fig. 14, the first stage samples the SIGNAL IN when C_1 goes low, timed to be at the center of the eye. The second stage resamples to prevent feedthrough while C_1 is high. If the eye is sufficiently open to eliminate decision errors, the

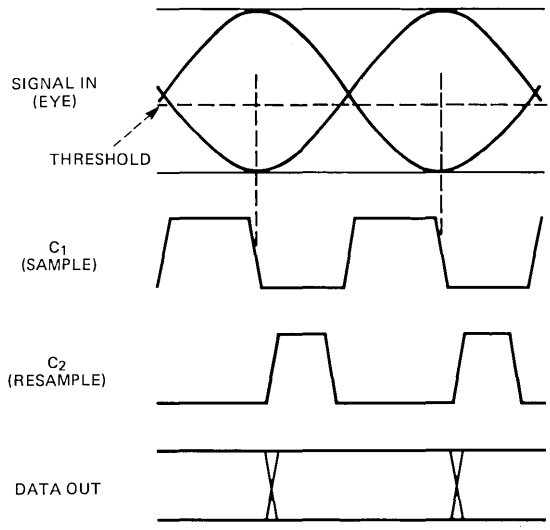

Fig. 14 — Decision circuit waveforms.

DATA OUT will be a logic-level version of the lightwave signal originally transmitted.

3.2 Timing recovery

The information for timing recovery is in the transitions of the SIGNAL IN (see Fig. 15). After some preprocessing of the signal, a local oscillator is locked to the transitions by a second-order phase-locked loop (PLL). The PLL, with a 3-dB bandwidth 1/1200 of the baud, limits the amount of timing jitter in the recovered clock. The pull-in range of the PLL is extended by a frequency comparator, permitting use of a low-tolerance (and inexpensive) oscillator.

3.2.1 Signal preprocessing

It is possible for low-frequency components of SIGNAL IN to cause timing jitter. Therefore the signal is high-pass filtered by a 60-MHz pole (approximating a differentiator); the information of the high-speed transitions is retained. See Fig. 15 for waveforms.

The signal is then processed by a full-wave rectifier (with dead zone) to produce a line in the frequency spectrum at the baud. The output of the full-wave rectifier is a series of current pulses corresponding to the transitions of SIGNAL IN.

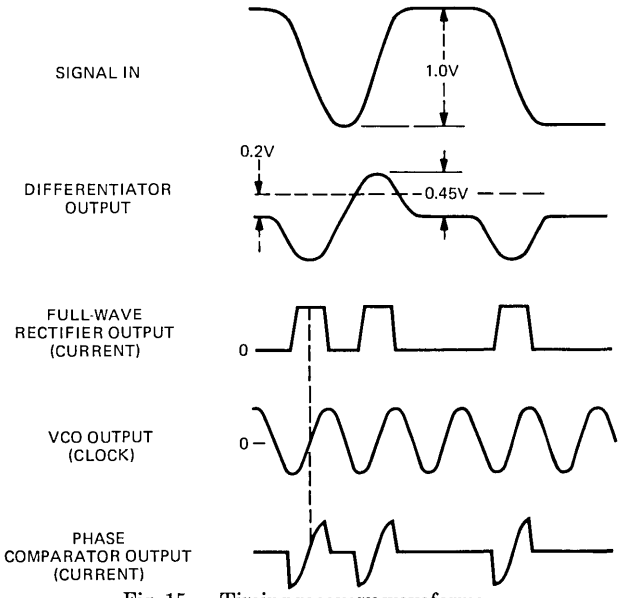

Fig. 15 — Timing recovery waveforms.

3.2.2 Phase-locked loop

The PLL comprises a phase comparator, a low-pass filter, and a voltage-controlled oscillator (VCO). Its input is the series of current pulses from the full-wave rectifier, and its output is the clock used by the decision circuit for sampling.

The phase comparator multiplies the clock by the PLL input, developing an average current proportional to their phase difference (for differences less than about 60 degrees). When the relative phase is zero, as shown in Fig. 15, the average output current is zero. The maximum average differential output of about 35 μA corresponds to a relative phase of 90 degrees.

The transfer function of the filter is $(1 + sC_0R_0)/sC_0$, where $C_0R_0 =$ 1 ms. Since the gain of the filter at dc is very great, offset of the center frequency of the VCO has a negligible contribution to the static phase offset of the clock.

An undesired differential offset current as large as 7 μA can appear at the input to the filter, causing up to 12 degrees static offset. It also causes the VCO frequency to drift when the PLL input signal is removed. If the input signal is interrupted for too long, the frequency drifts beyond the seize range of the PLL, and recovery time will be long. To assure seizure, the interrupt time must satisfy

$$\tau_i \leq R_0C_0\, I_{pc}/I_0 = 5 \text{ ms},$$

where I_{pc} is the current corresponding to a phase difference of 90 degrees,

and I_0 is the maximum offset current. When this is satisfied, measured recovery times are about 20 μs.

The voltage-controlled oscillator (VCO) has a center frequency of about 44.7 MHz. Its frequency can be varied over a range of ±10 percent according to the bias voltage applied to a varactor diode by the PLL filter. The VCO includes an AGC to maintain a 1.2-V p-p output.

The VCO is inexpensive because high stability is not required. As the power supply voltages vary over a range of ±10 percent, the VCO frequency varies by ±2 percent. As the temperature varies over a range of 65°C, the VCO frequency varies by ±1 percent. For nominal conditions, the frequency stays within ±2 percent from circuit to circuit. Therefore, the worst-case offset of the VCO over all conditions is ±5 percent. This is well within the control range of ±10 percent.

The nominal, closed-loop, 3-dB bandwidth f_0 of the PLL is 37 kHz. The noise bandwidth is $(\pi/2)\, f_0$. Due to variations in the gains of the phase comparator and VCO, f_0 was as low as 21 kHz and as high as 70 kHz for different circuits. The open-loop zero at 160 Hz introduced by the PLL filter causes up to 0.06-dB peaking in the closed-loop response.[10,11]

Since the phase comparator has a sinusoidal characteristic, the seize frequency f_s of the PLL equals its f_0 bandwidth.[12] The pull-in range of the unaided PLL is dependent on the offset current and can be as small as 55 kHz, or only 0.12 percent of the band.[12] This will not cover the ±10-percent control range of the VCO and the ±5 percent tolerance of the VCO; a pull-in range of at least ±15 percent is needed.

3.2.3 Frequency comparator

The pull-in range of the timing recovery circuit is extended to ±20 percent by a frequency comparator. The scheme was suggested by Bellisio[13] and is similar to an earlier proposal by Richman.[12] The additional circuitry needed consists of the second phase comparator, the low-pass filter, the slicers, and the multiplier shown at the top of Fig. 11.

The clock delivered to the second phase comparator is delayed 90 degrees from that delivered to the one in the PLL. When the PLL is out of lock, there is a beat note at the output of each phase comparator, and the two beat notes are 90 degrees out of phase. Which one is ahead in phase depends on the sign of the clock frequency error. The beat notes are squared up by slicers, and one of the square waves is differentiated to produce alternating positive and negative pulses. The product of the pulses with the other square wave is a train of either positive or negative pulses, depending on the sign of the frequency error. These current pulses are summed with the phase-error current at the input to the PLL filter and cause the PLL to pull in to its seize range. With the PLL in its seize range, the pulses cease and the PLL behaves as if there were no auxiliary pull-in circuitry.

The pull-in rate is proportional to the frequency comparator's average output current, which is plotted as a function of frequency difference in Fig. 16. The curve is linear near the origin. As the period of the difference frequency approaches the width of the current pulses, the curve falls off from the ideal, but it retains the right sign to beyond a frequency difference of ±20 percent.

The pull-in time is dependent on the difference between the initial VCO frequency and the baud. Figure 17 shows measured pull-in times for a typical circuit. Pull-in from a 10-percent frequency difference takes less than 50 ms.

3.2.4 Timing jitter

A regenerator retimes the phase of the data it transmits, but it can also introduce some jitter in the phase. Noise causes random jitter, and data dependence of the timing recovery circuit causes systematic jitter.

In a line of regenerators, this jitter accumulates and may become a problem for the terminal circuits. Each regenerator adds a certain amount of random and systematic jitter, characterized by the jitter power densities $\Phi_R(f)$ and $\Phi_S(f)$, respectively. (The unit of the "power" density is degrees^2/Hz.) The spectra can be considered, for all practical purposes, to be flat and equal to $\Phi_R(0)$ and $\Phi_S(0)$.

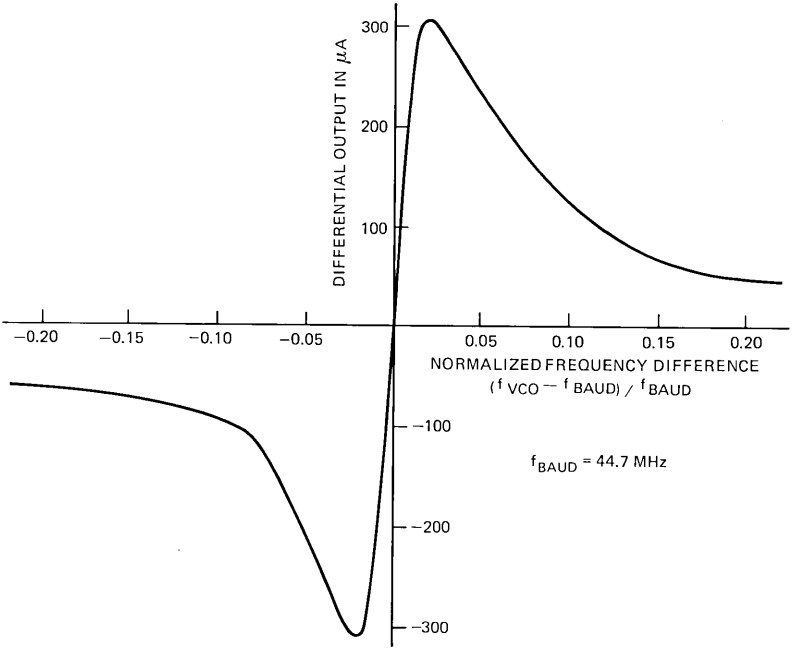

Fig. 16 — Typical frequency comparator characteristic.

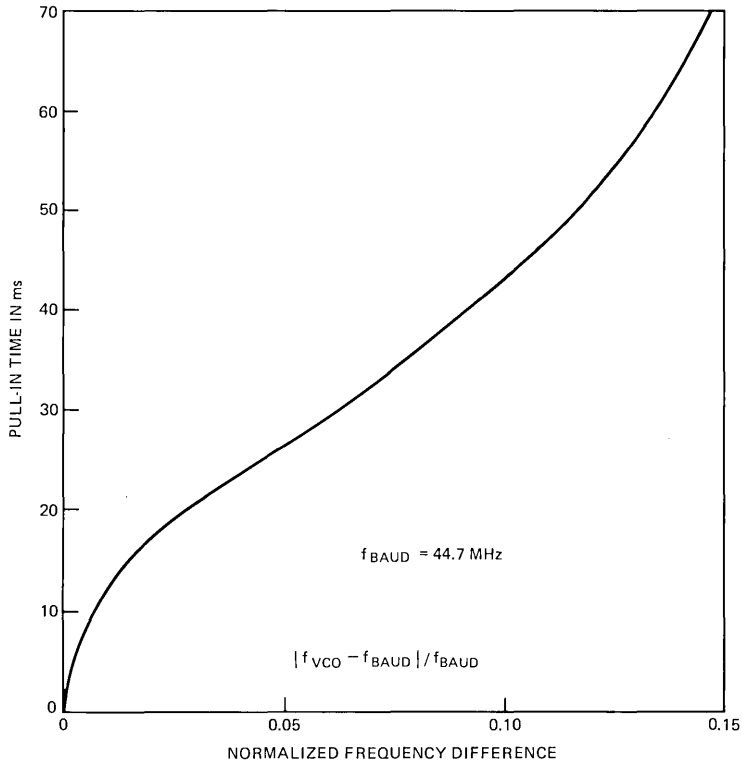

Fig. 17 — Typical pull-in times with aid of frequency comparator.

The accumulated jitter was measured for a line of 14 regenerators.[2,14] From this data the worst-case $\Phi_S(0)$ was calculated to be 33 degrees^2/MHz. This would correspond to 19 degrees rms of accumulated jitter for a line of 50 regenerators. The effect of $\Phi_R(0)$ was negligible.

IV. TRANSMITTER

The transmitter module accepts an ECL data signal and provides the data as an optical output from a fiber pigtail. The light source is a GaAlAs injection laser with an emission wavelength of 825 nm. Circuitry is included to monitor the laser output level and regulate it over time and temperature. A more complete description of the transmitter module is given by its designers and builders in Ref. 15.

A circuit diagram of the transmitter is shown in Fig. 18. When a positive-going pulse is present at DATA IN, the driver circuit applies a current pulse of about 35 mA to the laser, bringing it from below to above the lasing threshold. The pulses ride on top of a prebias current which improves switching speed and avoids chattering or oscillation of the light output.

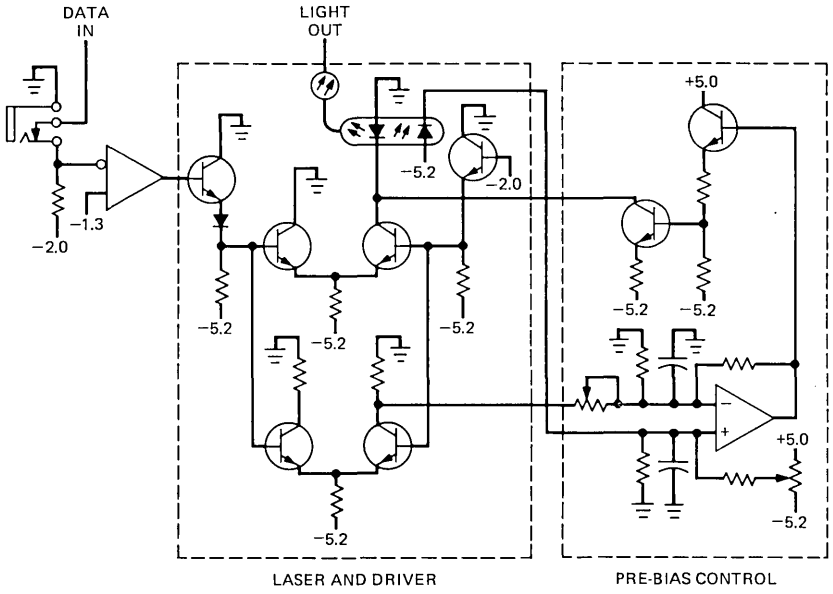

Fig. 18 — Transmitter circuit.

Through a feedback circuit, the prebias current is automatically established at a value required to maintain the light output of the laser constant. This circuit eliminates the changes in light output that would occur from changes in the threshold due to temperature and aging. As part of this control circuit, a pin photodiode senses the light output from the back face of the laser. The pin output correlates closely with the average light collected by the fiber pigtail at the other face of the lasing cavity. By deriving a reference from the DATA IN signal, the control is insensitive to the "ones" and "zeros" density in the data. At 25°C, the prebias current is typically about 100 mA, and at 50°C it is about 115 mA.

The varying density of "ones" in the data causes short-term heating and cooling of the laser. As a result, the laser output level varies at a rate faster than the response of the feedback control. Lasers are used that have a pattern dependence of the peak output power below 8 percent peak-to-peak.

For a balanced data signal, the average optical power available from the fiber pigtail is at least −3 dBm. The output power corresponding to a "one" is about 15 times that for a "zero."

The driver, laser, pin diode, and reference are contained in one package with cooling fins. The temperature of the package runs about 5°C above ambient. The remainder of the control circuit is contained in a second package.

A coaxial jack with normal-through contact provides an access point where the line signal can be interrupted and a test signal injected.

V. POWERING

The regenerator is powered by +5.0 V and −5.2 V with a typical power consumption of 3.1 W. For high supply voltages and the laser near end of life (high prebias), the power is estimated to be 3.9 W—0.9 in the receiver, 0.8 in the decider, and 2.2 in the transmitter. The supply voltages can vary by ±5 percent without affecting regenerator operation. In a subsequent regenerator modification, filtering was improved so that 100 mV p-p transients on the power line could be tolerated.

VI. CONCLUSION

The 45-Mb/s regenerator described here represents a practical design for a field environment. Feedback control of the avalanche photodiode gain and of the laser output level enable operation over a temperature range of 0 to 60°C. The regenerator has simple power requirements. Its input sensitivity and output power make useful regenerator spacings possible with currently available optical fiber. The wide AGC range permits the design to handle a wide range of regenerator spacings. The wide capture range of the timing circuit makes an expensive crystal unnecessary. The physical design is rugged and permits easy optical and electrical connection. Future efforts will reduce the three-module design to one module.

VII. ACKNOWLEDGMENTS

We gratefully acknowledge the contribution of Fred Radcliffe, now retired from Bell Laboratories, who was responsible for the design of the receiver module. Thanks are also due Richard Kerdock who carried out the recovery time and powering tests and Harry Proudfoot and Bob Hunter who provided valuable technical support.

REFERENCES

1. A. G. Chynoweth, "The Fiber Lightguide," Physics Today, May 1976, pp. 28–37.
2. R. S. Kerdock and D. H. Wolaver, "Performance of an Experimental Fiber-Optic Transmission System," Conference Record of National Telecommunications Conference, November 29 to December 1, 1976.
3. P. K. Runge, "An Experimental 50 Mb/s Fiber Optic PCM Repeater," IEEE Trans. Commun., *COM-24,* No. 4 (April 1976), pp. 413–418.
4. J. S. Cook and P. K. Runge, "An Exploratory Fiberguide Interconnection System," 2nd European Conf. on Optical Fiber Communication, Paris, September 27–30, 1976, pp. 253–256.
5. J. E. Goell, "An Optical Repeater with High-Impedance Input Amplifier," B.S.T.J., *53,* No. 4 (April 1974), pp. 629–643.
6. S. D. Personick, "Receiver Design for Digital Fiber Optic Communication Systems, Parts I and II," B.S.T.J., *52,* No. 6 (July–August 1973), pp. 843–886.

7. J. L. Hullett and T. V. Muoi, "A Feedback Receive Amplifier for Optical Transmission Systems," IEEE Trans. Commun., *COM-24,* No. 10 (October 1976), pp. 1180–1185.
8. R. G. Smith, C. A. Brackett, and H. W. Reinbold, "Optical Detector Package," B.S.T.J., this issue, pp. 1809–1822.
9. S. S. Cheng, unpublished work.
10. C. J. Byrne, "Properties and Design of the Phase Controlled Oscillator with a Sawtooth Comparator," B.S.T.J., *61,* No. 2 (March 1962), pp. 559–602.
11. A. J. Goldstein, "Analysis of the Phase-Controlled Loop with a Sawtooth Comparator," B.S.T.J., *61,* No. 2 (March 1962), pp. 603–633.
12. D. Richman, "Color-Carrier Reference Phase Synchronization Accuracy in NTSC Color Television," Proc. IRE, *42,* No. 1 (January 1954), pp. 106–133.
13. J. A. Bellisio, "A New Phase-Locked Timing Recovery Method for Digital Regenerators," Conference Record for International Conference on Communications, Philadelphia, June 14–16, 1976.
14. R. S. Kerdock and D. H. Wolaver, "Results of the Atlanta Lightwave System Experiment," B.S.T.J., this issue, pp. 1857–1879.
15. P. W. Shumate, Jr., F. S. Chen, and P. W. Dorman, "GaAlAs Laser Transmitter for Lightwave Transmission Systems," B.S.T.J., this issue, pp. 1823–1836.
16. M. R. Santana, M. J. Buckler, and M. J. Saunders, "Lightguide Cable Manufacture and Performance," B.S.T.J., this issue, pp. 1745–1757.

THE BELL SYSTEM TECHNICAL JOURNAL
Vol. 57, No. 6, July–August 1978
Printed in U.S.A.

Atlanta Fiber System Experiment:

Results of the Atlanta Experiment

By R. S. KERDOCK and D. H. WOLAVER

(Manuscript received October 20, 1977)

In the Atlanta System Experiment, a digital lightwave transmission system operating at 44.736 Mb/s was tested in an environment approximating field conditions. The system included a cable with 144 fibers pulled into a duct, lightguide cable splices, single-fiber connectors, a fiber distribution frame, optical regenerators employing avalanche photodiodes and GaAlAs lasers, and terminal equipment for interfacing to the standard DS3 signal format. A number of experiments were conducted to evaluate and gain experience with this digital lightwave transmission system. These included fiber crosstalk, fiber dispersion, timing jitter, system recovery, and dc powering. In this paper the configuration of the Atlanta lightwave system is briefly described, and experimental results are reported.

I. INTRODUCTION

Tests of an experimental lightwave transmission system operating at 44.736 Mb/s (DS3), the third level of the Bell System digital hierarchy, were begun by Bell Laboratories in January, 1976.[1-3] The system, operating in an environment simulating field conditions, included all the elements necessary for a practical transmission system at the DS3 rate: a small, ruggedized cable containing 144 fibers, lightguide cable splices, single-fiber connectors, a fiber distribution frame, regenerators* employing avalanche photodiodes and GaAlAs lasers, and terminal circuits to interface with the DS3 signal format.

The main goals of the system experiment were to gain experience with a digital lightwave transmission system and to obtain the data necessary to turn this new technology into practical telecommunication equipment.

* A regenerator is a 1-way device, a repeater comprises two 1-way regenerators.

Before the system experiment began, the individual elements comprised by the system were thoroughly tested and characterized. The system experiment brought all these elements together in a simulated field environment. Experiments were performed to measure important system parameters and to evaluate system performance. These included experiments on fiber crosstalk, fiber dispersion, timing jitter, system recovery, and dc powering.

II. SYSTEM DESCRIPTION

A 648-meter length of cable containing 144 fibers[4,14] was looped through an underground duct and two manholes so that both ends of the cable were accessible in a basement laboratory (see Fig. 1). Each end of the cable was spliced[5] to a short section of cable that fanned out to individual fibers terminating in a 12-by-12 optical connector array. The array, called the fiber distribution frame (FDF), provided convenient access to individual fibers. Optical patch cords with single-fiber connectors[6] were used to interconnect the fibers and to connect the fibers to the regenerators.

The regenerators[7] accept at their input an average optical power ranging from −20 to −55 dBm. The data format is an unrestricted, binary, nonreturn-to-zero signal that has been scrambled. The data rate is 44.736 Mb/s, the DS3 rate of the Bell System digital hierarchy. The output is a regenerated lightwave signal of 825-nm wavelength and an average power of at least −3 dBm. (Descriptions of the avalanche pho-

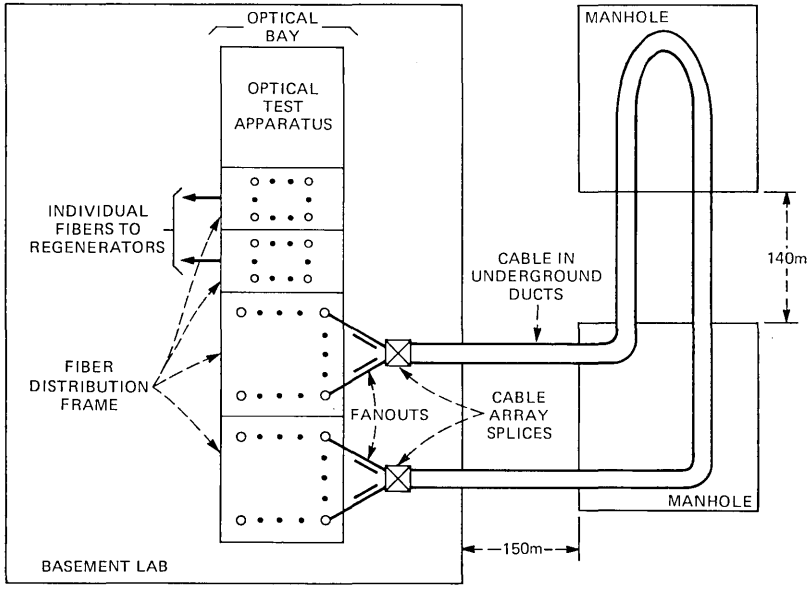

Fig. 1—Lightguide cable configuration showing access to individual fibers.

todiode[8] and GaAlAs laser[9] used in the regenerator are given elsewhere.) Optical patch cords are used to bring the input and output to the FDF.

The terminal circuits[2] provide the interface between the standard bipolar DS3 signal format and the unipolar format required by the regenerators. They also provide parity violation monitoring and removal. Figure 2 is a functional block diagram of the terminal circuits. Three pairs of terminal circuits were available.

These system elements were connected in various arrangements to form experimental setups. A typical experimental setup is shown in Fig. 3. As many as seven loops of the 648-m fibers were included between regenerators, and as many as 14 regenerators were included in a maintenance span.* Up to three maintenance spans could be connected in tandem. A signal source provided pseudo-random data with appropriate framing and parity bits.

III. CROSSTALK EXPERIMENT

In the configuration of the lightguide cable,[4] 12 fibers are placed side by side to form a ribbon, and 12 ribbons are stacked to form the cable

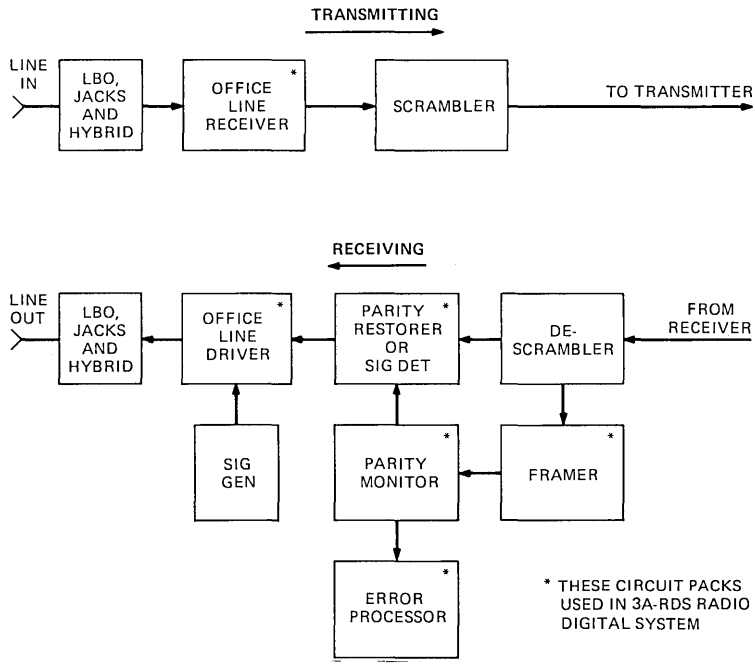

Fig. 2—Functional block diagram of the terminal circuits.

* For one experiment, fibers in a second lightguide cable 644 meters long were joined with low-loss splices to provide extra-long fiber lengths with up to 17 loops between regenerators.

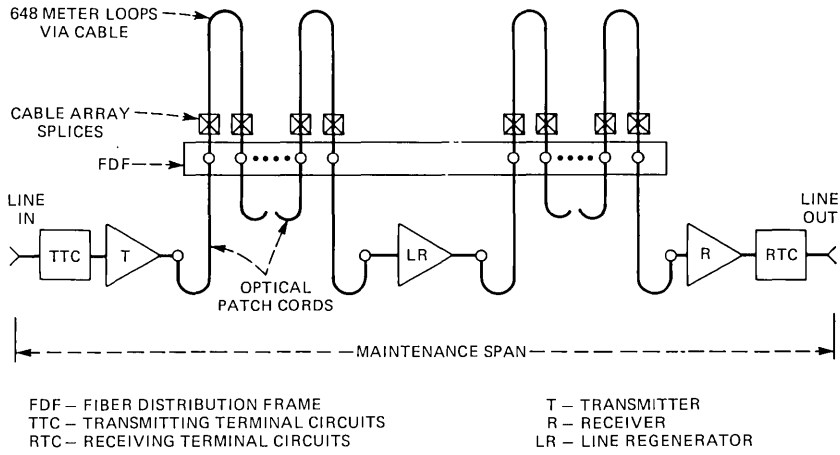

Fig. 3—Typical interconnection of system elements.

core. Thus most of the fibers have four neighbors. If stray light coupling is a problem, it would most likely be between neighboring fibers either along the length of the fibers or at cable splices.

The primary aim of this experiment was *not* to measure the amount of crosstalk coupling between fibers. Such data, obtained by a more sensitive technique, are reported elsewhere.[10] The purpose here was to measure the effect of crosstalk on system performance in terms of increased error rate. We also develop a model for the effect of crosstalk and compare measured results with a computer simulation.

3.1 Measured effect of crosstalk

Figure 4 shows the test arrangement for measuring the effect of crosstalk. Fiber A carries a lightwave signal with pseudorandom data, and the received signal is monitored for error rate. The level of the lightwave signal is adjusted by an optical attenuator so that the error rate is about 10^{-6}. (With a baud of 44.7 Mb/s and a count time of 10 seconds, there are about 447 error counts.) Then a lightwave signal 38 dB more powerful* is introduced into fiber B adjacent to fiber A. If this causes the measured error rate to increase by 14 percent or more (3σ of the count variation), there is defined to be measurable crosstalk.

Each of the 138 transmitting fibers in the cable was taken in turn as fiber A, and in each case the adjacent fibers (as many as four) were taken in turn as fiber B. In all, 456 fiber pairs were tested for crosstalk. If the measured error rate increased by a factor less than 1.14, the effect was attributed to statistical variation, and the pair was not investigated

* This is intended to be near the maximum signal level difference between two adjacent fibers in an actual application.

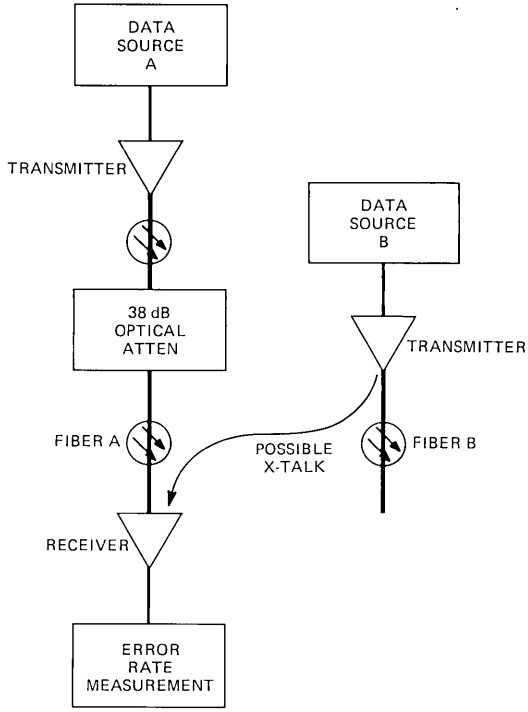

Fig. 4—Arrangement for crosstalk measurements.

further. There is some probability that actual crosstalk effects were overlooked. For example, an actual error rate increased factor of 1.30 would be overlooked with a probability of 3 percent.

Those fiber pairs with a measured error rate increase factor α more than 1.14 were tested again, measuring the error rates for 10 seconds. If α was again less than 1.14, the effect was attributed to statistical variation.

Two cases of fiber pairs with measurable crosstalk remained. The results are illustrated in Fig. 5. The arrows indicate the direction of the crosstalk, and α is the measured error rate increase factor. In determining α here, the error rates were measured for 100 seconds, giving a standard deviation of about 0.03 for α. The case with the greatest amount of crosstalk had $\alpha = 2.0$. This corresponds to a decrease of 0.25 dB in system sensitivity (see Fig. 5 of Ref. 7).

Both crosstalk situations involved fiber number 1-11. Subsequent investigation by Buckler and Miller[10] determined that crosstalk did not take place along the length of the fibers. An anomaly apparent in the splice of fiber 1-11 at the end labeled "W" produced the measurable crosstalk.

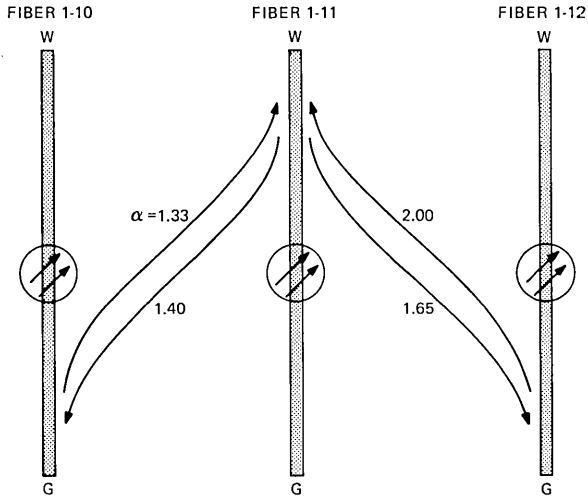

Fig. 5—Only case of measurable crosstalk. Arrows show direction of crosstalk. α is error rate increase factor.

The conclusion is that crosstalk measurably affecting the lightwave transmission system is indeed rare (two cases out of 456). Even the worst crosstalk case had a negligible effect on the system performance (0.25 dB decrease in sensitivity).

3.2 Model for effect of crosstalk

In this section, we develop a relation between strength of crosstalk interference and the error rate increase factor. The work is based in part on a computer simulation. There is one experimental data point.

As the interference from crosstalk is high (logical one) and low (logical zero), it increases the error rate of the main signal in two ways. Because of ac coupling in the receiver, it shifts the main signal both down and up by an amount Δ proportional to the interference power. This is equivalent to shifting the decision threshold up and down by Δ. When the interference is high, it also increases the error rate by increasing the shot noise and excess multiplication noise.[11]

In our case, the interference is high 50 percent of the time. We assume that the effect of low threshold and added noise is the product of the effect of each separately. Then the error rate increase factor is

$$\alpha = \tfrac{1}{2}(\alpha_t(\Delta) + \alpha_t(-\Delta)\alpha_n), \tag{1}$$

where α_t and α_n are the error rate increase factors due to threshold offset and light-associated noise, respectively.

The function $\alpha_t(\Delta)$ has been measured (see Fig. 12, "Error Rate Versus

Decision Threshold," of Ref. 7), and we can relate the offset to the interference power by

$$\Delta = 500(P_I/P_S)\text{mV}, \tag{2}$$

where P_I is the interference power and P_S is the signal power. To relate α to P_I/P_S we must also find α_n as a function of P_I/P_S.

If the crosstalk interference is constantly high (not PCM modulated), it will not shift the signal relative to the threshold because of ac coupling. Its only effect on the error rate will be through light-associated noise. This technique was used to measure α_n for one of the crosstalk cases in Fig. 5. For the case $\alpha = 1.65$, we measured $\alpha_n = 1.76$. Then from eqs. (1) and (2), P_I/P_S was calculated to be -17.3 dB for the modulated case. Since the signal in fiber B was 38 dB greater than the signal in fiber A, the crosstalk coupling was -55.3 dB for this case. This is in agreement with measurements by a different technique of the same crosstalk coupling.[10]

Only that one experimental point of α versus P_I/P_S was determined. To generate a complete curve, a computer simulation incorporating a Chernoff bound[12] was used to relate α_n to P_I/P_S. This, together with eqs. (1) and (2), gave the curve of error rate increase factor α versus interference-to-signal ratio in Fig. 6. The simulated results and the experimental point agree within a decibel.

IV. DISPERSION EXPERIMENT

When a pulse of light is launched into a fiber, the components of the pulse will arrive at the end of the fiber with different delays, depending upon the transit times for the modes. Therefore a transmitted pulse becomes dispersed in time as it travels through the fiber. Fibers with a graded index[13] are designed to reduce this effect, but some pulse spreading persists.

A spreading of the impulse response is equivalent to a reduction of the bandwidth. The bandwidths of the fibers in the cable are given in Ref. 14. The average 3-dB bandwidth (half-light power) of the 648-m cabled fibers is 690 MHz with a standard deviation of 286 MHz.

At a bit rate of 44.7 Mb/s, the effect of dispersion on system performance was expected to be small, so the six fibers with smallest bandwidth (high dispersion) were selected for a dispersion study. The average 3-dB bandwidth for the six is 177 MHz with a standard deviation of 27 MHz.

4.1 Measured effect of dispersion

The effect of dispersion was determined by comparing the system performance using high-dispersion fiber with the system performance using dispersionless attenuation (a neutral-density filter) in place of the

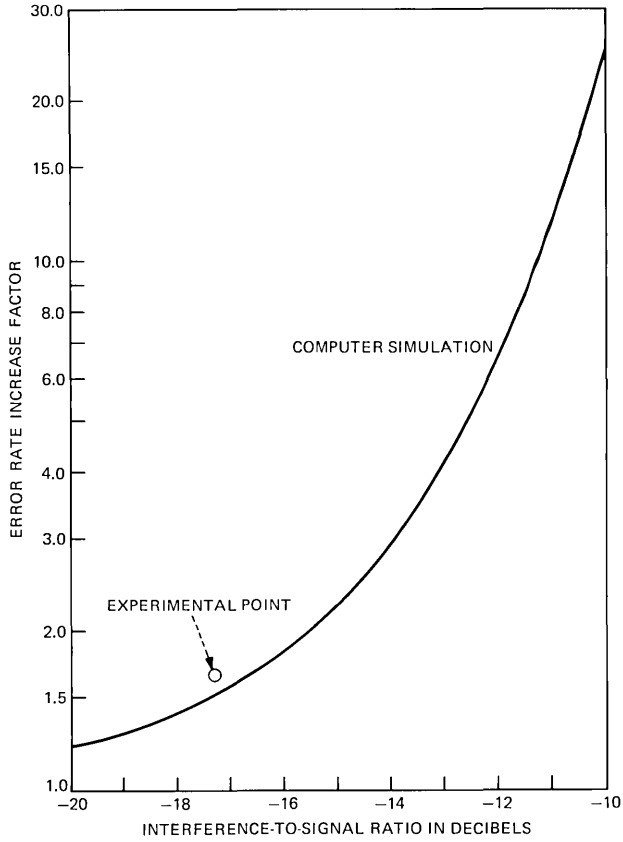

Fig. 6—Effect of crosstalk interference.

fiber. The measure of performance used here is the "system sensitivity"—the detected light power* for a 10^{-6} error rate. The decrease in sensitivity due to dispersion is called the "dispersion penalty."

From one to six of the high dispersion fibers were concatenated using optical jumpers. These fibers were included in the transmission path along with enough dispersionless attenuation to make the error rate 10^{-6}. Then the fibers were removed from the path, and the dispersionless attenuation was increased until the error rate was again 10^{-6}. The difference in detected light power for the two cases is the dispersion penalty for that length of fiber.

The dispersion penalty is plotted as a function of high-dispersion fiber length in Fig. 7. The highest penalty measured was only about 0.5 dB.

* The detected light power is calculated from the measured APD current. For this measurement, the APD bias is set for a known APD gain, so the primary current is known. The detected light power is 1.5 watts per ampere of primary current (for light with a wavelength of 825 nm).

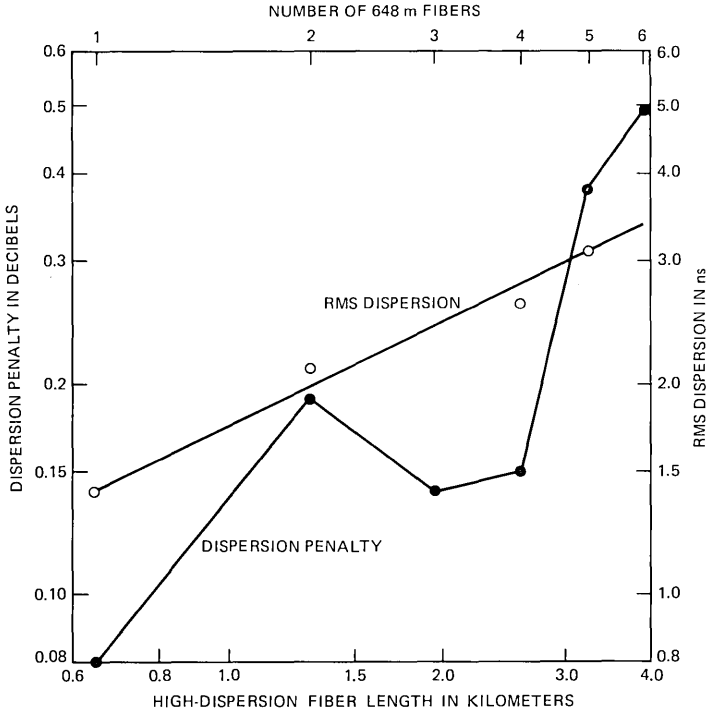

Fig. 7—Effect of high-dispersion fiber.

The curve should be monotonic increasing; the reversals are due to the limits of measurement accuracy.

4.2 Measured RMS dispersion

We have the dispersion penalties for a particular set of concatenated fibers. By measuring the dispersion of those fibers, we can extend the results to any fiber for which the dispersion is known.

The pulse responses for a few lengths of high-dispersion fiber were measured by S. D. Personick using the technique described in Ref. 14. Since the source pulse was only 0.5 ns wide, the pulse response can be considered to be an impulse response. The waveforms for four different lengths of the high-dispersion fiber are shown in Fig. 8. The impulse response broadens with increasing fiber length and approaches what is approximately a Gaussian waveform. Note that the waveform for the shortest fiber length is not smooth, indicating that mode mixing is not complete.

The impulse response is conveniently characterized by one parameter—the RMS dispersion σ defined by[11]

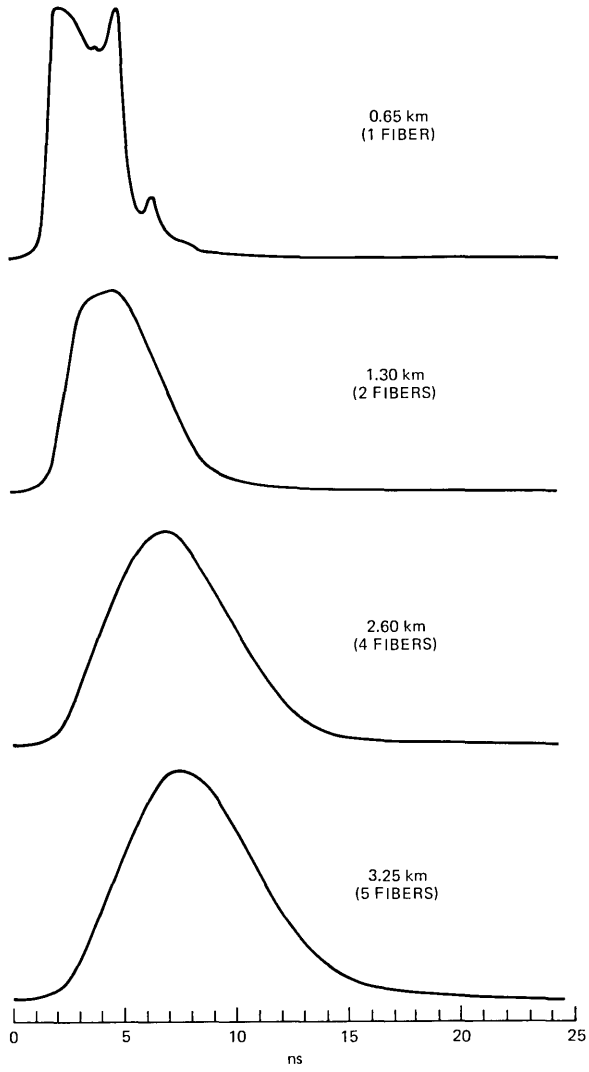

Fig. 8—Impulse responses of high-dispersion fiber.

$$\sigma^2 = \frac{\int t^2 h(t)dt}{\int h(t)dt} - \left[\frac{\int th(t)dt}{\int h(t)dt}\right]^2,$$

where $h(t)$ is the impulse response. The RMS dispersions for the four impulse responses in Fig. 8 are plotted in Fig. 7. The points lie close to a line with a slope of $\frac{1}{2}$, indicating a square-root dependence on length.

From the data in Fig. 7, we can determine the dispersion penalty

versus RMS dispersion (see the plot in Fig. 9). The curve through the data points was generated by a computer simulation using a Chernoff bound approximation of noise.[12] This curve holds for both high- and low-dispersion fiber. The corresponding lengths of high-dispersion fiber are indicated on a scale at the top of Fig. 9. For example, 7 km of high-dispersion fiber would have a dispersion penalty of about 1.0 dB. Even for this worst case, the dispersion penalty (for a bit rate of 44.7 Mb/s) is negligible compared to a loss of about 40 dB for 7 km of fiber.

4.3 Long fiber spans

There was some question whether the method of joining fibers at the fiber distribution frame adequately simulated field splicing methods in regard to dispersion characterization. Every time a 648-m fiber was added to a regenerator span, it was necessary also to add two optical fanouts with two splice interfaces and one optical patch cord with two connector interfaces (see Fig. 3). The numerous connectors and splices contribute significantly to the total loss of a fiber span, and they might also have significantly affected the measured dispersion by providing extra mode mixing.

To eliminate most of these connectors, an experiment was performed using a second cable. This 644-m cable was installed in the ducts in the

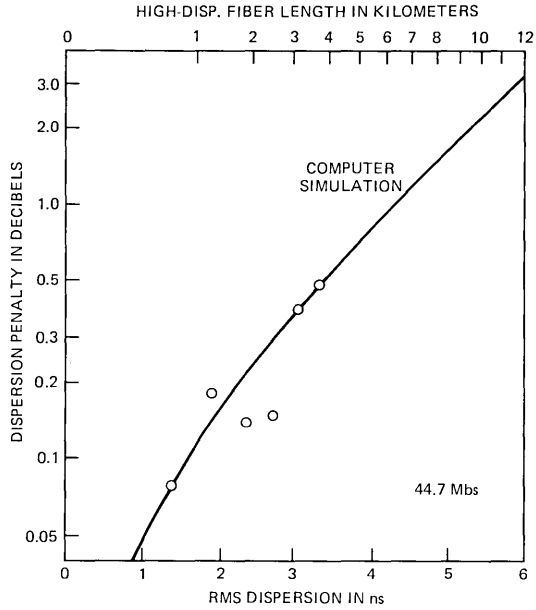

Fig. 9—Effect of RMS dispersion.

same manner as the first cable (see Fig. 1). For these tests, the fiber distribution frame was not used. Instead, fibers were concatenated using low-loss loose tube splices[15] to join individual fibers. One single-fiber connector was used at each end of the long concatenated fiber span to interconnect with the optical regenerators.

Two long fiber spans were constructed by C. M. Miller using these loose tube splices. Assuming that very little mode mixing occurred at the splices, the effect of fiber dispersion could now be accurately measured. Using the technique described above, the dispersion penalty was measured for each long span and compared to the span loss measured by M. J. Buckler.[1] One span was 10.3 km long with a dB loss of 49.2 and a dispersion penalty of 0.5 dB. The other span was 10.9 km in length and had a 47.9 dB loss and a dispersion penalty of 1.1 dB. It is clear that, as in the experiment using numerous connectors, the dispersion penalty is negligible compared to the loss. Therefore it is concluded that fiber-guide dispersion will have only a small effect on regenerator spacing at 44.7 Mb/s.

It should be noted that a length of nearly 11 km is not to be considered a "practical" regenerator spacing. In this experiment, low-loss fibers were selected, splicing losses were minimized, and very little allowance was made for operating margins. It has been estimated that these results translate into a regenerator spacing of approximately 7 km ($\approx$4 miles) for a practical transmission system employing current technology.

V. TIMING JITTER EXPERIMENT

In this experiment, a line of 14 regenerators was set up. The phase of the data at the output of each regenerator was compared with the clock phase of the data source—a maximum length pseudorandom sequence of length $2^{15} - 1$ scrambled by a 17-stage feedback register. In this way, the timing jitter accumulation was measured as a function of the number of regenerators.

Two types of jitter were investigated: random jitter and systematic jitter. In one experiment, as much random jitter as possible was introduced by operating each regenerator near an error rate of 10^{-6} (detected optical power near -55 dBm). The effect on the accumulated jitter was negligible. As will be explained below, random jitter tends to be swamped by systematic jitter as the number of regenerators in the line grows.

Two cases of systematic jitter were investigated. In one, offset current was purposely introduced in the phase-locked loop of each regenerator's timing recovery circuit. This caused a static timing offset μ of -12 degrees in each. In the other case, any offset current was nulled out to reduce μ to less than 1 degree. The measured results are shown in Fig. 10. That the jitter does not always increase monotonically with N is due to measurement error.

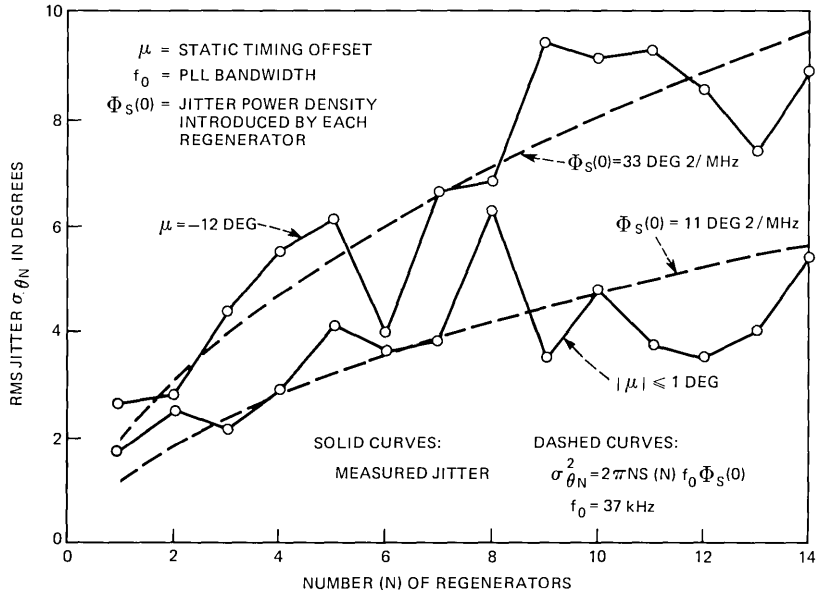

Fig. 10—Cumulative timing jitter. The function $S(N)$ is plotted in Fig. 11.

5.1 Jitter power density from fit to data

Each regenerator adds a certain amount of random jitter, caused by noise, and systematic jitter, caused by data dependence. We assume that each regenerator adds the same amount of jitter, and that the jitter power density spectra of the random and systematic components are $\Phi_R(f)$ and $\Phi_S(f)$, respectively. (The unit of the "power" density is degrees^2/Hz.) The spectra can be considered, for all practical purposes, to be flat and equal to $\Phi_R(0)$ and $\Phi_S(0)$. The cumulative RMS jitter $\sigma_{\theta N}$ is given by

$$\sigma_{\theta N}^2 = \sqrt{\pi N}\, R(N) f_0 \Phi_R(0) + 2\pi N S(N) f_0 \Phi_S(0), \tag{3}$$

where N is the number of regenerators, f_0 is the average PLL bandwidth, and $R(N)$ and $S(N)$ are "correction factors" needed for small N; they go to unity for large N (see Fig. 11). The first term, giving the dependence of N for random jitter, is due to DeLange.[16] The second term (systematic jitter) is due to Byrne, et al.[17]

In both experiments the measured spectra of the jitter power density displayed the notches associated with systematic jitter[17] (see Fig. 12). The depth of the notches indicated that the contribution from random jitter was insignificant. Therefore the RMS jitter $\sigma_{\theta N}$ should grow with $\sqrt{N}$, as seen from the second term in (3). Using this relation, we fitted curves to the measured data by selecting $\Phi_S(0)$ for each case. For $\mu = -12$ degrees, the fitted $\phi_S(0)$ is 33 deg^2/mHz and for $\mu < 1$ degree, the fitted $\Phi_S(0)$ is 11 deg^2/mHz.

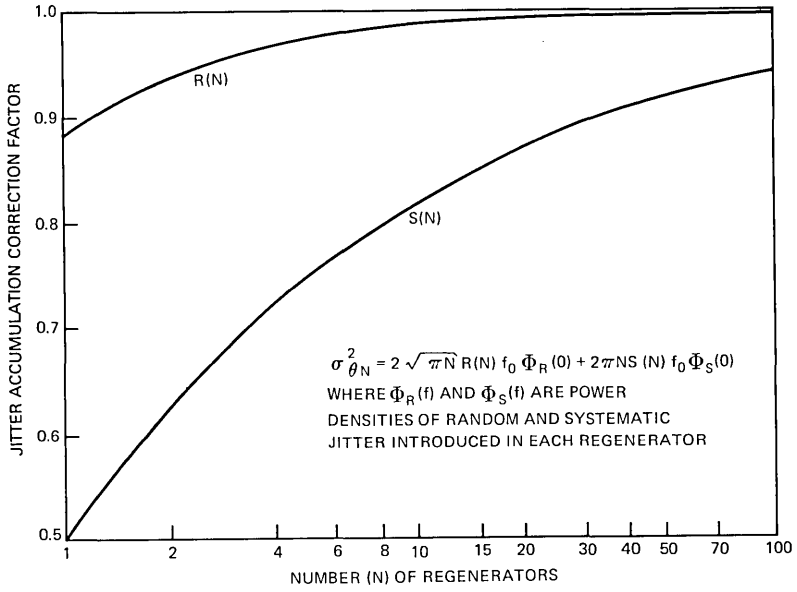

Fig. 11—Jitter accumulation correction factors.

5.2 Jitter power density calculated from model

Duttweiler[18] has done a computation of the jitter power densities $\Phi_R(0)$ and $\Phi_S(0)$ for a PLL that models the one used here fairly well. $\Phi_R(0)$ is calculated from the noise present at the output of the linear channel. $\Phi_S(0)$ is calculated from the static timing offset μ and from the pulse response of the linear channel (intersymbol interference). The analysis assumes a random data signal.

Using the pulse response in Fig. 9 of Ref. 7, the $\phi_S(0)$ for $\mu < 1$ degree was calculated to be 1.5 deg^2/MHz. This would produce only 37 percent of the measured jitter. The $\phi_S(0)$ for $\mu = -12$ degrees was calculated to be 7.7 deg^2/MHz. This would produce only 50 percent of the measured jitter. The discrepancy is not completely understood, but it may be due in part to the difference between random and pseudorandom data.

The measured data can be extrapolated by (3), neglecting random jitter. For $\mu = -12$ degrees and $N = 50$, the RMS jitter would be 19 degrees. This represents a worst case with the offset in the PLL of all regenerators at the maximum and in the same direction. Even this worst case is well within the capability of the terminal circuits, which can handle up to 30 degrees RMS jitter.

VI. SYSTEM RECOVERY EXPERIMENT

The objective of this experiment was to measure the response of the transmission system to signal interruptions of the sort that might be expected in actual application. We also wanted to gain an understanding

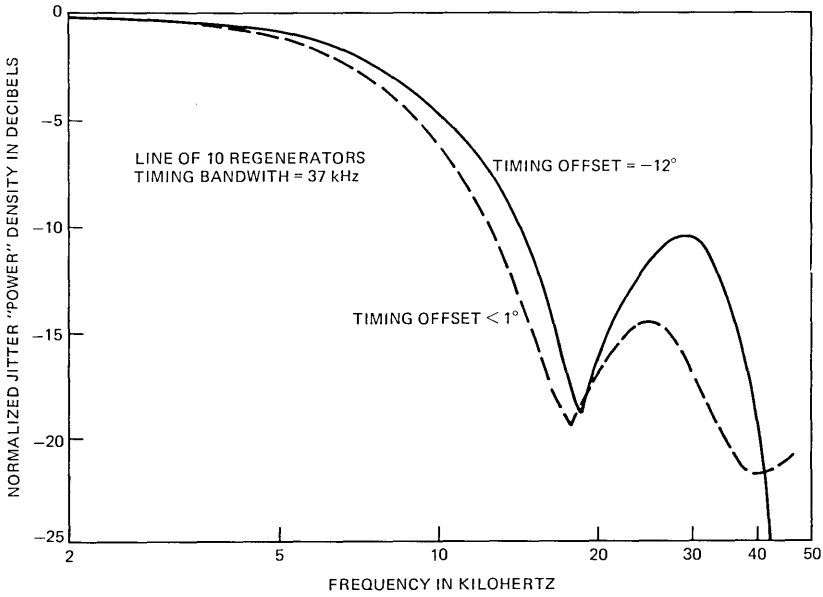

Fig. 12—Spectra of systematic jitter.

of the mechanisms affecting the recovery. To this end, recovery time was measured as a function of the interruption interval and the signal level. First we investigate the response of a single regenerator, then a line of regenerators in tandem, then a maintenance span with terminal circuits, and finally a number of maintenance spans in tandem.

In each test the data input to the system (or subsystem) was interrupted and set to logical "zero" for intervals of 0.2, 1.0, 3.0, and 10.0 ms. Following this, the data resumed.* The 0.2-ms interval is the expected maximum interruption that would be incurred during a protection switch. An interruption of 3.0 ms can occur due to the characteristics of the terminal circuits. A 10-ms interruption is typical of that during manual patching for service restoration or rolling.

6.1 Regenerator recovery

The input to a regenerator was supplied by a pseudorandom data source, and the output of the regenerator was monitored by a bit-error-rate test set (BERTS). The BERTS received a clock signal directly from the source so that it maintained synchronism during the interruption. The recovery time was defined as the time from the end of the interruption to the beginning of the first error-free second.

* Some tests were made in which the resumed data had a baud shifted 1.0 kHz from the original rate. However, this was found to have no measurable effect on the recovery time.

Typical regenerator recovery times are plotted in Fig. 13. The response is a function of both the interruption interval and the input signal level—the detected optical power. For interruptions up to 3.0 ms, the recovery times are 0.1 ms or less. For an interruption of 10 ms, the recovery times are between 0.4 and 4.0 ms. We will examine the mechanisms governing these responses.

Part of the recovery mechanism is illustrated in Fig. 14, which shows the signal at the decision point in the regenerator. After 0.3 ms or more of interruption time, the ac coupling in the linear channel causes the signal to be displaced upward by about 500 mV. When the data signal

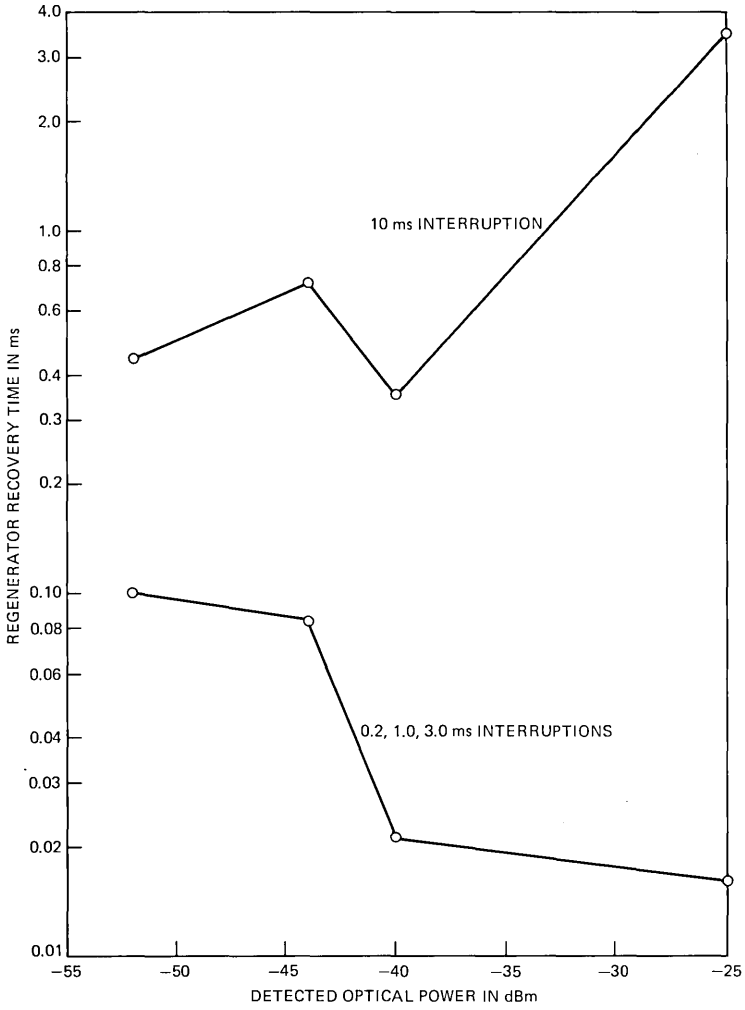

Fig. 13—Regenerator recovery times.

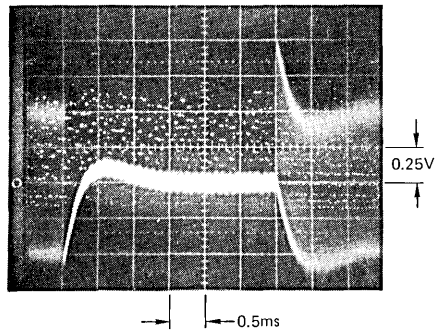

Fig. 14—Signal at decision point for 3.0-ms interruption and −44-dBm detected optical power.

returns, the signal in Fig. 14 drops to its proper position with the time constant of about 0.25 ms. The error rate is high until the "eye opening" moves down to include the decision threshold at −70 mV. Recovery is then complete. With greater detected optical power, the "eye" is more open, and the recovery time is shorter. This explains the characteristic of the lower curve in Fig. 13.

For a 0.2-ms interruption and high (−25 dBm) detected optical power, the "eye opening" does not have time to drift so far that it does not include the decision threshold upon the return of data. For this case the recovery might be expected to be immediate. However, another mechanism becomes important—the 15 μs recovery time of the phase-locked loop (PLL) in the timing circuitry. The result is that the response curve for a 0.2-ms interruption is about the same as that for 1.0-ms and 3.0-ms interruptions.

The upper curve in Fig. 13 indicates significantly greater recovery times for 10-ms interruptions. One reason for this is that the automatic gain control (AGC) has time to drift during the interruption so that the signal can be very large upon return of the data. In high (−25 dBm) detected optical power, this can lead to a saturation effect that incapacitates the linear channel of the regenerator for a number of milliseconds. This effect is shown in Fig. 15. After the data resume and the 0.25-ms transient is over, the signal remains unsymmetric for 2 to 4 ms. This indicates a badly distorted signal that results in errors.

For detected optical powers of −40 dBm and lower, the saturation effect does not occur. In this range, another mechanism dominates in causing longer recovery times for 10-ms interruptions. In some regenerators, there was enough offset in the PLL to cause it to drift out of its seize range during a 10-ms interruption. In that case, the recovery time of the PLL was about 0.5 ms.

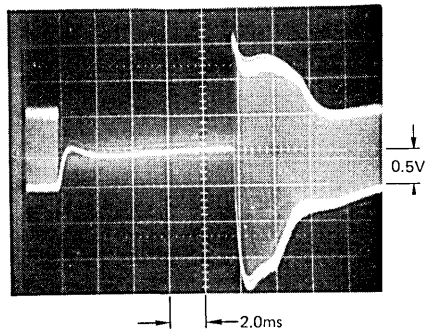

Fig. 15—Signal at decision point for 10-ms interruption and −25-dBm detected optical power.

6.2 Line recovery

Lines of as many as nine regenerators were constructed as in Fig. 3. In this part of the experiment, the terminal circuits were not included. The recovery times for various numbers of regenerators in tandem were measured by the method outlined for single regenerators. Typical results for a 3.0-ms interruption are plotted in Fig. 16. Notice that the recovery time grows more slowly than the number of regenerators.

It was not expected that the recovery time for a line of N regenerators

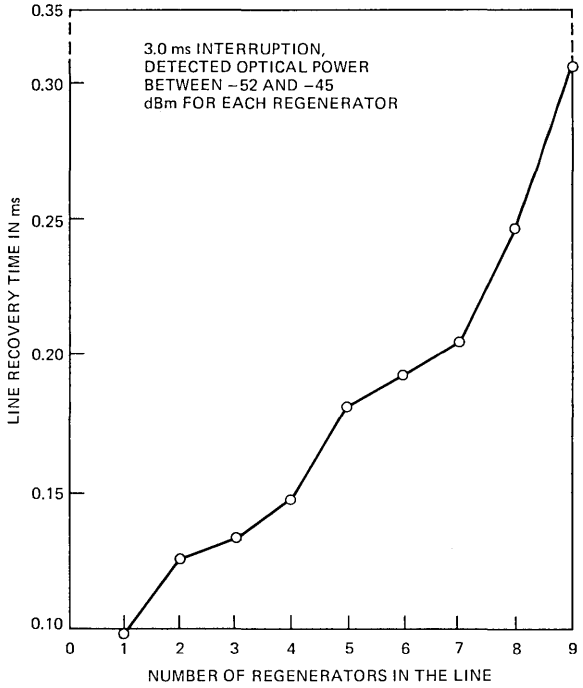

Fig. 16—Line recovery times.

would be N times the recovery time for one regenerator. The recovery mechanisms in the second regenerator can begin while the first regenerator is still recovering and putting out erroneous data.

The recovery of downstream regenerators is also affected by the activity of earlier regenerators *during* the interruption. With no lightwave signal at the input of the first regenerator, its PLL continues to free run. It continues to clock out whatever signal appears at the decision point, including noise. For example, Fig. 14 shows the noise meeting the decision threshold (−70 mV) after about 1.3 ms of interruption. For the rest of the interruption, the regenerator provides noise-like data to the second regenerator. For higher noise at the decision point, the interruption seen by the second regenerator becomes even more filled in.

The filling in of the interruption continues down the line of regenerators until only the first few tenths of a millisecond remain free of noise-like data. Figure 17 shows a typical example of the signal appearing at the decision point of the eighth regenerator in a line during a 10-ms interruption.

One effect of filling in the interruption is to keep the AGC from drifting out of adjustment. Therefore, the saturation effect, which causes long recovery times, can occur only in the first few regenerators in a line.

Another effect of filling in the interruption is to keep the PLL of each regenerator locked to the frequency of the PLL in the previous regenerator. This has little effect on the recovery time unless the PLL offset in one of the first few regenerators is large. In that case, the PLL drifts out of its seize range during a 10-ms interruption. If there is sufficient noise at the decision point, the noise-like data at the output cause all downstream regenerators to be pulled out of their seize range. For such a case, the recovery time for each regenerator is long, and line recovery times as high as 9 ms were measured for a line of nine regenerators.

Extrapolating the measured results to a line of 20 regenerators, we expect line recovery times of less than 1.0 ms for interruptions of 3 ms or less. Recovery times for interruptions longer than 3 ms can be greater.

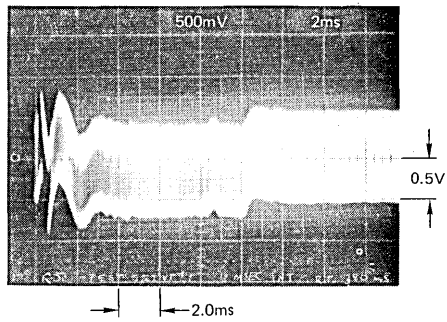

Fig. 17—Signal at the decision point of eighth regenerator in a line, illustrating the filling in of a 10-ms interruption.

It is planned to limit the PLL offset so that the PLL remains within its seize range for interruptions up to 10 ms. In that case, the expected line recovery time would be as much as 4 ms for interruptions from 3 to 10 ms. Such recovery times would be dominated by saturation effects in the first regenerator.

6.3 Maintenance span recovery

In this portion of the recovery experiment, the line of regenerators was extended to include the terminal circuit on each end (see Fig. 3). The recovery time was measured from DS3 interface to DS3 interface. The measurement method was, by necessity, different from that used for the regenerator and line recovery tests. The bit-error-rate test set that operates with the DS3 format requires framing to do bit error measurements, and the test set reframe time prevents accurate determination of recovery time. Therefore we need another measure of recovery time.

For some cases, the receive terminal circuit (RTC) itself provides a meaningful measure of recovery time. If the RTC is unable to frame on the data it receives for about 3 ms, it inserts a "blue signal" to satisfy downstream equipment. When the RTC is able to reframe, the blue signal is removed, and data transmission is resumed. We define maintenance span recovery time as the time from the end of the interruption to the removal of the blue signal by the RTC. One limitation of this definition is that only recovery times in response to interruptions of 3 ms or longer can be measured. Otherwise, the blue signal is not inserted. This is not a serious limitation, since the terminal circuits should have no effect on the recovery time for interruptions less than 3 ms.

The expected recovery time for a maintenance span is simply the line recovery time plus the reframe time of the RTC. This expectation was confirmed by recovery time measurements. The maximum average reframe time for the RTC is 1.5 ms. Therefore we expect a recovery time less than 5.5 ms for a maintenance span of 20 regenerators for interruptions of 3 to 10 ms. For interruptions less than 3 ms, we expect maintenance span recovery times less than 1.0 ms (the line recovery time).

6.4 System recovery for maintenance spans in tandem

Sufficient system elements were available to arrange three maintenance spans in tandem for a total transmission distance of 61 km (38 miles). With this arrangement it was possible to observe the effect of signal interrupts in one maintenance span on subsequent maintenance spans. These tests served to confirm the failure sectionalization capabilities of the receive terminal circuit (RTC) and uncovered no anomalies in system operation. If, during an interruption, all downstream main-

tenance spans have had time to reframe on the blue signal inserted by the RTC of the span experiencing the interruption, then the total system recovery time is simply the recovery time of the interrupted maintenance span. This also holds true, of course, if the interruption is less than 3 ms since all the RTCs start to reframe simultaneously when the data resume.

The system behavior is more complicated in the situation where downstream RTCs do not have time to frame on the failed span's blue signal during the interruption. In the worst case, the total system recovery time is the recovery time of the interrupted maintenance span plus the reframe times of the downstream RTCs.

The system recovery performance described here should be adequate to virtually insure that calls will not be dropped during normal maintenance activity.

VII. DC POWERING EXPERIMENT

The +5.0-Vdc and −5.2-Vdc supply voltages for the regenerators and terminal circuits were provided by dc-to-dc converters operating from 48 Vdc. In this experiment, we monitored system performance while inducing transients on the common power distribution bus. The results led to some modifications of the regenerator circuit.

Normal activity on a bay of equipment includes the connection and removal of regenerator units. (A regenerator draws about 150 mA from the +5.0 Vdc supply and 390 mA from the −5.2 Vdc supply.) The resulting transients appearing on the common power distribution bus must not impair the performance of working equipment in the bay.

Tests were made on a maintenance span in which each regenerator had a detected optical power between −52 and −45 dBm. It was found that the load change of connecting and removing one regenerator caused the system to make a significant number of errors. The sensitivity was traced to the regenerators and not the terminal circuits.

Further tests were made with even larger load changes to insure that worst-case situations would be covered with adequate margin. A load change of 790 mA on the −5.2-Vdc supply caused about 100 errors. A load change of 720 mA on the +5.0-Vdc supply would induce RTC out-of-frames.

Some waveforms accompanying this out-of-frame response are shown in Fig. 18. The voltage on the +5.0 Vdc supply bus shows a 200-mV spike and step change of 70 mV. This transient is a function of not only the current load change but also the bus impedance and the dc-to-dc converter characteristics. Figure 18 also shows the signal at the decision point in the regenerator. The 1-v transient during the recovery of dc level was the immediate cause of the errors.

One regenerator was modified to improve the filtering of the supply

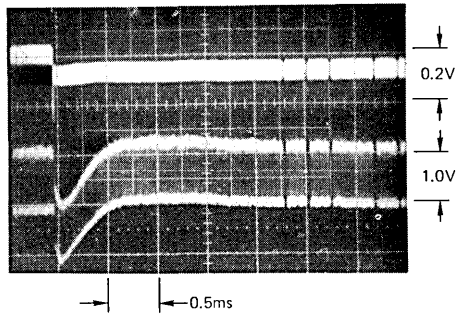

Fig. 18—Transients accompanying a step load change of 720 mA on the +5.0-Vdc supply. Upper trace: voltage on +5.0-Vdc supply buss. Lower trace: voltage at decision point in regenerator.

voltages in its linear channel. The above tests with load changes of about 720 mA were repeated on the modified regenerator. No errors resulted. Subsequently, all regenerators were similarly modified.

Another source of interference on the supply busses is from the dc-to-dc converters themselves. However, the specification for the power units guarantees 30 mV peak-to-peak or less ripple at their outputs. The tests on the modified regenerator assured us that transients up to 100 mV peak-to-peak cause negligible degradation. The conclusion is that the modified regenerator will tolerate all power supply transients and noise routinely incurred in an operating bay.

VIII. CONCLUSIONS

The Atlanta Fiber System Experiment was begun with high expectations for the system performance. There was some uncertainty due to lack of experience with lightwave systems; the Atlanta system was the Bell System's first complete lightwave system available in conditions approximating field environment. These experiments provided us with the needed experience, and in all cases the system met or exceeded our expectations.

Measurable crosstalk between fibers proved to be rare and to have only a negligible effect on system performance when it did occur. The effect of fiber dispersion is small compared to that of fiber loss; at 44.7 Mb/s the regenerator spacing is essentially loss-limited, not dispersion-limited. The jitter accumulation in a line of 50 regenerators should be well within the capability of the terminal circuits. System recovery time will be a fraction of interruption times caused by protection switches. This should virtually assure that no calls are dropped. The modified regenerator tolerates power supply transients and noise such as would be expected in a field application.

Through experience with the Atlanta lightwave system, we gained confidence in our technology. We were assured that the system and

equipment design will meet the conditions of a practical Bell System installation.

IX. ACKNOWLEDGMENTS

Much of the test circuitry used in the experiments was constructed by H. W. Proudfoot. We gratefully acknowledge his effort as well as that of M. J. Buckler, S. S. Cheng, V. J. Mazurczyk, and C. M. Miller in assisting with some of the tests. D. D. Sell provided valuable aid in designing the experiments and interpreting their results.

REFERENCES

1. R. S. Kerdock and D. H. Wolaver, "Performance of an Experimental Fiber-Optic Transmission System," Conference Record of National Telecommunications Conference, November 29 to December 1, 1976.
2. T. L. Maione and D. D. Sell, "Experimental Fiber-Optic Transmission System for Interoffice Trunks," IEEE Trans. on Communications, *COM-25,* No. 5 (May 1977), pp. 517–523.
3. I. Jacobs, "Lightwave Communications Passes Its First Test," Bell Laboratories Record, December 1976, pp. 291–297.
4. M. I. Schwartz, "Optical Fiber Cabling and Splicing," Technical Digest of Topical Meeting on Optical Transmission, Williamsburg, Virginia, January, 1975, pp. WAZ-1 to WAZ-4.
5. C. M. Miller, "A Fiber-Optic-Cable Connector," B.S.T.J., *54,* No. 9 (November 1975), pp. 1547–1555.
6. P. K. Runge and S. S. Cheng, "Demountable Single Fiber Optical Fiber Connectors and Their Measurement on Location," B.S.T.J., this issue, pp. 1771–1790.
7. T. L. Maione, D. D. Sell, and D. H. Wolaver, "Practical 45 Mb/s Regenerator for Lightwave Transmission," B.S.T.J., this issue, pp. 1837–1856.
8. R. G. Smith, C. A. Brackett, and H. W. Reinbold, "Optical Detector Package," B.S.T.J., this issue, pp. 1809–1822.
9. P. W. Shumate, Jr., F. S. Chen, and P. W. Dorman, "GaAlAs Laser Transmitter for Lightwave Transmission Systems," B.S.T.J., this issue, pp. 1823–1836.
10. M. J. Buckler and C. M. Miller, "Optical Crosstalk Evaluation for Two End-to-End Lightguide System Installations," B.S.T.J., this issue, pp. 1759–1770.
11. S. D. Personick, "Receiver Design for Digital Fiber Optical Communication Systems, I," B.S.T.J., *52,* No. 6 (July–August 1973), pp. 843–874.
12. S. D. Personick, P. Balaban, and J. H. Bobsin, "A Detailed Comparison of Four Approaches to the Calculation of the Sensitivity of Optical Fiber Systems Receivers," IEEE Trans. Communications, *COM-25,* No. 5 (May 1977), pp. 541–548.
13. A. G. Chynoweth, "The Fiber Lightguide," Physics Today, May 1976, pp. 28–37.
14. M. R. Santana, M. J. Buckler, and M. J. Saunders, "Lightguide Cable Manufacture and Performance," B.S.T.J., this issue, pp. 1745–1757.
15. C. M. Miller, "Loose Tube Splices for Optical Fiber," B.S.T.J., *54,* No. 7 (September 1975), pp. 1215–1225.
16. O. E. DeLange, "The Timing of High-Speed Regenerative Repeaters," B.S.T.J., *37,* No. 6 (November 1958), pp. 1455–1486.
17. C. J. Byrne, et al., "Systematic Jitter in a Chain of Digital Regenerators," B.S.T.J., *42,* No. 6 (November 1963), pp. 2692–2714.
18. D. L. Duttweiler, "The Jitter Performance of Phase-Locked Loops Extracting Timing from Baseband Data Waveforms," B.S.T.J., *55,* No. 1 (January 1976), pp. 37–58.

THE BELL SYSTEM TECHNICAL JOURNAL
Vol. 57, No. 6, July–August 1978
Printed in U.S.A.

Atlanta Fiber System Experiment:

The Chicago Lightwave Communications Project

By M. I. SCHWARTZ, W. A. REENSTRA, J. H. MULLINS, and J. S. COOK

(Manuscript received January 25, 1978)

The Bell System installed and is evaluating an exploratory lightwave communications system in downtown Chicago. In addition to regular interoffice trunk service, the system provides a range of telecommunications services to customers in Chicago's Brunswick Building, including voice, analog data, digital data, and PICTUREPHONE® *Meeting Service, a 4-MHz video service. This paper describes the transmission medium, its installation, and the system configuration, and includes some preliminary performance data.*

I. INTRODUCTION

The Atlanta Fiber System Experiment[1,2] utilizes cable ducts similar to those currently being installed in the telephone plant, but atypical of active Bell System ducts in that they were dry and uncrowded.

In 1976, new cable-placing methods and equipment were developed and tested at Bell Laboratories' Chester, New Jersey location. With these methods and equipment, optical fiber cables like those used in Atlanta[3] but containing only two ribbons (24 fibers) were installed in downtown Chicago in February 1977. The location was selected for the range of services that could be provided on fibers, as well as for the demanding cable route, representative of those found in busy, long-established metropolitan areas.

During the winter months, much of the Atlanta Experiment equipment was modified, replaced, or repackaged, and shipped to Chicago. On April 1, 1977 the first commercial traffic was carried on the new system, and on May 11 the Chicago Lightwave Communication System was fully cut over. Video encoders and other terminal equipment had been added so that the system could provide customer voice and data

service, and *PICTUREPHONE*® Meeting Service (PMS) as well as regular interoffice trunk service.

II. SYSTEM CONFIGURATION

Figure 1 is an overview of the Chicago Lightwave System. Standard video signals from a PMS customer in the Brunswick Building are digitally encoded and transmitted at the DS3 rate (44.7 Mb/s) using a pair of fibers (one for the return signal) in a 1-km long optical cable extending from the Brunswick Building to the Franklin Central Office (CO). There the fibers are connected directly to a pair of fibers in a second cable, 1.6 km long, between the Franklin CO and the Wabash CO. Thus, the length of this optical link is 2.6 km. The video is decoded and carried by standard means to the Television Operating Center (TOC) adjacent to the Wabash CO where it can be connected to standard intercity video circuits. Another pair of fibers in the second cable provides a two-way link between the TOC and a public PMS room at Illinois Bell Telephone (IBT) Headquarters, which is adjacent to the Franklin CO.

The Brunswick-to-Franklin cable also carries customer voice and data signals. Using three of its full capacity of 28 DS1 (1.54 Mb/s) channel inputs, an M13 multiplex combines 78 voice circuits and one 2.4-kb/s analog data signal from two *SLC**-40 (subscriber loop carrier) terminals, and two 4.8 kb/s digital data signals onto a single pair of optical fibers. The digital data signals are connected by a T1 (DS1 rate) circuit to the Canal St. Digital Data Service Office.

A third pair of fibers in the Franklin-Wabash cable carries 576 interoffice trunk circuits (24 DS1 channels). Here, again, M13 multiplexes combine signals from standard T1 systems to produce 44.7 Mb/s streams that pass through the fibers. Voice and data links are backed up by an operating spare fiber pair in each cable. All fiber links operate at 44.7 Mb/s, just as they did in Atlanta. The Franklin CO installation is shown in Fig. 2.

III. OPTICAL CABLE

The optical cable design used in Chicago is identical to the one used in Atlanta except that two ribbons (each containing 12 fibers produced by Western Electric—Atlanta) rather than 12 ribbons were used (Fig. 3). Three long cables, each approximately 1 km in length, and four short cables ranging from 160 to 460 m were made by Bell Laboratories for the project. Two fiber breaks occurred in one of the long cables and two breaks occurred in a 180-m cable; all breaks occurred in cable manufacture. The remaining four cables had no broken fibers. Two of the long cables and the three unbroken short cables were cut into ten cable segments of specified lengths. Half-connectors of the type reported pre-

* Trademark of Western Electric.

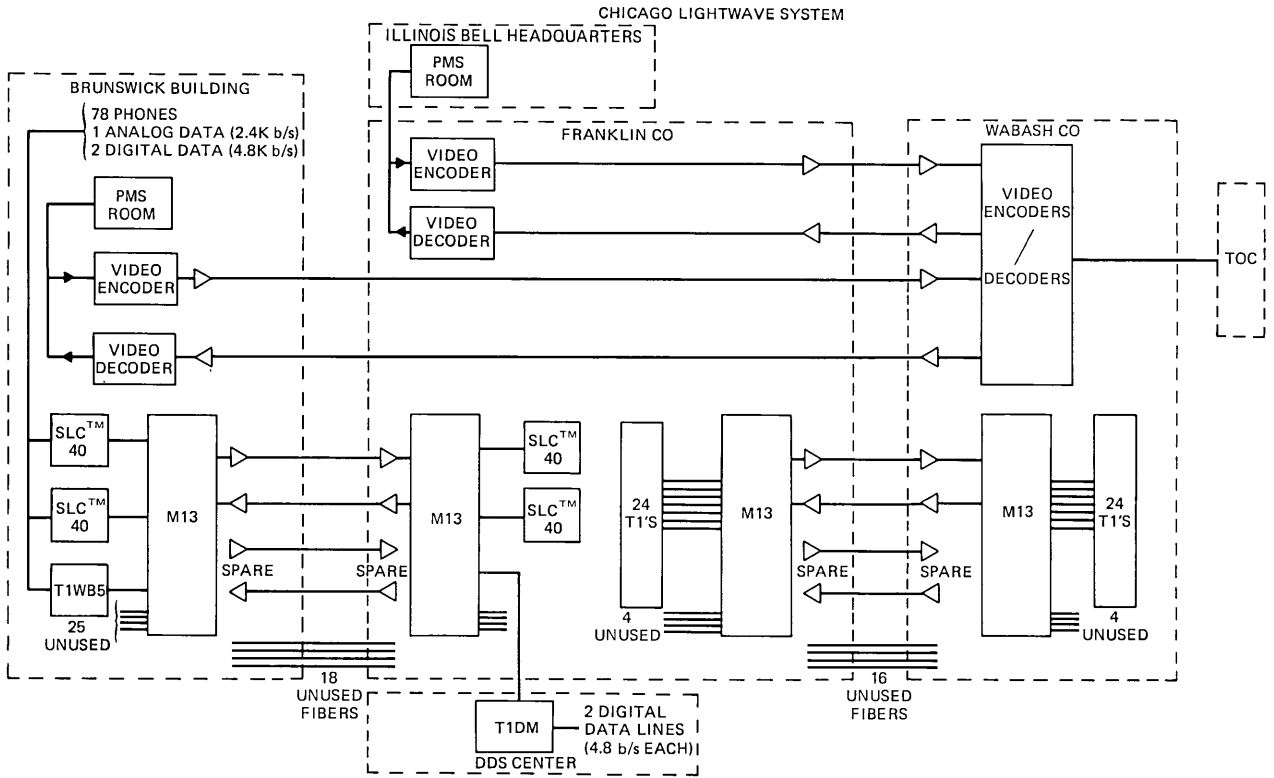

Fig. 1—Chicago lightwave system.

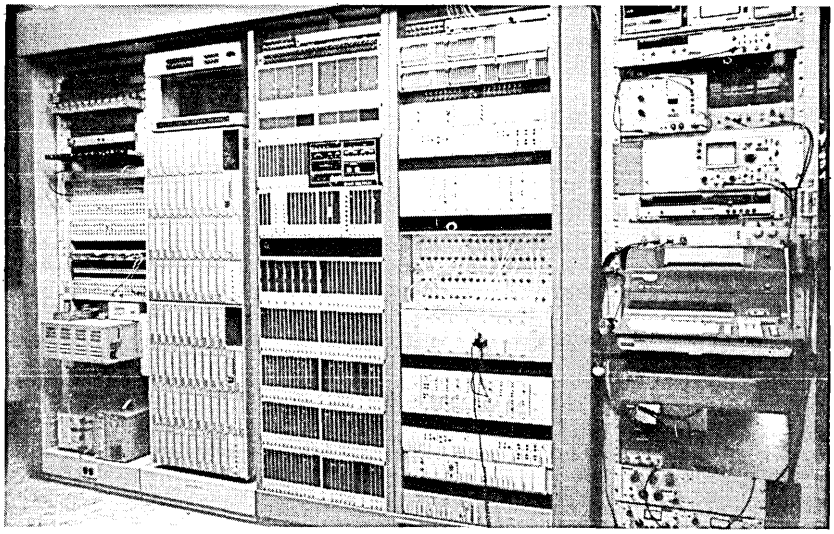

Fig. 2—Franklin Central Office installation.

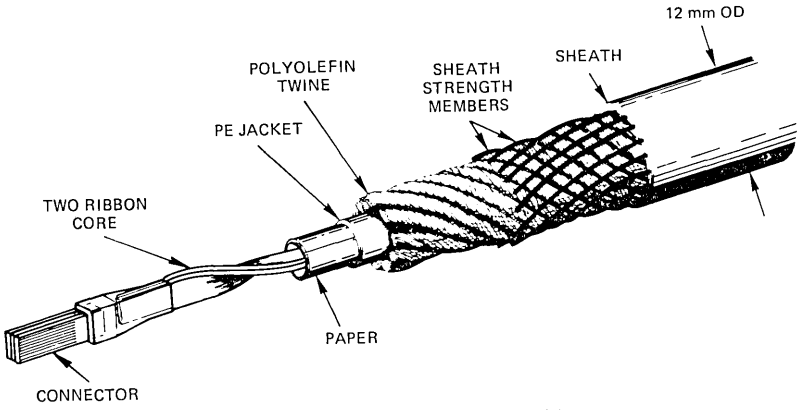

Fig. 3—Two-ribbon lightguide cable.

viously[4,5] were fabricated on all 10 cables. As a result, when the cables were installed in the field, splicing was a straightforward job that did not involve handling individual fibers. Figure 4 is a photograph of a half-connector formed on one end of a two-ribbon cable.

Figure 5 is a comparison of the loss histograms of the three long Chicago cables with the Atlanta Experiment cable.[3,4]

At the system wavelength of 0.82 microns, the mean loss of the Chicago cables was 5.1 dB/km, whereas the mean loss of the Atlanta Experiment cable was 6.0 dB/km. Most loss reduction is due to the smaller added loss (micro-bending loss) of 0.5 dB/km as opposed to 1.3 dB/km in the Atlanta Experiment.

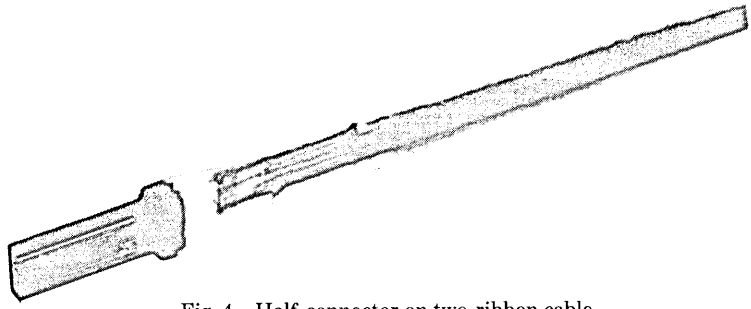

Fig. 4—Half-connector on two-ribbon cable.

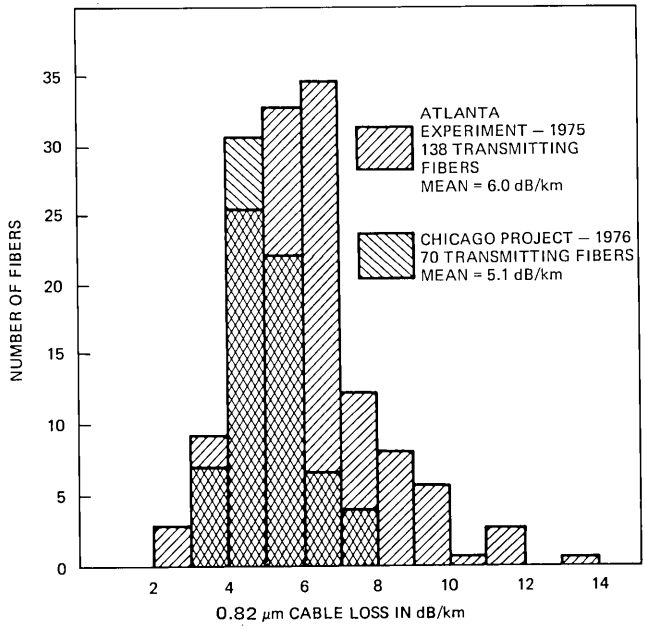

Fig. 5—Cabled fiber losses.

IV. CABLE INSTALLATION

Figure 6 shows the optical cable route connecting the Brunswick Building to the Franklin CO to the Wabash CO. Two short connectorized optical cables were installed from the cable vault to the equipment bay in the Franklin CO by WE and IBT personnel, and a similar intrabuilding cable was installed in the Wabash CO. The remaining seven connectorized cables were installed in underground ducts along the route with five outside plant manhole splices located as indicated in Fig. 6. Since there was no cable vault in the Brunswick Building, the cable entering the building ran directly to the equipment bay.

Before the installation of 12-mm O.D. optical cable, a polyethylene inner duct with an I.D. of 24 mm was installed inside the existing old tile

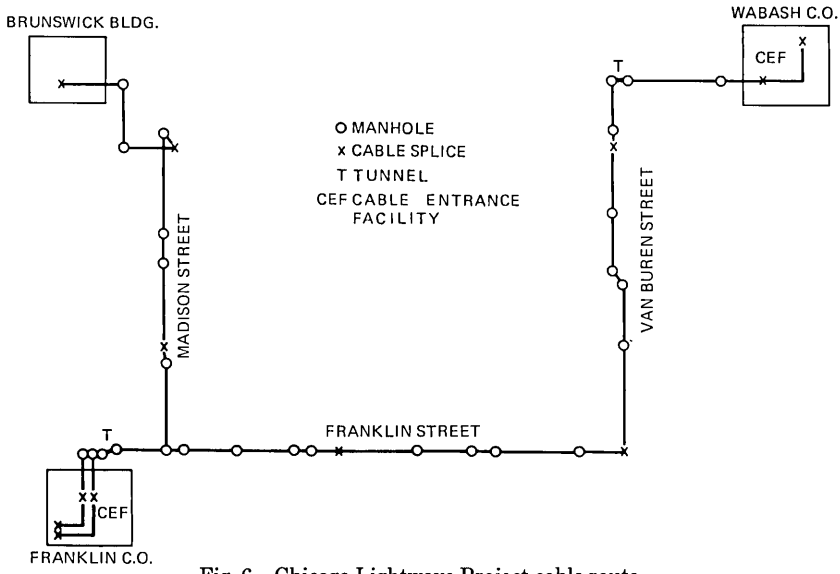

Fig. 6—Chicago Lightwave Project cable route.

duct by IBT personnel. The inner duct provided a controlled environment for the optical cable as well as a simple method of pressurizing around the optical cable. No problems were encountered in installing and splicing the inner duct. The optical cables were pulled into the inner duct and spliced by Bell Laboratories with the assistance of IBT personnel. Special optical cable installation equipment was designed and built by Bell Laboratories, including sheaves and a special reel and reel-handling assembly, that allowed cable to be payed out in opposite directions from an intermediate point. The two-way cable pull reduced the cable pulling tension when the cables were placed. All 10 cables were pulled in without any breakage in the installation process. The five cable manhole splices and seven inside building cable splices were made in a manner similar to that described previously.[4] The optical splices were enclosed and well protected by a special case inside a modified splice case. The splice cases also permitted pressurization continuity of the inner duct.

V. PERFORMANCE OF THE INSTALLED MEDIUM

After cable installation and splicing was completed, loss measurements were made on the two cable routes, Franklin-Brunswick and Wabash-Franklin. Loss histograms for the 24 fibers in each cable route are shown in Fig. 7. Based on these data and cable loss measurements alone, it is estimated that cable splice losses average about 0.5 dB per splice. Since the transmission distances are short in the Chicago route, the longest

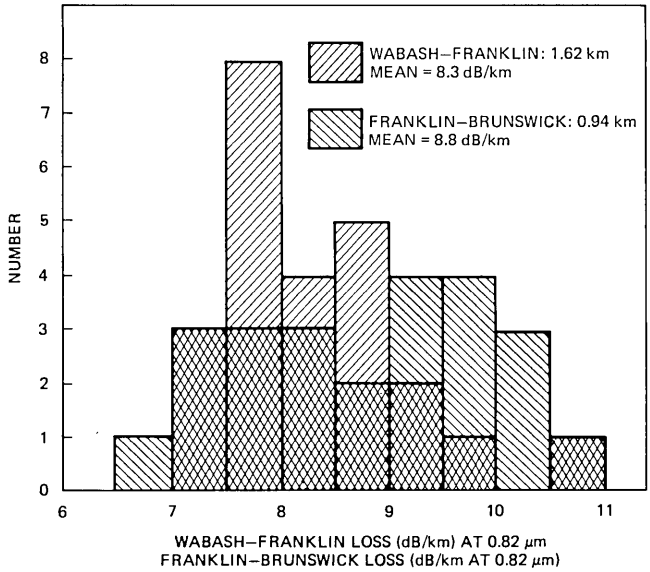

Fig. 7—Installed, spliced Chicago lightguide loss.

being about 2.6 km, neither the loss nor the bandwidth limit of the system is approached.

It is of interest to roughly estimate what the maximum regenerator spacing could be at the DS3 rate for a system using the Chicago technology. In doing this, we assume the following average values:

Allowable loss at DS3	= 46.0 dB
Single fiber connector loss*	= 0.5 dB
Cable splice loss	= 0.5 dB
Average connectorized unspliced cable length	= 350 m
Cabled fiber loss	= 5.1 dB/km

With these values, an average loss budget can be constructed (Table I). The results indicate that a spacing of about 6.5 km, including building cable, is achievable with this technology.†

VI. SYSTEM PERFORMANCE

The Chicago Lightwave Communication System was fully cut over on May 11, 1977 and has been carrying voice, data, and PMS to commercial customers on a trial basis since that time. A repeat of loss mea-

* In Chicago, an improved version of the single-fiber connector reported previously (Refs. 7–9) was used.

† This is intended to provide a rough estimate of regenerator spacing. An actual system design must account more carefully for loss distributions as well as for mean losses.

Table I — Estimating regenerator spacing at the 44.7 Mb/s rate, based on Chicago technology

Average loss budget

Item	No.	Loss (dB)
Single fiber connectors	4	2.0
Terminal cable splices	4	2.0
Building cables (2 × 130 m)	2	1.3
Outside cables (6.3 km)	18	32.2
Outside cable splices	17	8.5
		46.0

surements on the installed spliced medium, made two weeks after the initial measurements, showed no changes.

All spans except those used for video are continuously monitored. As of mid-December, 1977, the system had no outage; 75 percent of the days of operation had been error-free, 99.999 percent of seconds had been error-free, and one laser failure had occurred in 75,000 cumulative device hours, a record consistent with the expected mean time to failure of those devices in excess of 100,000 hours.

VII. ACKNOWLEDGMENTS

The work reported here, carried out under the auspices of AT&T, was accomplished through the extensive efforts and many individual contributions of WE, IBT, AT&T, and Bell Laboratories personnel. Its success stands as a tribute to the work and cooperation of everyone involved.

REFERENCES

1. I. Jacobs, "Atlanta Fiber System Experiment: Overview," B.S.T.J., this issue, pp. 1717–1721.
2. I. Jacobs, "Lightwave Communications Passes Its First Test," Bell Laboratories Record, *54,* No. 11 (Dec. 1976), pp. 291–297.
3. M. I. Schwartz, R. A. Kempf, and W. B. Gardner, "Design and Characterization of an Exploratory Fiber Optic Cable," Second European Conference on Optical Fiber Communications, Paris, Sept. 1976, pp. 311–314.
4. C. M. Miller, "A Fiber-Optic Cable Connector," B.S.T.J., *54,* No. 9 (Nov. 1975), pp. 1547–1555.
5. C. M. Miller and C. M. Schroeder, "Fiber Optic Array Splicing," 1976 IEEE/OSA Conference on Laser and Electro-Optical Systems, San Diego, May 1976.
6. M. J. Buckler and F. P. Partus, "Optical Fiber Transmission Properties Before and After Cable Manufacture," Digest of Topical Meeting on Optical Fiber Transmission II, Williamsburg, Virginia, Feb. 22–24, 1977, p. WA1.
7. J. S. Cook and P. Runge, "An Exploratory Fiberguide Interconnection System," Second European Conference on Optical Fiber Communications, Paris, Sept. 1976, pp. 253.
8. P. Runge, L. Curtis, and W. C. Young, "Precision Transfer Molded Single Fiber Connector Encapsulated Devices," Digest of Topical Meeting on Optical Fiber Transmission II, Williamsburg, Va., Feb. 22–24, 1977, p. WA4.
9. P. Runge and S. Cheng, "Demountable Single Fiber Optic Connectors and Their Measurement on Location," B.S.T.J., this issue, pp. 1771–1790.

Contributors to This Issue

Charles A. Brackett, B.S.E.E., 1962, M.S.E.E., 1963, M.S. (Physics), 1966, Ph.D., 1968, University of Michigan; Bell Laboratories, 1968—. Mr. Brackett has studied microwave circuits and low frequency phenomena in IMPATT oscillators, GaAs lasers, the coupling of GaAs lasers into optical fibers, receiver design for optical fiber communications, and optical fiber data link design. Member, IEEE, Sigma Xi, Tau Beta Pi, Eta Kappa Nu.

Michael J. Buckler, B.S.E.E., 1971, M.S.E.E., 1971, Georgia Institute of Technology; Bell Laboratories, 1971—. Mr. Buckler has worked on digital circuit and system design for high speed digital multiplexers and test equipment. He is currently engaged in optical waveguide design, analysis and characterization. Member, IEEE, OSA, Eta Kappa Nu.

F. S. Chen, B.S., 1951, National Taiwan University; M.S.E.E., 1955, Purdue University; Ph.D. 1959, The Ohio State University; Bell Laboratories, 1959—. Mr. Chen has worked in the development of ferrite devices, masers, and optical modulators, and is presently engaged in development of lightwave transmitter subsystems.

Steven Shui-uh Cheng, B.S., 1963, National Taiwan University; M.S., 1967, Tufts University; Ph.D., 1970, California Institute of Technology, all in physics; Bell Laboratories, 1971—. Between 1970 and 1971, Mr. Cheng participated in the first U.S. electron-position colliding-beam experiment at Harvard University. Since joining Bell Laboratories, he has worked on the millimeter waveguide system and recently on the fiber-optic transmission system. He is currently supervisor of the fiberguide applications group. Member, IEEE, American Physical Society, and Sigma Xi.

J. S. Cook, B.E.E., M.S. (Electrical Engineering), 1952, The Ohio State University. Bell Laboratories, 1952—. Mr. Cook has done research in the fields of traveling-wave tubes, microwave propagation and devices, antennas, and satellite communications. He has been working with optical fiber communication systems in recent years and currently heads a department responsible for development of optical fiber connectors and the special technology of optical fiber telecommunication systems. Senior member, IEEE, member, OSA, SPIE, Eta Kappa Nu, Tau Beta Pi, Sigma Xi.

Frank V. DiMarcello, B.S. (Geochemistry) 1960, Pennsylvania State University; M.S., (Ceramics) 1966, Rutgers University; Bell Laboratories, 1960—. Mr. DiMarcello has been involved in the development of glazes for ceramic substrates and the preparation and property evaluation of ceramics and glasses for various applications. He is currently involved in the preparation of glass-fiber optical waveguides.

Paul W. Dorman, B.S. (E.E.), 1972, Newark College of Engineering; Bell Laboratories, 1964—. Mr. Dorman's work has recently included studies of modulation characteristics of (Al,Ga)As injection lasers and development of practical modulator circuitry. Member, IEEE, Eta Kappa Nu, Tau Beta Pi.

Adrian R. Hartman, B.S. (E.E.), 1965, University of Pittsburgh; S.M. (E.E.), 1966, Prof. E.E., 1967, and Ph.D. (E.E.), 1970, Massachusetts Institute of Technology; Bell Laboratories, 1970—. Mr. Hartman has worked in the areas of solar energy conversion, low-temperature photoluminescence, GaP light-emitting diodes, GaAlAs double heterostructure lasers, optical detectors, bipolar integrated circuits, and switching devices. He is currently Supervisor of the Silicon Device Technology Group. Member, IEEE and Sigma Xi.

Ira Jacobs, B.S. (physics), magna cum laude, 1950, City College of New York; M.S. (physics), 1952, Ph.D. (physics), 1955, Purdue University; Bell Laboratories, 1955—. Mr. Jacobs became supervisor in the Communications and Electromagnetic Analysis Department of Bell Laboratories in 1960, participating in satellite communication and radar cross-section studies. In 1962 he was appointed Head of the Military Communication Analysis Department, with responsibilities for projects in satellite communication, deep space communication, and signal processing. He became Head of the Digital Transmission Analysis Department in 1967, where he managed design work on digital transmission systems. He was appointed Director of the Transmission Systems Research Center in 1969. There he was in charge of departments performing studies on transmission objectives, performance measurement, and human factor analysis. In 1970 he became Director of the Transmission Operations and Analysis Center, managing departments involved in transmission systems maintenance, testing, and performance analysis. From 1971 to 1976, Mr. Jacobs served as Director of the Digital Transmission Laboratory where his responsibilities included the development of planning tools and digital transmission facilities including the T1/OS,

T2, and T4M systems. In 1976, Mr. Jacobs became Director of the Wideband Transmission Facilities Laboratory, in charge of the design and development of digital transmission systems using optical fiber and coaxial cables, and the provision of the network services for radio and television broadcasting. Member, American Physical Society, IEEE, American Association for the Advancement of Science, Phi Beta Kappa, Sigma Xi, Sigma Pi Sigma.

Richard S. Kerdock, RCA Institutes, 1966; B.S.E.E., 1972, Polytechnic Institute of Brooklyn; M.S.E.E., 1975, Polytechnic Institute of New York; U.S. Air Force 1957–1961; New York Telephone Co. 1961–1962; Federal Electric Corp. (ITT) 1962–1963; Bell Laboratories 1966—. Since joining Bell Laboratories, Mr. Kerdock has done circuit and systems work on digital transmission systems. He worked on the development of the T2 Digital Line, and is presently involved in exploratory and early development of fiberguide transmission systems.

Theodore L. Maione, B.S.E.E., 1952, Massachusetts Institute of Technology; RCA, 1952; U.S. Army Signal Corps, 1952–1954; Communications Development Training Program, 1954–1956; Bell Laboratories, 1954—. Mr. Maione has worked on submarine cable systems and repeater design, general purpose communications test equipment for carrier and data systems, the T2 Digital Line, and lightwave communications system development. He currently has responsibility for lightwave terminal circuits and M12 and M13 multiplexes.

Hans Melchior, Dipl. E.E. and Dr. Sc. Tech., 1959 and 1965, Swiss Federal Institute of Technology, Zurich; Department of Advanced Electrical Engineering, Swiss Federal Institute of Technology, 1960–1965; Bell Laboratories, 1965–1976; Swiss Federal Institute of Technology, 1976—. As an Assistant and Research Associate at the Swiss Federal Institute, Mr. Melchior worked on noise problems of p-n junctions at breakdown, high injection effects, second breakdown in diodes and transistors, and tunnel diode mixers and oscillators. At Bell Laboratories, he worked on the development of high-speed avalanche photodiodes, thin-film photoconductors and noise problems in MOS devices.

Calvin M. Miller, B.S.E.E., 1963, North Carolina State University at Raleigh; M.S.E., 1966, Akron University; Goodyear Aerospace Corporation, 1963–1966; Martin Marietta Company, 1966–1967; Bell Laboratories, 1967—. Before joining Bell Laboratories, Mr. Miller designed electronic and optical components of side-looking radar processor equipment and control systems for reentry vehicles and aircraft flying simulators. At Bell Laboratories, Mr. Miller developed equipment and methods for transmission line characterization. His present interests are in the area of fiber optics as a practical transmission medium. He is supervisor of an exploratory optical fiber splicing group. Member, OSA.

Joe H. Mullins, B.S. (Physics), 1950, Texas A&M University; M.S. (Physics), 1954, Ph.D. (Physics), 1959, California Institute of Technology; California Institute of Technology, 1959–1967; Bell Laboratories, 1967—. Mr. Mullins worked on the Millimeter Waveguide System (WT4) during his first years at Bell Laboratories. In 1972, he was appointed Head, Fiberguide Trunk Development Department, with primary responsibility for the T2 transmission system, an intercity paired cable digital facility which was introduced into the Bell System in that year. In 1978 he became Director, Switching Operations Systems Laboratory. Member, American Institute of Physics, American Physical Society, American Association for the Advancement of Science, Sigma Xi; Senior member, IEEE.

Daryl L. Myers, B.S., 1953, Carnegie Institute of Technology; Western Electric, 1953—. Mr. Myers transferred from the Baltimore Works to the Product Engineering Control Center in Atlanta in 1969 and was assigned to the lightguide project in 1973. He is presently a Senior Staff Engineer responsible for fiber-drawing process development.

Fred P. Partus, Ph.D., 1971, Tulane University; Western Electric, 1971—. Mr. Partus' work on the lightguide project began in 1973 with internships at Bell Laboratories in Atlanta and Murray Hill. He is presently a Senior Engineer responsible for the process developments related to preform fabrication at the Western Electric Product Engineering Control Center in Atlanta.

W. A. Reenstra, B.S.E.E., 1947, M.S. (Physics), 1949, Rensselaer Polytechnic Institute; Bell Laboratories, 1942–1956; AT&T, 1956–1961; Bell Laboratories, 1961—. Mr. Reenstra's first assignment with Bell Laboratories was in the Switching Research Department, where he worked on the remote line concentrator. In 1961 he was appointed supervisor in the Systems Engineering Department and in 1965 became Head, Military Switching Systems Department. He is presently Head, Loop Plant Construction and Installation Department. Member, IEEE, American Physical Society.

Henry W. Reinbold, A.T., 1961, Temple University; B.S., 1973, Fairleigh Dickinson University; Bell Laboratories, 1961—. After joining Bell Laboratories in 1961, Mr. Reinbold became involved with ruby maser development, with emphasis on material studies. Later he worked with electro-optic light modulators and optical communication links. His present activity includes design of test apparatus used in evaluating various lightwave devices and subsystems.

Peter K. Runge, Dipl. Ing., 1963, Dr. Ing., 1967, Technical University of Braunschweig, Germany; Bell Laboratories, 1967—. Mr. Runge has been engaged in research of He-Ne and organic dye layers and exploratory development of fiber optic repeaters and single-fiber optic connectors. He is currently Supervisor of the Fiberguide Technology Group and is responsible for the development of single-fiber optic connectors.

M. R. Santana, B.S.E.E., 1970, University of Hartford; M.S.E.E., 1971, Georgia Institute of Technology; Bell Laboratories, 1970—. Mr. Santana has been continuously involved in cable design and development in the Loop Transmission Division. At present he is involved in optical fiber cable design, analysis, and testing. Member, IEEE, Kappa Mu.

M. J. Saunders, B.S. (Physics), 1950 and M.S. (Physics), 1952, University of Virginia; Ph.D. (Physics), 1956, University of Florida; Bell Laboratories, 1956—. Mr. Saunders has worked on a variety of optical problems and is currently investigating methods of determining the refractive index profiles of optical fibers and preforms. Member, Optical Society of America, New York Academy of Sciences, American Association for the Advancement of Sciences, and the Federation of American Scientists.

David P. Schinke, B.S., 1963, Central Methodist College; Ph.D., The University of Kansas; Bell Laboratories, 1968—. Mr. Schinke's fields of interest have included quantum electronics, thin film optics, and avalanche photodetectors.

Thomas E. Seidel, B.S. (Physics), 1957, St. Joseph's College, Pa.; M.S. (Physics), 1959, U. of Notre Dame; Ph.D. (Physics), 1965, Stevens Institute of Technology; RCA, 1959–1965; Bell Laboratories, 1965—. At Bell Laboratories, Mr. Seidel has worked on high field carrier transport, ion implantation and gettering phenomena in silicon and their device applications to microwave (IMPATT) devices, bipolar and MOS integrated circuits. In 1977, he held a teaching-research position at Cal Tech's Applied Physics Department. Member, American Physical Society, IEEE, ECS, and Bohmische Physical Society.

Morton I. Schwartz, B.E.E., 1956, City College of New York; M.E.E., 1959, Eng. Sci.D. 1964, New York University; ITT Laboratories, 1956–1962; Bell Laboratories, 1961—. At ITT, Mr. Schwartz' principal efforts were in the field of radar systems studies and design. At Bell Laboratories, he has been engaged in theoretical and experimental work in radar, sonar, and communications. Since 1972, he has been responsible for the exploratory development of optical fiber communication media which led to the Atlanta Lightwave Communications Experiments and to the Chicago Lightwave Communication Project. He is currently responsible for the development of optical fiber communications media.

Darrell D. Sell, B.A. 1962, St. Olaf College; Ph.D. (Physics), 1966, Stanford University, Bell Laboratories, 1967—. Mr. Sell joined Bell Laboratories in the physical research area and for six years carried out optical spectroscopic research on materials. He transferred to lightwave development work in 1973, where he has been involved in system design, testing, field evaluations, and lightwave regenerator development.

Paul W. Shumate, Jr., B.S. (physics), 1963, College of William and Mary; Ph.D. (physics), 1968, University of Virginia; Bell Laboratories, 1969—. Mr. Shumate's first assignments at Bell Laboratories included research on the physical properties of magnetic bubble materials and magnetic bubble memory devices. He transferred to the Integrated

Circuit Marketing and Applications Department in 1973, where he studied memory applications for integrated circuits. In 1975 he became Supervisor in the Lightwave Devices and Subsystems Department, where he directs the design and packaging of gallium-arsenide laser transmitters for use in future lightwave communications systems. Member, American Physical Society, Phi Beta Kappa, Sigma Xi, IEEE. Member of the IEEE Magnetics Advisory Committee and editor of the *IEEE Transactions on Magnetics.*

Richard G. Smith, B.S. E.E., 1958, M.S. E.E., 1959, Ph.D., 1963, Stanford University; Bell Laboratories, 1963—. Mr. Smith has been engaged in research and development in the areas of solid-state lasers, nonlinear optics, and electro-optic devices, and most recently in fiber optics. His current work involves the development of detectors and receivers for lightwave applications. Member, AIP, IEEE, Phi Beta Kappa, Tau Beta Pi.

John Williams, B.S. (Cer. E.) 1950, M.S. (Cer. E.), 1951, Prof. Degree (Cer. E.) 1969, University of Missouri–Rolla; Bell Laboratories, 1951—. Mr. Williams has been engaged in ceramic materials research and development of substrates for carbon film resistors and thin film circuits, ceramic dielectrics for microwave windows, and insulators in ocean cables. He is presently involved in the preparation of glass-fiber optical waveguides. Fellow, American Ceramic Society; Member, National Institute of Ceramic Engineers, ASTM-F-1.

Dan H. Wolaver, B.S.E.E., 1964, Rensselaer Polytechnic Institute; M.S.E.E., 1966, Ph.D. E.E., 1969, Massachusetts Institute of Technology; Bell Laboratories, 1969—. Mr. Wolaver has worked on margin monitoring in the T4M digital repeater. He is currently working on timing recovery and fault locating in fiberguide transmission systems. Member, Eta Kappa Nu, Tau Beta Pi, Sigma Xi, IEEE.

THE BELL SYSTEM TECHNICAL JOURNAL is abstracted or indexed by *Abstract Journal in Earthquake Engineering, Applied Mechanics Review, Applied Science & Technology Index, Chemical Abstracts, Computer Abstracts, Computer & Control Abstracts, Current Contents/Engineering, Technology & Applied Sciences, Current Contents/Physical & Chemical Sciences, Current Index to Statistics, Current Papers in Electrical & Electronic Engineering, Current Papers on Computers & Control, Electrical & Electronic Abstracts, Electronics & Communications Abstracts Journal, The Engineering Index, International Aerospace Abstracts, Journal of Current Laser Abstracts, Language and Language Behavior Abstracts, Mathematical Reviews, Metals Abstracts, Science Abstracts, Science Citation Index,* and *Solid State Abstracts Journal.* Reproductions of the Journal by years are available in microform from University Microfilms, 300 N. Zeeb Road, Ann Arbor, Michigan 48106.

Bell System